ABSTRACT

Title of Document:	ACTIVE ACOUSTIC METAMATERIALS
	Saeed Althamer, Doctor of Philosophy, 2015
Directed By:	Professor, Amr Baz, Department of Mechanical Engineering

A class of active acoustic metamaterial (*AAMM*) is presented. The proposed *AAMM* consists of an acoustic transmission line connected in parallel to an array of Helmholtz resonators that are provided with actively controlled boundaries. In this manner, the *AAMM* is in effect an assembly of periodic cells, each of which consists of a Helmholtz resonator connected in parallel to two sections of the transmission line. The two sections meet the Helmholtz resonator at its neck. The local control action at each Helmholtz resonator of a unit cell is generated by using a Proportional and Derivative (*PD*) as well as Fractional Derivative (*FD*) controllers. The controllers that rely in their operation on the measurement of the flow resulting from the deflection of the resonator boundary and the flow rates inside the two transmission line sections before and after the resonator. Such a single local control action is shown to be capable of controlling the local effective density and elasticity of each unit cell.

Lumped-parameter models are developed to model the dynamics and control characteristics of the *AAMM* under different gains for the *PD* controller and exponents of the *FD* controller. The models are exercised to demonstrate the ability of the *FD* controller in generating metamaterials with double negative effective density and elasticity over broad frequency ranges as compared to conventional Proportional and Derivative (*PD*) controllers.

With such capabilities, the development of *AAM* with *FD* control action may provide viable means for generating desirable spatial distributions of density and elasticity over broad frequency band using a small number of control actuators.

ACTIVE ACOUSTIC METAMATERIALS

By

Saeed Althamer

Dissertation submitted to the Faculty of the Graduate School of the
University of Maryland, College Park, in partial fulfillment
of the requirements for the degree of
Doctor of Philosophy
2015

Advisory Committee:
Professor Amr Baz, (Chair)
Professor Balakumar Balachandran
Assoc. Professor Nikhil Chopra
Asst. Professor Jin-Oh Hahn
Professor Alison Flatau (Dean's Representative)

ACKNOWLEDGMENTS

First of all, I would like to express my sincere gratitude to my committee chair Prof. Amr Baz for his immeasurable support and guidance throughout the course of this work. Dr. Baz has shown a perfect example of what an advisor has to be with his immense knowledge and professionalism.

I would like also to thank my thesis committee, Dr. Balakumar Balachandran, Dr. Nikhil Chopra, Dr. Jin-Oh Hahn, and Dr. Alison Flatau for their encouragement and helpful suggestions and comments.

Special thank goes to my colleagues and lab mates for providing me with the suitable working environment to excel in my work. Their encouragement and support was the key to survive all the challenges I have gone through during my school years.

Finally, to my parents, Thamer and Sara', and my siblings, Ali, Mohammad and Shomoukh, the ones who stood behind this work, there's no word that would express how grateful and appreciative I am more than thank you. Thank you for your love, support, motivation, and patience. I extend my thanks to include the two individuals, my Uncle Ali and Aunt Hilah, who have shown an infinite support and love for me throughout my journey.

Table of Contents

List of Figures:

List of Tables

Chapter 1: Introduction

1.1 Introduction to Metamaterials

Considerable interest in the field of metamaterials has been placed during the past decade as a viable means of redirecting waves. Such interest has stemmed from the unnatural characteristics and unique properties of these metamaterials that have enabled their use in numerous interesting and critical applications that cannot be achieved with natural materials existing in nature.

The term of metamaterials was coined nearly a decade ago by Walser (2001). The prefix "*meta*" originates from the Greek word for "*after*" or "*beyond*" and it was then defined as a "*macroscopic composites having a manmade, three-dimensional, periodic cellular architecture designed to produce an optimized combination, not available in nature, of two or more responses to specific excitation.*"

Since then, a wide class of metamaterials has been developed with unusual optical, electromagnetic, and acoustical properties. The design features and performance characteristics of these materials have been extensively reported, for example, by Lapine (2007), Shamonina and Solymar (2007), Gil *et al*. (2008) and Pope and Daley (2010). In most of these reported studies, the focus has been placed on passive metamaterials with fixed material properties. This limits considerably the potential of this class of materials as they can operate effectively only at specific operating conditions and their performance characteristics degrade dramatically if there is a need to operate at different conditions. This serious limitation manifests itself clearly by the narrow frequency band characteristics of passive metamaterials.

However, in this chapter, a radically different approach is considered where active acoustic metamaterials (*AAMM*) are investigated because of their ability of operating over wide frequency bands, adapting to varying external environment, and more importantly morphing from one functional configuration to another based on the mission requirements of the *AAMM*. This approach has been introduced by Baz (2009, 2010) and his associates Akl *et al*. (2010-2014).

The ultimate goal here is to outline the basic fundamentals and the associated underlying phenomena governing the operation of the *AAMM* and their application to several critical systems.

In general, the wave propagation patterns within this class of *AAMM* and the interacting acoustic fluid domains is governed by the spatial and spectral distributions of the two basic acoustic material properties: the density and bulk modulus.

Accordingly, engineering a particular material structure with arbitrary density and bulk modulus distributions would yield an acoustic domain with wave propagation pattern dependent on such distribution. Hence, the ultimate goal here is to present strategies for the design and synthesis of *AAMM* configurations that would allow for density and/or bulk modulus distributions that result in specific wave propagation patterns and mission configurations of the *AAMM* platform.

It is therefore the purpose of this chapter and dissertation is to summarize the efforts exerted in developing *AAMM* that have tunable and programmable mechanical and acoustic properties. Specifically, the *AAMM* under consideration consist of array of fluid cavities separated by piezoelectric boundaries. These boundaries control the stiffness of the individual cavities in such a way to control the dynamical density and bulk modulus. Various control strategies are considered to achieve different spectral and spatial control of the density and bulk modulus of this class of acoustic metamaterials.

To achieve these goals, this dissertation is organized in seven chapters. In chapter 1, a brief introduction is presented. In chapter 2, the need for metamaterials is motivated and the concept of the active acoustic metamaterial is introduced in chapter 3. In chapter 4, the theories governing the operation of the *AAMM* are presented. In chapter 5, numerical examples are considered to demonstrate the application of the active metamaterial to external and internal cloaks. In chapter 6, some performance characteristics of several components of the *AAMM* are presented. In chapters 7, *AAMM* with transmission line control boundaries is proposed. Additional controlling capabilities added to the *AAMM* with transmission line control boundaries to include Helmholtz control boundaries is studied rigorously in chapter 8. Then, a brief summary of the conclusions and the future work are outlined in chapter 9.

1.2. Why Active Metamaterials?

The need for active metamaterials can best be understood by considering the application region for conventional and natural materials as illustrated in Fig. 1.1. The figure shows such a region as plotted on the density (ρ) - bulk modulus (β) plan. It is clear that this region is very limited to be effective for critical applications such as perfect absorbers, perfect reflectors, beam shifters, or acoustics cloaks. The requirements for such critical applications will be discussed in detail in chapter 4. In all these applications, the ranges of density and bulk modulus that are required are actually far beyond what exists in nature. For example in air, perfect absorbers must have acoustic impedances $(Z = \sqrt{\rho\beta})$ equal to zero while perfect reflectors require impedances which are infinite. Although near perfect absorbers and reflectors can be achieved with conventional materials, no material exists that can behave as a perfect

absorber and then be morphed or programmed to become a perfect reflector. Metamaterials would provide a viable means for achieving such multi-functionality capabilities.

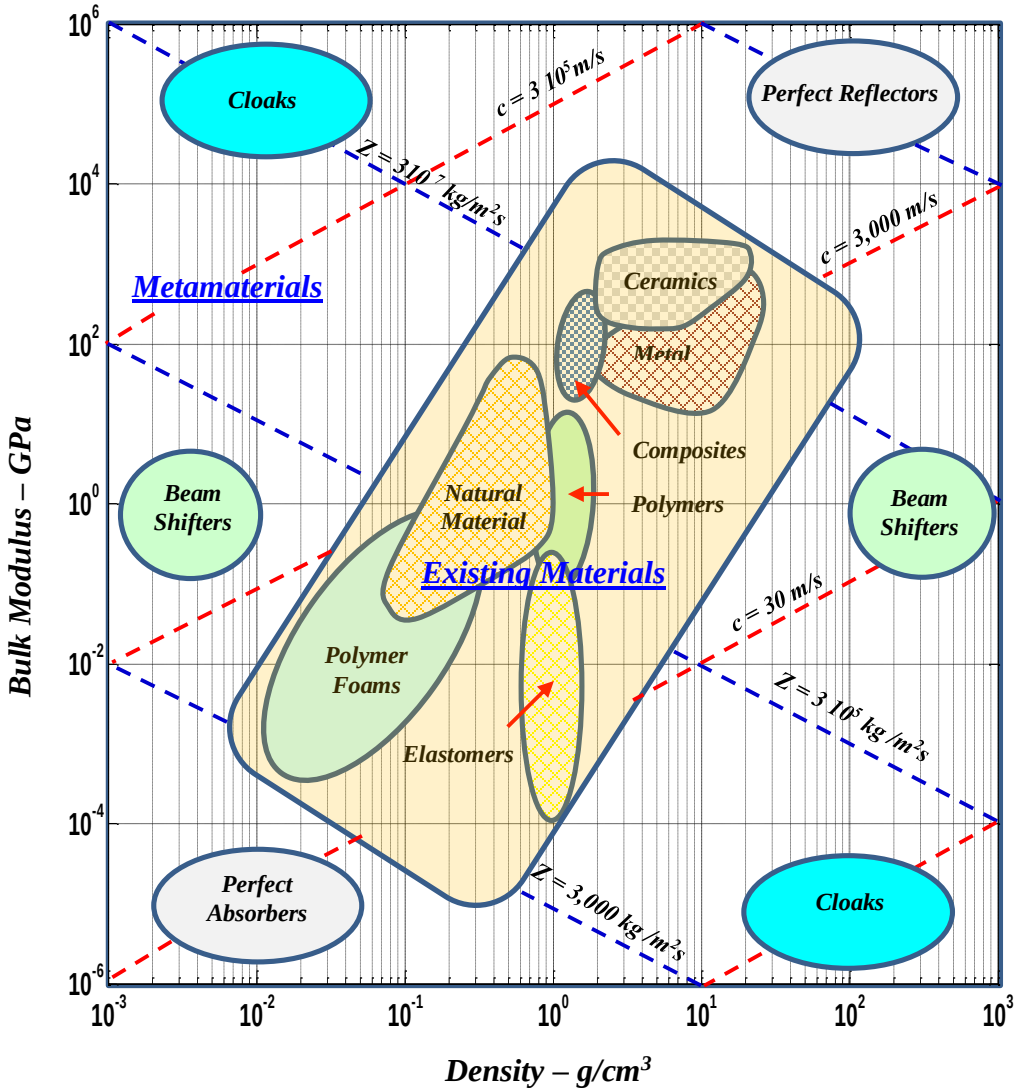

Fig. 1.1 - Regions of operation of existing materials, metamaterials, and potential applications
(*c*= sound speed, *Z*=impedance)

As for beam shifters, effective operation requires the assembly of metamaterial composites consisting of layers that have functionally graded acoustic impedances or sound speeds to enable desirable beam shifting and/or focusing characteristics. In order to practically achieve such characteristics in confined spaces with reasonable thicknesses, it is challenging if not impossible to use existing materials. It becomes imperative to rely on synthesizing metamatreial composites with not only steep impedance and/or sound speed changes as shown in Fig. 1.1. It may also be beneficial to provide these composites with tunable and programmable capabilities to enable morphing from just beam shifting to beam focusing and vice versa.

For acoustic cloaks, the situation is far more complicated as the material properties of the cloak must be anisotropic and vary orders of magnitude over the cloak volume in a manner which necessitates the use of metamaterials. These characteristics will be elaborated upon in section 4. The required metamaterial properties would span the entire space of the density-bulk modulus plan as shown in Fig. 1.1. The figure indicates that effective cloaks must be graded from a simultaneously very stiff and very light weight component, at one end, to a very soft and heavy ingredient at the other end. Such steep functionally graded properties cannot be realized with existing natural materials. Synthesized metamaterials can be programmed to map the desired functionally graded properties into its micro-structure.

More importantly, a metamaterial with such programmability or tunability characteristics can serve as platform that can be morphed to behave as acoustic cloak, beam shifter, perfect absorber, or perfect reflector as shown in Fig. 1.2. This morphing capability can be realized by imparting the necessary acoustic properties corresponding to moving around the corners and perimeter of the density-bulk modulus plan.

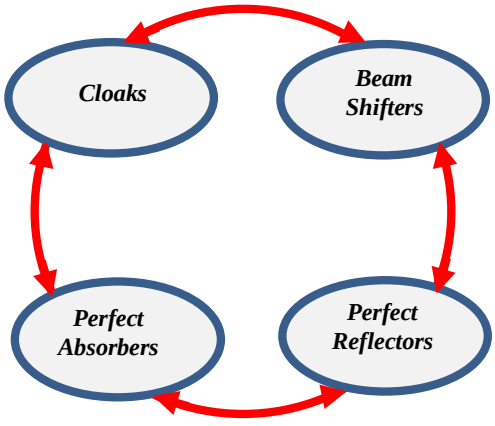

Fig. 1.2 – Morphing of an active acoustic metamaterial platform between different configurations according to mission requirements

1.3. Concept of Active Acoustic Metamaterial

In order to understand the concept and the structure of the active acoustic metamaterial, consider the structure of the external and internal acoustic cloaks (Fig. 1.3), the beam shifters (Fig. 1.4), and beam focusing device (Fig. 1.5). In Fig. 1.3, the external cloaks can potentially be used in hiding acoustically critical objects whereas the internal cloak can be employed to make the fuselages of aircraft and helicopters quiet and improve the interior acoustics inside auditoriums and meeting rooms. Note that the acoustic cloaks can be configured to treat objects either externally or internally in order to render these objects acoustically invisible. In Fig. 1.4a, the beam shifters can be utilized to enable the control of the directivity and dispersion characteristics of the waves as these waves propagate inside the metamaterial in order to shift the direction and slow/speed the sound propagation speed. A possible application can be used in the design of a metamaterial helmet for soldiers and athletes (Fig. 1.4b). The helmets are intended to protect the soldiers or the athletes from any brain injuries resulting from the exposure to blast or impact wave propagation by smoothly guiding and bending these waves around their heads to avoid any over-pressurization. Fig. 1.5 shows a schematic drawing of a metamaterial acoustic beam focusing device which can be useful in manufacturing, for example, hearing aids with high signal to noise ratio or for enhancing the efficiency of acoustic energy harvesters.

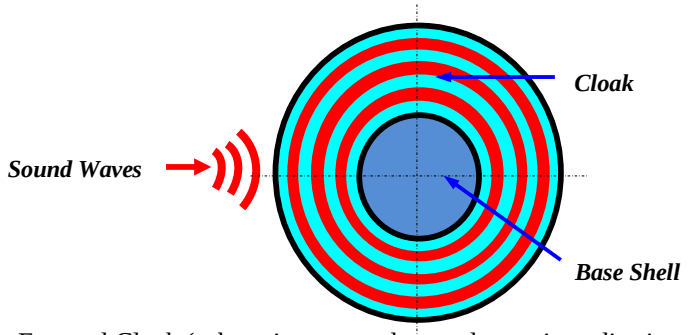

a. External Cloak (submarines, torpedoes, columns in auditorium, etc.)

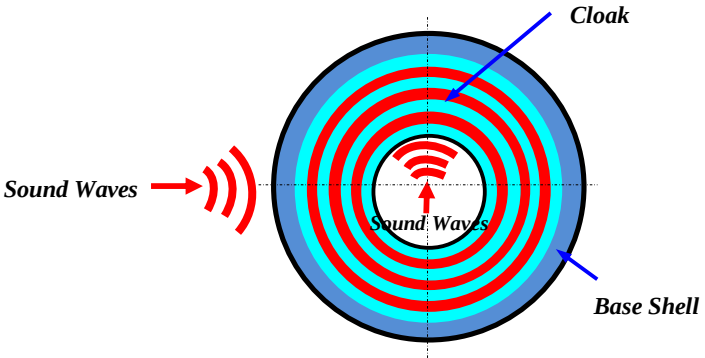

b. Internal Cloak (fuselage of aircraft, helicopter cabins, auditorium, etc.)

Fig. 1.3 – External and internal acoustic cloaks

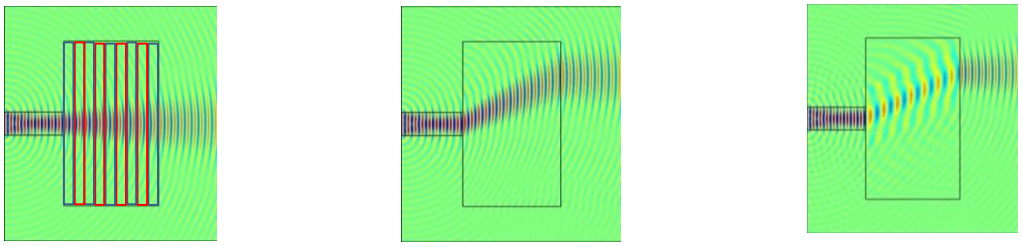

Original Beam | Directivity Control | Dispersion Control

(a) - Beam Shifters

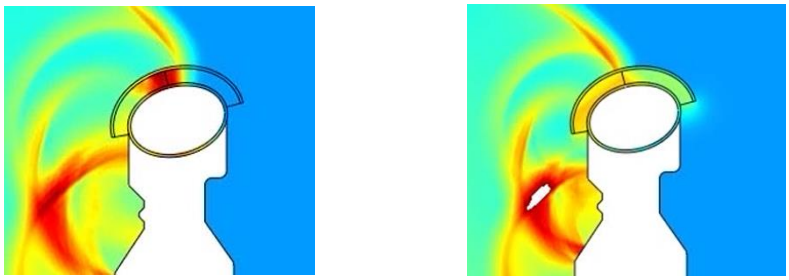

Conventional Helmet
(high pressures and fast waves)

Metamaterial Helmet
(low pressures and slow waves)

(b) - helmets

Fig. 1.4 – Beam shifting metamaterial devices

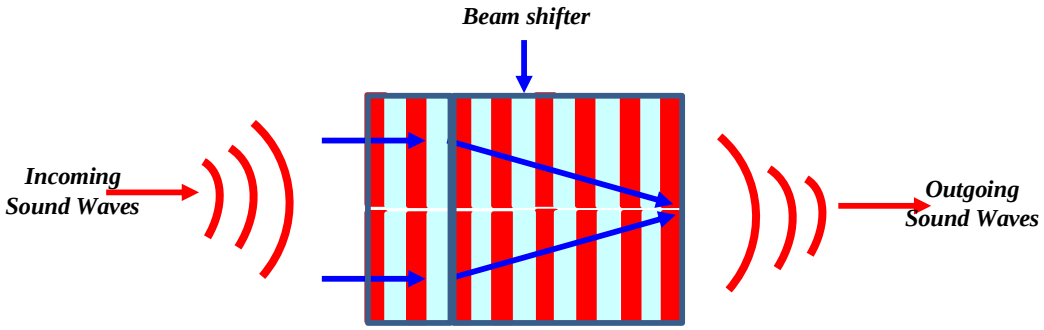

(a) – schematic drawing

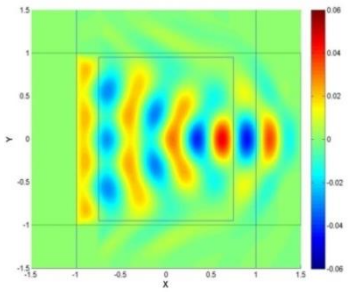

(b) – focusing capabilities of the device

Fig. 1.5 - Metamaterial acoustic beam focusing device

The systems and devices shown in Figs. 1.3 through 1.5 rely in their operation on engineered materials composed of periodically arranged composite cells of two or more materials, which are arranged in such a way to yield effective density and bulk modulus distributions that are otherwise unachievable with isotropic materials. The unit cell in all these examples is shown in Fig. 1.6. Note that the dimensions of these unit cells are designed to be much smaller than the wavelength of the encountered propagating waves in order to achieve homogenized domain with the targeted overall material properties. The parameters in designing the cell itself are its geometry, orientation in the macro-scale structure

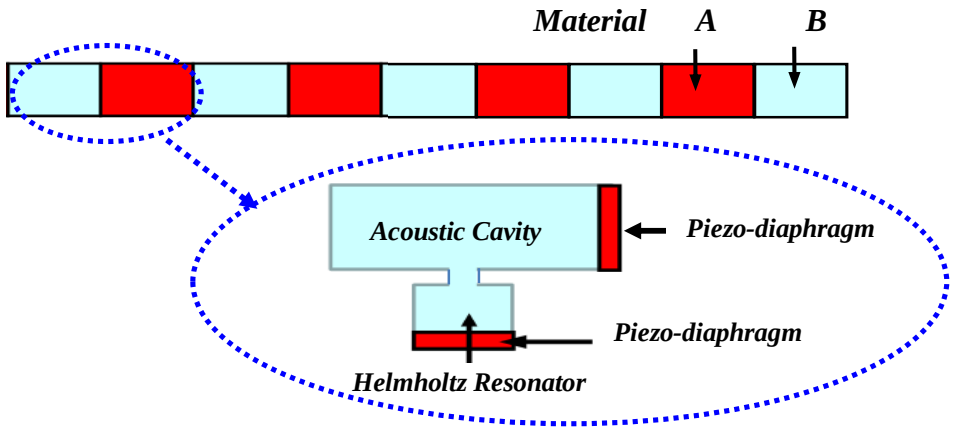

Fig. 1.6 – Structure of the active acoustic metamaterial

The preferred arrangement of the unit cell of the active acoustic metamaterial, shown in Fig.1.6, consists of arrays of fluid cavities that are separated by and provided with piezoelectric boundaries. These boundaries control the stiffness of the individual cavity and in turn control its dynamical density and bulk modulus. All the cavities and boundaries look mechanically the same to facilitate the manufacturing. However, with various control strategies, the individual piezo-boundaries can be programmed to achieve any desirable spectral and spatial distributions of the acoustical density and bulk modulus over the metamaterial volume.

1.4. Scope of the Dissertation

This dissertation aims at extending the current state-of-the-art of the field of *AAMM* by developing a new class of control strategies to effectively control and

enhance the performance of the current *AAMM*. Such an extension constitutes the major contribution of this dissertation.

The current *AAMM* rely in their operations on separate actuators to control the density and bulk modulus of a metamaterial unit cell. Furthermore, the adopted control strategies are based primarily on simple linear proportional-derivative (*PD*) control laws. In this dissertation, it is proposed to utilize single actuator to simultaneously both of the density and bulk modulus of the unit cell. More importantly, a nonlinear control law which employs fractional derivative (*FD*) controller in order to improve the performance of the current *AAMM*. The improvement is envisioned to be by enhancing the *AAMM* ability of operating over frequency bands that are wider than those possible with the simple linear proportional-derivative (*PD*) control laws.

The effectiveness of the proposed *FD* controller is demonstrated numerically and experimentally for metamaterial unit cells that are provided with ceramic piezoelectric actuators for control purposes and array of polymeric piezoelectric sensors for monitoring the operation of the unit cells.

Comparisons are also established between the performance of the proposed *FD* controller and that of the simple linear proportional-derivative (*PD*) control laws in order to emphasize the potential and merits of the *FD* control approach.

1.5. Organization of the Dissertation

In order to achieve the goals presented in the scope of the dissertation section, this dissertation is organized in seven chapters. In chapter 1, a brief introduction is presented. In chapter 2, configurations of passive acoustic metamaterials are introduced along with their performance characteristics. In chapter 3, the equivalent configurations of active acoustic metamaterials are presented and their performance characteristics are compared with those of the passive systems. In chapter 4, the *AAMM* configurations with stacked Helmholtz resonators are presented in an attempt to enhance the characteristics of the *AAMM* are presented. In chapter 5, *AAMM* with multiple Helmholtz resonators are presented and compared with different configurations of the *AAMM*. In chapter 6, some performance characteristics of several components of the *AAMM* are presented. In chapter 7, *AAMM* with Transmission Line Control Boundaries is proposed and investigated with two different configurations. In chapter 8, the two configurations of the *AAMM* with simultaneous transmission line and Helmholtz control boundaries is presented and studied. Then, a brief summary of the conclusions and the future work are outlined in chapter 9.

1.6. Summary

This chapter has presented a brief review of the field of acoustic metamaterials with a particular emphasis on the class of active acoustic metamaterials because of their ability of operating over wide frequency bands, adapting to varying external environment, and more importantly morphing from one functional configuration to another based on the mission requirements of the *AAMM*.

Furthermore, this chapter has outlined the scope and organization of this dissertation where the focus is placed on extending the current state-of-the-art by developing a new class of control strategies to effectively control and enhance the performance of the current *AAMM*. Such an extension constitutes the major contribution of this dissertation.

2.1 Dynamics of Transmission Line and Helmholtz Resonator

In this section the effect of the Helmholtz resonator on the transmission line of a wave carrying medium will be investigated. At first, the Helmholtz resonator cavity system parameters and dynamics will be presented. In addition to developing the dynamics of the transmission line element without the helmholtz cavity. Later, the helmholtz cavity is introduced to the transmission line element and the dynamics of the system is derived. Finally, the frequency response of the transmission line element with and without the helmholtz resonator including the effective system parameters will be studied.

a. Helmholtz resonator dynamics with flexible boundaries

The Helmholtz cavity is represented mechanically as mass-spring-damper system. The Helmholtz resonator system parameters are illustrated in Fig. 2.1 with resonating mass (m_r), spring (k_r) and damper (c_r), as introduced by Pope and Daley (2010). The Helmholtz cavity is equipped with flexible diaphragm at the end of the cavity. Spring (k_{end}) and damper (c_{end}) parameters are representing the flexible diaphragm encapsulating the fluid inside the cavity, see Fig.2.1.

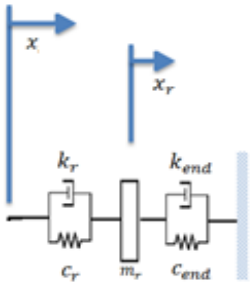

Fig. 2.1: Mechanical representation for the Helmholtz resonator with flexible boundary

The dynamics of the Helmholtz resonator with flexible diaphragm is formulated as such:

$$m_r s^2 X_r + (k_r + s c_r) X_r + (k_{end} + s\, c_{end}) X_r = 0$$

Where

X_r : represents the resonating mass's displacement.

b. Transmission line dynamics

The transmission line of a wave carrying medium is discretized into elements. Each element is represented as a system of mass-spring-damper system, see Fig.2.2. System parameters of transmission mass (m) and viscoelastic connection acting as spring (k) and damper (c) are respresenting the transmission line element mechanically as illustrated in Fig. 2.2.

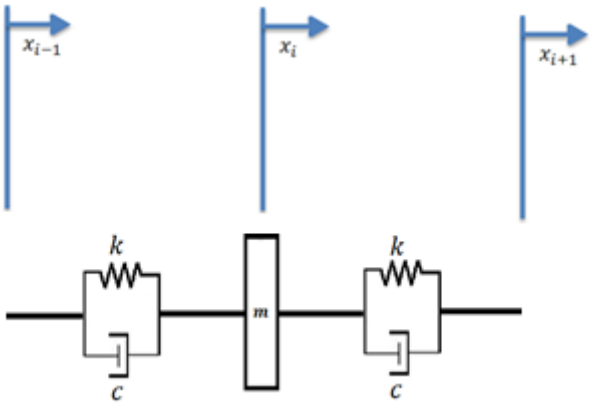

Fig. 2.2: Mechanical representation for the transmission line element

The dynamics of the transmission line element without helmhlotz resonator is formulated as such:

$$m\,s^2\,X_i + (k + sc)(2\,X_i - X_{i-1} - X_{i+1}) = 0$$

Table 2.1 Physical parameters of section 2.1

Parameter	m (kg)	k (N/m)	c (Ns/m)	m_r (kg)	k_r (N/m)	c_r (Ns/m)	k_{end} (N/m)	c_{end} (Ns/m)	No. of Cells
Values	0.01	100	0.1	0.1	1000	0.002	200	0.1	4

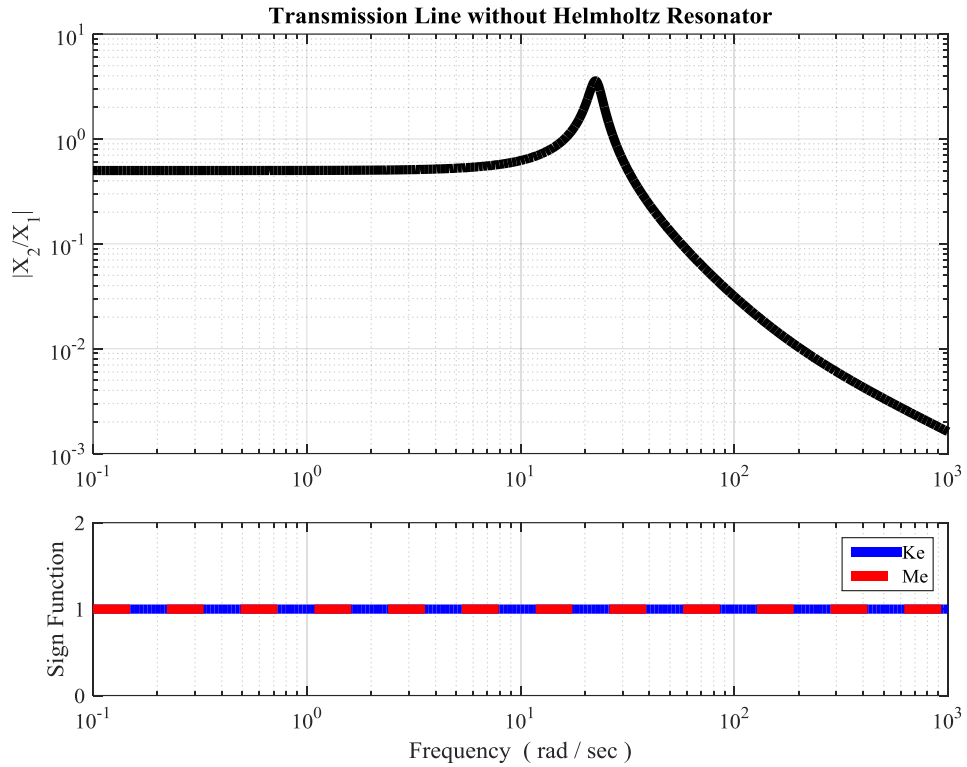

Fig. 2.3: Top: Frequency response $\left|\frac{X_2}{X_1}\right|$ of the single transmission line element. Bottom: Sign functions for the system effective parameters: mass (M_e) and stiffness(K_e)

The frequency response, absolute relative displacement$|X_1/X_0|$, for a single transmission line element has been plotted in the top part of Fig.2.3. On the frequency axis spanning from 0.1 rad/sec to 1000 rad/sec using parameters listed in table 2.1, this single transmission line element only exhibits a single resonance at 23 rad/sec.

It is evident, as it can be observed on the bottom part of Fig. 2.3, that the sign functions of the system effective parameters are maintained on their positive levels throughout the frequency range.

c. Transmission line with Helmholtz resonator

The helmholtz resonator has been attached to the transmission line element as an attempt to achieve effective parameters with the potential to embrace negative levels, Pope and Daley (2010). The helmholtz resonator will offer a great deal of controllability over the overall system response especially on the effective parameters.

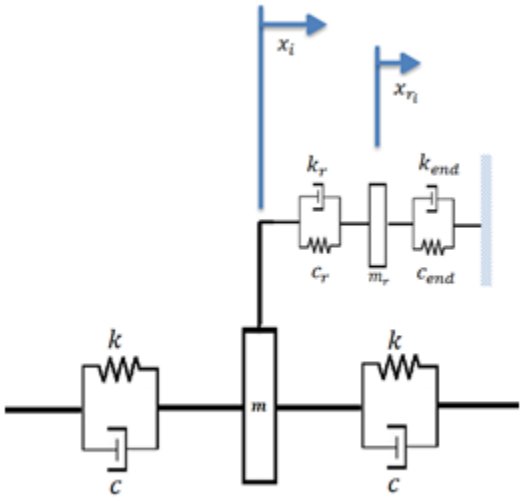

Fig. 2.4: Transmission line element with attached helmholtz resonator

a. Equation of motion of transmission line element with Helmholtz resonator

The equation of motion in here is including the helmholtz resonator parameters $(k_r\ , c_r)$ and motion information, X_r;

$$m\ s^2\ X_i + (k + sc)(2\ X_i - X_{i-1} - X_{i+1}) + (k_r + sc_r)(X_i - X_r) = 0$$

b. Equation of motion of the Helmholtz resonator attached to the transmission line

The equation of motion for the helmholtz is including a motion information, X_i, from the transmission line element which represents the transmission mass displacement;

$$m_r s^2 X_r + (k_r + s c_r)(X_r - X_i) + (k_{end} + s\, c_{end}) X_r = 0$$

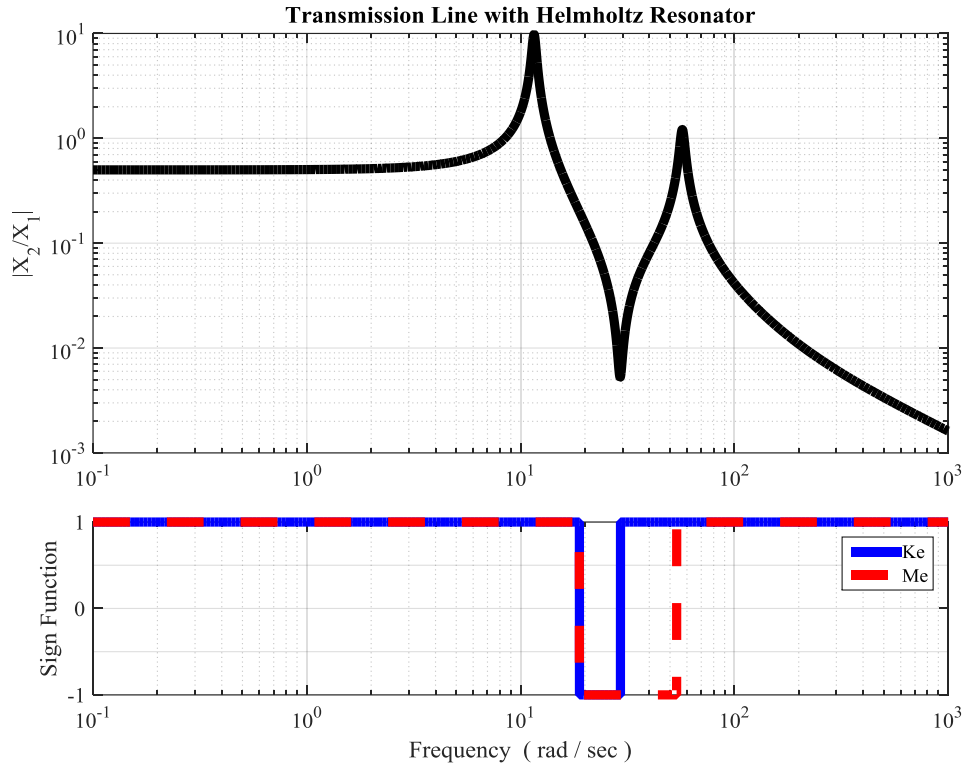

Fig. 2.5: Top: Frequency response $\left|\frac{X_2}{X_1}\right|$ of the single transmission line element. Bottom: Sign functions for the system effective parameters: mass (M_e) and stiffness(K_e)

The frequency response, absolute relative displacement$|X_1/X_0|$, for the single transmission line element with attached helmholtz resonator is shown at the top part of Fig. 2.5. It is evident that the system has exhibited two resonances, at 12 rad/sec and 60 rad/sec, with anti-resonance, at 30 rad/sec, in between caused by adding helmholtz resonator to the transmission element, see top part of Fig. 2.5.

A great deal of attenuation, bottom part Fig. 2.5, in the system response occured at the region of overlap when the effective parameters of the system became negative. At the moment when the effective parameters are of opposite signs ($K_e > 0\ and\ M_e < 0$), the system exhibited an anti-resonance. Following the anti-resonance, the system response has soon increased to cause the second resonance at the edge when the second

parameter, M_e, retrieved back to the positive levels joining the first parameter, K_e, and maintaining on these levels to the end.

System response using two unit cells

Periodic systems consisting of two transmission line elements with attached helmholtz resonators are presented in this section. Using the passive parameters listed in table 2.1, the system responses across the two elements for both cases have been illustrated in the top parts of Fig. 2.6 and Fig. 2.7. In addition, the levels of the periodic system effective parameters as the frequency changes will be investigated for the two cases without and with helmholtz resonators will discussed, bottom parts of Fig. 2.6 and Fig. 2.7.

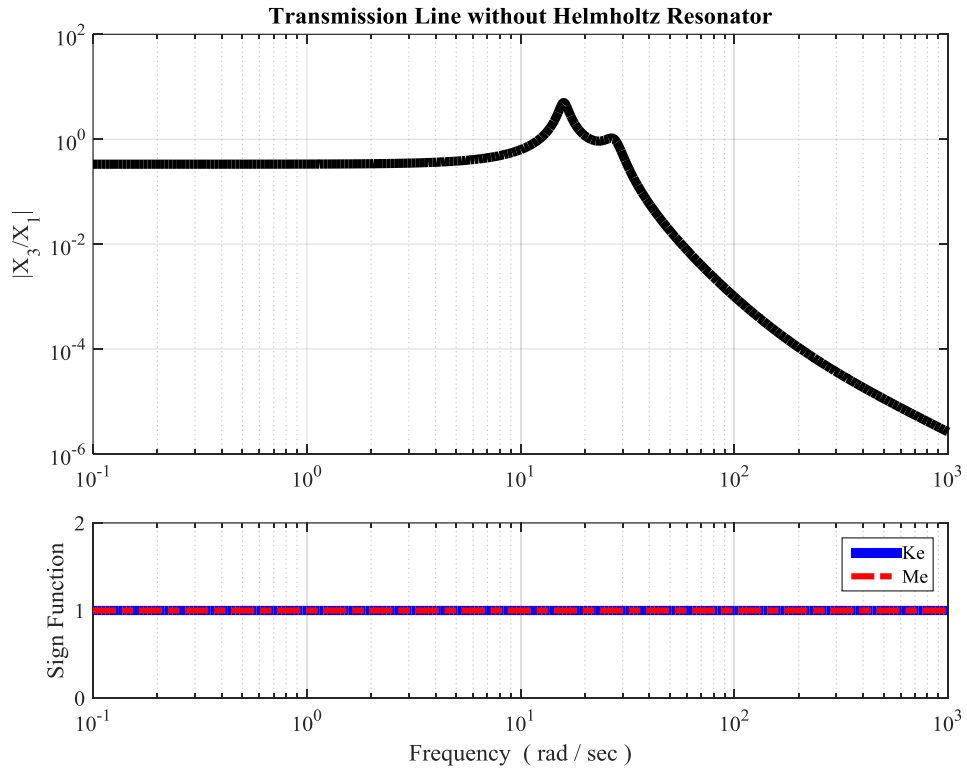

Fig. 2.6: Top: Frequency response $\left|\frac{X_3}{X_1}\right|$ of the two transmission-line elements without helmholtz resonator. Bottom: Sign functions for the system effective parameters: mass (M_e) and stiffness(K_e)

The frequency response, absolute relative displacement $|X_3/X_1|$, for a periodic system of two transmission line elements has been plotted in the top part of

Fig.2.6. On the frequency axis spanning from 0.1 rad/sec to 1000 rad/sec using parameters listed in table 2.1, this periodic system exhibits two resonances. The first resonance is observed at 16 rad/sec, whereas the second resonance is located at 28 rad/sec.

In the bottom part of Fig. 2.3, that the sign functions of the system effective parameters remained on positive levels throughout the frequency range.

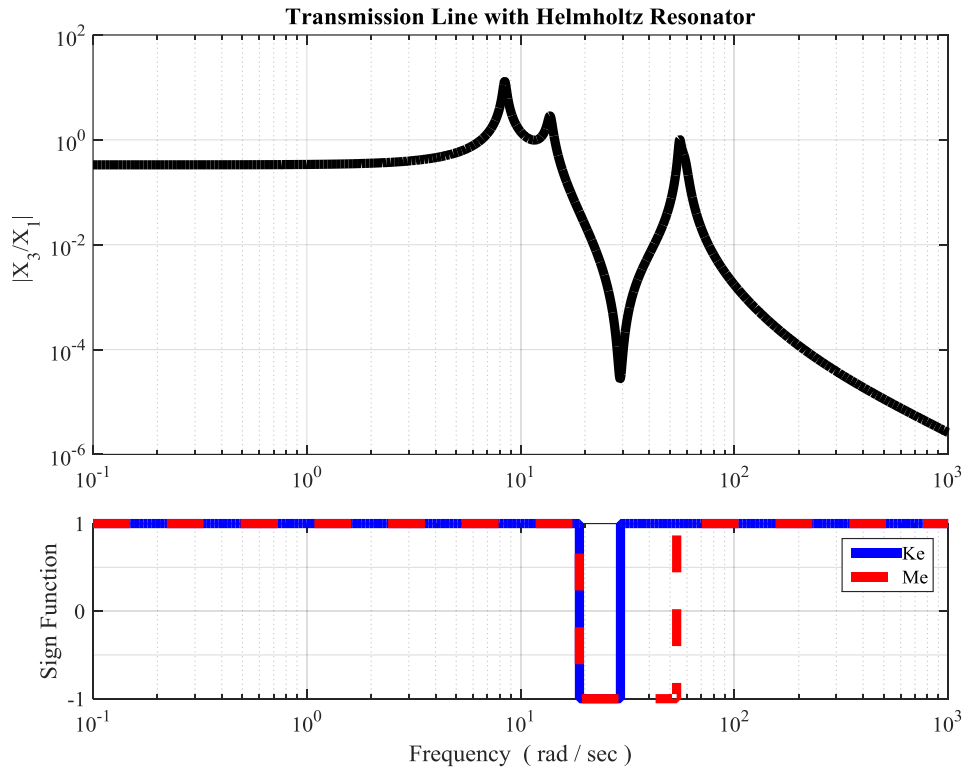

Fig. 2.7: Top: Frequency response $\left|\frac{X_3}{X_1}\right|$ of the two transmission-line elements with helmholtz resonator. Bottom: Sign functions for the system effective parameters: mass (M_e) and stiffness(K_e)

The frequency response, absolute relative displacement$|X_3/X_1|$, for the periodic system with two transmission-line elements with attached helmholtz resonator is shown at the top part of Fig. 2.7. It is obvious that the system has exhibited three resonances, at 8.5, 15 and 55 rad/sec, with anti-resonance, at 30 rad/sec, located between the last two resonances caused by adding helmholtz resonator to the transmission element, see top part of Fig. 2.7.

Attenuation in the response of the periodic system, bottom part Fig. 2.7, is observed, after the second resonance, at the region of overlap when the effective parameters of the system became negative at 20 rad/sec. At about 30 rad/sec when the effective parameters are of opposite signs ($K_e > 0 \; and \; M_e < 0$), the periodic system exhibited an anti-resonance. Following the anti-resonance at 30 rad/sec, the periodic system response has increased to form the second resonance, at 55 rad/sec, at the edge when the second parameter, M_e, retrieved back to the positive levels joining the first parameter, K_e, and maintaining on these levels to the end.

In conclusion, incorporating the helmholtz resonator into the structure of the transmission line element has influenced the dynamics of the single and periodic systems. The levels of the effective parameters determine the zones of attenuation, and the locations of resonances and anti-resonances. When the effective parameters have same sign levels, a resonance appears in the response of the system followed by attenuation in the response. On the other hand, when the effective parameters embrace opposite sign levels anti-resonance forms and increment in the system response follows.

2.2 The Structure of the Passive Metamaterial – Configuration 1

Passive acoustic metamaterials (*PAMM*) have traditionally been at the center of attention of the majority of the available studies. The *PAMM* in this section has been proposed and investigated by Pope and Daley (2010). In this section, the performance characteristics of *PAMM* are presented by developing a lumped parameter model of a preferred configuration of the *PAMM*. The first configuration of the considered *PAMM* design consists mainly of an array of Helmholtz resonators coupled to a main transmission line as shown in Fig. 2.8.

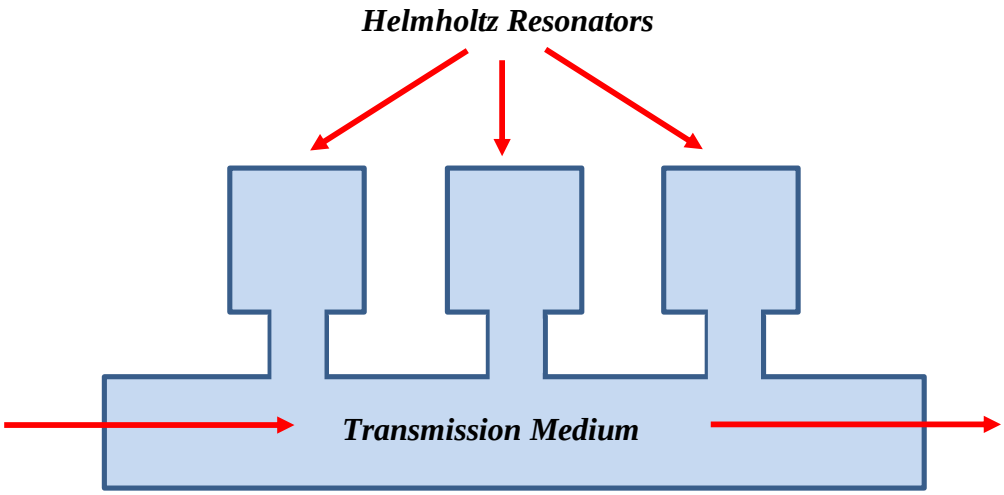

Fig. 2.8: Configuration 1 of the Passive Acoustic Metamaterial

2.3 Modeling of Configuration 1 of the Passive Metamaterial

The *PAMM* shown in Fig. 2.8 which consists of Helmholtz resonators/transmission line is modeled by arrays of coupled mass-spring-damper systems. The resulting lumped-parameter model is displayed in Fig. 2.9. In the figure, each Helmholtz resonator is represented by a spring k_r, mass m_r, and a damper c_r. The back of the Helmholtz resonator is assumed flexible and has a spring with a stiffness k_{end} and viscous damper with damping coefficient c_{end}. Also, in the figure, the transmission line is divided into discrete number of sections (elements). Each of these elements is modeled by a spring k, mass m, and a damper c.

Each Helmholtz resonator is connected, at its neck, to the transmission masses at one point along the transmission line (*e.g.* points i-1, i, i+1,…) as shown in Fig. 2.9.

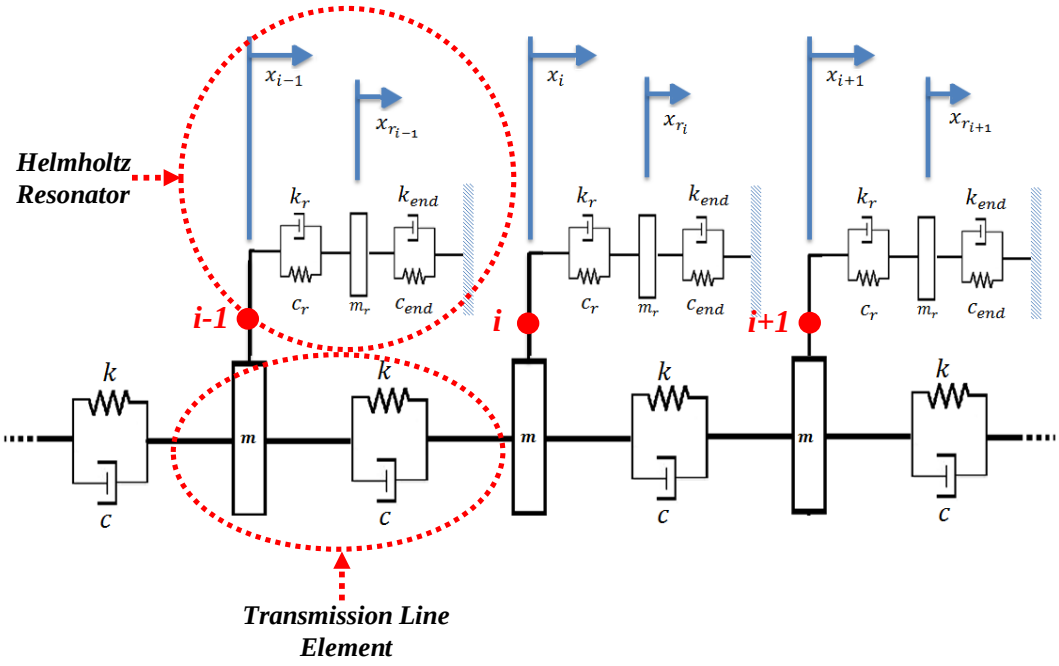

Fig. 2.9: Lumped-Parameter Model of Configuration 1 of the Passive Acoustic Metamaterial.

The dynamics of the lumped-parameter system is developed by writing the equation of motion of a unit cell consisting of a Helmholtz resonator and the transmission line element ***i*** as follows:

a. <u>The equation of motion of the i^{th} transmission element:</u>

Using the Laplace transformation, the equation of motion can be written as:

$$m\,s^2X_i + (k + s\,c)(2\,X_i - X_{i-1} - X_{i+1}) + (k_r + s\,c_r)(X_i - X_r) = 0 \qquad (2.1)$$

where X_i is the Laplace transform of the deflection x_i of the i^{th} transmission mass and X_r is the Laplace transform of the deflection x_r of the r^{th} Helmholtz resonator mass.

b. <u>The equation of motion of the Helmholtz Resonant Mass m_r:</u>

Similarly, in the Laplace domain, the equation of motion is written as:

$$m_r\,s^2X_r + (k_r + s\,c_r)(X_r - X_i) + (k_{end} + s\,c_{end})X_r = 0 \qquad (2.2)$$

Eq. (2.2) can be rewritten as:

$$[m_r\, s^2 + (K_r + s\, C_r) + (K_{end} + s\, C_{end})]\, X_r + (K_r + s\, C_r)(-X_i) = 0 \qquad (2.3)$$

This leads to:

$$X_r = \frac{(k_r + s\, c_r)}{m_r\, s^2 + (k_r + s\, c_r) + (k + s\, c_{end})} X_i \qquad (2.4)$$

Substituting for the resonant displacement X_r into the transmission mass's eq. (2.1), yields:

$$m\, s^2 X_i + (k + s\, c)(2\, X_i - X_{i-1} - X_{i+1}) + \frac{(k_r + s\, c_r)\left(m_r\, s^2 + (k_{end} + s\, c_{end})\right)}{m_r\, s^2 + (k_r + s\, c_r) + (k_{end} + s\, c_{end})} X_i = 0$$

Or

$$\left[m + \frac{(k_r + s\, c_r)\left(m_r\, s^2 + (k_{end} + s\, c_{end})\right)}{s^2\left(m_r\, s^2 + (k_r + s\, c_r) + (k_{end} + s\, c_{end})\right)}\right] s^2 X_i$$

$$+(k + s\, c)(2\, X_i - X_{i-1} - X_{i+1}) = 0 \qquad (2.5)$$

Eq. (2.5) yields the following effective mass, springs, and damper of the equivalent system shown in Fig. 2.3:

Effective lumped Mass:

$$m_e = m + \frac{\left(m_r s^2 + (k_{end} + s\, c_{end})\right)(k_r + s\, c_r)}{s^2\left(m_r s^2 + (k_r + s\, c_r) + (k_{end} + s\, c_{end})\right)} \qquad (2.6)$$

Effective lumped Stiffness:

$$k_e = k \qquad (2.7)$$

and

Effective lumped Damping Coefficient:

$$c_e = c \qquad (2.8)$$

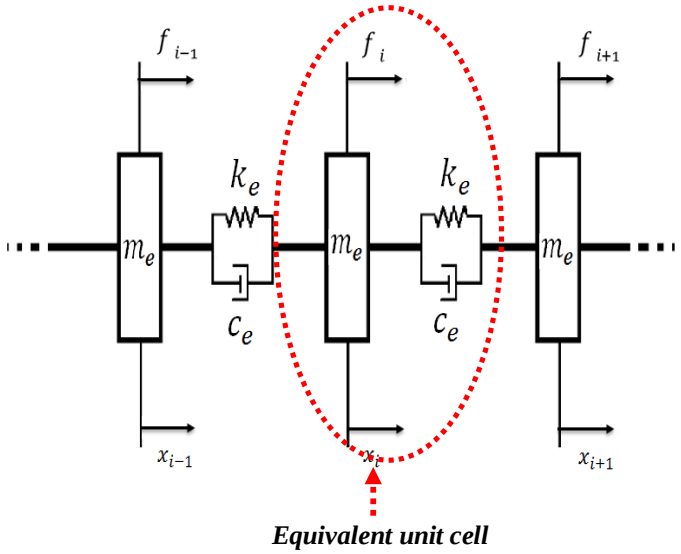

Fig. 2.10: Equivalent unit cell of the passive metamaterial.

As eq. (2.6) of the effective mass is mainly dependent on the frequency, hence, the metamaterial has the potential of achieving negative values. This is not the case for the effective stiffness or damping coefficient as both are positive and frequency-independent.

2.4 A Numerical Example

Consider a passive acoustic metamaterial with the physical parameters listed in Table 2.2. The metamaterial is excited at node 1 at the beginning of the transmission line with a swept sine wave and the response is monitored at node 4 at the end of the transmission line.

Table 2.2 Physical parameters of configuration 1 of the passive acoustic metamaterial, given as in Pope and Daley (2010)

Parameter	m (kg)	k (N/m)	c (Ns/m)	m_r (kg)	k_r (N/m)	c_r (Ns/m)	k_{end} (N/m)	c_{end} (Ns/m)	No. of Cells
Values	0.01	3000	0.1	0.1	1000	0.002	1000	100	4

Fig. 2.11a displays the frequency response of the magnitude of the transfer function $|X_4/X_1|$. Fig. 2.11b shows the sign of the effective mass m_e and stiffness k_e of the metamaterial array. It can be easily seen that below 20 *rad/s*, the metamaterial array exhibits negative effective mass whereas its effective stiffness remains positive throughout the considered frequency band.

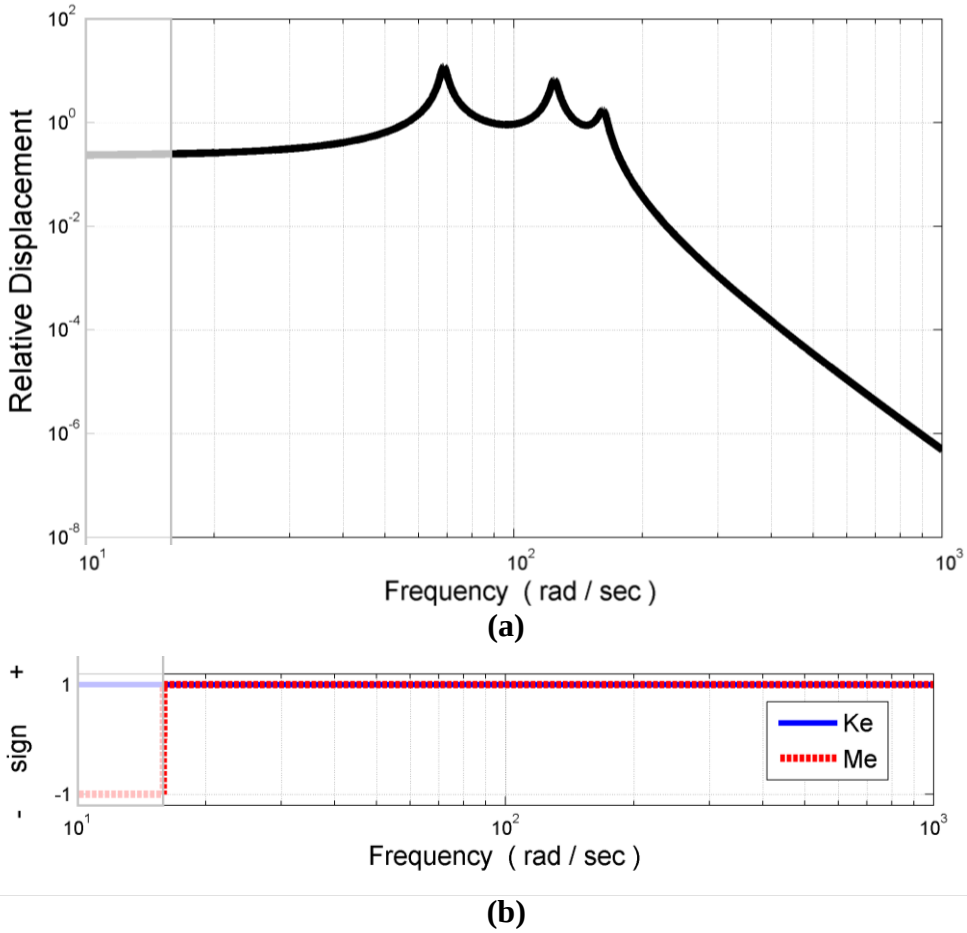

Fig. 2.11: Performance of configuration 1 of the passive metamaterial (a) - the frequency response of $|X_4/X_1|$, (b) sign of the effective mass and stiffness

2.5. The Structure of the Metamaterial – Configuration 2

In this section, the performance characteristics of another configuration of the *PAMM* are presented by also developing a lumped-parameter model of this configuration. In the configuration, the *PAMM* design consists mainly of an array of coupled Helmholtz resonators which interact with the main transmission line as shown in Fig. 2.12.

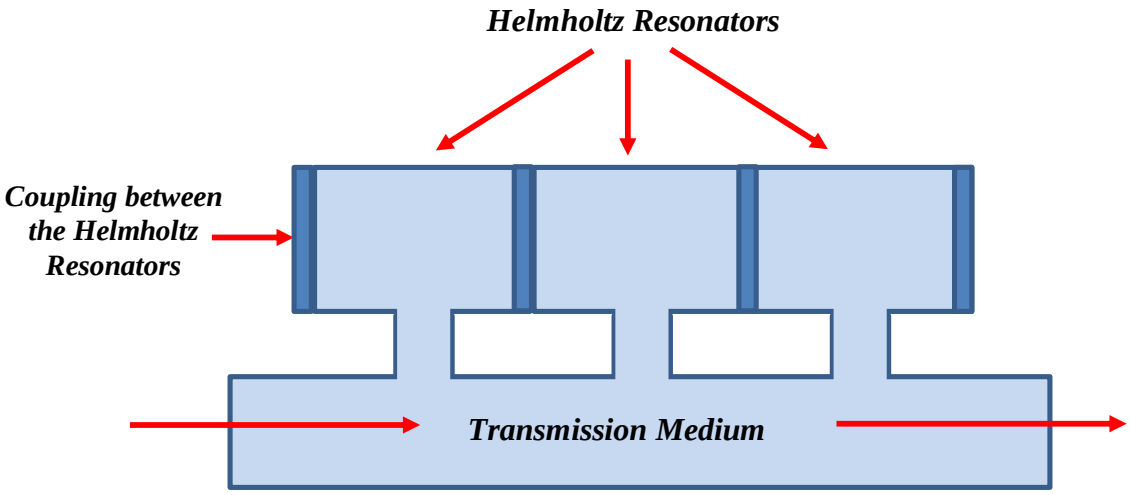

Fig. 2.12: Configuration 2 of the Passive Acoustic Metamaterial

2.6. Modeling of Configuration 2 of the Metamaterial

The *PAMM* shown in Fig. 2.12 which consists of Helmholtz resonators/transmission line is modeled by arrays of coupled mass-spring-damper systems. The side walls of the Helmholtz resonators are made of flexible walls. The resulting lumped-parameter model is displayed in Fig. 2.13. A similar passive acoustic metamaterial was proposed by M Reynolds and S Daley (2014) where solid-walled Helmholtz resonators are linked to each other through viscoelastic connections. Both *PAMM* designs hold the same mechanical representation and dynamics. In figure 2.13, each Helmholtz resonator is represented by a spring k_r, mass m_r, and a damper c_r. The sides of the Helmholtz resonators are coupled and are assumed flexible. These flexible boundaries have stiffness of k_r and damping coefficient c_r, matching the resonator parameters for simplicity. Also, in the figure, the transmission line is divided into discrete number of sections (elements). Each of these elements is modeled by a spring k, mass m, and a damper c.

Each Helmholtz resonator is connected, at its neck, to the transmission masses at one point along the transmission line (*e.g.* points i-1, i, i+1,…) as shown in Fig. 2.13.

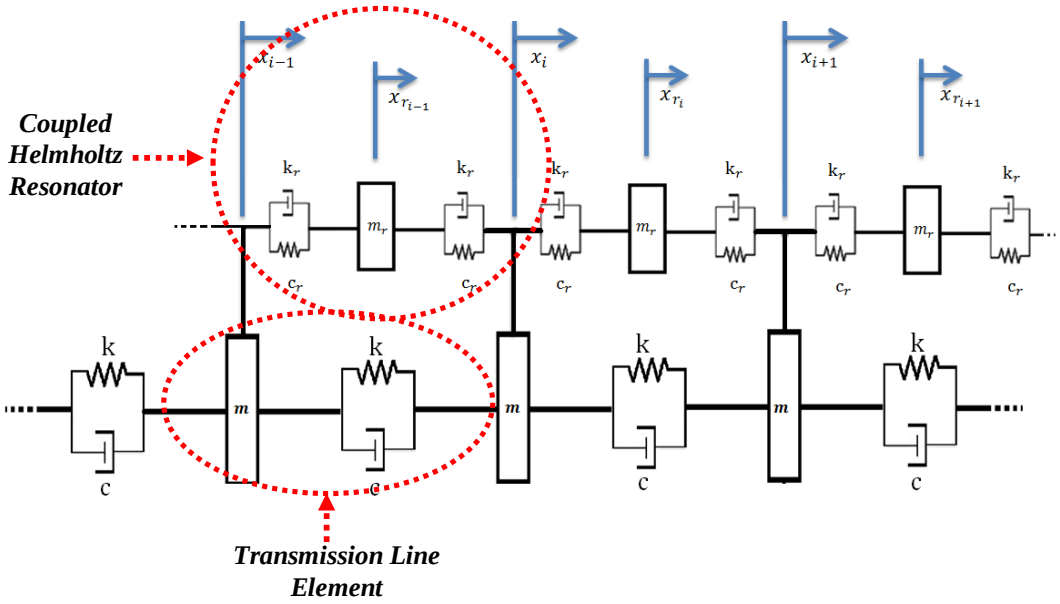

Fig. 2.13: Lumped-Parameter Model of Configuration 2 of the Passive Acoustic Metamaterial.

The dynamics of the lumped-parameter system is developed by writing the equation of motion of a unit cell consisting of a Helmholtz resonator and the transmission line element ***i*** as follows:

a. <u>The equation of motion of the i^{th} transmission element:</u>

Using the Laplace transformation, the equation of motion can be written as:

$$m_i\, s^2\, X_i + (k + s\, c)(2\, X_i - X_{i+1} - X_{i-1}) + (k_r + s c_r)\left(2X_i - X_{r_i} - X_{r_{i-1}}\right) = 0 \qquad (2.9)$$

b. <u>The equation of motion of the i^{th} Helmholtz Resonant Mass m_r:</u>

Similarly, in the Laplace domain, the equation of motion is written as:

$$m_r\, s^2 X_{r_i} + (k_r + s\, c_r)\left(2X_{r_i} - X_i - X_{i+1}\right) = 0 \qquad (2.10)$$

Eq. (2.10) can be rewritten as:

$$X_{r_i} = \frac{(k_r + s\,c_r)}{[m_r\,s^2 + 2(k_r + s\,c_r)]}(X_i + X_{i+1}) \qquad (2.11)$$

c. <u>The equation of motion of the *i*-1th Helmholtz Resonant Mass m_r:</u>

Similarly, in the Laplace domain, the equation of motion is written as:

$$m_r\,s^2 X_{r_{i-1}} + (k_r + s\,c_r)\left(2X_{r_{i-1}} - X_i - X_{i-1}\right) = 0 \qquad (2.12)$$

Eq. (2.12) can be rewritten as:

$$X_{r_{i-1}} = \frac{(k_r + s\,c_r)}{[m_r\,s^2 + 2(k_r + s\,c_r)]}(X_i + X_{i-1}) \qquad (2.13)$$

Substituting for the resonant displacements X_{r_i} and $X_{r_{i-1}}$ into the transmission mass's eq. (2.9), yields:

$$m_i\,s^2\,X_i + (k + s\,c)(2\,X_i - X_{i+1} - X_{i-1}) + (k_r + sc_r)\left(2X_i - \frac{(k_r + s\,c_r)(X_i + X_{i+1})}{[m_r\,s^2 + 2(k_r + s\,c_r)]} - \frac{(k_r + s\,c_r)(X_i + X_{i-1})}{[m_r\,s^2 + 2(k_r + s\,c_r)]}\right) = 0 \qquad (2.14)$$

Hence,

$$m_i\,s^2\,X_i + (k + s\,c)(2\,X_i - X_{i+1} - X_{i-1}) + (k_r + sc_r)\left(2X_i - \frac{2X_i(k_r + s\,c_r)}{m_r\,s^2 + 2(k_r + s\,c_r)} - \frac{(k_r + s\,c_r)(X_{i+1} + X_{i-1})}{m_r\,s^2 + 2(k_r + s\,k_r)}\right) = 0$$

Or

$$\left[m_i + \frac{2m_r(k_r + sc_r)}{m_r\,s^2 + 2(k_r + s\,c_r)}\right] s^2\,X_i + \left[(k + s\,c) + \frac{(k_r + s\,c_r)^2}{m_r\,s^2 + 2(k_r + s\,c_r)}\right](2\,X_i - X_{i+1} - X_{i-1}) = 0 \qquad (2.15)$$

This leads to the following final equation of motion of the equivalent system, which can still be represented by Fig. 2.10;

$$m_e\,s^2\,X_i + (k_e + s\,c_e)(2\,X_i - X_{i+1} - X_{i-1}) = 0 \qquad (2.16)$$

where,

$$m_e = m_i + \frac{2m_r(k_r+sc_r)}{m_r\, s^2+2(k_r+s\, c_r)}$$

and

$$k_e = (k + s\, c) + \frac{(k_r + s\, c_r)^2}{m_r\, s^2 + 2(k_r + s\, c_r)}$$

m_e denotes the system's effective mass and k_e defines the system's effective stiffness.

2.7. A Numerical Example

Consider a passive acoustic metamaterial of configuration 2 with the physical parameters listed in Table 2.2. The metamaterial is excited at node 1 at the beginning of the transmission line with a swept sine wave and the response is monitored at node 4 at the end of the transmission line.

.

Table 2.3 Physical parameters of configuration 2 of the passive acoustic metamaterial, used as in Pope and Daley (2010)

Parameter	m (*kg*)	k (*N/m*)	c (*Ns/m*)	m_r (*kg*)	k_r (*N/m*)	c_r (*Ns/m*)	*No. of Cells*
Values	0.01	3000	0.1	0.1	1000	0.002	10

Fig. 2.14a displays the frequency response of the magnitude of the transfer function $|X_{10}/X_1|$. Fig. 2.14b shows the sign of the effective mass m_e and stiffness k_e of the metamaterial array. It can be easily seen that between 22-75 *rad/s*, the metamaterial array exhibits negative effective mass whereas its effective stiffness has a negative value over a narrower band between 22-25 *rad/s*. Therefore, configuration 2 results in simultaneous double negative properties in the frequency range 22-25 *rad/s*.

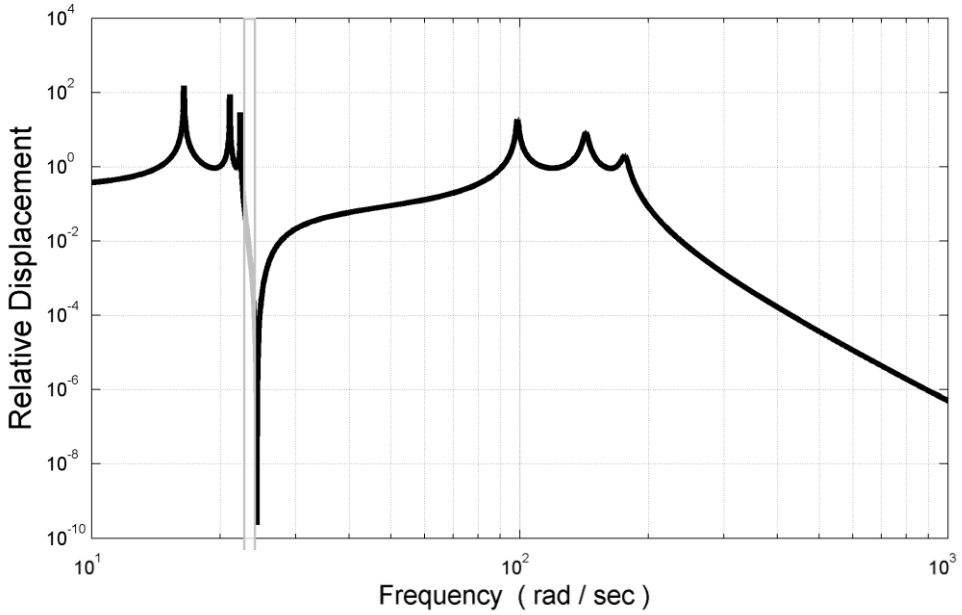

(a)

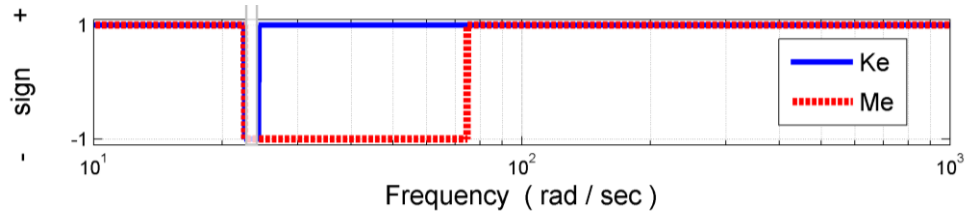

(b)

Fig. 2.14: Performance of configuration 2 of the passive metamaterial (a) - the frequency response of $|X_{10}/X_1|$, (b) sign of the effective mass and stiffness

2.8. Summary

This chapter has presented the effect of the Helmholtz resonator on the transmission line, a wave carrying medium. The influence of the helmholtz resonator on the dynamics of the system has impacted the response of the individual element and the periodic system and the effective parameters as well.

Also, this chapter has presented two configurations of the passive acoustic metamaterial which consist primarily from array of Helmholtz resonators coupled to a main transmission line. In configuration 1, the Helmholtz resonators are uncoupled whereas in configuration 2, the Helmholtz resonators are coupled through flexible boundaries.

Because of the basic design features of configuration 1, it is possible to encounter negative effective mass while the effective stiffness remains positive. In configuration 2, it is seen that both the effective mass and stiffness can simultaneously be negative.

The implications of such distinct design features can best be understood by considering the effective mass - effective stiffness map shown in Fig. 2.15.

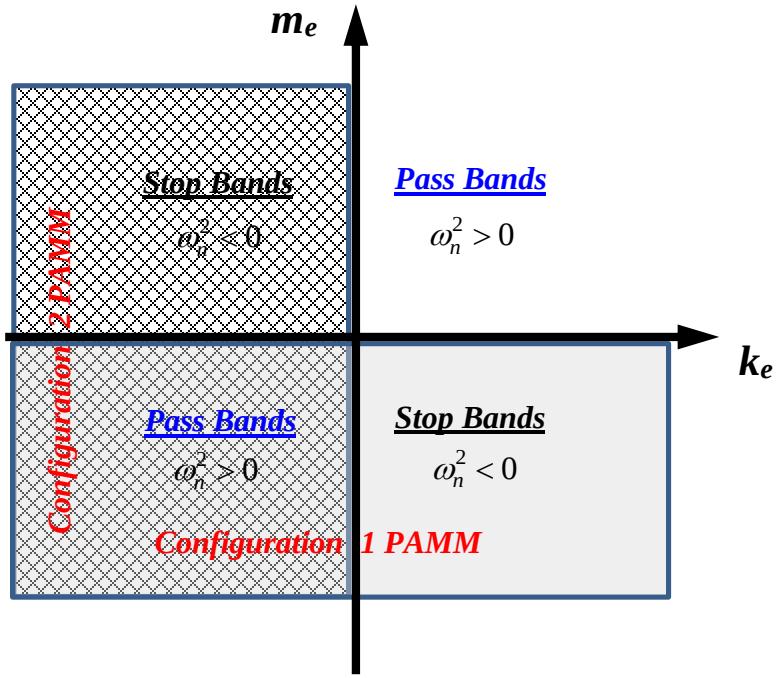

Fig. 2.15: Performance of configurations 1 and 2 of the passive metamaterial

Chapter 3: Active Acoustic Metamaterial

This chapter presents the design features and performance characteristics of a class of active acoustic metamaterials which in their passive mode of operation resemble and replicate exactly the behavior of the passive acoustic metamaterials presented in chapter 2.

Furthermore, the active acoustics metamaterials presented here modify the two passive configurations discussed in chapter 2 by adding active sensing, actuation, and appropriate control law capabilities.

In this chapter, two control laws are considered. These two laws include: simple linear proportional-derivative (*PD*) control law and a nonlinear control law which employs fractional derivative (*FD*) controller in order to improve the performance of the current *AAMM*. The improvements aim at enhancing the *AAMM* ability of operating over frequency bands that are wider than those possible with the simple linear proportional-derivative (*PD*) control laws.

More importantly, in this chapter, the controllers will utilize single actuator to simultaneously both of the density and bulk modulus of the unit metamaterial cell.

The effectiveness of the proposed *FD* controller is demonstrated for metamaterial unit cells that are provided with arrays of piezoelectric sensors and actuators. Comparisons are also presented between the performance of the proposed *FD* controller and that of the simple linear proportional-derivative (*PD*) control laws in order to emphasize the potential and merits of the *FD* control approach.

3.1. Active Control with Linear Control Laws

The design features and performance characteristics of different active acoustic metamaterial configurations are presented in this section when simple linear proportional-derivative (*PD*) control laws are employed. The active acoustic metamaterials throughout this chapter are based on the structures and controllers' designs that were proposed by Pope and Daley (2010).

3.1.1 Structure of the Active Metamaterial – Configuration 1

In the passive configuration 1, presented in chapter 2, the Helmholtz resonator has rigid walls trapping the fluid inside the cavity. This behavior of the trapped fluid has been simulated by a combination of spring and a damper with stiffness k_{end} and damping coefficient c_{end}.

In the modified active configuration 1, as studied by Pope and Daley (2010) and shown in Fig. 3.1, the passive stiffness k_{end} and damper c_{end} are replaced with active components k_c and c_c that functionally behave in the same manner. The stiffness of the active spring k_c, can be visualized as the gain of a proportional control action whereas the damping coefficient of the active damper c_c, can be considered as the gain of a derivative control action. Hence, the combination of the active components k_c and c_c is, in effect, equivalent to a Proportional-Derivative (*PD*) controller. In Fig. 3.1, such a combined control action is represented by the control force f_{c_i} which acts on the i^{th} Helmholtz resonator. This control force can be given by $f_{c_i} = -(k_c + s\,c_c)X_r$ where k_c and c_c are the active *P* and *D* components.

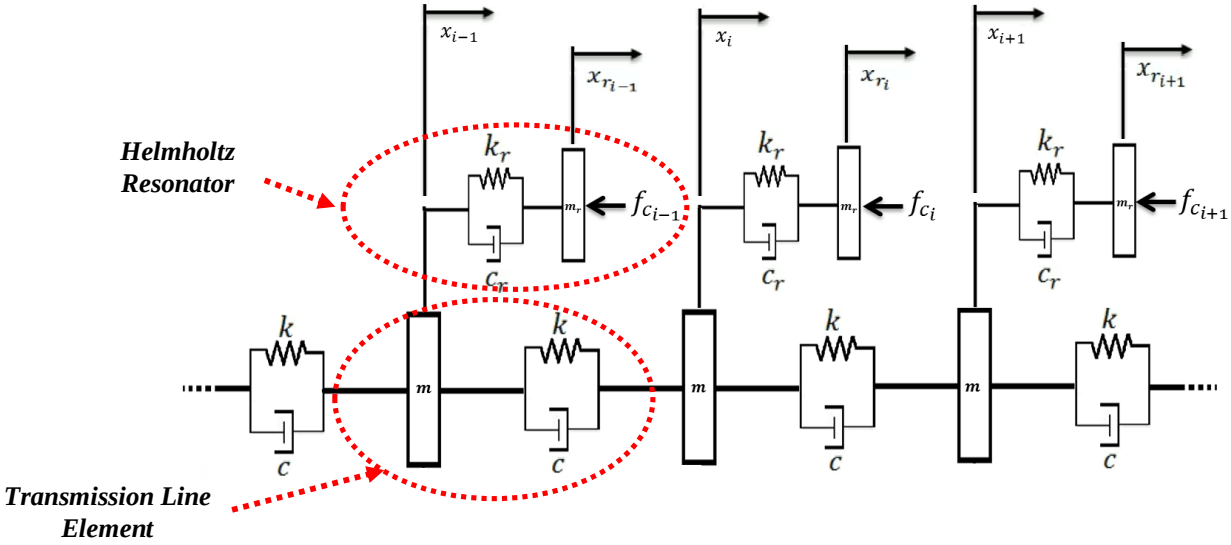

Fig. 3.1: Active control configuration 1 of the acoustic metamaterial

3.1.2 Modeling of Configuration 1 of the Active Metamaterial

The dynamics of the lumped-parameter system is developed by writing the equation of motion of a unit cell consisting of a Helmholtz resonator and the transmission line element ***i*** as follows:

a. <u>The equation of motion of the i^{th} transmission element:</u>

Using the Laplace transformation, the equation of motion can be written as:

$$m\,s^2X_i + (k + s\,c)(2\,X_i - X_{i-1} - X_{i+1}) + (k_r + s\,c_r)(X_i - X_r) = 0 \qquad (3.1)$$

b. <u>The equation of motion of the Helmholtz Resonant Mass m_r:</u>

Similarly, in the Laplace domain, the equation of motion is written as:

$$m_r\,s^2X_r + (k_r + s\,c_r)(X_r - X_i) = f_{c_i}$$

As $$f_{c_i} = -(k_c + s\,c_c)X_r \qquad (3.2)$$

Then, $$m_r\,s^2X_r + (k_r + s\,c_r)(X_r - X_i) + (k_c + s\,c_c)X_r = 0 \qquad (3.3)$$

Note that in eq. (3.3), the control action f_{c_i} is set to be proportional to only the displacement X_r of the resonant mass m_r.

Eq. (3.3) can be rewritten as:

$$[m_r\,s^2 + (k_r + s\,c_r) + (k_c + s\,c_c)]\,X_r + (k_r + s\,c_r)(-X_i) = 0 \qquad (3.4)$$

This leads to:

$$X_r = \frac{(k_r + s\,c_r)}{m_r\,s^2 + (k_r + s\,c_r) + (k_c + s\,c_c)}X_i \qquad (3.5)$$

Substituting for X_r into the transmission mass's eq. (3.1):

$$m\,s^2X_i + (k + s\,c)(2\,X_i - X_{i-1} - X_{i+1}) + (k_r + s\,c_r)\left(X_i - \frac{(k_r + s\,c_r)}{m_r\,s^2 + (k_r + s\,c_r) + (k_c + s\,c_c)}X_i\right) = 0$$

or

$$\left[m + \frac{(k_r + s\,c_r)\big(m_r\,s^2 + (k_c + s\,c_c)\big)}{s^2\big(m_r\,s^2 + (k_r + s\,c_r) + (k_c + s\,c_c)\big)}\right] s^2X_i + (k + s\,c)(2\,X_i - X_{i-1} - X_{i+1}) = 0 \qquad (3.6)$$

Eq. (3.6) yields the following effective mass, spring, and damper of the equivalent system shown in Fig. 3.1:

Effective lumped Mass:

$$m_e = m + \frac{\left(m_r s^2 + (k_c + s\, c_c)\right)(k_r + s\, c_r)}{s^2\left(m_r s^2 + (k_r + s\, c_r) + (k_c + s\, c_c)\right)} \tag{3.7}$$

Effective lumped Stiffness:

$$k_e = k \tag{3.8}$$

and

Effective lumped damping coefficient:

$$c_e = c \tag{3.9}$$

As eq. (3.7) of the effective mass is mainly dependent on the frequency, hence, the metamaterial has the potential of achieving a negative parameter. This is not the case for the effective stiffness or damping coefficient as both are positive and frequency-independent.

3.1.3. Numerical Examples

Consider the active acoustic metamaterial of configuration 1 with the physical parameters listed in Table 3.1. The metamaterial is excited at node 1 at the beginning of the transmission line with a swept sine wave and the response is monitored at node 4 at the end of the transmission line.

Table 3.1 Physical parameters of configuration 1 of the active acoustic metamaterial

Parameter	m (kg)	k (N/m)	c (Ns/m)	m_r (kg)	k_r (N/m)	c_r (Ns/m)	k_c (N/m)	c_c (Ns/m)	No. of Cells
Values	0.01	3000	0.1	0.1	1000	0.002	1000	0.1	4

Fig. 3.2a displays the frequency response of the magnitude of the transfer function $|X_4/X_1|$. Fig. 3.2b shows the sign of the effective mass m_e and stiffness k_e of the metamaterial array. It can be easily seen that between 0-50 *rad/s*, the metamaterial array exhibits negative effective mass whereas its effective stiffness remains positive throughout the considered frequency range.

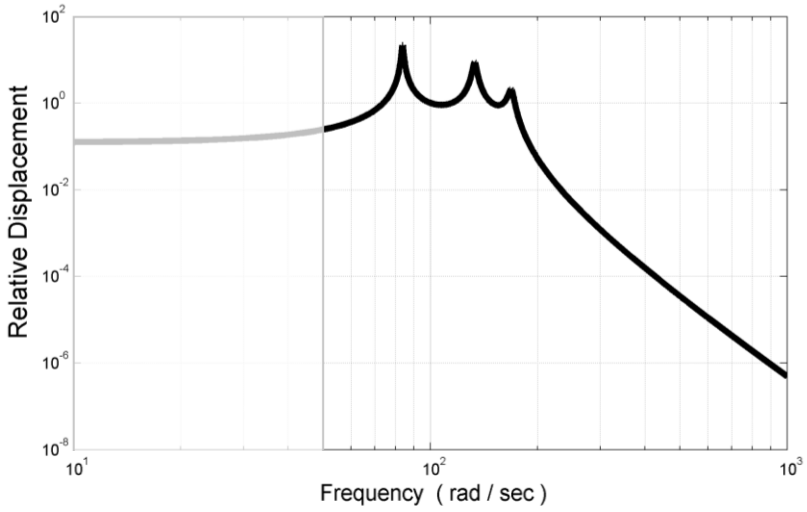

(a)

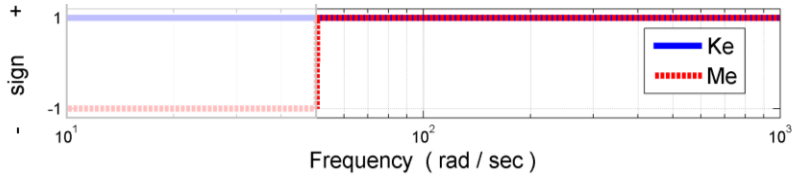

(b)

Fig. 3.2: Performance of configuration 1 of the active metamaterial (a) - the frequency response of $|X_4/X_1|$, (b) sign of the effective mass and stiffness

3.1.4. Preferred Design of Configuration 1 of the Active Metamaterial

The active acoustic metamaterial design which was introduced by Pope and Daley (2010) and is shown schematically in Fig. 3.1 can be physically realized using an array of piezoelectric sensors and actuators to generate the control actions f_{c_i}. Fig.3.3 displays a possible placement strategy of the piezoelectric sensors and actuators in the preferred design of configuration 1 of the active metamaterial. In this

arrangement, the end cap of each Helmholtz resonator is provided with a *PZT* piezoelectric bimorph for generating a *PD* control action f_{c_i} which is proportional to the deflection x_{r_i}. The displacement x_{r_i} is monitored by an array of *PVDF* sensors which are labeled as the *H*-sensors in Fig. 3.3. These sensors are capable of measuring the pressure gradient inside the Helmholtz which is linearly proportional to the velocity $\dot{x}_{r_i}$ according to Euler's equations of fluids.

In a similar manner, the displacements x_i*'s* of the transmission line elements are monitored using another set of *PVDF* sensors which are labeled as the *T*-sensors in Fig. 3.3.

With these sensing capabilities, the local control actions f_{c_i} can be generated either to be proportional to the Helmholtz displacement x_{r_i} only or to be proportional to any linear combination of the Helmholtz displacement x_{r_i} and the displacements of the neighboring transmission line elements x_i's.

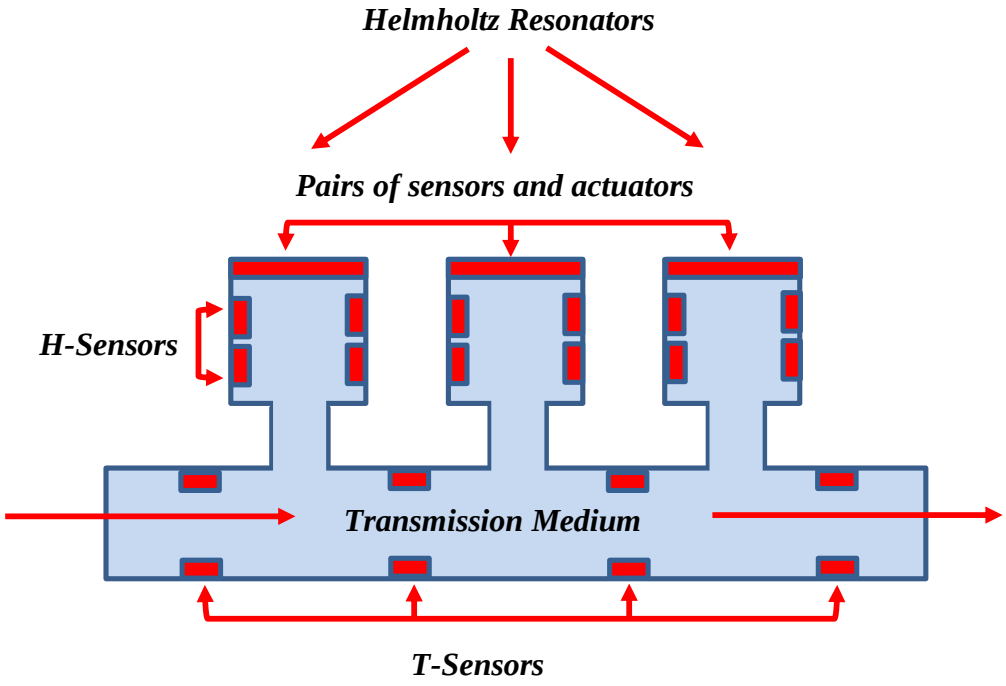

Fig. 3.3: Schematic drawing of the active acoustic metamaterial.

Note that in the case of *AAMM* of configuration 1 the control actions f_{c_i}, given by eq. (3.2), is generated to be proportional to the Helmholtz displacement x_{r_i} only. As will be discussed later, configuration 2 of the *AAMM* requires the use of linear combination of the Helmholtz displacement x_{r_i} and the displacements of the neighboring transmission line elements x_i's. With such linear combination, it will be shown that the control performance can be enhanced considerably and single actuator can be used to simultaneously control both the density and bulk modulus of the *AAMM* unit cell.

3.1.5. Structure of the Active Metamaterial – Configuration 2

In this configuration, the control action as proposed by Pope and Daley (2010) is generated to be proportional to a linear combination of the Helmholtz displacement x_{r_i} and the displacements of the neighboring transmission line elements x_i's such as:

$$f_{c_i} = (k_c + s\, c_c)\left(X_{i-1} + X_{i+1} - 2X_{r_i}\right) \tag{3.10}$$

where k_c and c_c are the proportional and derivative control gains.

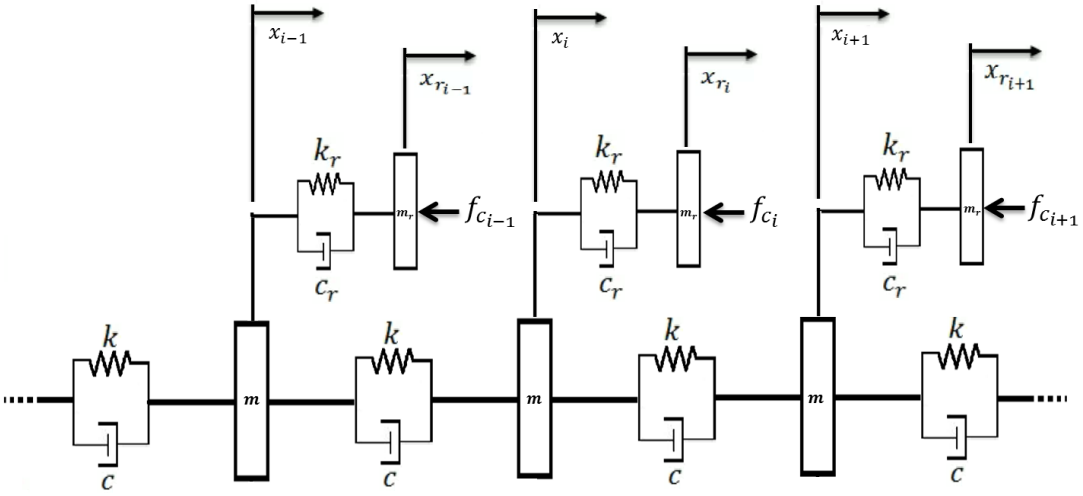

Fig. 3.4: Schematics drawing of configuration 2 of the active metamaterial.

3.1.6. Modeling of Configuration 2 of the Active Metamaterial

The dynamics of the lumped-parameter system is developed by writing the equation of motion of a unit cell consisting of a Helmholtz resonator and the transmission line element ***i*** as follows:

a. <u>The equation of motion of the i^{th} transmission element:</u>

Using the Laplace transformation, the equation of motion can be written as:

$$ms^2X_i + (k + s\,c)(X_i - X_{i+1}) + (k + sc)(X_i - X_{i-1}) + (k_r + s\,c_r)\left(X_i - X_{r_i}\right) = F_i \quad (3.11)$$

b. <u>The equation of motion of the Helmholtz resonant mass m_r:</u>

In the Laplace domain:

$$m_r s^2 X_{r_i} + (k_r + s\,c_r)\left(X_{r_i} - X_i\right) = f_{ci} \quad (3.12)$$

where:

c the acoustic equivalent mechanical damper of the tranmission medium.
c_r the acoustic equivalent mechanical damper of the Helmholtz resonator.
c_c the desired acoustic equivalenet mechanical damping

F_i the external applied force
f_{Ci} the control force.
k the acoustic equivalent mecanical stiffness modulus of the transmission medium
k_c the desired acoustic stiffness modulus gain generated by the controller
k_r the acoustic equivalent mecanical stiffness modulus of the Helmholtz resonantor
s Laplace complex number
X_i the displacement of the transmission (medium)mass.
X_r the displacement of the first resonant mass.

The equivalent lumped-parameter system:

Combining eqs. (3.10), and (3.12) gives:

$$m_r s^2 X_{r_i} + (k_r + s\,c_r)\left(X_{r_i} - X_i\right) = (k_c + s\,c_c)(X_{i-1} + X_{i+1} - 2X_{r_i})$$

This yields

$$X_{r_i} = \frac{(k_r+s\,c_r)X_i+(k_c+s\,c_c)}{\left(m_r s^2+(k_r+s\,c_r)+2(k_c+s\,c_c)\right)}(X_{i-1} + X_{i+1}) \qquad (3.13)$$

Now, substituting X_{r_i} into eq. (3.11) of the transmission medium yields:

$$ms^2 X_i + (k + s\,c)(X_i - X_{i+1}) + (k + s\,c)(X_i - X_{i-1})$$

$$+(k_r + s\,c_r)\left(X_i - \frac{(k_r + s\,c_r)X_i + (k_c + s\,c_c)(X_{i-1} + X_{i+1})}{\left(m_r s^2 + (k_r + s\,c_r) + 2(k_c + s\,c_c)\right)}\right) = F_i$$

or

$$m\,s^2 X_i + \frac{m_r(k_r + s\,c_r)}{\left(m_r s^2 + (k_r + s\,c_r) + 2(k_c + s\,c_c)\right)} s^2 X_i$$

$$-(k + s\,c)(X_{i-1} + X_{i+1} - 2X_i)$$

$$-\frac{(K_r+s\,C_r)(K_c+s\,C_c)}{\left(m_r s^2+(K_r+s\,C_r)+2(K_c+s\,C_c)\right)}(X_{i-1} + X_{i+1} - 2X_i) = F_i \qquad (3.14)$$

Eq. (3.14) results in the following equation of motion of the equivalent lumped-parameter system of configuration 2 of the *AAMM:*

$$m_e\,s^2 X_i - (k_e + s\,c_e)\,(X_{i-1} + X_{i+1} - 2X_i) = F_i \qquad (3.15)$$

Where,

The effective mass:

$$m_e = m + \frac{m_r(k_r + s\,c_r)}{m_r s^2 + (k_r + s\,c_r) + 2(k_c + s\,c_c)} \tag{3.16}$$

and,

The effective stiffness:

$$k_e = k + \boldsymbol{Real}\left[s\,c + \frac{(k_r + s\,c_r)(k_c + s\,c_c)}{\left(m_r s^2 + (k_r + s\,c_r) + 2(k_c + s\,c_c)\right)}\right] \tag{3.17}$$

The equivalent system is shown schematically in Fig. 3.5.

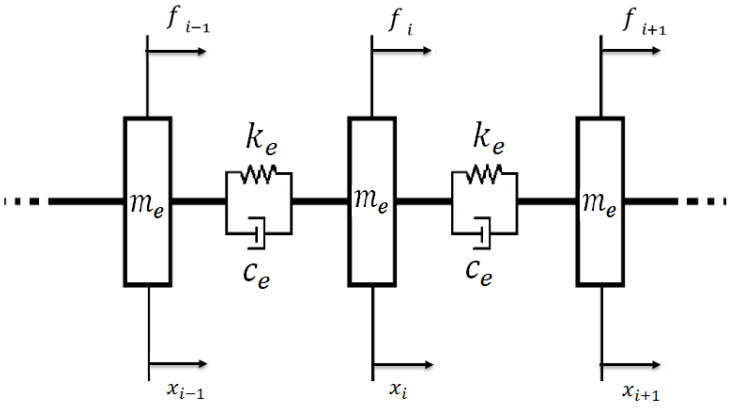

Fig.3.5: Equivalent lumped-parameter system of configuration 2 of the active acoustic metamaterials

3.1.7. A Numerical Example

Consider the active acoustic metamaterial of configuration 2 with the physical parameters listed in Table 3.2. The metamaterial is excited at node 1 at the beginning of the transmission line with a swept sine wave and the response is monitored at node 4 at the end of the transmission line.

Table 3.2 Physical parameters of configuration 2 of the active acoustic metamaterial, used as in Pope and Daley (2010)

Parameter	m (kg)	k (N/m)	c (Ns/m)	m_r (kg)	k_r (N/m)	c_r (Ns/m)	k_c (N/m)	c_c (Ns/m)	*No. of Cells*
Values	0.01	3000	0.1	0.1	1000	0.002	2100	0.1	4

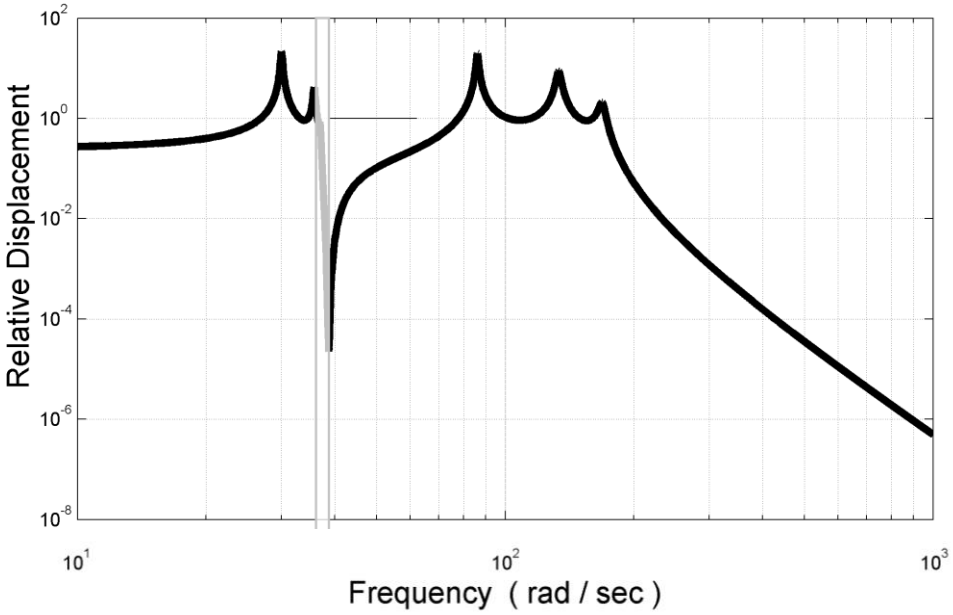

(a)

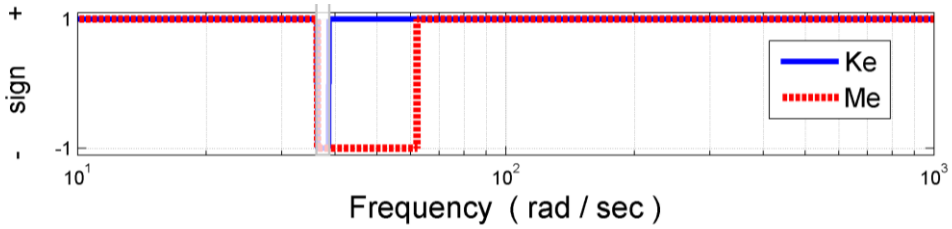

(b)

Fig. 3.6: Performance of configuration 1 of the active metamaterial (a) - the frequency response of $|X_4/X_1|$, (b) sign of the effective mass and stiffness

Fig. 3.6a displays the frequency response of the magnitude of the transfer function $|X_4/X_1|$ as plotted in Pope and Daley (2010). Fig. 3.6b shows the sign of the effective mass m_e and stiffness k_e of the metamaterial array. It can be easily seen that between 35-52 *rad/s*, the metamaterial array exhibits negative effective mass whereas its effective stiffness has a negative value over a narrower band between 35-40 *rad/s*. Therefore, configuration 2 results in simultaneous double negative properties in the frequency range 35-40 *rad/s*.

The figure indicates an improvement of the width of the double negative zone to be 5 *rad/s* as compared to that obtained from configuration 1 which resulted only in 3 *rad/s* zone. However, this resulting frequency bandwidth of double negative properties is still very narrow for practical applications.

3.2. Active Control with Fractional Derivative Controller:

3.2.1. Fractional Order Systems

The fractional order systems have various advantages depending on the objective for which the system is designed for; whether for stability or reducing the steady state error of the system or both (Monje *et al*., 2010).

In fractional order system control, it's commonly known that one of the main advantages of the Fractional Derivative (*FD*) type controllers is achieving a relative stability to the controlled system. On the other hand, the Fractional Integral (*FI*) order controllers are of great importance when eliminating the steady state error of the system. Fractional derivative controllers have more to offer in the field of metamaterials and in particular on improving the operating bandwidth of metamaterials. In this section, the effectiveness and the merits of developing active acoustic metamaterials with fractional derivative controllers are investigated in comparison to active acoustic metamaterials with simple linear Proportional and Derivative controllers (*PD*).

The parameters of *FD* controller are optimized to achieve desirable frequency response characteristics.

3.2.2. Modeling of Configuration 2 of the Active Metamaterial with Fractional Derivative Controller

One of the main objectives of using a fractional Derivative type controller is because of its flexibility on designing the controller and better system response (Monje *et al*., 2010). A simple structure of the *FD* controller is proposed such that the control action f_{c_i} is generated using the following control law:

$$f_{c_i} = (c_c s^{\alpha} + k_c)(X_{i-1} + X_{i+1} - 2X_{r_i}) \tag{3.18}$$

In eq. (3.18), the *FD* controller is a non-linear proportional-derivative with the derivative control action is raised to power α is a positive fraction where $0 < \alpha < 1$. The exponent is adding an extra active parameter to the previously introduced control active by Pope and Daley (2010) to help improve the response of the system.

The dynamics of the lumped-parameter system is developed by writing the equation of motion of a unit cell consisting of a Helmholtz resonator and the transmission line element ***i*** as follows:

a. The equation of motion of the i^{th} transmission element:

Using the Laplace transformation, the equation of motion can be written as:

$$ms^2X_i + (k + cs)(X_i - X_{i+1}) + (k + cs)(X_i - X_{i-1}) + (k_r + c_r s)(X_i - X_{ri}) = F_i \quad (3.19)$$

b. The equation of motion of the Helmholtz resonant mass m_r:

In the Laplace domain:

$$m_r s^2 X_{ri} + (k_r + c_r s)(X_{ri} - X_i) = f_c \quad (3.20)$$

where

- c the acoustic equivalent mechanical damper of the tranmission medium.
- c_r the acoustic equivalent mechanical damper of the Helmholtz resonator.
- c_c the desired acoustic equivalenet mechanical damping
- F_i the external applied force
- f_{Ci} the control force.
- k the acoustic equivalent mecanical stiffness modulus of the transmission medium
- k_c the desired acoustic stiffness modulus gain generated by the controller
- k_r the acoustic equivalent mecanical stiffness modulus of the Helmholtz resonantor
- s Laplace complex number
- X_i the displacement of the transmission (medium)mass.
- X_r the displacement of the first resonant mass.

The equivalent lumped-parameter system:

Combining eqs. (3.18), and (3.20) gives:

$$m_r s^2 X_{ri} + (k_r + c_r s)(X_{ri} - X_i) = (k_c + c_c s^{\alpha})(X_{i-1} + X_{i+1} - 2X_{ri})$$

Or

$$\left(m_r s^2 + (k_r + c_r s) + 2(k_c + c_c s^{\alpha})\right) X_{ri}$$

$$= (k_r + c_r s)X_i + (k_c + c_c s^{\alpha})(X_{i-1} + X_{i+1}) \quad (3.21)$$

This leads to:

$$X_{ri} = \frac{(k_r+c_r s)X_i+(k_c+c_c s^{\alpha})}{(m_r s^2+(k_r+c_r s)+2(k_c+c_c s^{\alpha}))}(X_{i-1} + X_{i+1}) \quad (3.22)$$

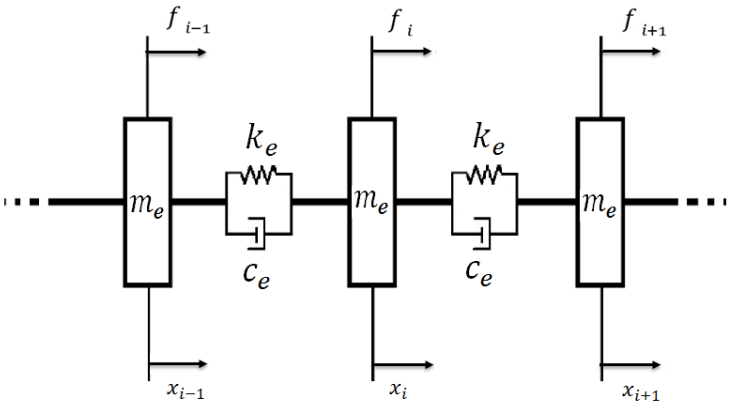

Fig. 3.7: Equivalent Lumped-parameter model of Configuration 2 Active Acoustic Metamaterial with Fractional Derivative Controller

Eliminating X_{ri} between eqs. (3.19) and (3.22), yields:

$$ms^2X_i + (k + cs)(X_i - X_{i+1}) + (k + cs)(X_i - X_{i-1})$$

$$+(k_r + c_r s)\left(X_i - \frac{(k_r + c_r s)X_i + (k_c + c_c s^{\alpha})(X_{i-1} + X_{i+1})}{(m_r s^2 + (k_r + c_r s) + 2(k_c + c_c s^{\alpha}))}\right) = F_i$$

or

$$m\, s^2X_i + \frac{m_r(k_r + c_r s)}{(m_r s^2 + (k_r + c_r s) + 2(k_c + c_c s^{\alpha}))}s^2X_i$$

$$-(k + cs)(X_{i-1} + X_{i+1} - 2X_i)$$

$$-\frac{(k_r+c_r s)(k_c+c_c s^{\alpha})}{(m_r s^2+(k_r+c_r s)+2(k_c+c_c s^{\alpha}))}(X_{i-1} + X_{i+1}-2X_i) = F_i \quad (3.23)$$

or

$$m_e\, s^2 X_i - (k_e + s\, c_e)\,(X_{i-1} + X_{i+1} - 2X_i) = F_i \tag{3.24}$$

where:

The Effective Mass:

$$m_e = m + \frac{m_r(k_r + c_r s)}{m_r s^2 + (k_r + c_r s) + 2(k_c + c_c s^{\alpha})} \tag{3.25}$$

$$m_e = m_{e_{REAL}} + i\, m_{e_{IMAG}}$$

where:

$$m_{e_{REAL}} = m + \boldsymbol{real}\big(G_M(s,\alpha)\big) \tag{3.26}$$

$$m_{e_{IMAG}} = \boldsymbol{imag}\big(G_M(s,\alpha)\big) \tag{3.27}$$

$$G_M(s,\alpha) = \frac{m_r(k_r + c_r s)}{m_r s^2 + (k_r + c_r s) + 2(k_c + c_c s^{\alpha})} \tag{3.28}$$

The Effective Stiffness:

$$k_e = k + \boldsymbol{real}\big(G(s,\alpha)\big) \tag{3.29}$$

where:

$$G_k(s,\alpha) = \frac{(k_r + c_r s)(k_c + c_c s^{\alpha})}{m_r s^2 + (k_r + c_r s) + 2(k_c + c_c s^{\alpha})} \tag{3.30}$$

with $s = i\,\omega$.

The Effective Damping Coeeficient:

$$c_e = c + \frac{\boldsymbol{imag}\big(G_k(i\omega,\alpha)\big)}{\omega} \tag{3.31}$$

Substituting eqs. (3.25) through (3.31) into eq. (3.24) with *s* replaced by *iω*, gives:

$$-\left(m_{e_{REAL}} + i\, m_{e_{IMAG}}\right) \omega^2 X_i - \left(k_e + i\omega\, c_e\right)\left(X_{i-1} + X_{i+1} - 2X_i\right) = F_i \quad (3.32)$$

$$-\left(m_{e_{REAL}} + i\, m_{e_{IMAG}}\right) \omega^2 X_i + 2\left(k_e + i\,\omega\, c_e\right) X_i =$$

$$\underbrace{F_i + \left(k_e + i\,\omega\, c_e\right)\left(X_{i-1} + X_{i+1}\right)}_{F_T} \quad (3.33)$$

i.e.

$$-m_{e_{REAL}}\, \omega^2 X_i + i\omega\left(\, 2\, c_e - \,\omega\, m_{e_{IMAG}}\right) X_i \;+\; 2k_e\, X_i = F_T \quad (3.34)$$

Hence, eq. (3.34) reduces to:

$$-\, m_{e_m} w^2 X_i + iw\, c_{e_m} X_i + k_{e_m} X_i = F_T \quad (3.35)$$

where:

$$m_{e_m} = m_{e_{REAL}}$$

$$c_{e_m} = \, 2\, c_e - \,\omega\, M_{e_{IMAG}}$$

$$k_{e_m} = 2\, k_e$$

with,

$$\mathrm{m_{e_m}} = \text{The effective mass of the modified lumped} - \text{system}$$

$$k_{e_m} = \text{The effective stiffness of the modified lumped} - \text{system}$$

$$c_{e_m} = \text{The effective damper of the modified lumped} - \text{system}$$

3.2.3. A Numerical Example

Consider the active acoustic metamaterial of configuration 2 with fractional derivative controller. The system has the physical parameters listed in Table 3.3. The

metamaterial is excited at node 1 at the beginning of the transmission line with a swept sine wave and the response is monitored at node 10 at the end of the transmission line.

Table 3.3 Physical parameters of configuration 3 of the active acoustic metamaterial with *PD* and *FD* controllers

Parameter	m (kg)	k (N/m)	c (Ns/m)	m_r (kg)	k_r (N/m)	c_r (Ns/m)	k_c (N/m)	c_c (Ns/m)	*No. of Cells*
Values	**0.01**	**2,000**	**0.1**	**1**	**1,500**	**0.002**	**150,000**	**40**	**10**

Fig. 3.8a shows the magnitude of the relative displacement across ten cascaded transmission elements $|X_{10}/X_1|$. Fig. 3.8b shows the sign of the effective mass m_e and stiffness k_e of the metamaterial array. It can be easily seen that between 93-95.2 *rad/s*, the metamaterial array exhibits negative effective mass whereas its effective stiffness has a negative value over a wider band between 93-105 *rad/s*. Therefore, configuration 2 with linear *PD* controller results in simultaneous double negative properties in the frequency range 93-95.2 *rad/s*.

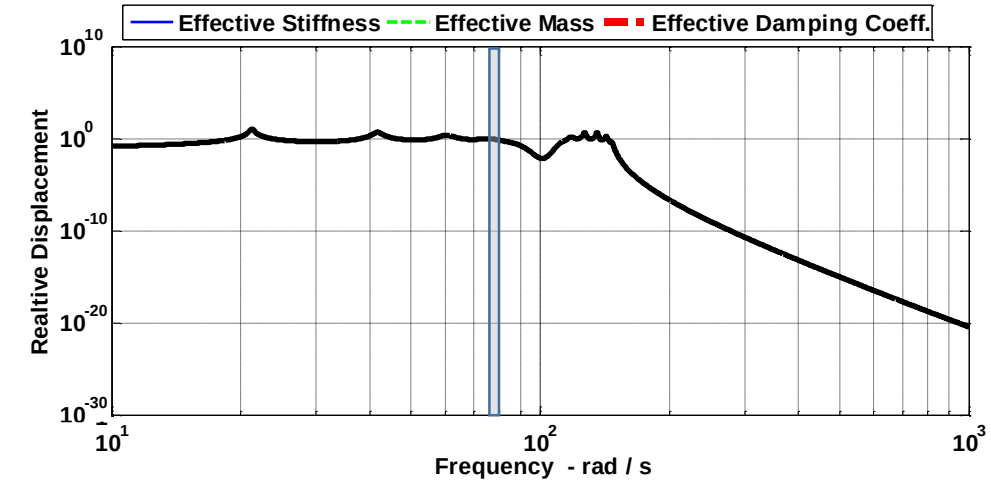

(a)

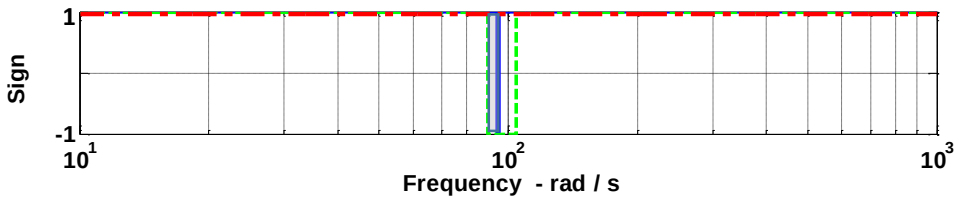

(b)

Fig. 3.8 : The Active Acoustic Metamaterial model with linear *PD* Controller.

Fig. 3.9, shows a close-up look on the metamaterial behavior for the frequency ranging from (80-115 rad/sec) to show more efficiently the narrowness of that double negative overlap frequency zone.

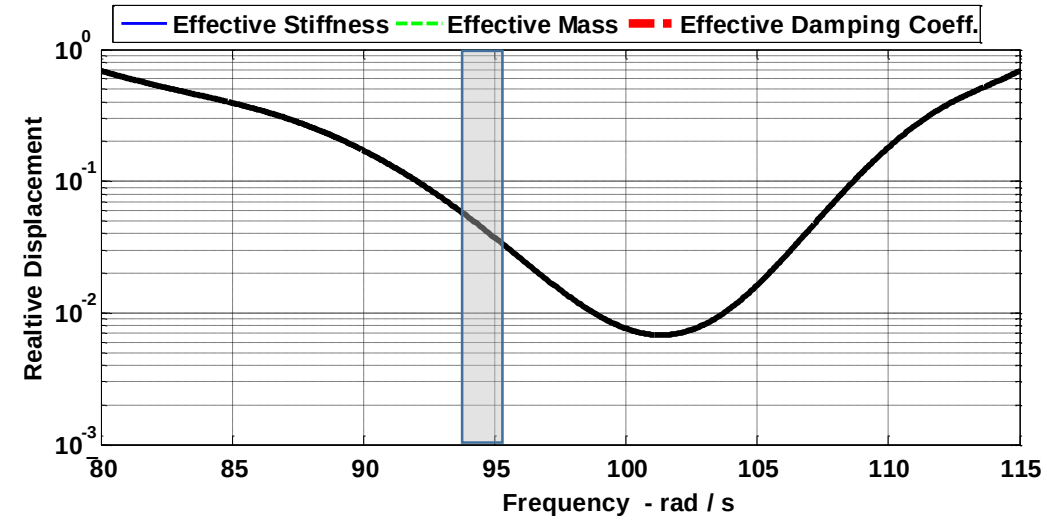

(a)

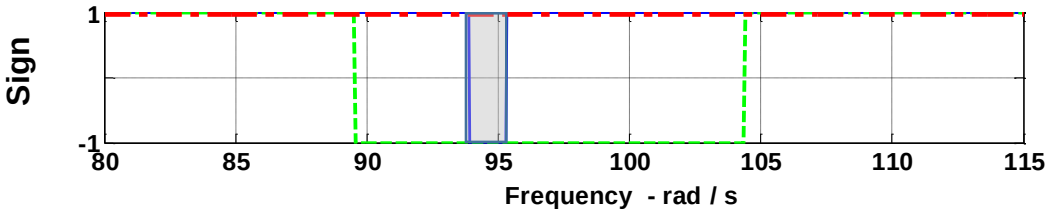

(b)

Fig. 3.9 : A close-up of the behavior of the Active Acoustic Metamaterial model with linear *PD* Controller in the frequency zone 80-115 rad/s.

Fig. 3.10 illustrates the performance of the active acoustic metamaterial with a *FD* controller when $\alpha = 0.1$. The figure shows that the *FD* controller has increased considerably the frequency range of double negative properties. Specifically, the *FD* controller has magnified that overlap frequency range by a factor of seven as compared to that obtained by using the *PD* controller.

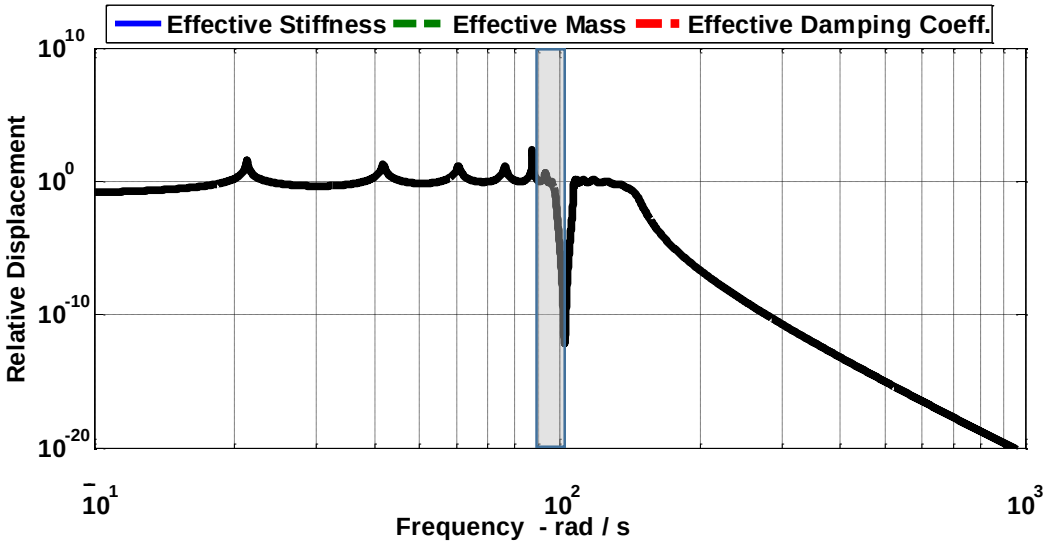

(a)

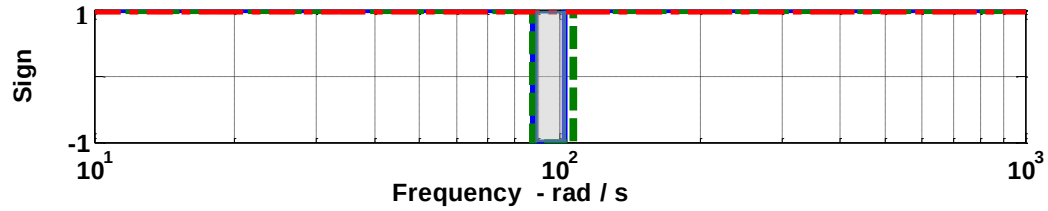

(b)

Fig. 3.10 : The Active Acoustic Metamaterial model with nonlinear *FD* controller $\alpha = 0.1$.

Such a magnification can be easily seen by considering the close-up view displayed in Fig. 3.11 which indicates that the overlap zone extends between 87-102 rad/s as compared to 93-95.2 rad/s for the case of *PD* controller.

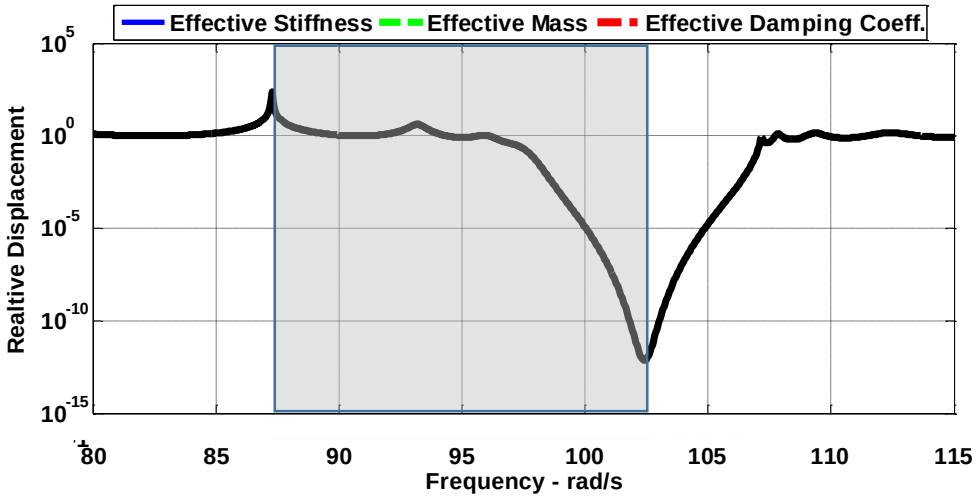

(a)

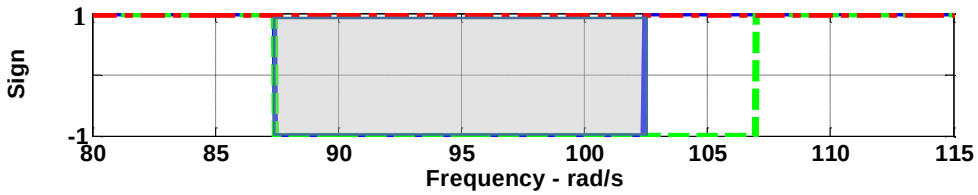

(b)

Fig. 3.11 : A close-up of the behavior of the Active Acoustic Metamaterial model with nonlinear *FD* Controller when α=0.1 in the frequency zone 80-115 rad/s.

3.2.4. Stability Analysis of the Active Acoustic Metamaterial:

In the previous section, the effect of controller design on the width of the frequency zone of double negative parameters has been investigated for linear *PD* and nonlinear *FD* controllers.

In this section, the system stability is studied by computing the sign of the effective damping coefficients for the linear *PD* and nonlinear *FD* controllers for the considered numerical examples.

Fig. 3.12a displays plots of signs of the effective mass, stiffness, and damping coefficient for the nonlinear *FD* controller with α=0.1. Fig. 3.12b shows the corresponding characteristics for the case of the linear *PD* controller.

It is evident in both cases that the sign of the damping coefficient remains positive throughout the considered frequency range. More importantly, the sign of the damping coefficient remains positive over the double negative properties zones of

operation. Hence, both controllers can provide in a stable manner zones with double negative properties.

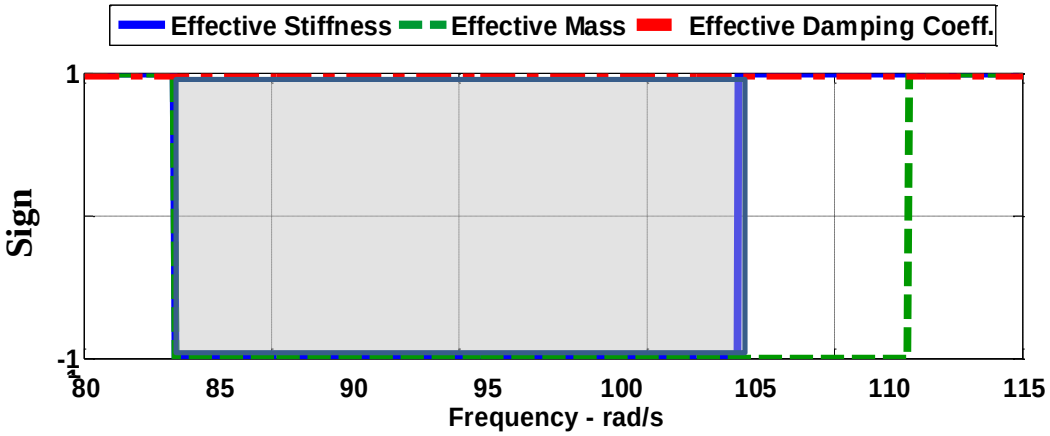

(a)

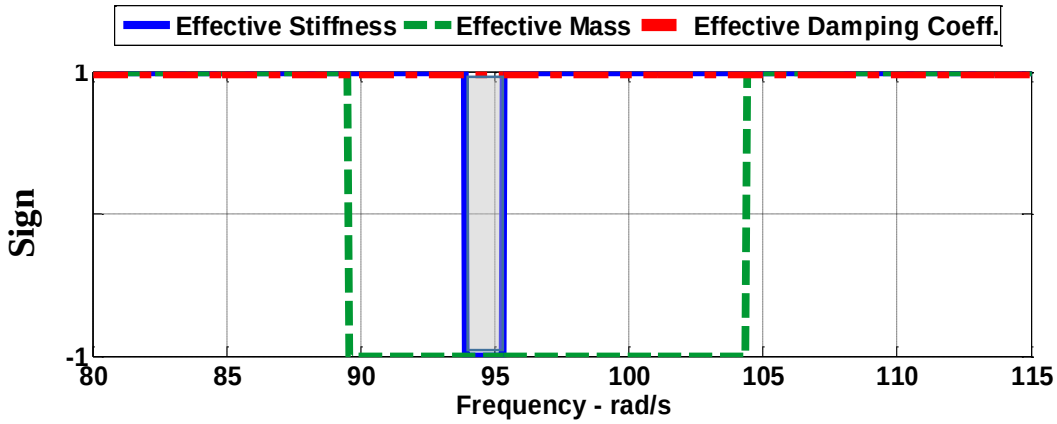

(b)

Fig. 3.12: Signs of the effective mass, stiffness, and damping coefficient of the active acoustic metamaterial with:
(a) - *FD* controller with α=0.1. (b) *PD* controller.

3.3. Summary

This chapter has presented two configurations of the *AAMM* whereby the control actions are generated either by linear *PD* and nonlinear *FD* controllers. In the first considered configuration, the local control action f_{c_i} is generated to be proportional to the Helmholtz displacement x_{r_i} only. This strategy enables the control of only the effective mass of the *AAMM* while the effective stiffness remains unaffected or uncontrolled. Accordingly, an additional controller is needed to control the stiffness of the *AAMM*.

However, in the second configuration of the *AAMM*, the local control action f_{c_i} is generated to be a linear combination of the Helmholtz displacement x_{r_i} and the displacements of the neighboring transmission line elements x_i's. This strategy enables the simultaneous control of the effective mass and stiffness of the *AAMM* with one control actuator. Accordingly, this simplifies considerably the design, physical and practical realization, and reliability of the *AAMM*.

A major contribution of this chapter is the consideration of a nonlinear fractional derivative (*FD*) controller to control the acoustic properties of the *AAMM* instead of the conventional proportional and derivative (*PD*) controller. It is demonstrated here that the use of the *FD* controller has significantly magnified the frequency bandwidth where negative effective mass and stiffness are obtained simultaneously as compared to that obtained by using the *PD* controller. Such significant magnification is shown to be achieved without compromising the stable operation of the *AAMM*.

Chapter 4 Active Acoustic Metamaterial with Stacked Helmholtz Resonators

4.1. Overview

In this chapter, another favorable configuration of the *AAMM* is presented. The proposed configuration consists again of an array of Helmholtz resonators which are coupled with an acoustic transmission line. However, each of the considered Helmholtz resonators is designed to be an assembly of stacked Helmholtz resonators (*SHR*). It is envisioned that with such stacking of the resonators, it would be possible to capitalize on the dynamics of the resulting system to enhance the overall performance of the *AAMM*.

In this chapter, the equations governing the interactions of the stacked Helmholtz resonators with the transmission line are developed. The performance characteristics of the *AAMM/SHR* system are presented when linear *PD* or nonlinear *FD* controllers are employed. Comparisons are established between the characteristics of the *AAMM/SHR* with the different controllers to emphasize the effectiveness and merits of the nonlinear *FD* controller as compared to the linear *PD* controller.

4.2. Concept of the Active Acoustic Metamaterial with Stacked Helmholtz Resonators:

4.2.1 The Structure of the Metamaterial *AAMM/SHR*:

The *AAMM/SHR* system in its bulk form is consisting of several stacked up Helmholtz resonators which are spatially distributed and connected to a wave carrying medium as shown in Fig. 4.1. Emphasis is placed here on double-stacked Helmholtz resonators. The *AAMM* introduced by Pope and Daley (2010) with a single resonator has influenced the design of *AAMM/SHR*.

4.2.2 Lumped-Parameter Modeling of the Metamaterial *AAMM/SHR*:

The structure of the metamaterial unit cell consists of a section of the transmission line which is connected at a single point to a double-neck Helmholtz resonator. A schematic drawing of the equivalent lumped-parameter model of a unit cell of the *AAMM/SHR* is shown Fig. 4.2.

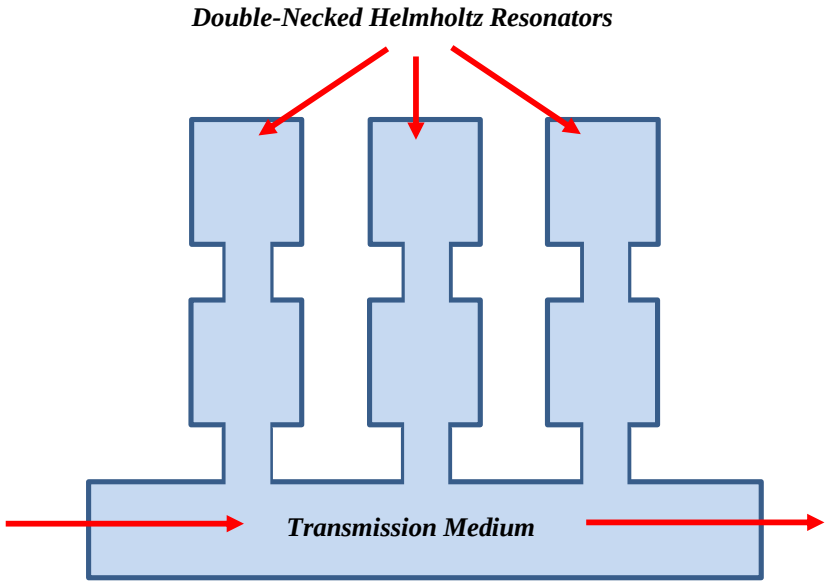

Fig. 4.1: Schematic drawing of *AAMM* with double-necked Helmholtz resonators

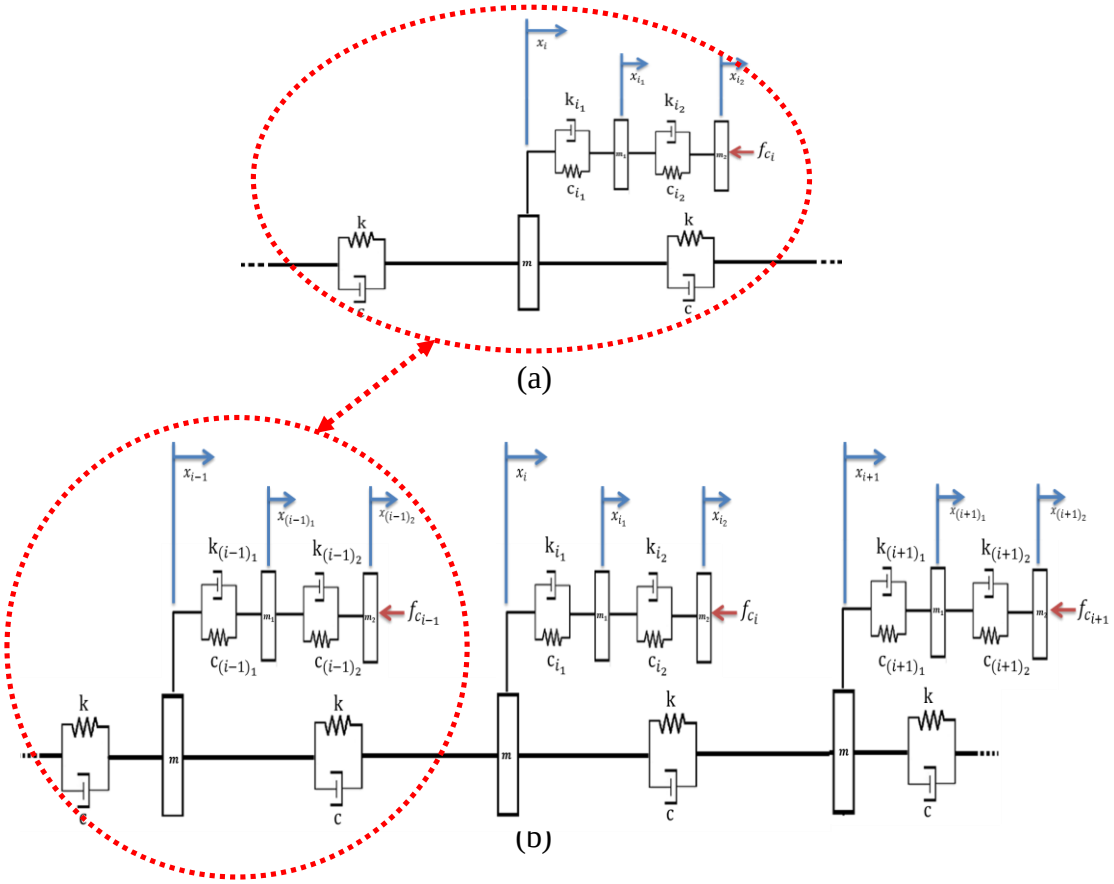

Fig. 4.2: Lumped-parameter model of a unit cell (a) of an active acoustic metamaterial (b) with a double-necked Helmholtz resonator.

For the unit cell shown in Fig. 4.2, each transmission line element has 3 parameters: mass $\boldsymbol{m}$, stiffness $\boldsymbol{k}$, and damping coefficient $\boldsymbol{c}$. Associated with each of these elements is an array of $\boldsymbol{n}$ stacked Helmholtz resonators, each of which has three parameters. These are namely: resonator mass $\boldsymbol{m_i}$, spring $\boldsymbol{k_i}$, and damper $\boldsymbol{c_i}$ where $i = 1,2,\ldots,n$. This leads, for a passive unit cell, to a total number of parameters P_p equal to $3n+3$. When the cell is provided with active capabilities, two additional parameters are added, These additional parameters are the control gains $\boldsymbol{k_c}$ and $\boldsymbol{c_c}$. Hence, the total number of associated with an *AAMM/SHR* is $P_a = 3n+5$.

These parameters govern the behavior of the acoustic metamaterial and control its operating frequency range.

4.3. Control with A Linear Proportional and Derivative (*PD*) Controller

The dynamics of the lumped-parameter system is developed by writing the equation of motion of a unit cell consisting of a Helmholtz resonator and the transmission line element ***i*** as follows:

a. <u>The equation of motion of the i^{th} transmission element:</u>

Using the Laplace transformation, the equation of motion can be written as:

$$m\,s^2X_i + (k + s\,c)(2X_i - X_{i-1} - X_{i+1}) + (k_1 + sc_1)\left(X_i - X_{i_1}\right) = F_i \qquad (4.1)$$

where: F_i : is an applied external force.

b. <u>The equation of motion of the first Helmholtz resonant mass m_1:</u>

In the Laplace domain:

$$m_1 s^2 X_{i_1} + (k_1 + sc_1)\left(X_{i_1} - X_i\right) + (k_2 + s\,c_2)\left(X_{i_1} - X_{i_2}\right) = 0 \qquad (4.2)$$

c. <u>The equation of motion of the second Helmholtz resonant mass m_2:</u>

In the Laplace domain:

$$m_2\,s^2\,X_{i_2} + (k_2 + s\,c_2)\left(X_{i_2} - X_{i_1}\right) = \boldsymbol{f_c} \qquad (4.3)$$

d. The control action:

In this chapter, the control action $\boldsymbol{f_c}$, as introduced by Pope and Daley (2010), is generated to be proportional to a linear combination of the Helmholtz displacement x_{r_i} and the displacements of the neighboring transmission line elements x_i's. This strategy enables the simultaneous control of the effective mass and stiffness of the *AAMM* with one control actuator as demonstrated in Chapter 3. Hence, the control action $\boldsymbol{f_c}$ such that:

$$\boldsymbol{f_c} = (k_c + s\,c_c)\big(2X_{i_2} - X_{i+1} - X_{i-1}\big) \tag{4.4}$$

The equivalent lumped-parameter system:

Combining eqs. (4.3), and (4.4) gives:

$$m_2\,s^2\,X_{i_2} + (k_2 + s\,c_2)\big(X_{i_2} - X_{i_1}\big)$$

$$+(k_c + s\,c_c)\big(2X_{i_2} - X_{i+1} - X_{i-1}\big) = 0 \tag{4.5}$$

This yields to:

$$X_{i_2} = \frac{(k_2+s\,c_2)X_{i_1}+(k_c+s\,c_c)}{[m_2\,s^2+(k_2+s\,c_2)+2(k_c+s\,c_c)\,]}(X_{i+1} + X_{i-1}) \tag{4.6}$$

Substituting eq. (4.6) into eq. (4.2), gives

$$[m_1 s^2 + (k_1 + s\,c_1) + (k_2 + s\,c_2)]X_{i_1}$$

$$= (k_1 + s\,c_1)X_i +$$

$$\frac{(k_2+s\,c_2)^2X_{i_1}+(k_2+s\,c_2)(k_c+s\,c_c)(X_{i+1}+X_{i-1})}{[m_2\,s^2+(k_2+s\,c_2)+2(k_c+s\,c_c)\,]} \tag{4.7}$$

Let:

$$a_1 = [m_2\,s^2 + (k_2 + s\,c_2) + 2(k_c + s\,c_c)\,]$$

and

$$a_2 = \left[m_1 s^2 + (k_1 + sc_1) + (k_2 + s\,c_2) - \frac{(k_2+s\,c_2)^2}{a_1}\right] \tag{4.8}$$

Then, eq. (4.7) reduces to:

$$X_{i_1} = \left[\frac{a_1(k_1+sc_1)\,X_i+(k_2+s\,c_2)(k_c+s\,c_c)(X_{i+1}+X_{i-1})}{a_1 a_2}\right] \quad (4.9)$$

Finally, inserting eq. (4.9) into eq. (4.1) yields:

$$m\,s^2X_i + (k + s\,c)(2X_i - X_{i-1} - X_{i+1}) + (k_1 + sc_1)X_i$$

$$-\left[\frac{a_1(k_1+sc_1)^2X_i+(k_1+sc_1)(k_2+s\,c_2)(k_c+s\,c_c)(X_{i+1}+X_{i-1})}{a_1 a_2}\right] = F_i \quad (4.10)$$

Let:

$$\boldsymbol{b} = [m_2\,m_1\,s^2\;(k_1 + sc_1) + m_2\,(k_2 + s\,c_2)(k_1 + sc_1)$$

$$+m_1(k_1 + sc_1)\big((k_2 + s\,c_2) + 2\,(k_c + s\,c_c)\big)] \quad (4.11)$$

Then, eq. (4.10) reduces to:

$$\left[m + \frac{b}{a_1 a_2}\right]s^2\,X_i + \left[(k + s\,c) + \frac{(k_1 + sc_1)(k_2 + s\,c_2)(k_c + s\,c_c)}{a_1 a_2}\right]\times$$

$$(2X_i - X_{i+1} - X_{i-1}) = F_i \quad (4.12)$$

The equivalent lumped-parameter system equation of motion reduces to:

$$m_e\,s^2\,X_i + (k_e + s\,c_e)(2X_i - X_{i+1} - X_{i-1}) = F_i \quad (4.13)$$

where:

<u>The effective mass of the equivalent-system:</u>

$$m_e = m + \frac{b}{a_1 a_2} = m_{e_{REAL}} + i\,m_{e_{IMAG}} \quad (4.14)$$

$where$:

$$m_{e_{REAL}} = m + \boldsymbol{real}\left(G_M(s)\right) \quad , \quad m_{e_{IMAG}} = \boldsymbol{imag}\left(G_M(s)\right)$$

$$G_M(s) = \frac{b}{a_1 a_2}, \quad \text{and} \quad s = i\,\omega \tag{4.15}$$

The effective stiffness of the equivalent-system:

$$k_e = k + \boldsymbol{real}\left(G_k(s)\right) \tag{4.16}$$

where:

$$G_k(s) = \frac{(k_1 + s c_1)(k_2 + s\,c_2)(k_c + s\,c_c)}{a_1 a_2} \tag{4.17}$$

The effective damping of the equivalent-system:

$$c_e = c \; + \frac{\boldsymbol{imag}\left(G_k(i\omega)\right)}{\omega} \tag{4.18}$$

Then, the equation of motion of the equivalent system is given by:

$$m_e\, s^2 X_i - (k_e + s\, c_e)\,(X_{i-1} + X_{i+1} - 2X_i) = F_i \tag{4.19}$$

Eq. (4.19) can be described in the frequency as follows:

$$-\left(m_{e_{REAL}} + i\, m_{e_{IMAG}}\right)\omega^2 X_i - (k_e + i\omega\, c_e)\,(X_{i-1} + X_{i+1} - 2X_i) = F_i$$

or

$$-\left(M_{e_{REAL}} + i\, M_{e_{IMAG}}\right)\omega^2 X_i + 2\,(K_e + i\,\omega\, C_e)\, X_i =$$

$$\underbrace{F_i + (K_e + i\,\omega\, C_e)(X_{i-1} + X_{i+1})}_{F_T}$$

This leads to:

$$-m_{e_{REAL}}\,\omega^2 X_i + i\omega\left(2\,c_e - \omega\, m_{e_{IMAG}}\right) X_i + 2k_e\, X_i = F_T \qquad (4.20)$$

Eq. (4.20) can be rewritten as:

$$-m_{e_m}\omega^2 X_i + i\omega\, c_{e_m} X_i + k_{e_m} X_i = F_T \qquad (4.21)$$

where:

$$m_{e_m} = m_{e_{REAL}} \qquad (4.22)$$

$$c_{e_m} = 2\,c_e - \omega\, m_{e_{IMAG}} \qquad (4.23)$$

$$k_{e_m} = 2\,k_e \qquad (4.24)$$

$$F_T = F_i + (k_e + i\,\omega\, c_e)(X_{i-1} + X_{i+1}) \qquad (4.25)$$

e. Notes on The Effective Properties

The effective properties of the equivalent system, as described by eqs. (4.22) through (4.24), have special structures that are worthy of additional comments:

i. The effective mass:

The effective mass equation, eq. (4.14), includes two components. The first component is positive real and equals the mass m of the transmission line element. The second component is a frequency-dependent term which depends on the resonant mass, stiffness and damper elements. This component can cause the effective mass to assume a negative value over certain frequency range. The structure of the frequency-dependent term is fractional function which is of strictly proper order. This means that the order of the nominator is less than that of the denominator. In other words, this term vanishes the Laplace complex number approaches infinity.

In fact, the effective mass is a complex number. The real part is considered as the actual effective mass of the metamaterial system, whereas, the imaginary part is treated as a loss term of the total energy of the system. Accordingly, this loss term has to be included in the total effective damping coefficient alongside with the main damping element c_e, described by eq. (4.23).

ii. **The effective stiffness:**

Similarly the effective stiffness consists of two terms. The first term is the stiffness $\boldsymbol{k}$ which characterizes the compressibility property of the fluid medium in the transmission line. The second term is a complex function that has similar structure as the effective damping coefficient of the system. Only the real part of this term is considered, eq. (4.17).

Note also that the complex term is fractional function which is strictly proper with its numerator is assembled in a unique manner. The numerator is structured in the form of a product of the stiffness and damping coefficient of the stacked Helmholtz resonators such that: $(k_1 + s\,c_1)(k_2 + s\,c_2)$ ... $(k_i + s\,c_i)$. Furthermore, the product is also multiplied by the transfer function of the active gains $(k_c + s\,c_c)$.

Therefore, the order of the numerator is equal to number of stacked resonators plus the order of the transfer function of the active gains. For example, a triple-neck metamaterial, for instance, has three stiffness-damper combinations in addition to the active gains. Thus, the order of the numerator is of the fourth order $(k_1 + s\,c_1)(k_2 + s\,c_2)(k_3 + s\,c_3)(k_c + s\,c_c)$. Empirically, one can generalize a formula for the order of numerator $n + 1$.

4.4. Control with A Fractional Derivative (*FD*) Controller

The fractional order systems have various advantages depending on the objective for which the system is designed for; whether for stability or reducing the steady state error of the system or both (Monje *et al.*, 2010).

In fractional order system control, it's commonly known that one of the main advantages of the Fractional Derivative (*FD*) type controllers is achieving a relative stability to the controlled system. On the other hand, the Fractional Integral (*FI*) order controllers are of great importance when eliminating the steady state error of the system. Fractional derivative controllers have more to offer in the field of metamaterials and in particular on improving the operating bandwidth of metamaterials. In this section, the effectiveness and the merits of developing active acoustic metamaterials with fractional derivative controllers are investigated in comparison to active acoustic metamaterials with simple linear Proportional and Derivative controllers (*PD*).

The parameters of *FD* controller are optimized to achieve desirable frequency response characteristics.

The proposed equation of the fractional derivative controller is in the form:

$$\boldsymbol{f_c} = (k_c + s^{\alpha} c_c)\left(2X_{i_2} - X_{i+1} - X_{i-1}\right) \tag{4.26}$$

a. Metamaterial with Double Necked Helmholtz Resonator with *FD* Controller:

Eq. (4.12) can be easily modified to describe the behavior of the metamaterial with FD controller to assume the following form:

$$\left[m + \frac{b(s,\alpha)}{a_1 a_2}\right] s^2 X_i + \left[(k + s\,c) + \frac{(k_1 + sc_1)(k_2 + s\,c_2)(k_c + s^{\alpha}\,c_c)}{a_1 a_2}\right] (2X_i - X_{i+1} - X_{i-1}) = F_i \tag{4.27}$$

where:

$$\boldsymbol{b}(s,\alpha) = \left[m_2\, m_1\, s^2\ (k_1 + sc_1) + m_2\,(k_2 + s\,c_2)(k_1 + sc_1) + m_1(k_1 + sc_1)\left((k_2 + s\,c_2) + 2\,(k_c + s^{\alpha}\,c_c)\right)\right] \tag{4.28}$$

This leads to the following equivalent lumped-parameter system:

$$m_e\, s^2\, X_i + (k_e + s\,c_e)(2X_i - X_{i+1} - X_{i-1}) = F_i \tag{4.29}$$

Where:

<u>The effective mass of the equivalent-system:</u>

$$m_e = m + \frac{b}{a_1 a_2} = m_{e_{REAL}} + i\, m_{e_{IMAG}} \tag{4.30}$$

where:

$$m_{e_{REAL}} = m + \boldsymbol{real}\left(G_M(s)\right) \quad , \quad m_{e_{IMAG}} = \boldsymbol{imag}\left(G_M(s)\right)$$

$$G_M(s) = \frac{b}{a_1 a_2}, \quad \text{and} \quad s = i\,\omega \tag{4.31}$$

The effective stiffness of the equivalent-system:

$$k_e = k + \boldsymbol{real}\big(G_k(s)\big) \tag{4.32}$$

where:

$$G_k(s) = \frac{(k_1 + s c_1)(k_2 + s\,c_2)(k_c + s^{\alpha}\,c_c)}{a_1 a_2} \tag{4.33}$$

The effective damping of the equivalent-system:

$$c_e = c\ + \frac{\boldsymbol{imag}\big(G_k(i\omega)\big)}{\omega} \tag{4.34}$$

Then, the equation of motion of the equivalent system is given by:

$$m_e\, s^2 X_i - (k_e + s\, c_e)\,(X_{i-1} + X_{i+1} - 2X_i) = F_i \tag{4.35}$$

Eq. (4.35) can be described in the frequency as follows:

$$-\big(m_{e_{REAL}} + i\, m_{e_{IMAG}}\big)\,\omega^2 X_i - (k_e + i\omega\, c_e)\,(X_{i-1} + X_{i+1} - 2X_i) = F_i$$

or

$$-\big(M_{e_{REAL}} + i\, M_{e_{IMAG}}\big)\,\omega^2 X_i + 2\,(K_e + i\,\omega\, C_e)\,X_i =$$

$$\underbrace{F_i + (K_e + i\,\omega\, C_e)(X_{i-1} + X_{i+1})}_{F_T}$$

This leads to:

$$-m_{e_{REAL}}\,\omega^2 X_i + i\omega\left(2\,c_e - \omega\, m_{e_{IMAG}}\right) X_i + 2k_e\, X_i = F_T \qquad (4.36)$$

Eq. (4.36) can be rewritten as:

$$-m_{e_m}\omega^2 X_i + i\omega\, c_{e_m} X_i + k_{e_m} X_i = F_T \qquad (4.37)$$

where:

$$m_{e_m} = m_{e_{REAL}} \qquad (4.38)$$

$$c_{e_m} = 2\,c_e - \omega\, m_{e_{IMAG}} \qquad (4.39)$$

$$k_{e_m} = 2\,k_e \qquad (4.40)$$

$$F_T = F_i + (k_e + i\,\omega\, c_e)(X_{i-1} + X_{i+1}) \qquad (4.41)$$

4.5. Numerical Examples and Discussions:

a. <u>Performance of a single Halmholtz resonator</u>

Consider the active acoustic metamaterial with single Helmholtz with proportional derivative controller. The system has the physical parameters listed in Table 4.1. The metamaterial is excited at node 1 at the beginning of the transmission line with a swept sine wave and the response is monitored at node 10 at the end of the transmission line.

Table 4.1 Physical parameters of the active acoustic metamaterial with single Helmholtz resonator

Parameter	m (*kg*)	k (*N/m*)	c (*Ns/m*)	m_{r1} (*kg*)	k_{r1} (*N/m*)	c_{r1} (*Ns/m*)	k_c (*N/m*)	c_c (*Ns/m*)	*No. of Cells*
Values	**0.01**	**2000**	**0.1**	**1.6**	**1800**	**0.002**	**6999**	**10**	**10**

Fig. 4.3.a shows the magnitude of the relative displacement across ten cascaded transmission elements $|X_{10}/X_1|$. Fig. 4.3b shows the sign of the effective mass m_e and stiffness k_e of the metamaterial array. It can be easily seen that between 15-70 *rad/s*, the metamaterial array exhibits negative effective mass whereas its effective stiffness has a negative value over a wider band between 15-18 *rad/s*. Therefore, the *AAMM*

with linear *PD* controller results in simultaneous double negative properties in the frequency range 15-18 *rad/s*.

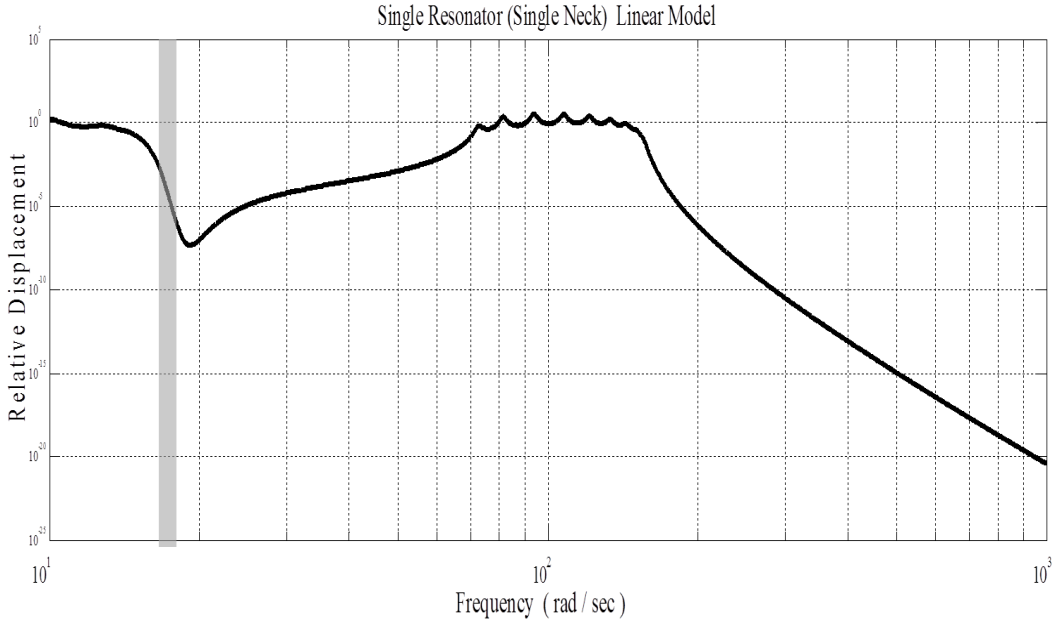

(a)

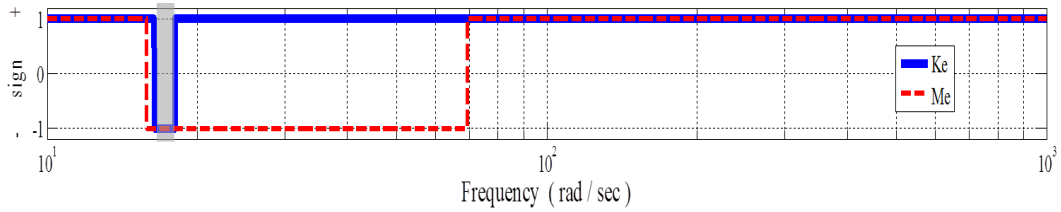

(b)

Fig.4.3: Active acoustic metamaterial with single Helmholtz resonator.
(a) the frequency response of $|X_{10}/X_1|$, (b) sign of the effective mass and stiffness

(b) – Comparisons between Single and stacked Helmholtz resonators

***i.* – High Frequency Range:**

1 – Linear PD Controller

Consider the active acoustic metamaterial with single Helmholtz with fractional derivative controller. The system has the physical parameters listed in Table 4.2. The metamaterial is excited at node 1 at the beginning of the transmission line with a swept sine wave and the response is monitored at node 10 at the end of the transmission line.

Table 4.2 Physical parameters of the active acoustic metamaterial with single and stacked Helmholtz resonators in addition to Table 4.1

Parameter	m_{r2} (*kg*)	k_{r2} (*N/m*)	c_{r2} (*Ns/m*)	*No. of Cells*
Values	**1**	**2500**	**0.002**	**10**

Fig. 4.4 shows a comparison between the frequency bandwidth of the double negative properties zones of *AAMM* with a single and double neck Helmholtz resonators. Fig. 4.4a shows the sign of the effective mass m_e and stiffness k_e of the metamaterial with a single Helmholtz resonator. It can be easily seen that between 55-80 *rad/s*, the metamaterial array exhibits negative effective mass whereas its effective stiffness has a negative value over a wider band between 55-62 *rad/s*. Therefore, the *AAMM* with linear *PD* controller results in simultaneous double negative properties in the frequency range 55-62 *rad/s*.

Fig. 4.4b displays the sign of the effective mass m_e and stiffness k_e of the metamaterial with a double Helmholtz resonators. It can be easily seen that between 34-90 *rad/s*, the metamaterial array exhibits negative effective mass whereas its effective stiffness has a negative value over a wider band between 34-43 *rad/s*. Therefore, the *AAMM* with linear *PD* controller results in simultaneous double negative properties in the frequency range 34-43 *rad/s*.

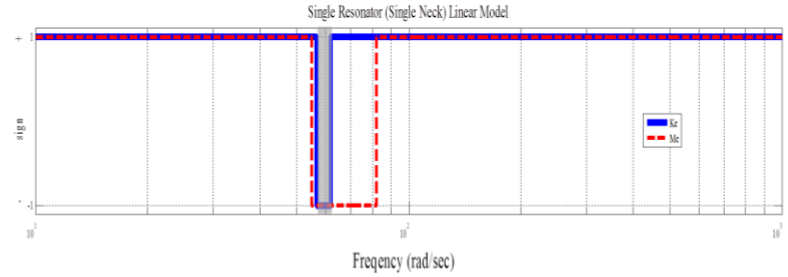

(a)

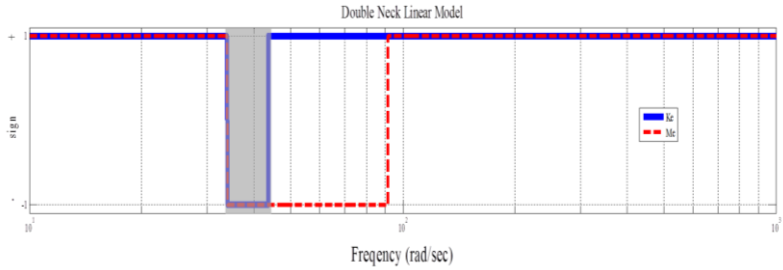

(b)

Fig. 4.4: Comparison between the frequency bandwidth of double negative properties zones (a) single neck (b) double neck

2 – Nonlinear FD Controller

The effect of providing the *AAMM* with a *FD* controller on the frequency bandwidth of double negative properties zones is investigated when the metamaterial is integrated with double-necked Helmholtz resonators.

Fig. 4.5 displays the sign of the effective mass m_e and stiffness k_e of the metamaterial for different values of the *FD* exponent α. It can be easily seen that the widest frequency band of double negative properties zone is obtained when α=0.1. The width of the obtained zone is between 34-55 *rad/s*.

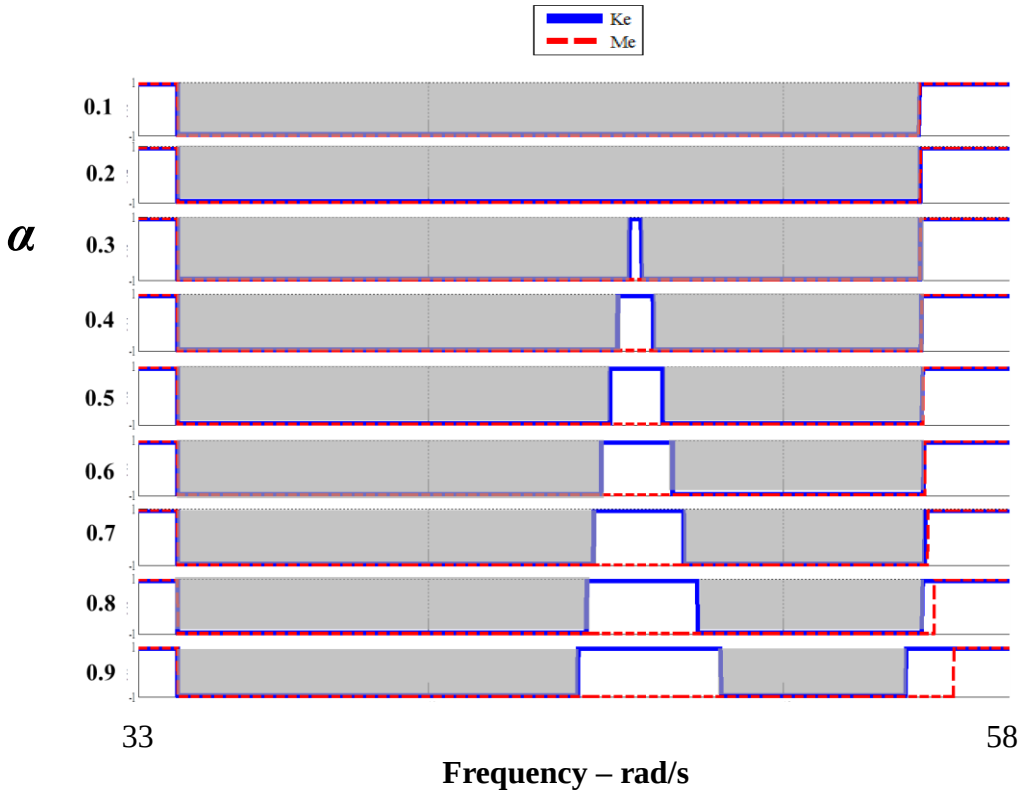

Fig. 4.5: The effect of the exponent α in the Fractional Derivative controller on the double negative parameters characteristics of a metamaterial with double-necked Helmholtz resonators

A comparison between the characteristics of *AAMM* with double-necked Helmholtz resonator controlled by *FD* controller, *AAMM* with double-necked Helmholtz resonator controlled by *PD* controller, and *AAMM* with single-necked Helmholtz resonator controlled by *PD* controller are shown in Fig. 4.6. It is evident

that the use of *FD* controller with a double-necked resonators has resulted in the widest frequency bandwidth of double negative properties zones.

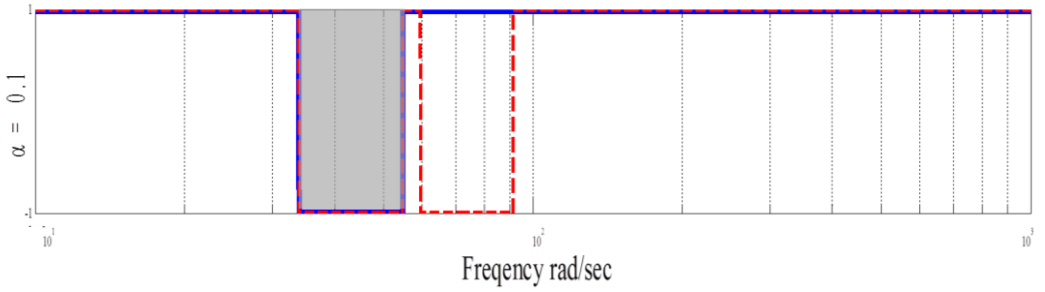

(a)

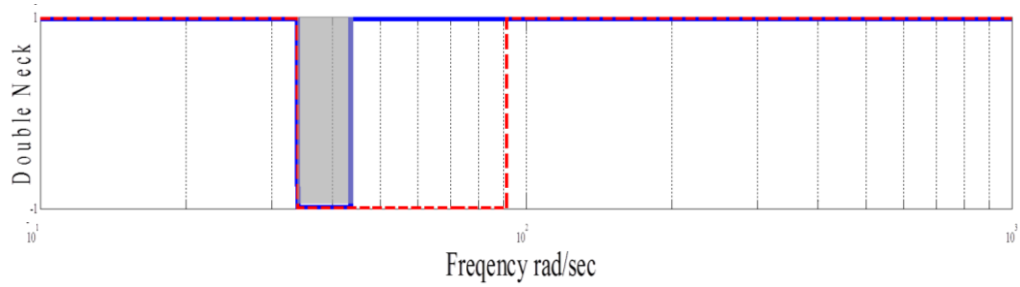

(b)

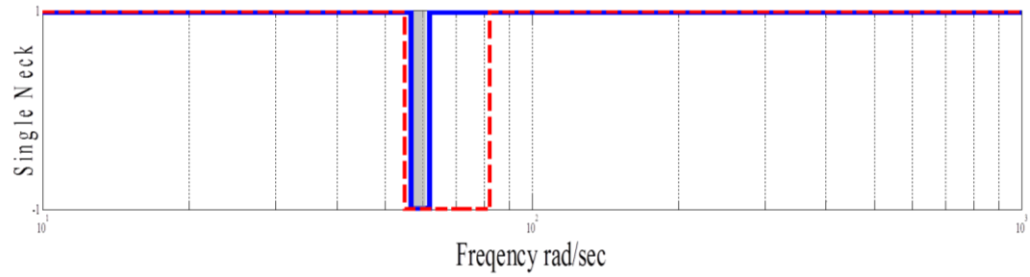

(c)

Fig. 4.6: Comparison between the frequency bandwidth of double negative properties zones of *AAMM* with single neck resonator and *PD* controller, with double neck resonator and *PD* controller, and double neck resonator with *FD* controller

***ii.* – Low Frequency Range:**

It is important to note that Fig. 4.6 indicated that the use of the double-necked Helmholtz resonators has resulted in two effects as compared to the use of the single-necked arrangement. In the first effect, the frequency bandwidth of double negative properties zone is increased whereas the second effect is manifested by a shift of the zone to lower frequency range.

Another example is considered here. The metamaterial characteristics are summarized in Table 4.3.

Table 4.3 Physical parameters of the active acoustic metamaterial with double-necked Helmholtz resonators and *PD* controller in addition to Table 4.1

Parameter	m_{r2} (kg)	k_{r2} (N/m)	c_{r2} (Ns/m)	*No. of Cells*
Values	**1**	**2500**	**0.002**	**10**

A comparison between the characteristics of *AAMM* with a single-necked Helmholtz resonator, and those with double-necked Helmholtz resonator controlled by *PD* controller are shown in Fig. 4.7. It is evident that the use of a double-necked resonator has increased the frequency bandwidth of double negative properties zone from 10-14 *rad/s* to 17-18 *rad/s* for the single-necked resonator. Furthermore, the double negative properties zone is shifted to start from 10 *rad/s* instead 17 *rad/s* for the case of a single-necked resonator.

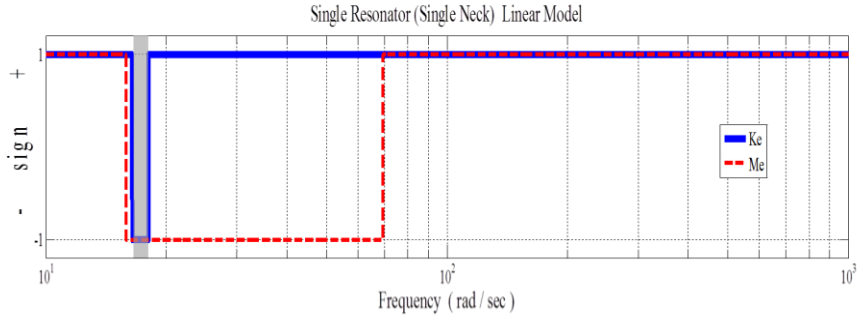

(a)

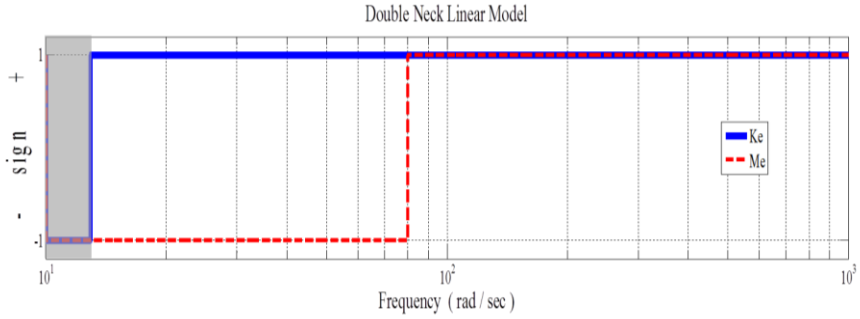

(b)

Fig. 4.7: Comparison between the frequency bandwidth of double negative properties zones of *AAMM* with single neck resonator (a) and with double neck resonator and *PD* controller (b)

Fig. 4.8 displays the sign of the effective mass m_e and stiffness k_e of the metamaterial for different values of the *FD* exponent α. It can be easily seen that the widest frequency band of double negative properties zone is obtained when α=0.1. The width of the obtained zone is between 10-17 *rad/s*.

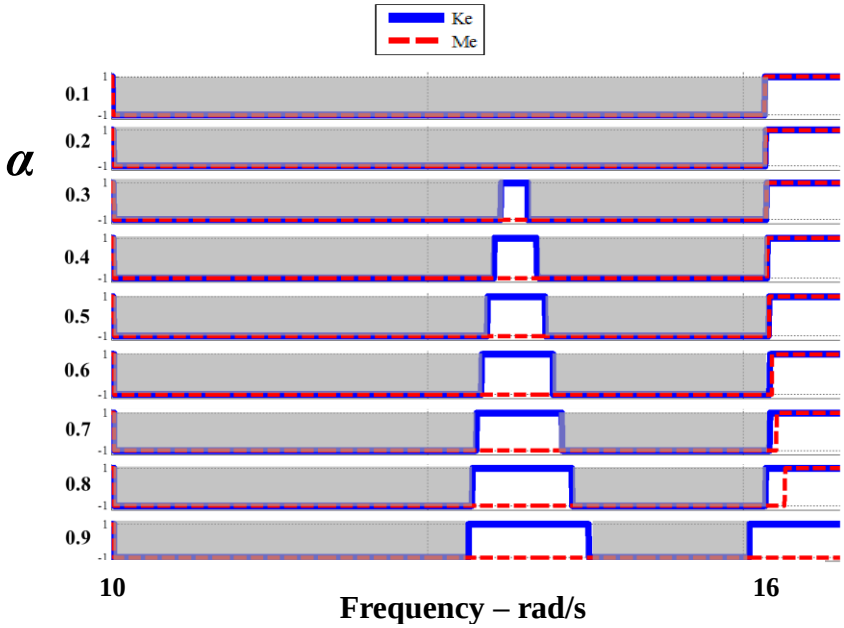

Fig. 4.8: The effect of the exponent α in the Fractional Derivative controller on the double negative parameters characteristics of a metamaterial with double-necked Helmholtz resonators

A comparison between the characteristics of *AAMM* with double-necked Helmholtz resonator controlled by *FD* controller, *AAMM* with double-necked Helmholtz resonator controlled by *PD* controller, and *AAMM* with single-necked Helmholtz resonator controlled by *PD* controller are shown in Fig. 4.9. It is evident that the use of *FD* controller with a double-necked resonators has resulted in the widest frequency bandwidth of double negative properties zones.

.

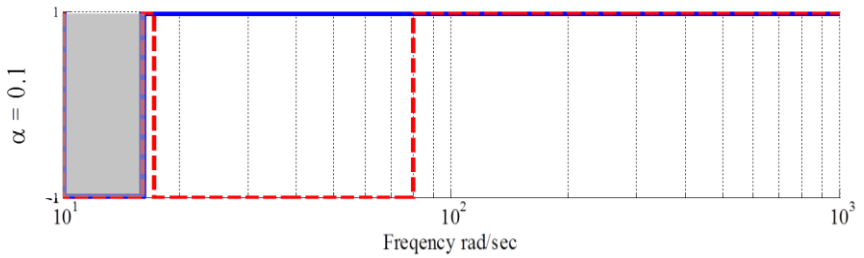

(a)

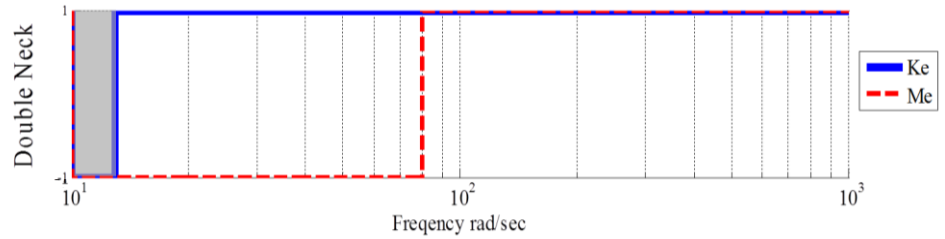

(b)

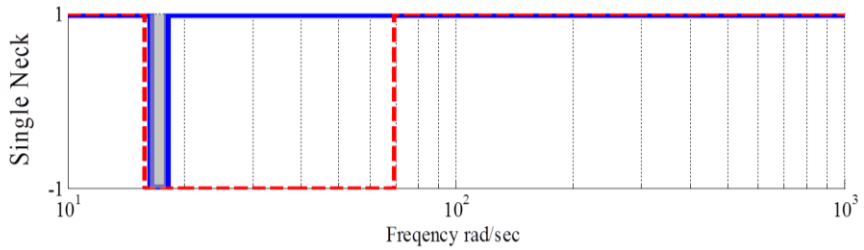

(c)

Fig. 4.9: Comparison between the frequency bandwidth of double negative properties zones of *AAMM* with single neck resonator and *PD* controller, with double neck resonator and *PD* controller, and double neck resonator with *FD* controller at low frequency range.

4.6. Comparison between the Frequency Response Characteristics

a. High Frequency Zone

In this section, comparisons are presented between the frequency response characteristics of *AAMM* with double-neck Helmholtz resonators controlled by linear *PD* controller and nonlinear *FD* controller for high frequency operation. These comparisons are displayed in Figs. 4.10 and 4.11 respectively.

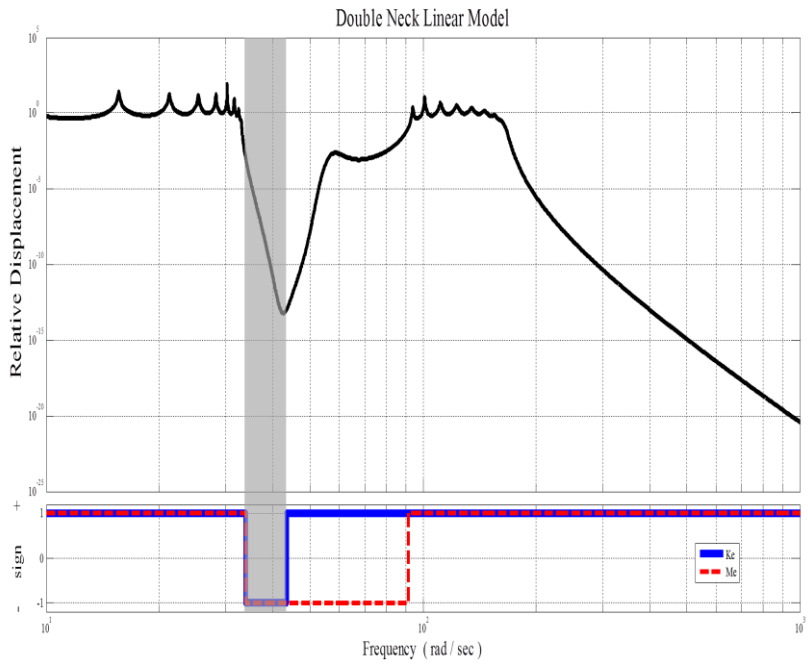

Fig. 4.10: The frequency response (a) and sign of the effective mass and stiffness (b) for an *AAMM* with double-necked resonators and *PD* controller, at high frequency range.

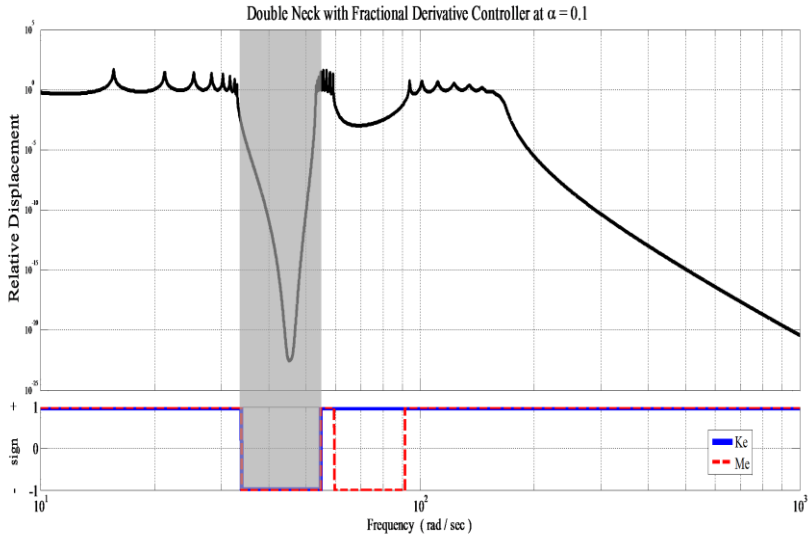

Fig. 4.11: The frequency response (a) and sign of the effective mass and stiffness (b) for an *AAMM* with double-necked resonators and *FD* controller, at high frequency range.

b. Low Frequency Zone

In this section, comparisons are presented between the frequency response characteristics of *AAMM* with double-neck Helmholtz resonators controlled by linear *PD* controller and nonlinear *FD* controller for low frequency operation. These comparisons are displayed in Figs. 4.12 and 4.13 respectively.

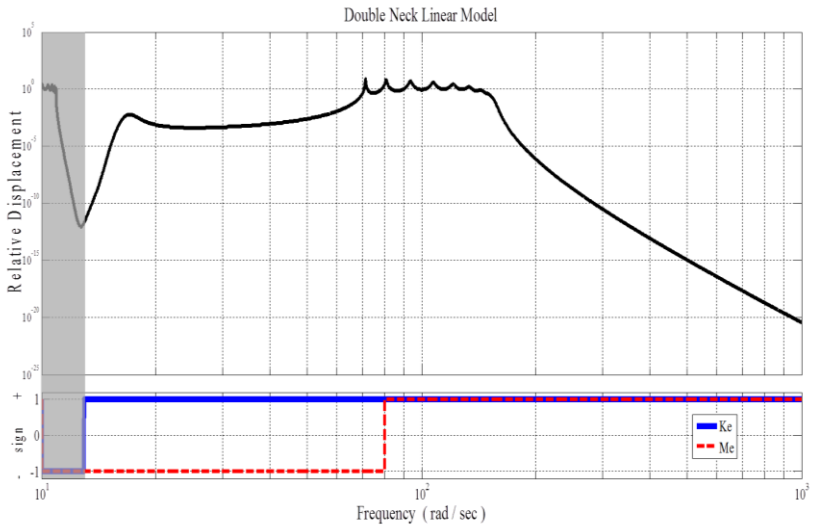

Fig. 4.12: The frequency response (a) and sign of the effective mass and stiffness (b) for an *AAMM* with double-necked resonators and *PD* controller, at low frequency range.

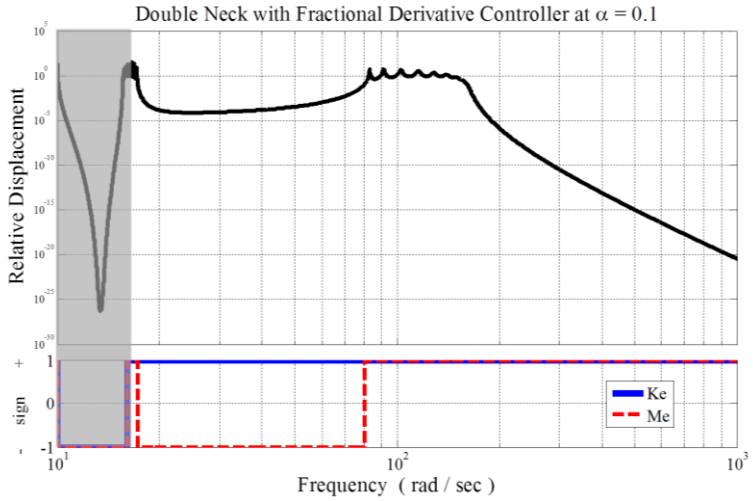

Fig. 4.13: The frequency response (a) and sign of the effective mass and stiffness (b) for an *AAMM* with double-necked resonators and *FD* controller, at low frequency range.

4.7. Summary

This chapter has presented a viable configuration of the *AAMM* which consists of an array of stacked Helmholtz resonators which are coupled with an acoustic transmission line.

The equations governing the interactions of the stacked Helmholtz resonators with the transmission line are developed. The performance characteristics of the *AAMM/SHR* system are presented when linear *PD* or nonlinear *FD* controllers are employed. Comparisons are established between the characteristics of the *AAMM/SHR* with the different controllers to emphasize the effectiveness and merits of the nonlinear *FD* controller as compared to the linear *PD* controller.

It is seen that the use of the double-necked Helmholtz resonators has resulted in broadening the frequency bandwidth of double negative properties zone and shifting of the zone to lower frequency range. It is observed that the employing *FD* controller has enhanced considerably the characteristics of the *AAMM* by further stretching the frequency bandwidth of double negative properties zone and shifting it more to much lower frequency range.

5.1. Overview

In this chapter, another preferred design of the active acoustic metamaterials is introduced in an attempt to enhance the width of the double negative properties zones.

In the proposed design, multiple Helmholtz resonators (*MHR*) are connected to each of the discrete points defining the transmission line. These *MHR* are distributed annularly around the connection point of the transmission line as shown in Fig. (5.1).

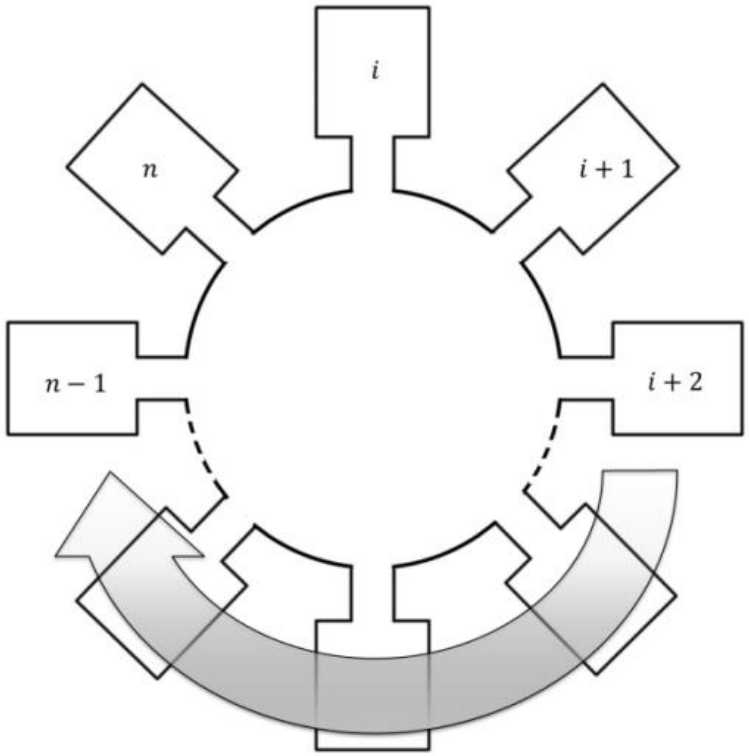

Fig. 5.1: Schematic drawing of Multi-Helmholtz-Resonators (*MHR*) active acoustic metamaterial

5.2. Concept of the Active Acoustic Metamaterial with Multiple Helmholtz Resonators (*MHR*):

5.2.1. The Structure of the Metamaterial *AAMM/MR*:

The *AAMM* consisting of multiple Helmholtz resonators (*MHR*) which are evenly distributed along the circumference of the unit cell as shown in Fig. 5.1. These multiple sets are spatially distributed and connected to a wave carrying medium as shown in Fig. 5.2. Emphasis is placed here on using *MHR* with double and triple Helmholtz resonators. The *AAMM* introduced by Pope and Daley (2010) with a single resonator has influenced the design of *AAMM/MHR*.

5.2.2. Lumped-Parameter Modeling of the Metamaterial *AAMM/MHR*:

The structure of the metamaterial unit cell consists of a section of the transmission line which is connected at a single point to multiple Helmholtz resonators. A schematic drawing of the equivalent lumped-parameter model of a unit cell of the *AAMM/MHR* is shown Fig. 5.3.

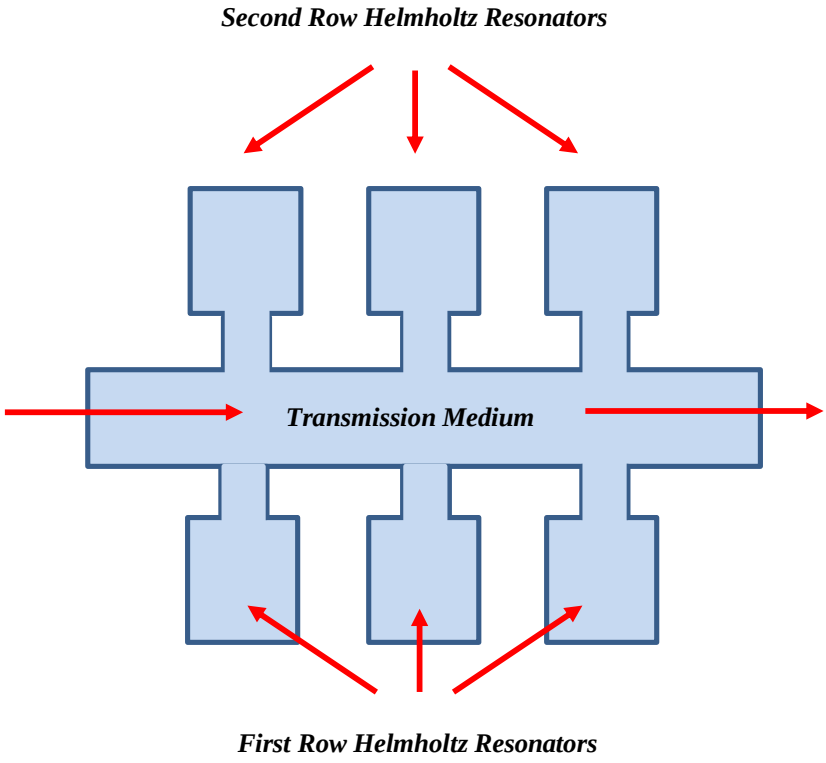

Fig. 5.2: Schematic drawing of *AAMM* with Multiple Double Helmholtz resonators

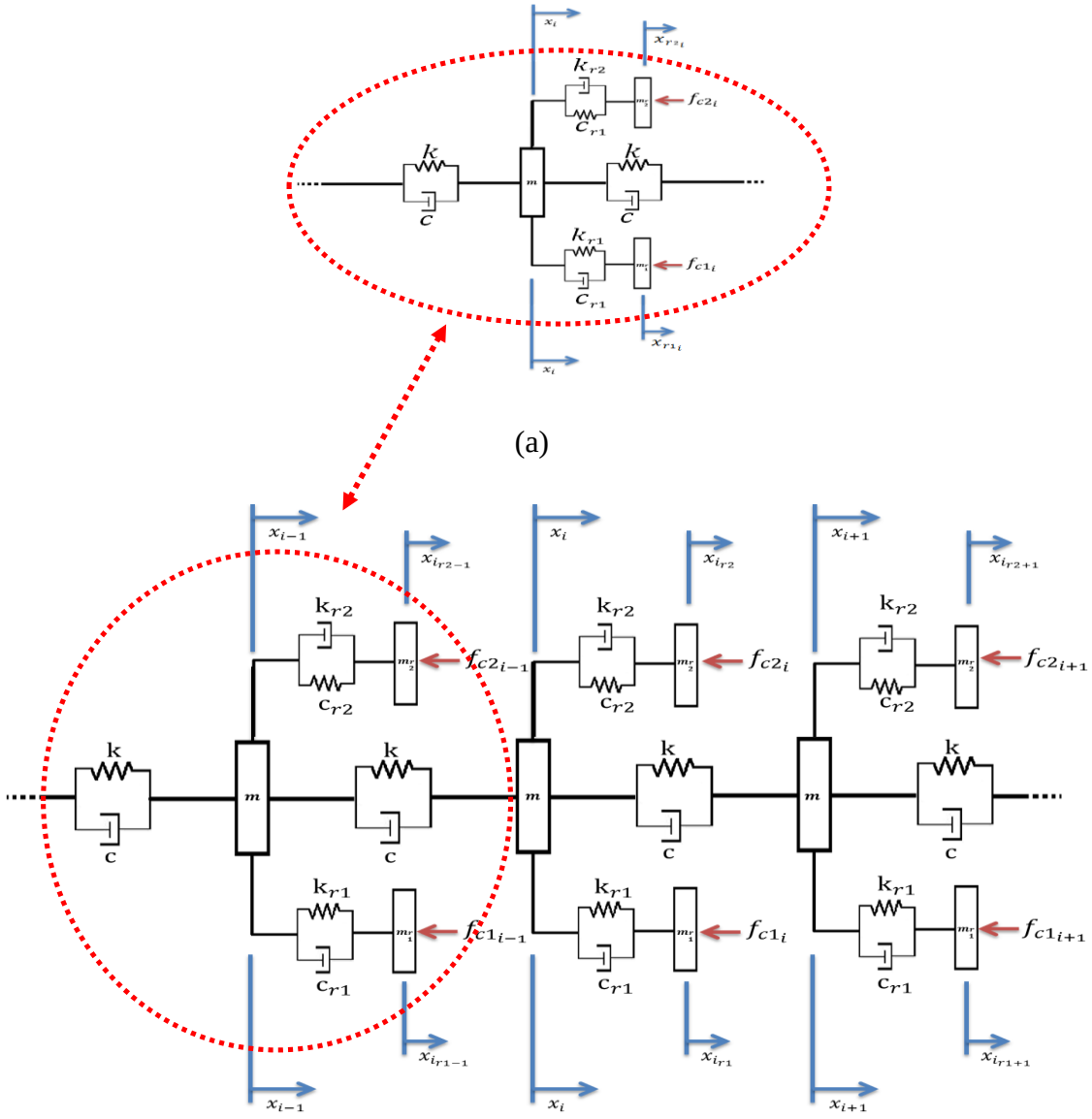

Fig. 5.3: Lumped-parameter model of a unit cell (a) of an active acoustic metamaterial and entire assembly of multi-cells (b)

For the unit cell shown in Fig. 5.3, each transmission line element has 3 parameters: mass ***m***, stiffness ***k***, and damping coefficient ***c***. Associated with each of these elements is a set of ***n*** multiple Helmholtz resonators, each of which has three

parameters. These are namely: resonator mass $\boldsymbol{m_i}$, spring $\boldsymbol{k_i}$, and damper $\boldsymbol{c_i}$ where $i = 1,2,\ldots,n$. This leads, for a passive unit cell, to a total number of parameters P_p equal to $3n+3$. When the cell is provided with active capabilities, ($2\boldsymbol{n}$) additional parameters are added, These additional parameters are the control gains $\boldsymbol{k_c}$ and $\boldsymbol{c_c}$. Hence, the total number of associated with an *AAMM/MHR* is $P_a = 5n+3$.

These parameters govern the behavior of the acoustic metamaterial and control its operating frequency range.

5.2.3. Modeling of the Active Acoustic Metamaterial with Multi-Double Resonators:

The dynamics of the lumped-parameter system is developed by writing the equation of motion of a unit cell consisting of multiple Helmholtz resonators and the transmission line element ***i*** as follows:

a. The equation of motion of the i^{th} transmission element:

Using the Laplace transformation, the equation of motion can be written as:

$$m\,s^2X_i + (k + s\,c)(2X_i - X_{i-1} - X_{i+1}) + (k_{r1} + sc_{r1})\left(X_i - X_{i_{r1}}\right)$$

$$+(k_{r2} + sc_{r2})\left(X_i - X_{i_{r2}}\right) = F_i \qquad (5.1)$$

where: F_i : is an applied external force.

b. The equation of motion of the first Helmholtz resonant mass m_1:

In the Laplace domain:

$$m_{r1}s^2X_{i_{r1}} + (k_{r1} + sc_{r1})\left(X_{i_{r1}} - X_i\right) = \boldsymbol{f}_{i_{c1}} \qquad (5.2)$$

c. The equation of motion of the second Helmholtz resonant mass m_2:

In the Laplace domain:

$$m_{r2}s^2X_{i_{r2}} + (k_{r2} + sc_{r2})\left(X_{i_{r2}} - X_i\right) = \boldsymbol{f}_{i_{c2}} \qquad (5.3)$$

d. <u>The control action</u>:

In this chapter, the control action $\boldsymbol{f_{i_{ci}}}$, as introduced by Pope and Daley (2010), is applied to every Helmholtz resonator individually. The generated control action is proportional to a linear combination of the Helmholtz displacement x_{r_i} and the displacements of the neighboring transmission line elements x_i's. This approach enables the simultaneous control of the effective mass and stiffness of the *AAMM* with multiple control actuators. Hence, the control actions $\boldsymbol{f_{i_{ci}}}$ such that:

i. The controlled force applied on the *first* connected Helmholtz resonator, $f_{i_{c1}}$:

$$\boldsymbol{f}_{i_{c1}} = (k_{c1} + sc_{c1})(2X_{i_{r1}} - X_{i+1} - X_{i-1}) \tag{5.4}$$

ii. The controlled force applied on the *second* connected Helmholtz resonator, $f_{i_{c2}}$:

$$\boldsymbol{f}_{i_{c2}} = (k_{c2} + sc_{c2})(2X_{i_{r2}} - X_{i+1} - X_{i-1}) \tag{5.5}$$

<u>The equivalent lumped-parameter system:</u>

Combining eqs. (5.4), and (5.2) gives:

$$\begin{aligned} &m_{r1}s^2X_{i_{r1}} + (k_{r1} + sc_{r1})\big(X_{i_{r1}} - X_i\big) + \\ &(k_{c1} + sc_{c1})\big(2X_{i_{r1}} - X_{i+1} - X_{i-1}\big) = 0 \end{aligned} \tag{5.6}$$

This yields to:

$$X_{r1} = \frac{(k_{r1}+s\,c_{r1})X_i-(k_{c1}+s\,C_{c1})(-X_{i+1}-X_{i-1})}{[m_{r1}\,s^2+(k_{r1}+s\,c_{r1})+2(k_{c1}+s\,c_{c1})]} \tag{5.7}$$

Also, combining eqs. (5.5), and (5.3) gives:

$$X_{r2} = \frac{(k_{r2}+s\,c_{r2})\,X_i-(k_{c2}+s\,c_{c2})(-X_{i+1}-X_{i-1})}{[m_{r2}\,s^2+(k_{r2}+s\,c_{r2})+2(k_{c2}+s\,c_{c2})]} \tag{5.8}$$

Substituting eqs. (5.7), and (5.8) into eq. (5.1), gives

$$m\,s^2\,X_i + (k + s\,c)(2X_i - X_{i+1} - X_{i-1}) + [(k_{r1} + s\,c_{r1}) + (k_{r2} + s\,c_{r2})]X_i$$

$$- \frac{(k_{r1} + s\, c_{r1})^2 X_i - (k_{r1} + s\, c_{r1})(k_{c1} + s\, c_{c1})(-X_{i+1} - X_{i-1})}{[m_{r1}\, s^2 + (k_{r1} + s\, c_{r1}) + 2(k_{c1} + s\, c_{c1})]}$$

$$- \frac{(k_{r2}+s\, c_{r2})^2\, X_i - (k_{r2}+s\, c_{r2})(k_{c2}+s\, c_{c2})(-X_{i+1}-X_{i-1})}{[m_{r2}\, s^2+(k_{r2}+s\, c_{r2})+2(k_{c2}+s\, c_{c2})]} = 0 \qquad (5.9)$$

Let:

$$a_1 = [m_{r1}\, s^2 + (k_{r1} + s\, c_{r1}) + 2(k_{c1} + s\, c_{c1})]$$

Also,

$$a_2 = [m_{r2}\, s^2 + (k_{r2} + s\, c_{r2}) + 2(k_{c2} + s\, c_{c2})] \qquad (5.10)$$

Finally, eq. (5.9) reduces to:

$$\left[m + \frac{m_{r1}a_2(k_{r1} + s\, c_{r1}) + m_{r2}a_1(k_{r2} + s\, c_{r2})}{a_1 a_2}\right] s^2\, X_i$$

$$+ \left[k + s\, c + \frac{a_2(k_{r1} + s\, c_{r1})\,(k_{c1} + s\, c_{c1}) + a_1(k_{r2} + s\, c_{r2})(k_{c2} + s\, c_{c2})}{a_1 a_2}\right] \times$$

$$(2X_i - X_{i+1} - X_{i-1}) = 0 \qquad (5.11)$$

The equivalent lumped-parameter system equation of motion reduces to:

$$m_e\, s^2\, X_i + (k_e + s\, c_e)(2X_i - X_{i+1} - X_{i-1}) = F_i \qquad (5.12)$$

where:

The effective mass of the equivalent-system:

$$m_e = m + \frac{m_{r1}a_2(k_{r1} + s\, c_{r1}) + m_{r2}a_1(k_{r2} + s\, c_{r2})}{a_1 a_2}$$

$$= m_{e_{REAL}} + i\, m_{e_{IMAG}} \tag{5.13}$$

where:

$$m_{e_{REAL}} = m + \boldsymbol{real}\big(G_M(s)\big) \quad , \quad m_{e_{IMAG}} = \boldsymbol{imag}\big(G_M(s)\big)$$

$$G_M(s) = \frac{m_{r1}a_2(k_{r1}+s\,c_{r1}) + m_{r2}a_1(k_{r2}+s\,c_{r2})}{a_1 a_2},$$

and $\quad s = i\,\omega \tag{5.14}$

The effective stiffness of the equivalent-system:

$$k_e = k + \boldsymbol{real}\big(G_k(s)\big) \tag{5.15}$$

where:

$$G_k(s) = \frac{a_2(k_{r1}+s\,c_{r1})\,(k_{c1}+s\,c_{c1}) + a_1(k_{r2}+s\,c_{r2})(k_{c2}+s\,c_{c2})}{a_1 a_2} \tag{5.16}$$

The effective damping of the equivalent-system:

$$c_e = c + \frac{\boldsymbol{imag}\big(G_k(i\omega)\big)}{\omega} \tag{5.17}$$

Then, the equation of motion of the equivalent system is given by:

$$m_e\, s^2 X_i - (k_e + s\, c_e)\,(X_{i-1} + X_{i+1} - 2X_i) = F_i \tag{5.18}$$

Eq. (5.18) can be described in the frequency as follows:

$$-\big(m_{e_{REAL}} + i\, m_{e_{IMAG}}\big)\,\omega^2 X_i - (k_e + i\omega\, c_e)\,(X_{i-1} + X_{i+1} - 2X_i) = F_i$$

or

$$-\big(M_{e_{REAL}} + i\, M_{e_{IMAG}}\big)\,\omega^2 X_i + 2\,(K_e + i\,\omega\, C_e)\,X_i =$$

$$\underbrace{F_i + (K_e + i\,\omega\,C_e)(X_{i-1} + X_{i+1})}_{F_T}$$

This leads to:

$$-m_{e_{REAL}}\,\omega^2 X_i + i\omega\left(2\,c_e - \omega\,m_{e_{IMAG}}\right)X_i + 2k_e\,X_i = F_T \qquad (5.19)$$

Eq. (4.20) can be rewritten as:

$$-m_{e_m}\omega^2 X_i + i\omega\,c_{e_m}X_i + k_{e_m}X_i = F_T \qquad (5.20)$$

where:

$$m_{e_m} = m_{e_{REAL}} \qquad (5.21)$$

$$c_{e_m} = 2\,c_e - \omega\,m_{e_{IMAG}} \qquad (5.22)$$

$$k_{e_m} = 2\,k_e \qquad (5.23)$$

$$F_T = F_i + (k_e + i\,\omega\,c_e)(X_{i-1} + X_{i+1}) \qquad (5.24)$$

5.3.Modeling of the Active Acoustic Metamaterial with Triple Resonators:

Similarly, the procedure in which this section will be conducted is in the same manner as in the previous section 5.2.

a. <u>The equation of motion of the i^{th} transmission element:</u>

Using the Laplace transformation, the equation of motion can be written as:

$$\begin{aligned} &m\,s^2X_i + (k + s\,c)(2X_i - X_{i-1} - X_{i+1}) \\ &\quad +(k_{r1} + sc_{r1})\left(X_i - X_{i_{r1}}\right) \\ &\quad +(k_{r2} + sc_{r2})\left(X_i - X_{i_{r2}}\right) \\ &+(k_{r3} + sc_{r3})\left(X_i - X_{i_{r3}}\right) = F_i \end{aligned} \qquad (5.25)$$

where: F_i : is an applied external force.

b. <u>The equation of motion of the *first* Helmholtz resonant mass m_1:</u>

In the Laplace domain:

$$m_{r1}s^2X_{i_{r1}} + (k_{r1} + sc_{r1})\left(X_{i_{r1}} - X_i\right) = \boldsymbol{f}_{i_{c1}} \quad (5.26)$$

c. <u>The equation of motion of the *second* Helmholtz resonant mass m_2:</u>

In the Laplace domain:

$$m_{r2}s^2X_{i_{r2}} + (k_{r2} + sc_{r2})\left(X_{i_{r2}} - X_i\right) = \boldsymbol{f}_{i_{c2}} \quad (5.27)$$

d. <u>The equation of motion of the *third* Helmholtz resonant mass m_2:</u>

In the Laplace domain:

$$m_{r3}s^2X_{i_{r3}} + (k_{r3} + sc_{r3})\left(X_{i_{r3}} - X_i\right) = \boldsymbol{f}_{i_{c3}} \quad (5.28)$$

e. <u>The control action</u>:

In this chapter, the control action $\boldsymbol{f}_{\boldsymbol{i_{ci}}}$ is applied to every Helmholtz resonator individually, as used by Pope and Daley (2010). The generated control action is proportional to a linear combination of the Helmholtz displacement x_{r_i} and the displacements of the neighboring transmission line elements x_i's. This approach enables the simultaneous control of the effective mass and stiffness of the *AAMM* with multiple control actuators. Hence, the control actions $\boldsymbol{f}_{\boldsymbol{i_{ci}}}$ such that:

i. The controlled force applied on the *first* connected Helmholtz resonator, $f_{i_{c1}}$:

$$\boldsymbol{f}_{i_{c1}} = (k_{c1} + sc_{c1})(2X_{i_{r1}} - X_{i+1} - X_{i-1}) \quad (5.29)$$

ii. The controlled force applied on the *second* connected Helmholtz resonator, $f_{i_{c2}}$:

$$\boldsymbol{f}_{i_{c2}} = (k_{c2} + sc_{c2})(2X_{i_{r2}} - X_{i+1} - X_{i-1}) \quad (5.30)$$

iii. The controlled force applied on the *third* connected Helmholtz resonator, $f_{i_{c3}}$:

$$\boldsymbol{f}_{i_{c3}} = (k_{c3} + sc_{c3})(2X_{i_{r3}} - X_{i+1} - X_{i-1}) \quad (5.31)$$

The equivalent lumped-parameter system:

Combining eqs. (5.29), and (5.26) gives:

$$m_{r1}s^2X_{i_{r1}} + (k_{r1} + sc_{r1})\left(X_{i_{r1}} - X_i\right) + (k_{c1} + sc_{c1})\left(2X_{i_{r1}} - X_{i+1} - X_{i-1}\right) = 0 \quad (5.32)$$

This yields to:

$$X_{r1} = \frac{(k_{r1}+s\,c_{r1})X_i-(k_{c1}+s\,C_{c1})(-X_{i+1}-X_{i-1})}{[m_{r1}\,s^2+(k_{r1}+s\,c_{r1})+2(k_{c1}+s\,c_{c1})]} \quad (5.33)$$

Also, Combining eqs. (5.30), and (5.27) gives:

$$X_{r2} = \frac{(k_{r2}+s\,c_{r2})\,X_i-(k_{c2}+s\,c_{c2})(-X_{i+1}-X_{i-1})}{[m_{r2}\,s^2+(k_{r2}+s\,c_{r2})+2(k_{c2}+s\,c_{c2})]} \quad (5.34)$$

And, Combining eqs. (5.31), and (5.28) gives:

$$X_{r3} = \frac{(k_{r3}+s\,c_{r3})\,X_i-(k_{c3}+s\,c_{c3})(-X_{i+1}-X_{i-1})}{[m_{r3}\,s^2+(k_{r3}+s\,c_{r3})+2(k_{c3}+s\,c_{c3})]} \quad (5.35)$$

Substituting eqs. (5.33), (5.34) and (5.35) into eq. (5. 25), gives

$$m\,s^2\,X_i + (k + s\,c)(2X_i - X_{i+1} - X_{i-1})$$

$$+[(k_{r1} + s\,k_{r1}) + (k_{r2} + s\,c_{r2}) + (k_{r3} + s\,c_{r3})]X_i$$

$$-\frac{(k_{r1} + s\,c_{r1})^2X_i - (k_{r1} + s\,c_{r1})\,(k_{c1} + s\,c_{c1})(-X_{i+1} - X_{i-1})}{[m_{r1}\,s^2 + (K_{r1} + s\,c_{r1}) + 2(K_{c1} + s\,c_{c1})]}$$

$$-\frac{(k_{r2} + s\,c_{r2})^2\,X_i - (k_{r2} + s\,c_{r2})(k_{c2} + s\,c_{c2})(-X_{i+1} - X_{i-1})}{[m_{r2}\,s^2 + (k_{r2} + s\,c_{r2}) + 2(k_{c2} + s\,c_{c2})]}$$

$$-\frac{(k_{r3}+s\,c_{r3})^2\,X_i-(k_{r3}+s\,c_{r3})(k_{c3}+s\,c_{c3})(-X_{i+1}-X_{i-1})}{[m_{r3}\,s^2+(k_{r3}+s\,c_{r3})+2(k_{c3}+s\,c_{c3})]} = 0 \quad (5.36)$$

Let:

$$a_1 = [m_{r1}\,s^2 + (K_{r1} + s\,c_{r1}) + 2(K_{c1} + s\,c_{c1})]$$

Also,

$$a_2 = [m_{r2}\, s^2 + (k_{r2} + s\, c_{r2}) + 2(k_{c2} + s\, c_{c2})]$$

$$a_3 = [m_{r3}\, s^2 + (k_{r3} + s\, c_{r3}) + 2(k_{c3} + s\, c_{c3})]$$

Eq.(5.36) reduces to:

$$\begin{bmatrix} m \\ +\frac{m_{r1} a_2\, a_3 (k_{r1} + s\, c_{r1})}{a_1\, a_2\, a_3} \\ +\frac{m_{r2} a_1\, a_3 (k_{r2} + s\, c_{r2})}{a_1\, a_2\, a_3} \\ +\frac{m_{r3} a_1\, a_2 (k_{r3} + s\, c_{r3})}{a_1\, a_2\, a_3} \end{bmatrix} s^2\, X_i$$

$$+ \begin{bmatrix} (k + s\, c) \\ +\frac{a_1 a_2 (k_{r3} + s\, c_{r3})(k_{c3} + s\, c_{c3})}{a_1\, a_2\, a_3} \\ +\frac{a_3 a_2 (k_{r1} + s\, c_{r1})\,(k_{c1} + s\, c_{c1})}{a_1\, a_2\, a_3} \\ +\frac{a_3 a_1 (k_{r2} + s\, c_{r2})(k_{c2} + s\, c_{c2})}{a_1\, a_2\, a_3} \end{bmatrix} (2X_i - X_{i+1} - X_{i-1}) = 0 \qquad (5.37)$$

The equivalent lumped-parameter system equation of motion reduces to:

$$m_e\, s^2\, X_i + (k_e + s\, c_e)(2X_i - X_{i+1} - X_{i-1}) = F_i \qquad (5.38)$$

where:

The effective mass of the equivalent-system:

$$m_e = m + \frac{m_{r1} a_2\, a_3 (k_{r1} + s\, c_{r1})}{a_1\, a_2\, a_3} + \frac{m_{r2} a_1\, a_3 (k_{r2} + s\, c_{r2})}{a_1\, a_2\, a_3} + \frac{m_{r3} a_1\, a_2 (k_{r3} + s\, c_{r3})}{a_1\, a_2\, a_3}$$

$$= m_{e_{REAL}} + i\, m_{e_{IMAG}} \qquad (5.39)$$

$where$:

$$m_{e_{REAL}} = m + \boldsymbol{real}\big(G_M(s)\big) \quad , \quad m_{e_{IMAG}} = \boldsymbol{imag}\big(G_M(s)\big)$$

$$G_M(s) = \frac{m_{r1}a_2\,a_3(k_{r1}+s\,c_{r1})+m_{r2}a_1\,a_3(k_{r2}+s\,c_{r2})+m_{r3}a_1\,a_2(k_{r3}+s\,c_{r3})}{a_1\,a_2\,a_3},$$

and $\quad s = i\,\omega$ (5.40)

The effective stiffness of the equivalent-system:

$$k_e = k + \boldsymbol{real}\big(G_k(s)\big) \tag{5.41}$$

where:

$$G_k(s) = \frac{a_1a_2(k_{r3}+s\,c_{r3})(k_{c3}+s\,c_{c3})}{a_1\,a_2\,a_3} + \frac{a_3a_2(k_{r1}+s\,c_{r1})\,(k_{c1}+s\,c_{c1})}{a_1\,a_2\,a_3} + \frac{a_3a_1(k_{r2}+s\,c_{r2})(k_{c2}+s\,c_{c2})}{a_1\,a_2\,a_3} \tag{5.42}$$

The effective damping of the equivalent-system:

$$c_e = c\ + \frac{\boldsymbol{imag}\big(G_k(i\omega)\big)}{\omega} \tag{5.43}$$

Then, the equation of motion of the equivalent system is given by:

$$m_e\,s^2X_i - (k_e + s\,c_e)\,(X_{i-1} + X_{i+1} - 2X_i) = F_i \tag{5.44}$$

Eq. (5.18) can be described in the frequency as follows:

$$-\big(m_{e_{REAL}} + i\,m_{e_{IMAG}}\big)\,\omega^2X_i - (k_e + i\omega\,c_e)\,(X_{i-1} + X_{i+1} - 2X_i) = F_i$$

or

$$-\big(M_{e_{REAL}} + i\,M_{e_{IMAG}}\big)\,\omega^2X_i + 2\,(K_e + i\,\omega\,C_e)\,X_i =$$

$$\underbrace{F_i + (K_e + i\,\omega\,C_e)(X_{i-1} + X_{i+1})}_{F_T}$$

This leads to:

$$-m_{e_{REAL}}\,\omega^2 X_i + i\omega\left(2\,c_e - \omega\, m_{e_{IMAG}}\right) X_i + 2k_e\, X_i = F_T \qquad (5.45)$$

Eq. (4.20) can be rewritten as:

$$-m_{e_m}\omega^2 X_i + i\omega\, c_{e_m} X_i + k_{e_m} X_i = F_T \qquad (5.46)$$

where:

$$m_{e_m} = m_{e_{REAL}} \qquad (5.47)$$

$$c_{e_m} = 2\,c_e - \omega\, m_{e_{IMAG}} \qquad (5.48)$$

$$k_{e_m} = 2\,k_e \qquad (5.49)$$

$$F_T = F_i + (k_e + i\,\omega\, c_e)(X_{i-1} + X_{i+1}) \qquad (5.50)$$

5.4. Numerical Examples and Discussions:

a. Performance of The Active Acoustic Metamaterial with Multi-Double Halmholtz resonators:

Consider the active acoustic metamaterial with multi-double Helmholtz resonators. The system has the physical parameters listed in Table 5.1 for a high frequency case and in Table 5.2 for the low frequency case. The metamaterial is excited at node 1 at the beginning of the transmission line with a swept sine wave and the response is monitored at node 4 at the end of the transmission line.

Table 5.1 Physical parameters of the active acoustic metamaterial with Multi-Double Helmholtz resonators for the High frequency case

Parameter	m (*kg*)	k (*N/m*)	c (*Ns/m*)	m_r (*kg*)	k_r (*N/m*)	c_r (*Ns/m*)	k_c (*N/m*)	c_c (*Ns/m*)	*No. of Cells*
Values	**0.01**	**2000**	**0.1**	**11**	**1500**	**0.002**	**150000**	**40**	**4**

Parameter	m_{r1} (*kg*)	k_{r1} (*N/m*)	c_{r1} (*Ns/m*)	k_{c1} (*N/m*)	c_{c1} (*Ns/m*)
Values	**1**	**1500**	**0.002**	**150000**	**40**

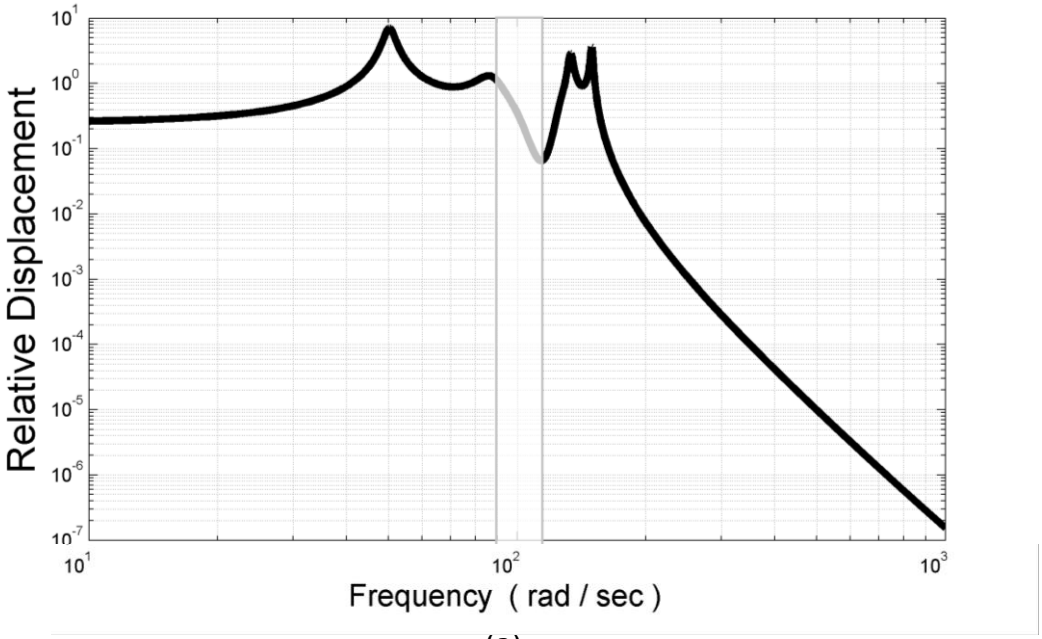

(a)

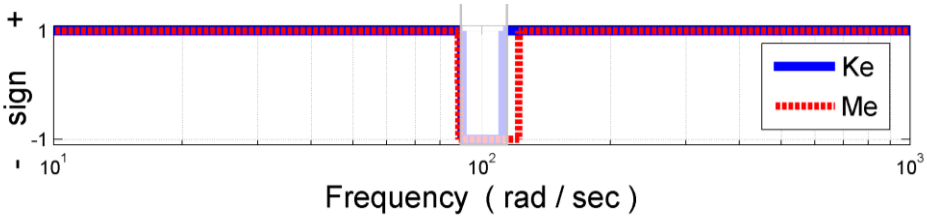

(b)

Fig. 5.4: The frequency response (a) and sign of the effective mass and stiffness (b) for an *AAMM* with double Helmholtz resonators and *PD* controller at high frequency

Fig. 5.4a displays the frequency response of the magnitude of the transfer function $|X_4/X_1|$. Fig. 5.4b shows the sign of the effective mass m_e and stiffness k_e of the metamaterial array. It can be easily seen that between 90-120 *rad/s*, the metamaterial array exhibits negative effective mass whereas its effective stiffness has a negative value over a narrower band between 90-110 *rad/s*. Therefore, using double Helmholtz resonators results in simultaneous double negative properties in the frequency range 90-110 *rad/s*.

Fig. 5.5 displays the corresponding characteristics for a single Helmholtz resonator for comparison purposes.

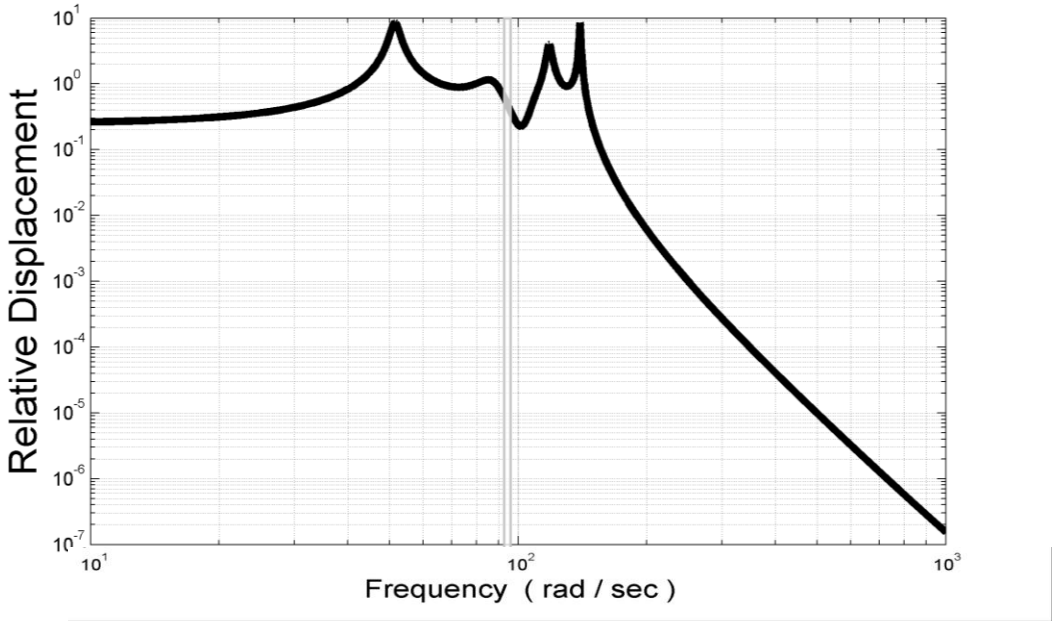

(a)

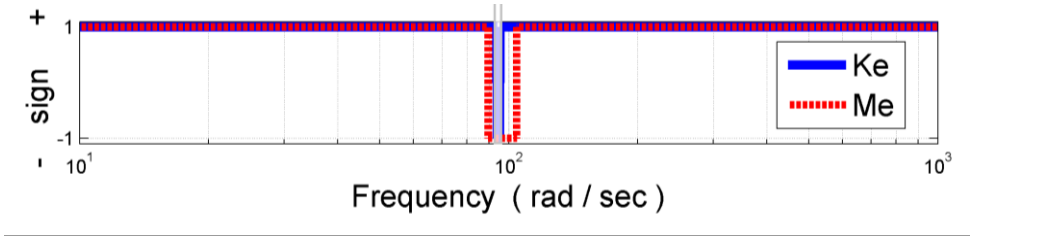

(b)

Fig. 5.5: The frequency response (a) and sign of the effective mass and stiffness (b) for an *AAMM* with single Helmholtz resonator and *PD* controller at high frequency

The figures indicate an improvement of the width of the double negative zone to be 20 *rad/s* with double Helmholtz resonators as compared to that obtained with single resonator which resulted only in 5 *rad/s* zone.

Table 5.2 Physical parameters of the active acoustic metamaterial with Multi-Double Helmholtz resonators for the Low frequency case

Parameter	m (*kg*)	k (*N/m*)	c (*Ns/m*)	m_r (*kg*)	k_r (*N/m*)	c_r (*Ns/m*)	k_c (*N/m*)	c_c (*Ns/m*)	*No. of Cells*
Values	**0.01**	**3000**	**0.1**	**0.1**	**1000**	**0.002**	**2100**	**0.1**	**4**

Parameter	m_{r1} (*kg*)	k_{r1} (*N/m*)	c_{r1} (*Ns/m*)	k_{c1} (*N/m*)	c_{c1} (*Ns/m*)
Values	**0.1**	**1000**	**0.002**	**2100**	**0.1**

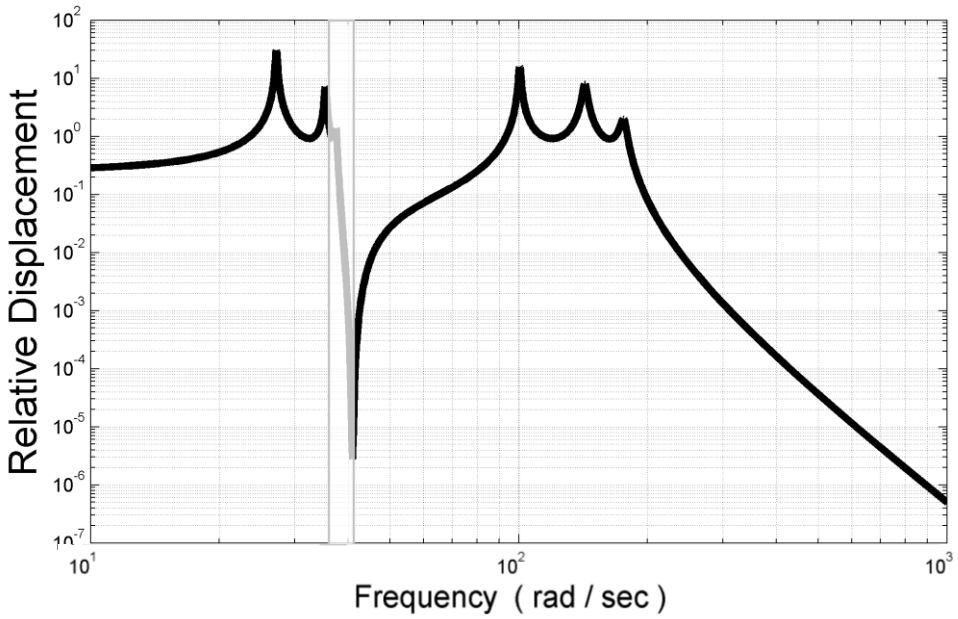

(a)

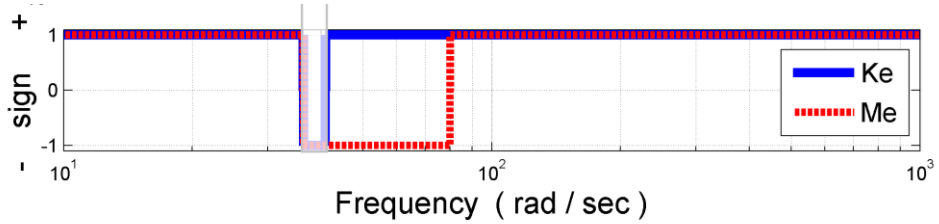

(b)

Fig. 5.6: The frequency response (a) and sign of the effective mass and stiffness (b) for an *AAMM* with double resonators and *PD* controller at low frequency

Fig. 5.6a displays the frequency response of the magnitude of the transfer function $|X_4/X_1|$. Fig. 5.6b shows the sign of the effective mass m_e and stiffness k_e of the metamaterial array. It can be easily seen that between 35-80 *rad/s*, the metamaterial array exhibits negative effective mass whereas its effective stiffness has a negative value over a narrower band between 35-40 *rad/s*. Therefore, *AAMM* with double resonators results in simultaneous double negative properties in the frequency range 35-40 *rad/s*.

Fig. 5.7 displays the corresponding characteristics for a single Helmholtz resonator for comparison purposes.

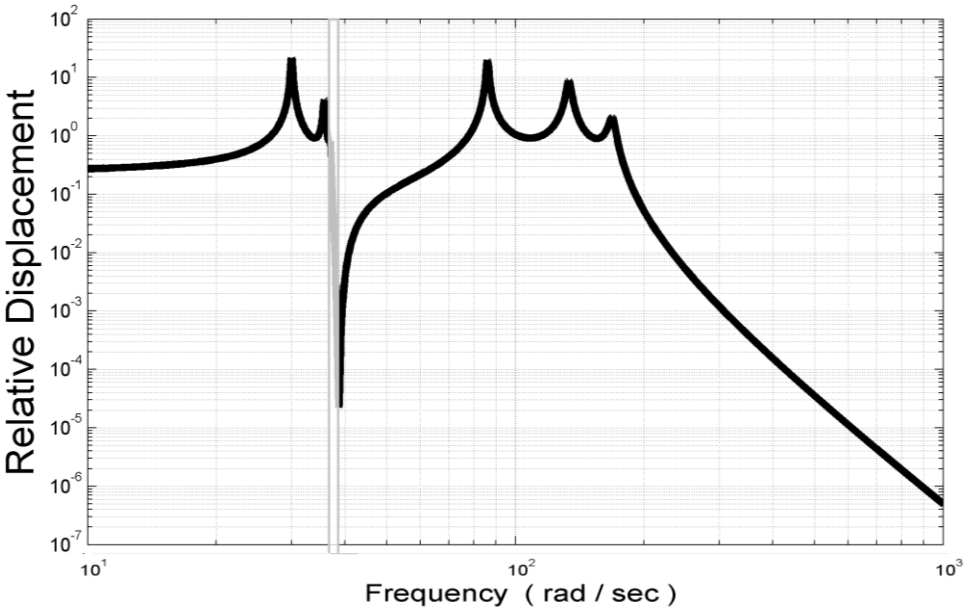

(a)

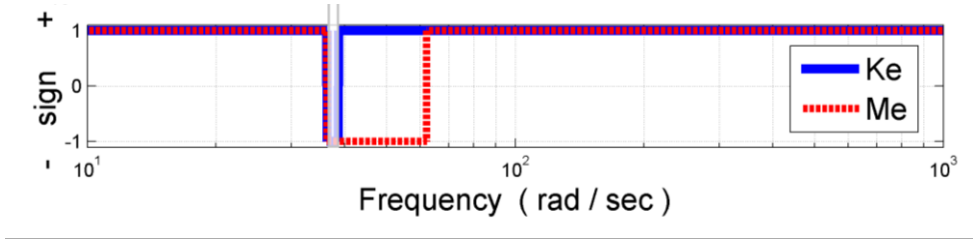

(b)

Fig. 5.7: The frequency response (a) and sign of the effective mass and stiffness (b) for an *AAMM* with single Helmholtz resonator and *PD* controller at low frequency

The figures indicate an improvement of the width of the double negative zone to be 5 *rad/s* with double Helmholtz resonators as compared to that obtained with single resonator which resulted only in 2 *rad/s* zone.

b. Performance of The Active Acoustic Metamaterial with Multi-Triple Halmholtz resonators:

This system has the same physical parameters listed in Table 5.1 for the high frequency case, and in Table 5.2 for the low frequency case. The additional physical parameters due to the extra Helmholtz resonator are matching the other resonator's parameters, see Table 5.3. The metamaterial is excited at node 1 at the beginning of the transmission line with a swept sine wave and the response is monitored at node 4 at the end of the transmission line.

Table 5.3 Additional Physical parameters of the active acoustic metamaterial with Triple Helmholtz resonators due to the third resonator

(a) - High frequency case:

Parameter	m_{r2} (*kg*)	k_{r2} (*N/m*)	c_{r2} (*Ns/m*)	k_{c2} (*N/m*)	c_{c2} (*Ns/m*)
Values	1	1500	0.002	150000	40

(b) - Low frequency case:

Parameter	m_{r2} (*kg*)	k_{r2} (*N/m*)	c_{r2} (*Ns/m*)	k_{c2} (*N/m*)	c_{c2} (*Ns/m*)
Values	0.1	1000	0.002	2100	0.1

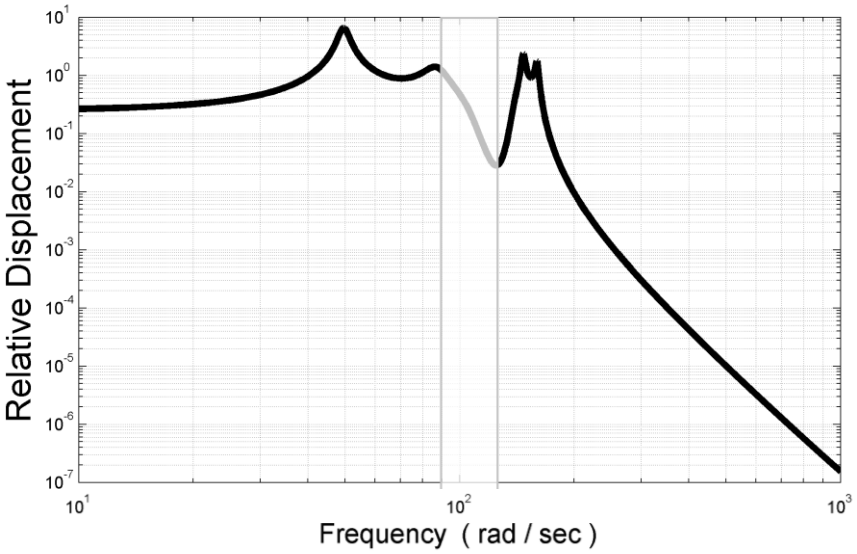

(a)

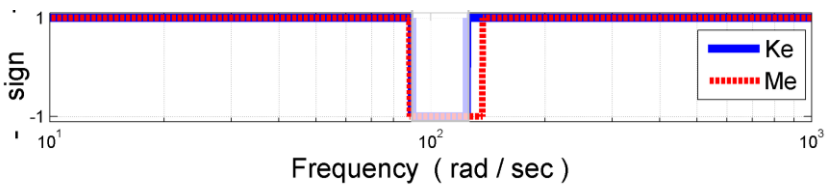

(b)

Fig. 5.8: The frequency response (a) and sign of the effective mass and stiffness (b) for an *AAMM* with triple Helmholtz resonators and *PD* controller at high frequency

Fig. 5.8a displays the frequency response of the magnitude of the transfer function $|X_4/X_1|$. Fig. 5.8b shows the sign of the effective mass m_e and stiffness k_e of the metamaterial array. It can be easily seen that between 90-150 *rad/s*, the metamaterial array exhibits negative effective mass whereas its effective stiffness has a negative value over a narrower band between 90-130 *rad/s*. Therefore, the configuration with triple Helmholtz resonators results in simultaneous double negative properties in the frequency range 90-130 *rad/s*.

The figure indicates an improvement of the width of the double negative zone to be 40 *rad/s* for the case of triple Helmholtz resonators as compared to that obtained from double Helmholtz resonators which resulted only in 30 *rad/s* zone as shown in

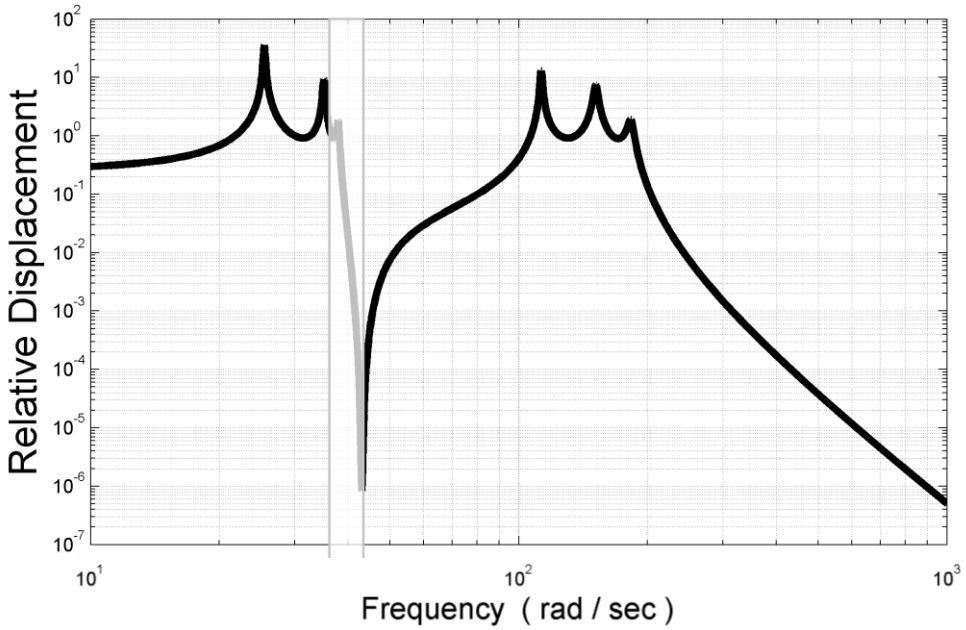

(a)

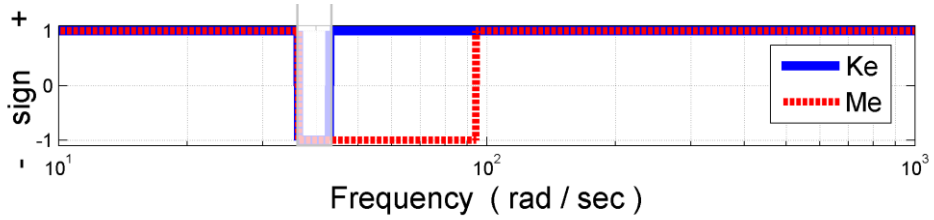

(b)

Fig. 5.9: The frequency response (a) and sign of the effective mass and stiffness (b) for an *AAMM* with triple Helmholtz resonators and *PD* controller at low frequency

Fig. 5.10a displays the frequency response of the magnitude of the transfer function $|X_4/X_1|$. Fig. 5.10b shows the sign of the effective mass m_e and stiffness k_e of the metamaterial array. It can be easily seen that between 35-95 *rad/s*, the metamaterial array exhibits negative effective mass whereas its effective stiffness has a negative value over a narrower band between 35-43 *rad/s*. Therefore, configuration with triple Helmholtz resonators results in simultaneous double negative properties in the frequency range 35-43 *rad/s*.

The figure indicates an improvement of the width of the double negative zone to be 8 *rad/s* for the case of triple Helmholtz resonators as compared to that obtained from the double Helmholtz resonators which resulted only in 5 *rad/s* zone as shown in Fig. 5.7.

5.5. Summary

This chapter has presented *AAMM* configurations consisting of multiple Helmholtz resonators (*MHR*) which are evenly distributed along the circumference of the unit cell. These multiple sets are intended as means for increasing the width of the double negative properties zones. Emphasis is placed in this chapter on using *MHR* with double and triple Helmholtz resonators.

It is shown that increasing the number of the *MHR* associated with each transmission element results in considerable improvement of the width of the double negative properties zones.

6.1. Overview

In this chapter, another configuration of the *AAMM* is presented. The prototype of the *AAMM* unit cell has been provided with transmission line control capabilities. These capabilities can be easily seen by considering Fig. 6.1. In particular, the *AAMM* consists of arrays of transmission line cavities that are separated by and provided with piezoelectric boundaries. These boundaries control the stiffness of the individual cavity and in turn control its dynamical density and bulk modulus. Connected to these transmission line cavities are a set of Helmholtz resonators which have passive flexible boundaries. With such control capabilities, it would be possible to evaluate the effectiveness and merits of controlling the acoustic properties through the transmission line piezo-boundaries.

Fig. 6.2 shows a schematic drawing of the equivalent lumped-parameter model of the experimental *AAMM* with transmission line control boundaries.

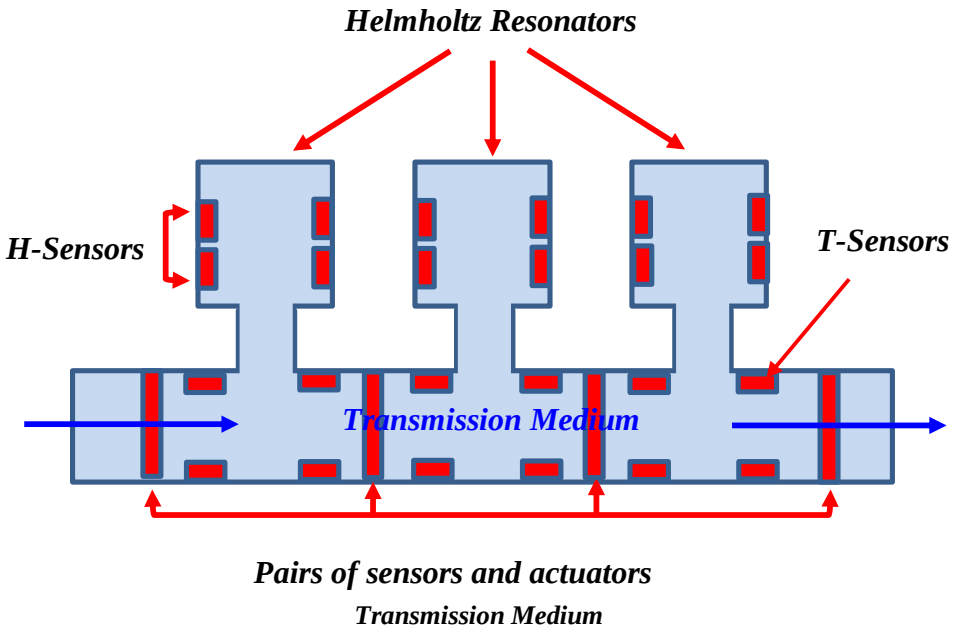

Fig. 6.1 - Active acoustic metamaterial with transmission line control boundaries

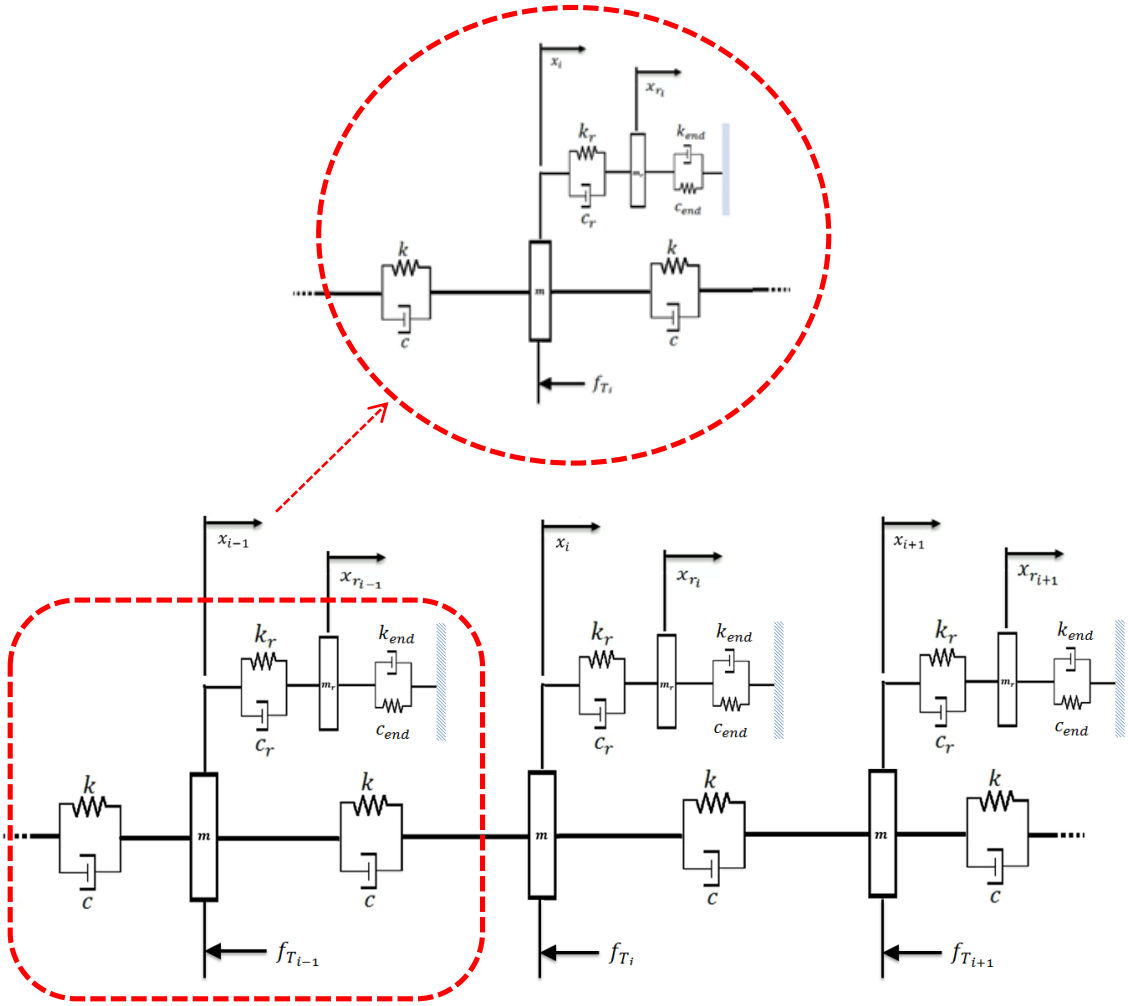

Fig. 6.2 - Lumped-parameter model of the active acoustic metamaterial with transmission line control boundaries

6.2. Concept of the Active Acoustic Metamaterial with Transmission Line Control Boundaries:

6.2.1 The Structure of the Metamaterial *AAMM/TC*:

The *AAMM/TC* system in its bulk form is consisting of array of Helmholtz resonators which are spatially distributed and connected to a wave carrying medium. The carrying medium, transmission line, has been separated and provided with active piezoelectric boundaries as shown in Fig. 6.1.

In this design two different control configurations have been implemented in the *AAMM/TC*. In this *AAMM/TC,* the Helmholtz cavity is represented by a spring k_{end} and damper c_{end} which are the characteristics of the flexible diaphragm in the back of the Helmholtz cavity. The control action design introduced by Pope and Daley (2010) influences the control action designs proposed in this chapter with different active gains and motion combinations.

In the first configuration and specially in the control action applied directly to the transmission line $\boldsymbol{f_T}$, the controller is proportional to a linear combination of the transmission line mass displacement, X_i, of the unit cell in addition to the other adjacent transmission line masses before, X_{i-1}, and after, X_{i+1}, as $f_T = (k_T + s\,c_T)(2X_{\boldsymbol{i}} - X_{i+1} - X_{i-1})$ where k_T and c_T are the active transmission spring and damper gains.

In the second control action configuration, however, the linear combination that carries the information of motion of the system has been toggled to count for the motion of the attached Helmholtz resonator, X_r, replacing the displacement of transmission mass of the unit cell, X_i. Similarly as in the control action introduced by Pope and Daley (2010). While keeping on the adjacent transmission masses, $X_{i-1}\ and\ X_{i-1}$, the second configuration of the control action is given as $f_T = (k_T + s\,c_T)(2X_{\boldsymbol{r}} - X_{i+1} - X_{i-1})$ where k_T and c_T are the active transmission gains.

6.2.2 Structure of the *AAMM/TC* with Control Configuration 1:

In this configuration, the control force, $\boldsymbol{f_T}$, is applied directly to the transmission line mass. The controller in $\boldsymbol{f_T}$ is proportional to a linear combination of the transmission line mass displacement, X_i, of the unit cell and to the other adjacent transmission line masses before, X_{i-1}, and after, X_{i+1}. The control action applied to the transmission line in this configuration is given as $f_T = (k_T + s\,c_T)(2X_{\boldsymbol{i}} - X_{i+1} - X_{i-1})$, where k_T and c_T are the active transmission spring and damper gains.

6.2.3 Modeling of the *AAMM/TC* with Control Configuration 1:

The dynamics of the lumped-parameter system is developed by writing the equation of motion of a unit cell consisting of a Helmholtz resonator and the transmission line element ***i*** as follows:

a. The equation of motion of the i^{th} transmission element:

Using the Laplace transformation, the equation of motion can be written as:

$$m\,s^2X_i + (k + s\,c)(2X_i - X_{i+1} - X_{i-1}) + (k_r + s\,c_r)(X_i - X_r) + f_T = 0 \quad (6.1)$$

As

$$f_T = (k_T + s\,c_T)(2X_{\boldsymbol{i}} - X_{i+1} - X_{i-1}) \quad (6.2)$$

Then,

$$m\,s^2X_i + (k + s\,c)(2X_i - X_{i+1} - X_{i-1}) + (k_r + s\,c_r)(X_i - X_r) + (k_T + s\,c_T)(2X_i - X_{i+1} - X_{i-1}) = 0 \quad (6.3)$$

b. The equation of motion of the Helmholtz Resonant Mass m_r:

Similarly, in the Laplace domain, the equation of motion is written as:

$$m_r s^2X_r + (k_r + s\,c_r)(X_r - X_i) + (k_{end} + s\,c_{end})X_r = 0 \quad (6.4)$$

Eq. (6.4) can be rewritten as:

$$[m_r s^2 + (k_r + s\,c_r) + (k_{end} + s\,c_{end})]\,X_r - (k_r + s\,c_r)X_i = 0 \quad (6.5)$$

This leads to:

$$X_r = \frac{(k_r + s\,c_r)}{[m_r s^2 + (k_r + s\,c_r) + (k_{end} + s\,c_{end})]}\,X_i \quad (6.6)$$

Substituting for X_r into the transmission mass's eq. (6.3):

$$m\,s^2X_i + (k + s\,c)(2X_i - X_{i+1} - X_{i-1}) + (k_r + s\,c_r)\left(X_i - \frac{(k_r+s\,c_r)}{[m_rs^2+(k_r+s\,c_r)+(k_{end}+s\,c_{end})]}\,X_i\right) + (k_T + s\,c_T)(2X_i - X_{i-1} - X_{i+1}) = 0 \quad (6.7)$$

Or

$$\left\{m + \frac{m_r(k_r + s\,c_r)}{m_rs^2 + (k_r + s\,c_r) + (k_{end} + s\,c_{end})}\right\} s^2X_i + \left\{k + s\,c + \frac{m_r(k_T + s\,c_T)s^2 + (k_T + s\,c_T)(k_r + s\,c_r) + (k_T + s\,c_T)(k_{end} + s\,c_{end})}{m_rs^2 + (k_r + s\,c_r) + (k_{end} + s\,c_{end})}\right\}(2X_i - X_{i+1} - X_{i-1}) = F_T$$

Where:

$$F_T = \left(\frac{m_r(k_T + s\,c_T)s^2}{m_rs^2 + (k_r + s\,c_r) + (k_{end} + s\,c_{end})}\right)(2X_i - X_{i+1} - X_{i-1}) - \left(\frac{(k_r+s\,c_r)(k_{end}+s\,c_{end})}{m_rs^2+(k_r+s\,c_r)+(k_{end}+s\,c_{end})}\right)X_i \quad (6.8)$$

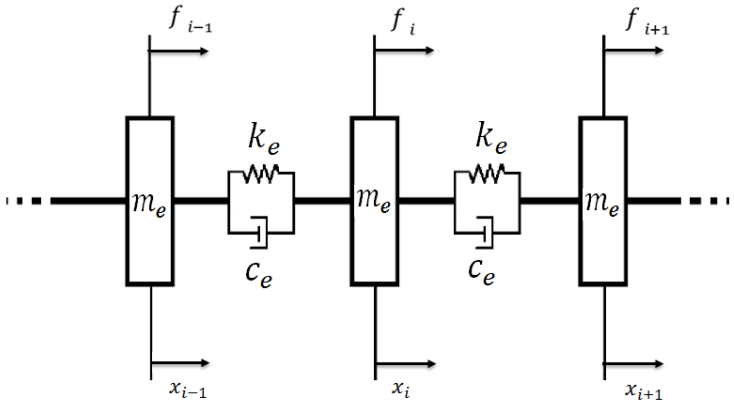

Fig.6.3: Equivalent lumped-parameter system of configuration 1 of the *AAMM/TC*

Eq. (6.10) results in the following equation of motion of the equivalent lumped-parameter system for the control action configuration 1 of the *AAMM/TC* shown in Fig. 6.3.

$$m_e\, s^2 X_i - (k_e + s\, c_e)\,(X_{i-1} + X_{i+1} - 2X_i) = 0 \qquad (6.9)$$

Where:

The effective mass of the equivalent-system:

$$m_e = m + \frac{m_r(k_r + s\, c_r)}{m_r s^2 + (k_r + s\, c_r) + (k_{end} + s\, c_{end})} = m_{e_{REAL}} + i\, m_{e_{IMAG}} \qquad (6.10)$$

where:

$$m_{e_{REAL}} = m + \boldsymbol{real}\big(G_M(s)\big) \quad , \quad m_{e_{IMAG}} = \boldsymbol{imag}\big(G_M(s)\big)$$

$$G_M(s) = \frac{m_r(k_r + s\, c_r)}{m_r s^2 + (k_r + s\, c_r) + (k_{end} + s\, c_{end})}, \quad \text{and} \quad s = i\,\omega \qquad (6.11)$$

The effective stiffness of the equivalent-system:

$$k_e = k + \boldsymbol{real}\big(G_k(s)\big) \qquad (6.12)$$

Where:

$$G_k(s) = \frac{(k_T + s\, c_T)[(k_r + s\, c_r) + (k_{end} + s\, c_{end})]}{m_r s^2 + (k_r + s\, c_r) + (k_{end} + s\, c_{end})} \qquad (6.13)$$

The effective damping of the equivalent-system:

$$c_e = c + \frac{\boldsymbol{imag}\left(G_k(i\omega)\right)}{\omega} \tag{6.14}$$

Eq. (6.9) can be described in the frequency as follows:

$$-\left(m_{e_{REAL}} + i\, m_{e_{IMAG}}\right) \omega^2 X_i - (k_e + i\omega\, c_e)\,(X_{i-1} + X_{i+1} - 2X_i) = F_i$$

or

$$-\left(M_{e_{REAL}} + i\, M_{e_{IMAG}}\right) \omega^2 X_i + 2\,(K_e + i\,\omega\, C_e)\, X_i =$$

$$\underbrace{F_i + (K_e + i\,\omega\, C_e)(X_{i-1} + X_{i+1})}_{F_T}$$

This leads to:

$$-m_{e_{REAL}}\, \omega^2 X_i + i\omega\left(\, 2\, c_e - \,\omega\, m_{e_{IMAG}}\right) X_i \;+\; 2k_e\, X_i = F_T \tag{6.15}$$

Eq. (6.17) can be rewritten as:

$$-\, m_{e_m} \omega^2 X_i + i\omega\, c_{e_m} X_i + k_{e_m} X_i = F_T \tag{6.16}$$

Where:

$$m_{e_m} = m_{e_{REAL}} \tag{6.17}$$

$$c_{e_m} = \, 2\, c_e - \,\omega\, m_{e_{IMAG}} \tag{6.18}$$

$$k_{e_m} = 2\, k_e \tag{6.19}$$

$$F_T = F_i + (k_e + i\,\omega\, c_e)(X_{i-1} + X_{i+1}) \tag{6.20}$$

6.2.7 Numerical Examples and Discussions:

Performance of The Active Acoustic Metamaterial with transmission line control boundaries, control configuration 1 :

Consider the active acoustic metamaterial with transmission line control boundaries. The system has the physical parameters listed in Table 6.1 for a high frequency case, in Table 6.2 for the mid-range frequency case, and Table 6.3 for the high frequency case. The metamaterial is excited at node 1 at the beginning of the transmission line with a swept sine wave and the response is monitored at node 4 at the end of the transmission line.

Table 6.1 Physical parameters of the active acoustic metamaterial with transmission line control boundaries, control configuration 1, for the High frequency case

Parameter	m (kg)	k (N/m)	c (Ns/m)	m_r (kg)	k_r (N/m)	c_r (Ns/m)	k_c (N/m)	c_c (Ns/m)	*No. of Cells*
Values	**0.01**	**2000**	**0.1**	**0.8**	**1000**	**0.002**	**2100**	**0.1**	**4**

Parameter	k_T (N/m)	c_T (Ns/m)	k_{end} (N/m)	c_{end} (Ns/m)
Values	$10k_c$	$0.001c_c$	$100k_r$	$0.001c_r$

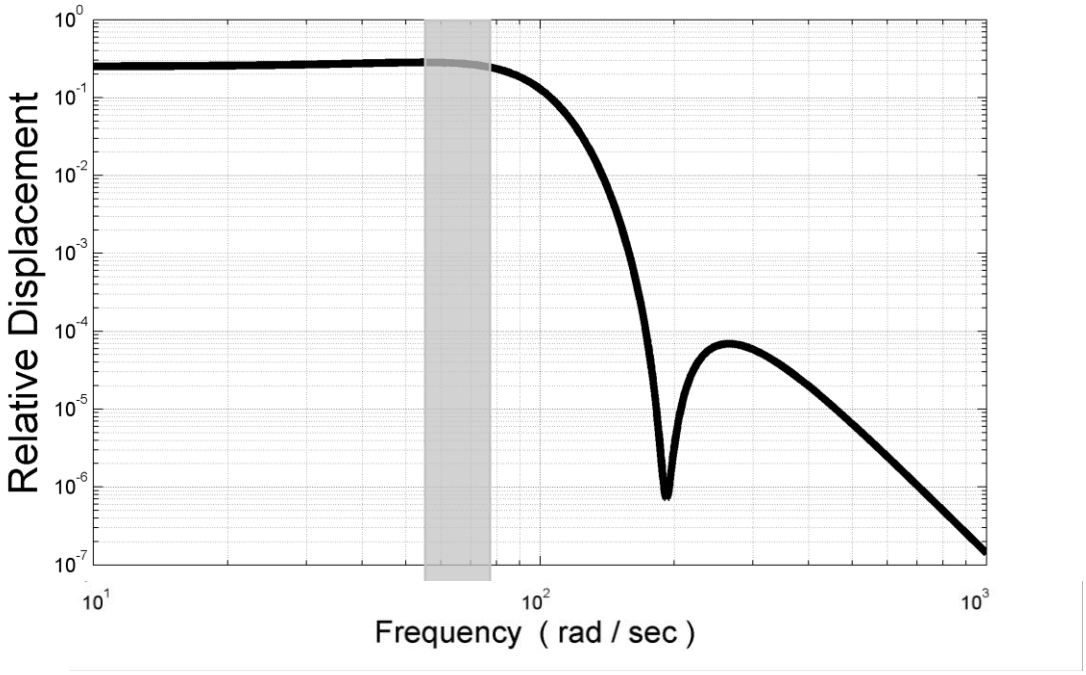

(a)

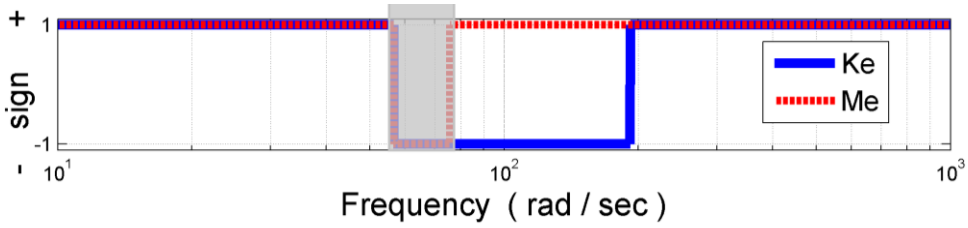

(b)

Fig. 6.4: The frequency response (a) and sign of the effective mass and stiffness (b) for an *AAMM/TC* configuration 1 at high frequency

Fig. 6.4a displays the frequency response of the magnitude of the transfer function $|X_4/X_1|$. Fig. 6.4b shows the sign of the effective mass m_e and stiffness k_e of the metamaterial array. It can be easily seen that between 57-76 *rad/s*, the metamaterial array exhibits negative effective mass whereas its effective stiffness has a negative value near the same band between 57-192 *rad/s*. Therefore, using the *AAMM/TC* resonators results in simultaneous double negative properties in the frequency range 57-76*rad/s*.

Table 6.2 Physical parameters of the active acoustic metamaterial with transmission line control boundaries, control configuration 1, for the mid-range frequency case

Parameter	m (kg)	k (N/m)	c (Ns/m)	m_r (kg)	k_r (N/m)	c_r (Ns/m)	k_c (N/m)	c_c (Ns/m)	*No. of Cells*
Values	0.01	2000	0.1	0.5	1000	0.002	2100	0.1	4

Parameter	k_T (N/m)	c_T (Ns/m)	k_{end} (N/m)	c_{end} (Ns/m)
Values	$10k_c$	$0.001c_c$	$10k_r$	$0.001c_r$

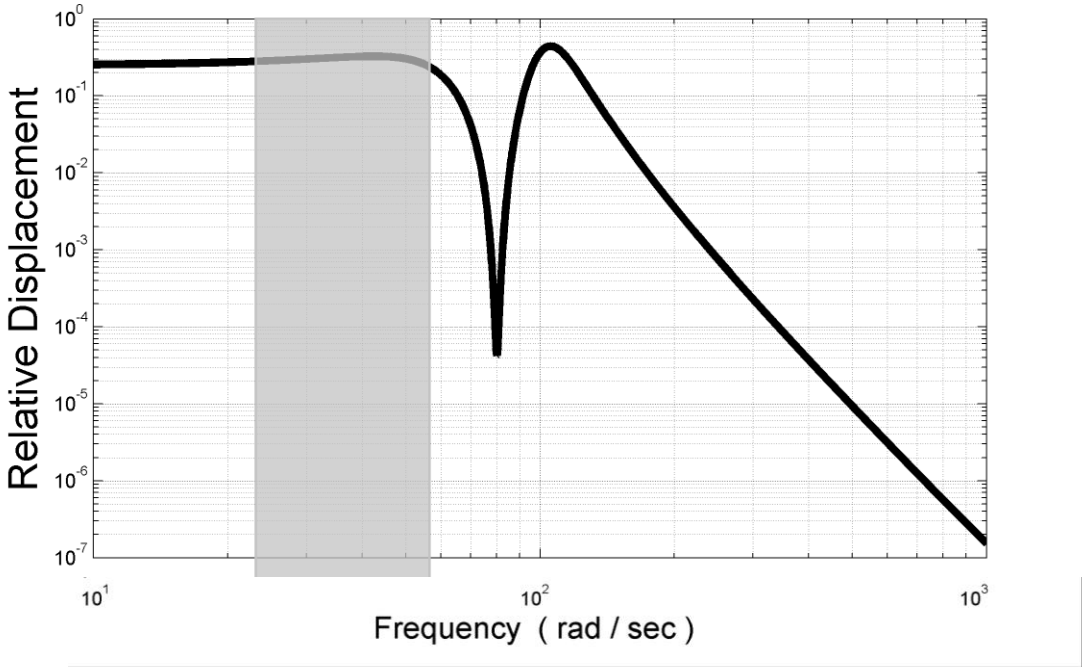

(a)

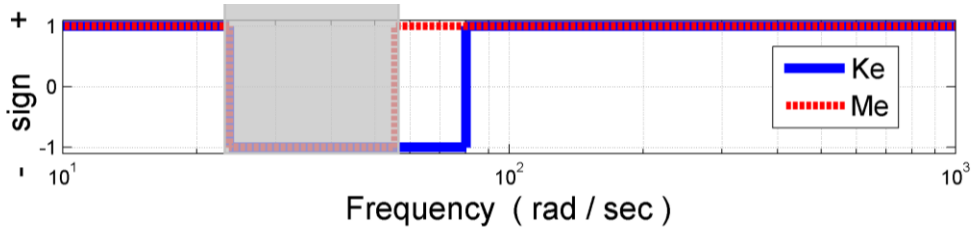

(b)

Fig. 6.5: The frequency response (a) and sign of the effective mass and stiffness (b) for an *AAMM/TC* configuration 1 at mid-range frequency

Table 6.3 Physical parameters of the active acoustic metamaterial with transmission line control boundaries, control configuration 1, for the low frequency case

Parameter	m (kg)	k (N/m)	c (Ns/m)	m_r (kg)	k_r (N/m)	c_r (Ns/m)	k_c (N/m)	c_c (Ns/m)	No. of Cells
Values	0.01	2000	0.1	0.5	1000	0.002	2100	0.1	4

Parameter	k_T (N/m)	c_T (Ns/m)	k_{end} (N/m)	c_{end} (Ns/m)
Values	$10k_c$	$0.01c_c$	$1k_r$	$0.1c_r$

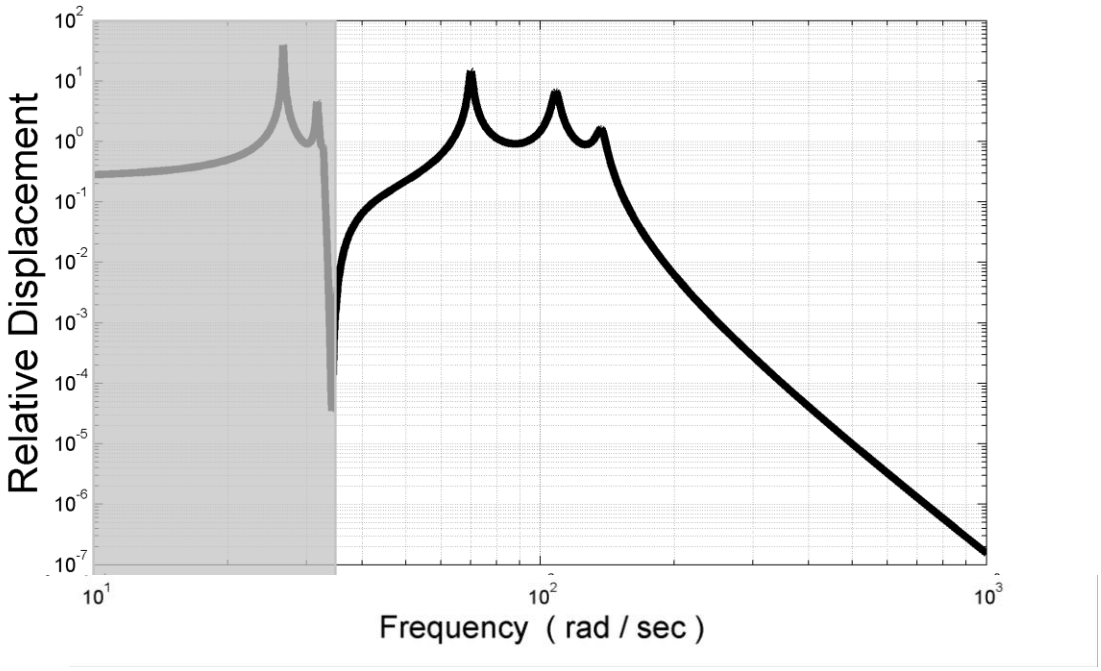

(a)

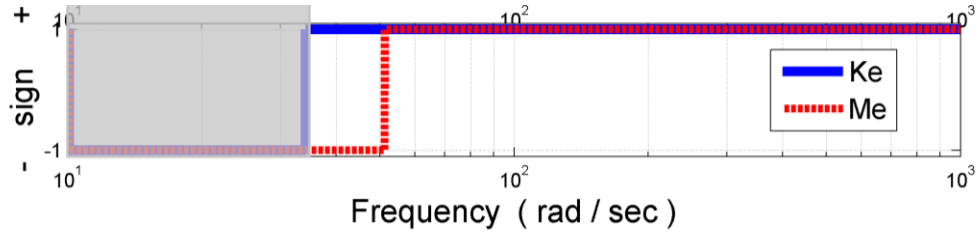

(b)

Fig. 6.6: The frequency response (a) and sign of the effective mass and stiffness (b) for an *AAMM/TC* configuration 1 at low frequency

Fig. 6.5a displays the frequency response of the magnitude of the transfer function $|X_4/X_1|$. Fig. 6.5b shows the sign of the effective mass m_e and stiffness k_e of the metamaterial array. It can be easily seen that between 24-56 *rad/s*, the metamaterial array exhibits negative effective mass whereas its effective stiffness has a negative value over a band between 24-80 *rad/s*. Therefore, using the *AAMM/TC* resonators results in simultaneous double negative properties in the frequency range 24-56 *rad/s*.

Fig. 6.4a displays the frequency response of the magnitude of the transfer function $|X_4/X_1|$. Fig. 6.4b shows the sign of the effective mass m_e and stiffness k_e of the metamaterial array. It can be easily seen that between 12-52 *rad/s*, the metamaterial array exhibits negative effective mass whereas its effective stiffness has a negative value over a band between 12-15 *rad/s*. Therefore, using the *AAMM/TC* resonators results in simultaneous double negative properties in the frequency range 12-15 *rad/s*.

Figures 6.4, 6.5, 6.6 show the capability of the *AAMM/TC* on achieving a double negative property response on various frequency ranges. The *AAMM/TC* can be tuned to bring double negativity to high, mid-range, and low frequency regions. This tenability feature of the active acoustic metamaterial is depending mainly on the passive and active parameters.

6.2.5 Structure of the *AAMM/TC* with Control Configuration 2:

In this control action configuration, however, the linear combination that carries the information of motion of the system has been toggled to count for the motion of the attached Helmholtz resonator, X_r, replacing the displacement of transmission mass of the unit cell, X_i. While keeping on the adjacent transmission masses, $X_{i-1}\ and\ X_{i-1}$, the second configuration of the control action is given as $f_T = (k_T + s\,c_T)(2X_{\boldsymbol{r}} - X_{i+1} - X_{i-1})$ where k_T and c_T are the active transmission gains.

6.2.6 Modeling of the *AAMM/TC* with Control Configuration 2:

The dynamics of the lumped-parameter system is developed by writing the equation of motion of a unit cell consisting of a Helmholtz resonator and the transmission line element ***i*** as follows:

a. <u>The equation of motion of the i^{th} transmission element:</u>

Using the Laplace transformation, the equation of motion can be written as:

$$m\,s^2X_i + (k + s\,c)(2X_i - X_{i+1} - X_{i-1}) +$$

$$(k_r + s\,c_r)(X_i - X_r) + f_T = 0 \tag{6.21}$$

As

$$f_T = (k_T + s\,c_T)(2X_r - X_{i+1} - X_{i-1}) \tag{6.22}$$

Then,

$$m\,s^2X_i + (k + s\,c)(2X_i - X_{i+1} - X_{i-1}) + (k_r + s\,c_r)(X_i - X_r) + (k_T + s\,c_T)(2X_r - X_{i+1} - X_{i-1}) = 0 \tag{6.23}$$

b. The equation of motion of the Helmholtz Resonant Mass m_r:

Similarly, in the Laplace domain, the equation of motion is written as:

$$m_r s^2 X_r + (k_r + s\,c_r)(X_r - X_i) + (k_{end} + s\,c_{end})X_r = 0 \tag{6.24}$$

Eq. (6.24) can be rewritten as:

$$[m_r s^2 + (k_r + s\,c_r) + (k_{end} + s\,c_{end})]\,X_r - (k_r + s\,c_r)X_i = 0 \tag{6.25}$$

This leads to:

$$X_r = \frac{(k_r + s\,c_r)}{[m_r s^2 + (k_r + s\,c_r) + (k_{end} + s\,c_{end})]}\,X_i \tag{6.26}$$

Substituting for X_r into the transmission mass's eq. (6.23):

$$m\,s^2X_i + (k + s\,c)(2X_i - X_{i+1} - X_{i-1}) + (k_r + s\,c_r)X_i + [2(k_T + s\,c_T) - (k_r + s\,c_r)]\frac{(k_r + s\,c_r)}{[m_r s^2 + (k_r + s\,c_r) + (k_{end} + s\,c_{end})]}\,X_i + (k_T + s\,c_T)(-X_{i-1} - X_{i+1}) = 0 \tag{6.27}$$

Or

$$\left\{m + \frac{m_r(k_r + s\,c_r)}{m_r s^2 + (k_r + s\,c_r) + (k_{end} + s\,c_{end})}\right\} s^2 X_i$$
$$+ \left[k + s\,c + \frac{(k_T + s\,c_T)(k_r + s\,c_r)}{m_r s^2 + (k_r + s\,c_r) + (k_{end} + s\,c_{end})}\right](2X_i - X_{i+1} - X_{i-1})$$
$$= F_T$$

Where:

$$F_T = -\left\{\frac{(k_{end} + s\,c_{end})(k_r + s\,c_r)}{m_r s^2 + (k_r + s\,c_r) + (k_{end} + s\,c_{end})}\right\} X_i$$
$$- \left[\frac{m_r(k_T + s\,c_T)s^2 + (k_{end} + s\,c_{end})(k_T + s\,c_T)}{m_r s^2 + (k_r + s\,c_r) + (k_{end} + s\,c_{end})}\right](-X_{i-1} - X_{i+1}) \qquad (6.28)$$

Eq. (6.10) results in the following equation of motion of the equivalent lumped-parameter system for the control action configuration 1 of the *AAMM/TC* shown in Fig. 6.3.

$$m_e\, s^2 X_i - (k_e + s\,c_e)\,(X_{i-1} + X_{i+1} - 2X_i) = 0 \qquad (6.29)$$

Where:

The effective mass of the equivalent-system:

$$m_e = m + \frac{m_r(k_r + s\,c_r)}{m_r s^2 + (k_r + s\,c_r) + (k_{end} + s\,c_{end})} = m_{e_{REAL}} + i\, m_{e_{IMAG}} \qquad (6.30)$$

Where:

$$m_{e_{REAL}} = m + \boldsymbol{real}\big(G_M(s)\big) \quad , \quad m_{e_{IMAG}} = \boldsymbol{imag}\big(G_M(s)\big)$$

$$G_M(s) = \frac{m_r(k_r + s\,c_r)}{m_r s^2 + (k_r + s\,c_r) + (k_{end} + s\,c_{end})}, \quad \text{and} \quad s = i\,\omega \qquad (6.31)$$

The effective stiffness of the equivalent-system:

$$k_e = k + \boldsymbol{real}\big(G_k(s)\big) \tag{6.32}$$

Where:

$$G_k(s) = \frac{(k_T + s\,c_T)(k_r + s\,c_r)}{m_r s^2 + (k_r + s\,c_r) + (k_{end} + s\,c_{end})} \tag{6.33}$$

The effective damping of the equivalent-system:

$$c_e = c + \frac{\boldsymbol{imag}\big(G_k(i\omega)\big)}{\omega} \tag{6.34}$$

Eq. (6.29) can be described in the frequency as follows:

$$-\big(m_{e_{REAL}} + i\,m_{e_{IMAG}}\big)\,\omega^2 X_i - (k_e + i\omega\,c_e)\,(X_{i-1} + X_{i+1} - 2X_i) = F_i$$

$$or$$

$$-\big(M_{e_{REAL}} + i\,M_{e_{IMAG}}\big)\,\omega^2 X_i + 2\,(K_e + i\,\omega\,C_e)\,X_i =$$

$$\underbrace{F_i + (K_e + i\,\omega\,C_e)(X_{i-1} + X_{i+1})}_{F_T}$$

This leads to:

$$-m_{e_{REAL}}\,\omega^2 X_i + i\omega\,\big(\,2\,c_e - \,\omega\,m_{e_{IMAG}}\big)\,X_i \;+\; 2k_e\,X_i = F_T \tag{6.35}$$

Eq. (6.35) can be rewritten as:

$$-\,m_{e_m}\omega^2 X_i + i\omega\,c_{e_m} X_i + k_{e_m} X_i = F_T \tag{6.36}$$

Where:

$$m_{e_m} = m_{e_{REAL}} \tag{6.37}$$

$$c_{e_m} = 2\,c_e - \omega\, m_{e_{IMAG}} \tag{6.38}$$

$$k_{e_m} = 2\,k_e \tag{6.39}$$

$$F_T = F_i + (k_e + i\,\omega\,c_e)(X_{i-1} + X_{i+1}) \tag{6.40}$$

6.2.7 Numerical Examples and Discussions:

Performance of The Active Acoustic Metamaterial with transmission line control boundaries, control configuration 2 :.

Consider the active acoustic metamaterial with transmission line control boundaries. The system has the physical parameters listed in Table 6.4 for a high frequency case, in Table 6.5 for the mid-range frequency case, and Table 6.6 for the high frequency case. The metamaterial is excited at node 1 at the beginning of the transmission line with a swept sine wave and the response is monitored at node 4 at the end of the transmission line.

Table 6.4 Physical parameters of the active acoustic metamaterial with transmission line control boundaries, control configuration 2, for the High frequency case

Parameter	m (kg)	k (N/m)	c (Ns/m)	m_r (kg)	k_r (N/m)	c_r (Ns/m)	k_c (N/m)	c_c (Ns/m)	*No. of Cells*
Values	**0.01**	**2000**	**0.1**	**0.9**	**1000**	**0.002**	**2100**	**0.1**	**4**

Parameter	k_H (N/m)	c_H (Ns/m)	k_T (N/m)	c_T (Ns/m)
Values	$100k_c$	c_c	$0.1k_c$	c_c

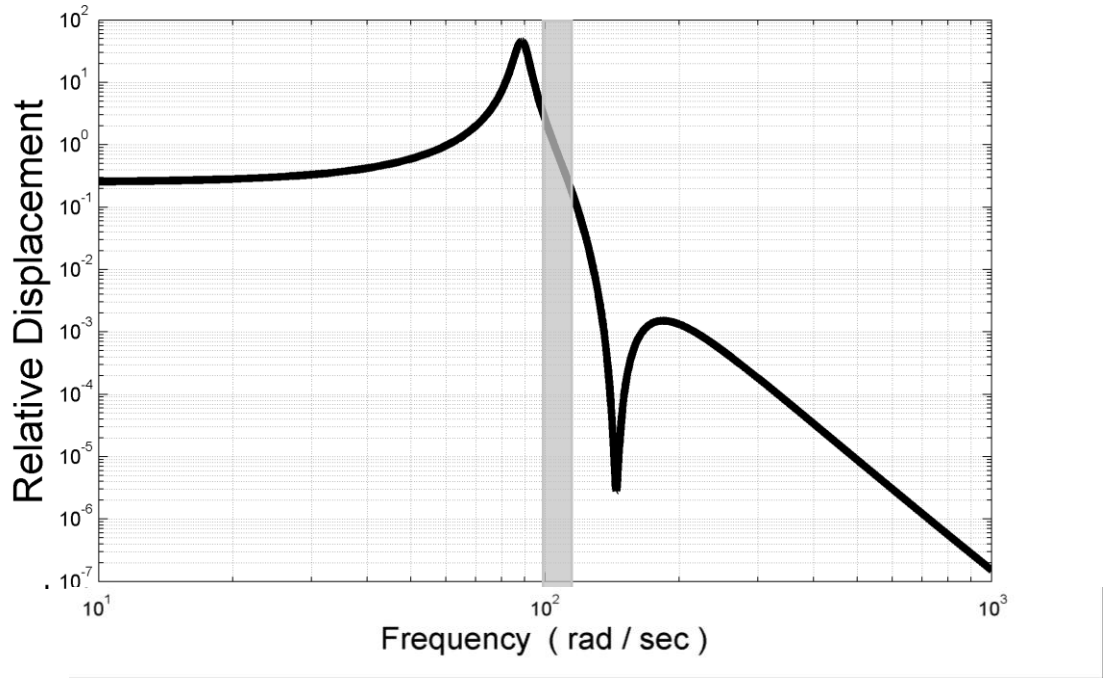

(a)

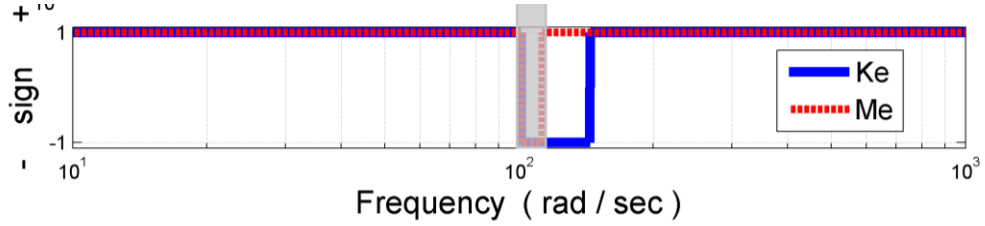

(b)

Fig. 6.7: The frequency response (a) and sign of the effective mass and stiffness (b) for an *AAMM/TC* configuration 2 at high frequency

Fig. 6.7a displays the frequency response of the magnitude of the transfer function $|X_4/X_1|$. Fig. 6.7b shows the sign of the effective mass m_e and stiffness k_e of the metamaterial array. It can be easily seen that between 101-113 *rad/s*, the metamaterial array exhibits negative effective mass whereas its effective stiffness has a negative value near the same band between 101-145*rad/s*. Therefore, using the *AAMM/TC* resonators results in simultaneous double negative properties in the frequency range 101-113 *rad/s*.

Table 6.5 Physical parameters of the active acoustic metamaterial with transmission line control boundaries, control configuration 2, for the mid-range frequency case

Parameter	m (kg)	k (N/m)	c (Ns/m)	m_r (kg)	k_r (N/m)	c_r (Ns/m)	k_c (N/m)	c_c (Ns/m)	No. of Cells
Values	0.01	2000	0.1	0.9	1000	0.002	2100	0.1	4

Parameter	k_H (N/m)	c_H (Ns/m)	k_T (N/m)	c_T (Ns/m)
Values	$10k_c$	c_c	$0.1k_c$	c_c

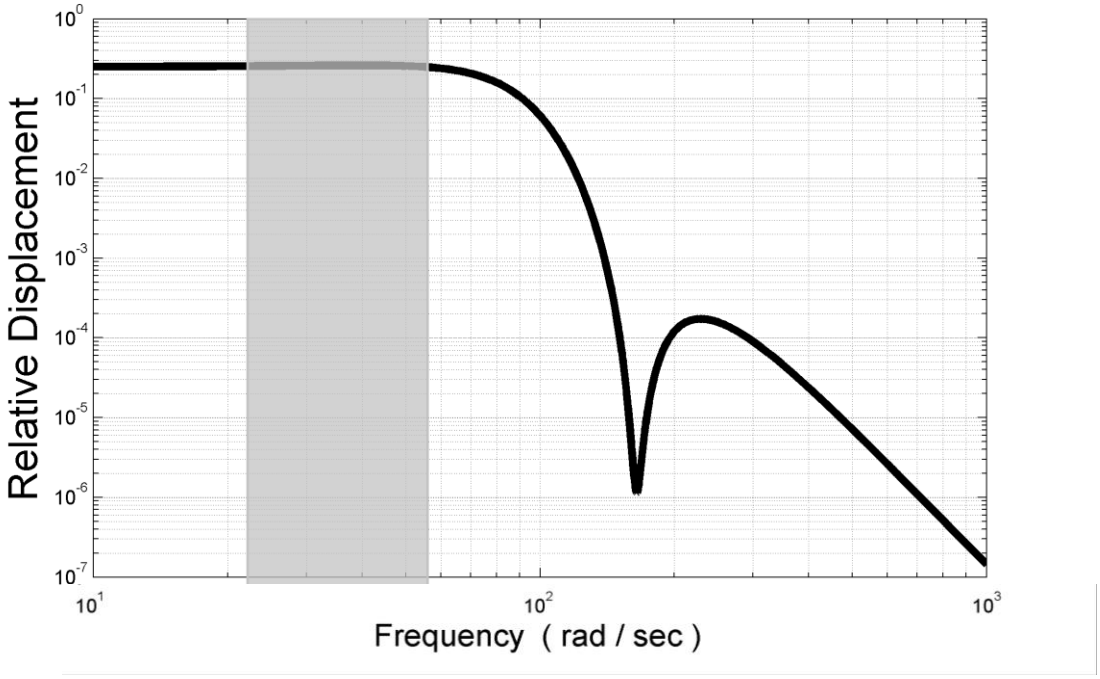

(a)

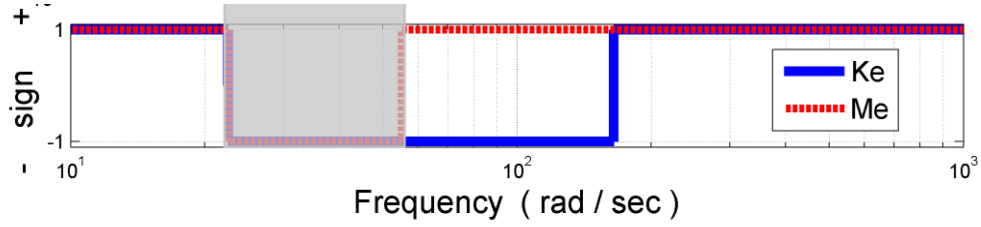

(b)

Fig. 6.8: The frequency response (a) and sign of the effective mass and stiffness (b) for an *AAMM/TC* configuration 2 at mid-range frequency

Fig. 6.8a displays the frequency response of the magnitude of the transfer function $|X_4/X_1|$. Fig. 6.8b shows the sign of the effective mass m_e and stiffness k_e of the metamaterial array. It can be easily seen that between 22-56 *rad/s*, the metamaterial array exhibits negative effective mass whereas its effective stiffness has a negative value over a band between 22-165 *rad/s*. Therefore, using the *AAMM/TC* resonators results in simultaneous double negative properties in the frequency range 22-56 *rad/s*.

Table 6.6 Physical parameters of the active acoustic metamaterial with transmission line control boundaries, control configuration 2, for the low frequency case

Parameter	m (kg)	k (N/m)	c (Ns/m)	m_r (kg)	k_r (N/m)	c_r (Ns/m)	k_c (N/m)	c_c (Ns/m)	*No. of Cells*
Values	**0.01**	**2000**	**0.1**	**0.9**	**1000**	**0.002**	**2100**	**0.1**	**4**

Parameter	k_H (N/m)	c_H (Ns/m)	k_T (N/m)	c_T (Ns/m)
Values	$1k_c$	c_c	$0.1k_c$	c_c

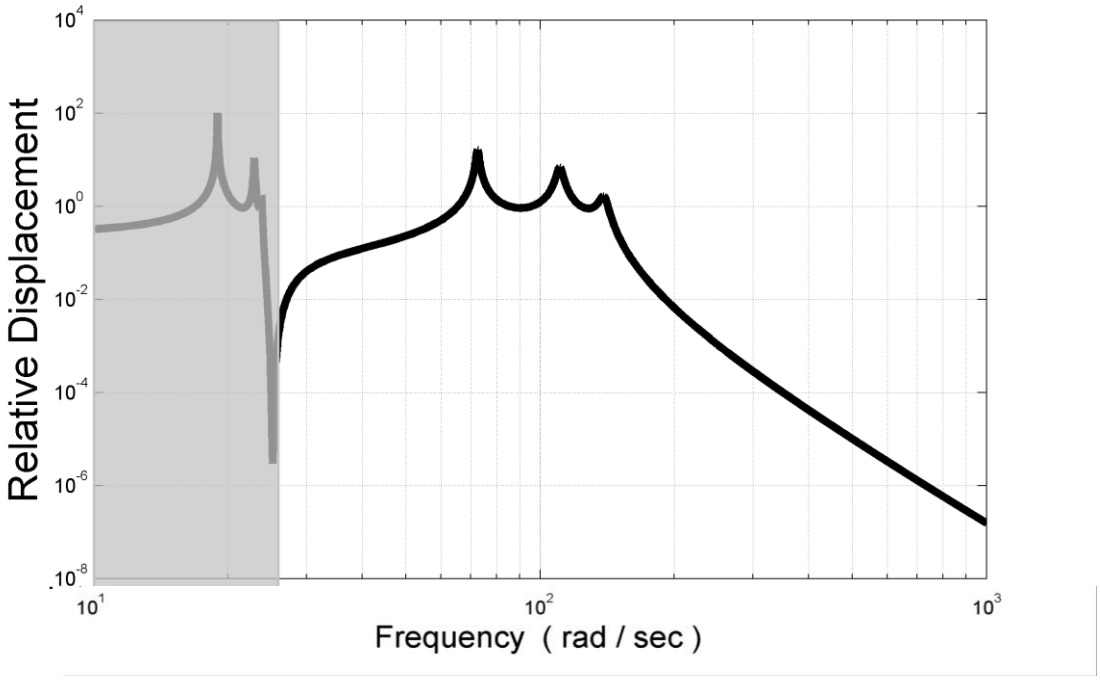

(a)

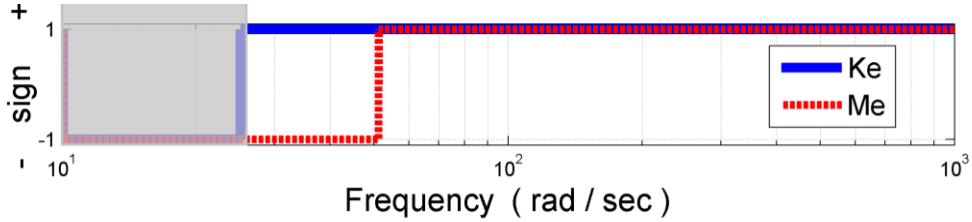

(b)

Fig. 6.9: The frequency response (a) and sign of the effective mass and stiffness (b) for an *AAMM/TC* configuration 2 at low frequency

Fig. 6.9a displays the frequency response of the magnitude of the transfer function $|X_4/X_1|$. Fig. 6.9b shows the sign of the effective mass m_e and stiffness k_e of the metamaterial array. It can be easily seen that between 10-52 *rad/s*, the metamaterial array exhibits negative effective mass whereas its effective stiffness has a negative value over a band between 10-26 *rad/s*. Therefore, using the *AAMM/TC* resonators results in simultaneous double negative properties in the frequency range 10-26 *rad/s*.

Figures 6.7, 6.8, 6.9 show the capability of the *AAMM/TC* on achieving a double negative property response on various frequency ranges. The *AAMM/TC* can be tuned to bring double negativity to high, mid-range, and low frequency regions. This tenability feature of the active acoustic metamaterial is depending mainly on the passive and active parameters.

6.3. Summary

This chapter has presented *AAMM* configuration consists of arrays of transmission line cavities that are separated by and provided with piezoelectric boundaries. These boundaries control the stiffness of the individual cavity and in turn control its dynamical density and bulk modulus. Connected to these transmission line cavities are a set of Helmholtz resonators which have passive flexible boundaries. The transmission line control action insures the achievement of double negative parameter response of the metamaterial.

Various control configurations have been presented in this chapter. Each of these control configurations has offered a great deal of negativity response over certain frequency bandwidths. Moreover, the control configurations have succeeded in bringing the double negative parameter response into various frequency ranges, high, mid-range and low frequency ranges.

Chapter 7: Active Acoustic Metamaterial With Simultaneous Transmission Line and Helmholtz Control Boundaries

7.1 Overview

In this chapter, another powerful configuration of the *AAMM* is presented. The prototype of the *AAMM* unit cell has been provided with additional control capabilities. These capabilities can be easily seen by considering Fig. 7.1. In particular, the *AAMM* consists of arrays of transmission line cavities that are separated by and provided with piezoelectric boundaries. These boundaries control the stiffness of the individual cavity and in turn control its dynamical density and bulk modulus. Connected to these transmission line cavities are a set of Helmholtz resonators which have also flexible piezoelectric boundaries to also simultaneously control the dynamical density and bulk modulus. With such dual control capabilities, it would be possible to evaluate the effectiveness and merits of controlling the acoustic properties through the transmission line piezo-boundaries or the Helmholtz piezo-boundaries.

Fig. 7.2 shows a schematic drawing of the equivalent lumped-parameter model of the experimental *AAMM* with simultaneous transmission line and Helmholtz control boundaries.

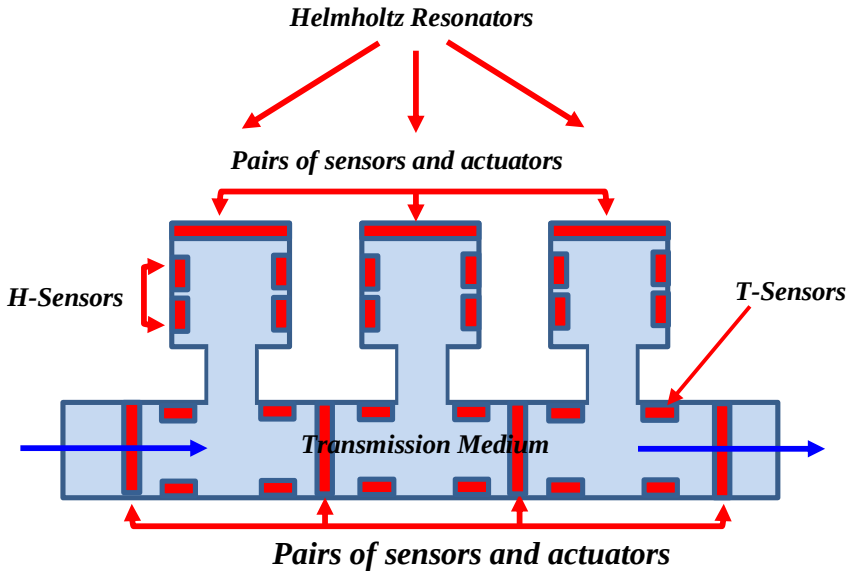

Fig. 7.1 - Active acoustic metamaterial with simultaneous transmission line and Helmholtz control boundaries

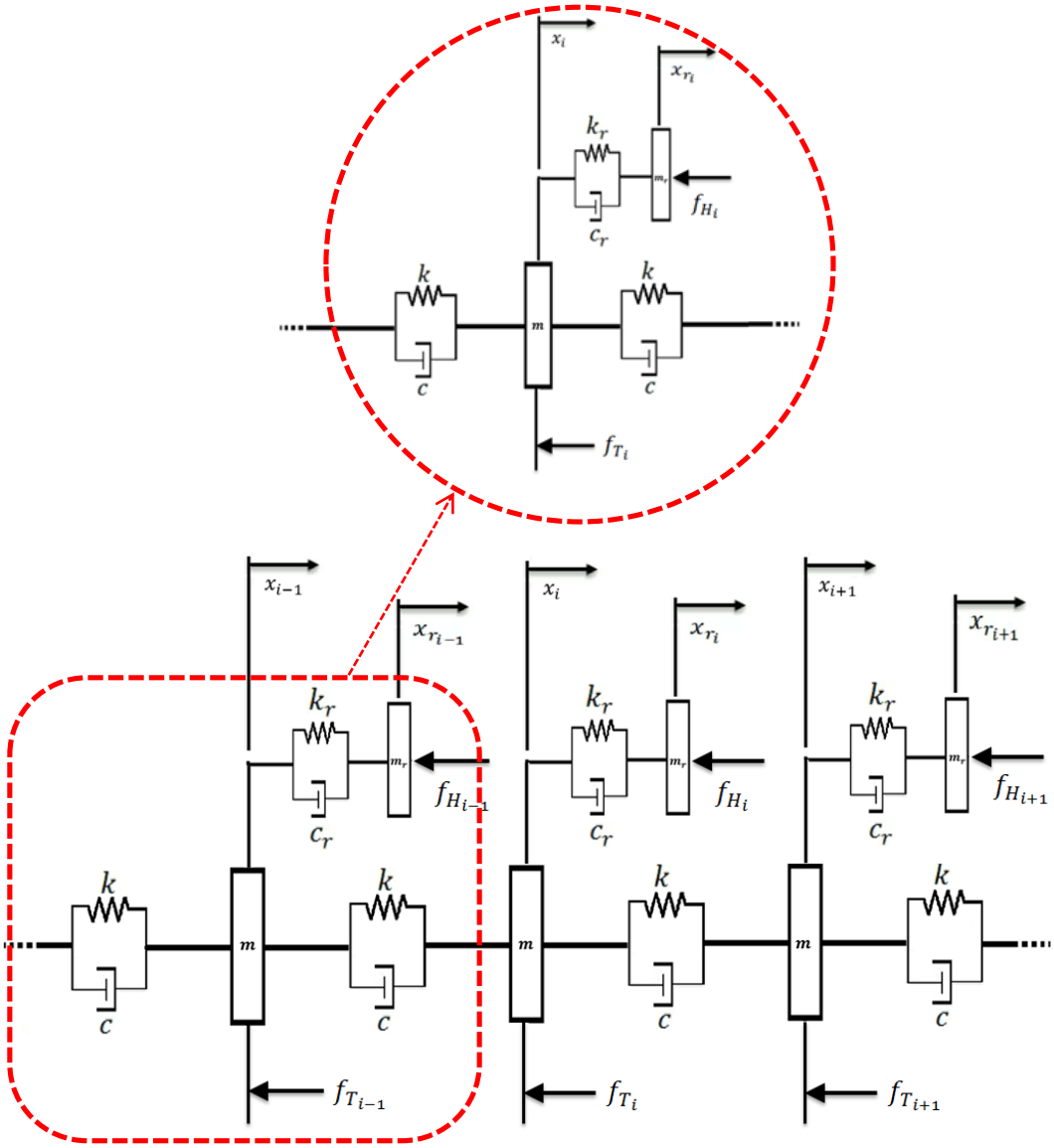

Fig. 7.2 - Lumped-parameter model of the active acoustic metamaterial with simultaneous transmission line and Helmholtz control boundaries

7.2 Concept of the Active Acoustic Metamaterial with Simultaneous Transmission Line And Helmholtz Control Boundaries:

7.2.1. The Structure of the Metamaterial *AAMM/THC*:

The *AAMM/THC* system in its bulk form is consisting of array of actively controlled Helmholtz resonators which are spatially distributed and connected to a wave carrying medium. The carrying medium, transmission line, has been separated and provided with active piezoelectric boundaries as shown in Fig. 7.1.

In this design two different control configurations have been implemented in the *AAMM/THC*. Both in which the control action applied to the Helmholtz resonators $\boldsymbol{f_H}$ would remain the same. In this *AAMM/THC*, the control action applied to the Helmholtz is holding the same form of controller that was introduced earlier, Pope and Daley (2010). The control force applied to the Helmholtz resonator is formulated as $f_H = (k_H + s\, c_H)(2X_{\boldsymbol{r}} - X_{i+1} - X_{i-1})$, where k_H and c_H are active spring and damper gains. The control action design introduced by Pope and Daley (2010) influences the control action designs proposed in this chapter with different active gain and motion combinations.

In the first configuration and specially in the control action applied directly to the transmission line $\boldsymbol{f_T}$, the controller is proportional to a linear combination of the transmission line mass displacement, X_i, of the unit cell in addition to the other adjacent transmission line masses before, X_{i-1}, and after, X_{i+1}, as $f_T = (k_T + s\, c_T)(2X_{\boldsymbol{i}} - X_{i+1} - X_{i-1})$ where k_T and c_T are the active transmission spring and damper gains.

In the second control action configuration, however, the linear combination that carries the information of motion of the system has been toggled to count for the motion of the attached Helmholtz resonator, X_r, replacing the displacement of transmission mass of the unit cell, X_i. While keeping on the adjacent transmission masses, $X_{i-1}\ and\ X_{i-1}$, the second configuration of the control action is given as $f_T = (k_T + s\, c_T)(2X_{\boldsymbol{r}} - X_{i+1} - X_{i-1})$ where k_T and c_T are the active transmission gains.

7.2.2. Structure of the *AAMM/THC* with Control Configuration 1:

In this configuration, the control force, $\boldsymbol{f_T}$, is applied directly to the transmission line mass. The controller in $\boldsymbol{f_T}$ is proportional to a linear combination of the transmission line mass displacement, X_i, of the unit cell and to the other adjacent transmission line masses before, X_{i-1}, and after, X_{i+1}. The control action applied to the transmission line in this configuration is given as $f_T = (k_T + s\, c_T)(2X_{\boldsymbol{i}} - X_{i+1} - X_{i-1})$, where k_T and c_T are the active transmission spring and damper gains.

a. Modeling of the *AAMM/THC* with Control Configuration 1:

The dynamics of the lumped-parameter system is developed by writing the equation of motion of a unit cell consisting of a Helmholtz resonator and the transmission line element ***i*** as follows:

b. <u>The equation of motion of the i^{th} transmission element:</u>

Using the Laplace transformation, the equation of motion can be written as:

$$m\,s^2X_i + (k + s\,c)(2X_i - X_{i+1} - X_{i-1}) + (k_r + s\,c_r)(X_i - X_r) + f_T = 0 \quad (7.1)$$

As

$$f_T = (k_T + s\,c_T)(2X_i - X_{i+1} - X_{i-1}) \quad (7.2)$$

Then,

$$m\,s^2X_i + (k + s\,c)(2X_i - X_{i+1} - X_{i-1}) + (k_r + s\,c_r)(X_i - X_r) + (k_T + s\,c_T)(2X_i - X_{i+1} - X_{i-1}) = 0 \quad (7.3)$$

c. <u>The equation of motion of the Helmholtz Resonant Mass m_r:</u>

Similarly, in the Laplace domain, the equation of motion is written as:

$$m_r s^2X_r + (k_r + s\,c_r)(X_r - X_i) + f_H = 0 \quad (7.4)$$

As

$$f_H = (k_H + s\,c_H)(2X_r - X_{i+1} - X_{i-1}) \quad (7.5)$$

Then,

$$m_r s^2X_r + (k_r + s\,c_r)(X_r - X_i) + (k_H + s\,c_H)(2X_r - X_{i+1} - X_{i-1}) = 0 \quad (7.6)$$

Eq. (7.6) can be rewritten as:

$$[m_r s^2 + (k_r + s\,c_r) + 2(k_H + s\,c_H)]\,X_r - (k_r + s\,c_r)X_i + (k_H + s\,c_H)(-X_{i+1} - X_{i-1}) = 0 \quad (7.7)$$

This leads to:

$$X_r = \frac{(k_r+s\,c_r)X_i-(k_H+s\,c_H)(-X_{i+1}-X_{i-1})}{m_r s^2+(k_r+s\,c_r)+2(k_H+s\,c_H)} \tag{7.8}$$

Substituting for X_r into the transmission mass's eq. (7.3), yields:

$$\begin{aligned} & m\,s^2X_i + (k+s\,c)(2X_i - X_{i+1} - X_{i-1}) + (k_r + s\,c_r)X_i \\ & -\frac{(k_r + s\,c_r)^2X_i - (k_H + s\,c_H)(k_r + s\,c_r)(-X_{i+1} - X_{i-1})}{m_r s^2 + (k_r + s\,c_r) + 2(k_H + s\,c_H)} \\ & +(k_T + s\,c_T)(2X_i - X_{i+1} - X_{i-1}) = 0 \end{aligned} \tag{7.9}$$

Or

$$\begin{aligned} & \left\{m + \frac{m_r(k_r+s\,c_r)}{m_r s^2+(k_r+s\,c_r)+2(k_H+s\,c_H)}\right\} s^2X_i \\ & +\left\{(k+s\,c) + (k_T + s\,c_T) + \frac{(k_H + s\,c_H)(k_r + s\,c_r)}{m_r s^2 + (k_r + s\,c_r) + 2(k_H + s\,c_H)}\right\} \\ & (2X_i - X_{i+1} - X_{i-1}) = 0 \end{aligned} \tag{7.10}$$

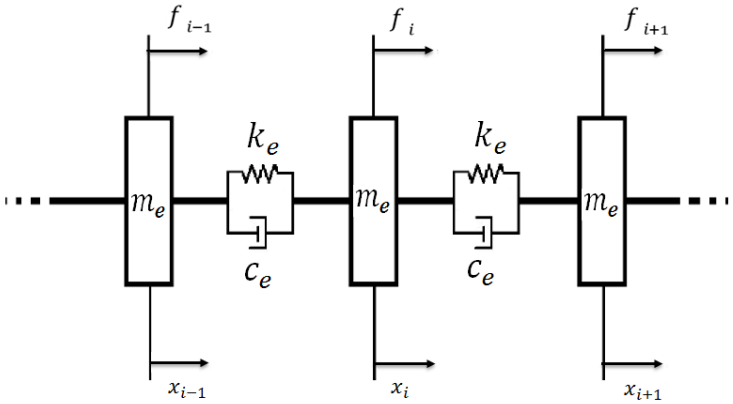

Fig.7.3: Equivalent lumped-parameter system of configuration 1 of the *AAMM/THC*

Eq. (7.10) results in the following equation of motion of the equivalent lumped-parameter system for the control action configuration 1 of the *AAMM/THC* shown in Fig. 7.3.

$$m_e\, s^2 X_i - (k_e + s\, c_e)\,(X_{i-1} + X_{i+1} - 2X_i) = 0 \qquad (7.11)$$

where:

The effective mass of the equivalent-system:

$$m_e = m + \frac{m_r(k_r + s\, c_r)}{m_r s^2 + (k_r + s\, c_r) + 2(k_H + s\, c_H)} = m_{e_{REAL}} + i\, m_{e_{IMAG}} \qquad (7.12)$$

where:

$m_{e_{REAL}} = m + \boldsymbol{real}\big(G_M(s)\big)$, $m_{e_{IMAG}} = \boldsymbol{imag}\big(G_M(s)\big)$, and

$G_M(s) = \frac{m_r(k_r + s\, c_r)}{m_r s^2 + (k_r + s\, c_r) + 2(k_H + s\, c_H)}$, and $s = i\,\omega$ (7.13)

The effective stiffness of the equivalent-system:

$$k_e = k + k_T + \boldsymbol{real}\big(G_k(s)\big) \qquad (7.14)$$

where:

$$G_k(s) = \frac{(k_H + s\, c_H)(k_r + s\, c_r)}{m_r s^2 + (k_r + s\, c_r) + 2(k_H + s\, c_H)} \qquad (7.15)$$

The effective damping of the equivalent-system:

$$c_e = c + c_T + \frac{\boldsymbol{imag}\big(G_k(i\omega)\big)}{\omega} \qquad (7.16)$$

Eq. (7.11) can be described in the frequency as follows:

$$-\big(m_{e_{REAL}} + i\, m_{e_{IMAG}}\big)\,\omega^2 X_i - (k_e + i\omega\, c_e)\,(X_{i-1} + X_{i+1} - 2X_i) = F_i$$

or

$$-\left(M_{e_{REAL}} + i\, M_{e_{IMAG}}\right) \omega^2 X_i + 2\,(K_e + i\,\omega\, C_e)\, X_i =$$

$$\underbrace{F_i + (K_e + i\,\omega\, C_e)(X_{i-1} + X_{i+1})}_{F_T}$$

This leads to:

$$-m_{e_{REAL}}\, \omega^2 X_i + i\omega \left(\, 2\, c_e - \,\omega\, m_{e_{IMAG}}\right) X_i \;+\; 2k_e\, X_i = F_T \qquad (7.17)$$

Eq. (7.17) can be rewritten as:

$$-\, m_{e_m} \omega^2 X_i + i\omega\, c_{e_m} X_i + k_{e_m} X_i = F_T \qquad (7.18)$$

where:

$$m_{e_m} = m_{e_{REAL}}\ , \qquad (7.19)$$

$$c_{e_m} = \,2\, c_e - \,\omega\, m_{e_{IMAG}}\ , \qquad (7.20)$$

$$k_{e_m} = 2\, k_{e,} \qquad (7.21)$$

$$F_T = F_i + (k_e + i\,\omega\, c_e)(X_{i-1} + X_{i+1})\ . \qquad (7.22)$$

7.2.3. Numerical Examples and Discussions:

a. Performance of The Active Acoustic Metamaterial with simultaneous transmission line and Helmholtz control boundaries, control configuration 1 :

Consider the active acoustic metamaterial with simultaneous transmission line and Helmholtz control boundaries. The system has the physical parameters listed in Table 7.1 for a high frequency case, in Table 7.2 for the mid-range frequency case, and Table 7.3 for the high frequency case. The metamaterial is excited at node 1 at the

beginning of the transmission line with a swept sine wave and the response is monitored at node 4 at the end of the transmission line.

Table 7.1 Physical parameters of the active acoustic metamaterial with simultaneous transmission line and Helmholtz control boundaries, control configuration 1, for the High frequency case

Parameter	m (*kg*)	k (*N/m*)	c (*Ns/m*)	m_r (*kg*)	k_r (*N/m*)	c_r (*Ns/m*)	k_c (*N/m*)	c_c (*Ns/m*)	*No. of Cells*
Values	0.01	2000	0.1	0.9	1000	0.002	2100	0.1	4
Parameter	k_H (*N/m*)		c_H (*Ns/m*)		k_T (*N/m*)		c_T (*Ns/m*)		
Values	$100k_c$		c_c		$0.1k_c$		c_c		

Fig. 7.4a displays the frequency response of the magnitude of the transfer function $|X_4/X_1|$. Fig. 7.4b shows the sign of the effective mass m_e and stiffness k_e of the metamaterial array. It can be easily seen that between 109-120 *rad/s*, the metamaterial array exhibits negative effective mass whereas its effective stiffness has a negative value near the same band between 109-119 *rad/s*. Therefore, using the *AAMM/THC* resonators results in simultaneous double negative properties in the frequency range 109-119 *rad/s*.

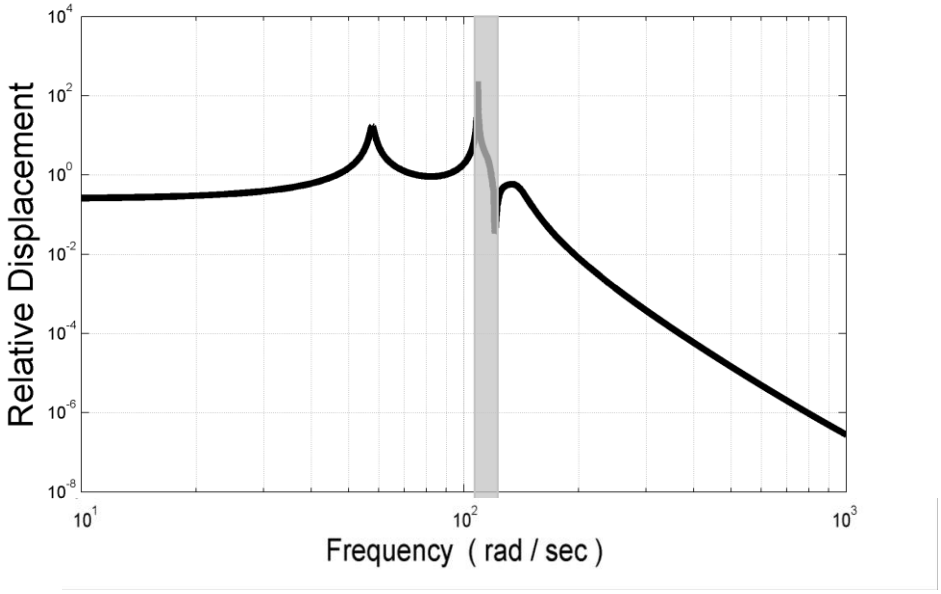

(a)

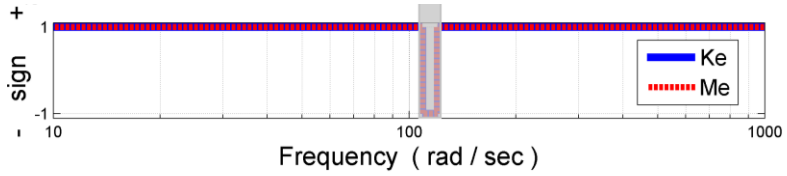

(b)

Fig. 7.4: The frequency response (a) and sign of the effective mass and stiffness (b) for an *AAMM/THC* configuration 1 at high frequency

Table 7.2 Physical parameters of the active acoustic metamaterial with simultaneous transmission line and Helmholtz control boundaries, control configuration 1, for the mid-range frequency case

Parameter	m (kg)	k (N/m)	c (Ns/m)	m_r (kg)	k_r (N/m)	c_r (Ns/m)	k_c (N/m)	c_c (Ns/m)	No. of Cells
Values	0.01	2000	0.1	0.9	1000	0.002	2100	0.1	4

Parameter	k_H (N/m)	c_H (Ns/m)	k_T (N/m)	c_T (Ns/m)
Values	$10k_c$	c_c	$0.1k_c$	c_c

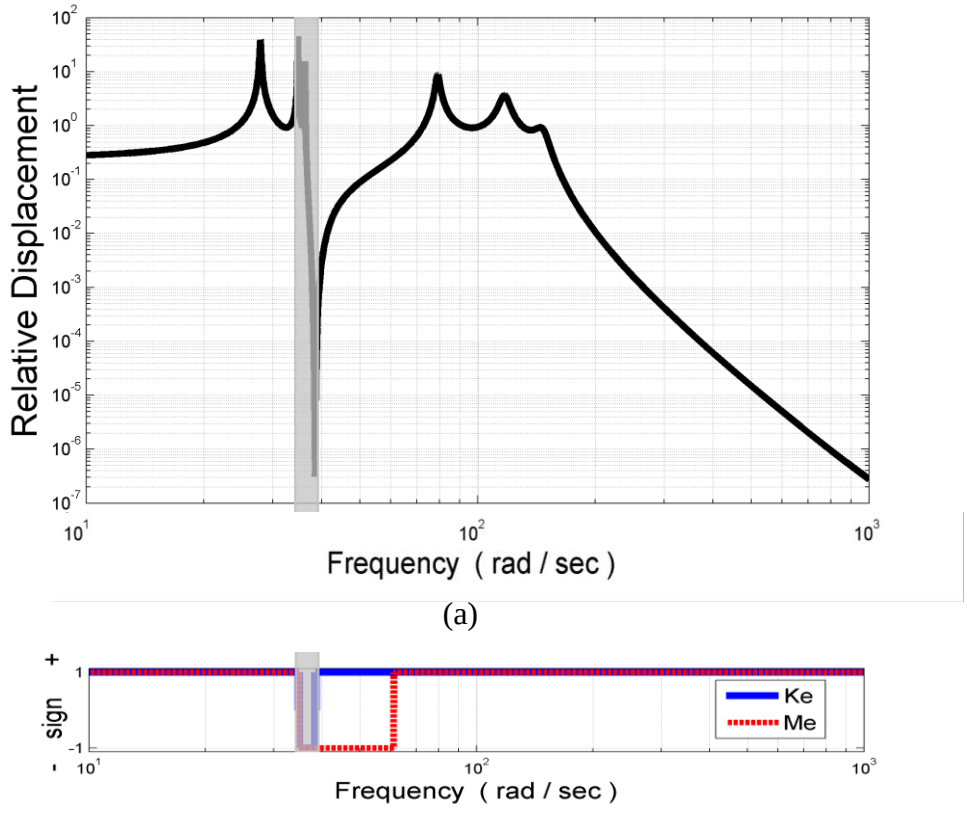

Fig. 7.5: The frequency response (a) and sign of the effective mass and stiffness (b) for an *AAMM/THC* configuration 1 at mid-range frequency

Fig. 7.5a displays the frequency response of the magnitude of the transfer function $|X_4/X_1|$. Fig. 7.5b shows the sign of the effective mass m_e and stiffness k_e of the metamaterial array. It can be easily seen that between 35-62 *rad/s*, the metamaterial array exhibits negative effective mass whereas its effective stiffness has a negative

value over a band between 34-39 *rad/s*. Therefore, using the *AAMM/THC* resonators results in simultaneous double negative properties in the frequency range 34-39 *rad/s*.

Table 7.3 Physical parameters of the active acoustic metamaterial with simultaneous transmission line and Helmholtz control boundaries, control configuration 1, for the low frequency case

Parameter	m (*kg*)	k (*N/m*)	c (*Ns/m*)	m_r (*kg*)	k_r (*N/m*)	c_r (*Ns/m*)	k_c (*N/m*)	c_c (*Ns/m*)	*No. of Cells*
Values	0.01	2000	0.1	0.9	1000	0.002	2100	0.1	4
Parameter	k_H (*N/m*)		c_H (*Ns/m*)		k_T (*N/m*)		c_T (*Ns/m*)		
Values	$1k_c$		c_c		$0.1k_c$		c_c		

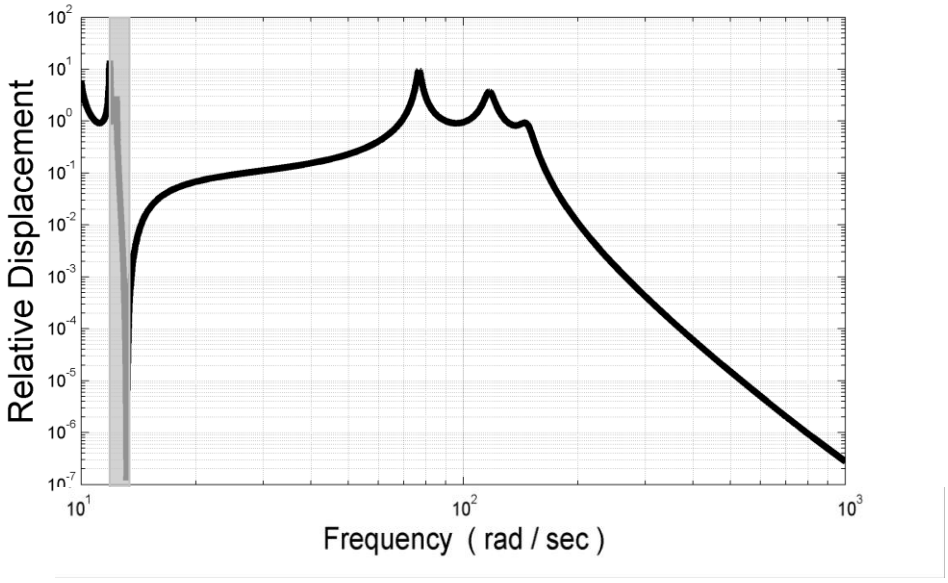

(a)

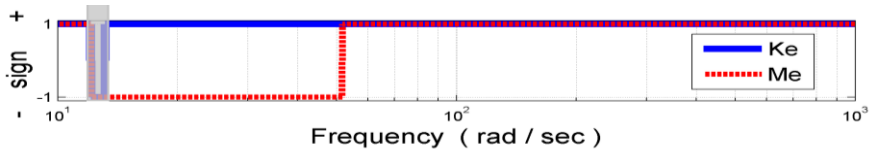

(b)

Fig. 7.6: The frequency response (a) and sign of the effective mass and stiffness (b) for an *AAMM/THC* configuration 1 at low frequency

Fig. 7.4a displays the frequency response of the magnitude of the transfer function $|X_4/X_1|$. Fig. 7.4b shows the sign of the effective mass m_e and stiffness k_e of the metamaterial array. It can be easily seen that between 12-52 *rad/s*, the metamaterial array exhibits negative effective mass whereas its effective stiffness has a negative value over a band between 12-15 *rad/s*. Therefore, using the *AAMM/THC* resonators results in simultaneous double negative properties in the frequency range 12-15 *rad/s*.

Figures 7.4, 7.5, 7.6 show the capability of the *AAMM/THC* on achieving a double negative property response on various frequency ranges. The *AAMM/THC* can be tuned to bring double negativity to high, mid-range, and low frequency regions. This tenability feature of the active acoustic metamaterial is depending mainly on the passive and active parameters.

7.2.4. Structure of the *AAMM/THC* with Control Configuration 2:

In this control action configuration, however, the linear combination that carries the information of motion of the system has been toggled to count for the motion of the attached Helmholtz resonator, X_r, replacing the displacement of transmission mass of the unit cell, X_i. While keeping on the adjacent transmission masses, X_{i-1} *and* X_{i-1}, the second configuration of the control action is given as $f_T = (k_T + s\,c_T)(2X_{\boldsymbol{r}} - X_{i+1} - X_{i-1})$ where k_T and c_T are the active transmission gains.

7.2.5. Modeling of the *AA MM/THC* with Control Configuration 2:

The dynamics of the lumped-parameter system is developed by writing the equation of motion of a unit cell consisting of a Helmholtz resonator and the transmission line element ***i*** as follows:

a. <u>The equation of motion of the i^{th} transmission element:</u>

Using the Laplace transformation, the equation of motion can be written as:

$$m\,s^2X_i + (k + s\,c)(2X_i - X_{i+1} - X_{i-1}) + (k_r + s\,c_r)(X_i - X_r) + f_T = 0 \qquad (7.23)$$

As

$$f_T = (k_T + s\,c_T)(2X_{\boldsymbol{r}} - X_{i+1} - X_{i-1}) \tag{7.24}$$

Then,

$$m\,s^2X_i + (k + s\,c)(2X_i - X_{i+1} - X_{i-1}) +$$

$$(k_r + s\,c_r)(X_i - X_r) + (k_T + s\,c_T)(2X_r - X_{i+1} - X_{i-1}) = 0 \tag{7.25}$$

b. <u>The equation of motion of the Helmholtz Resonant Mass m_r:</u>

Similarly, in the Laplace domain, the equation of motion is written as:

$$m_r s^2 X_r + (k_r + s\,c_r)(X_r - X_i) + f_H = 0 \tag{7.26}$$

As

$$f_H = (k_H + s\,c_H)(2X_{\boldsymbol{r}} - X_{i+1} - X_{i-1}) \tag{7.27}$$

Then,

$$m_r s^2 X_r + (k_r + s\,c_r)(X_r - X_i) +$$

$$(k_H + s\,c_H)(2X_{\boldsymbol{r}} - X_{i+1} - X_{i-1}) = 0 \tag{7.28}$$

Eq. (7.28) can be rewritten as:

$$[m_r s^2 + (k_r + s\,c_r) + 2(k_H + s\,c_H)]\,X_r -$$

$$(k_r + s\,c_r)X_i + (k_H + s\,c_H)(-X_{i+1} - X_{i-1}) = 0 \tag{7.29}$$

This leads to:

$$X_r = \frac{(k_r + s\,c_r)X_i - (k_H + s\,c_H)(-X_{i+1} - X_{i-1})}{m_r s^2 + (k_r + s\,c_r) + 2(k_H + s\,c_H)} \tag{7.30}$$

Substituting for X_r into the transmission mass's eq. (7.3):

$$m\,s^2X_i + (k + s\,c)(2X_i - X_{i+1} - X_{i-1}) +$$

$$(k_r + s\,c_r)X_i + [2(k_T + s\,c_T) - (k_r + s\,c_r)]$$

$$\frac{(k_r+s\,c_r)X_i-(k_H+s\,c_H)(-X_{i+1}-X_{i-1})}{m_r s^2+(k_r+s\,c_r)+2(k_H+s\,c_H)} + (k_T + s\,c_T)(-X_{i+1} - X_{i-1}) = 0 \qquad (7.31)$$

Or

$$\left\{m + \frac{m_r(k_r + s\,c_r)}{m_r s^2 + (k_r + s\,c_r) + 2(k_H + s\,c_H)}\right\} s^2\,X_i$$

$$+\left\{(k + s\,c) + \frac{(k_T + s\,c_T)(k_r + s\,c_r)}{m_r s^2 + (k_r + s\,c_r) + 2(k_H + s\,c_H)} + \frac{(k_H + s\,c_H)(k_r + s\,c_r)}{m_r s^2 + (k_r + s\,c_r) + 2(k_H + s\,c_H)}\right\}(2X_i - X_{i+1} - X_{i-1})$$

$$= \underbrace{-\left[\frac{m_r(k_T+s\,c_T)s^2}{m_r s^2+(k_r+s\,c_r)+2(k_H+s\,c_H)}\right](-X_{i+1} - X_{i-1})}_{F_T} \qquad (7.32)$$

Eq. (7.32) results in the following equation of motion of the equivalent lumped-parameter system for the control action configuration 1 of the *AAMM/THC* shown in Fig. 7.3.

$$m_e\,s^2X_i - (k_e + s\,c_e)\,(X_{i-1} + X_{i+1} - 2X_i) = 0 \qquad (7.33)$$

Where:

The effective mass of the equivalent-system:

$$m_e = m + \frac{m_r(k_r+s\,c_r)}{m_r s^2+(k_r+s\,c_r)+2(k_H+s\,c_H)} = m_{e_{REAL}} + i\,m_{e_{IMAG}} \qquad (7.34)$$

where:

$$m_{e_{REAL}} = m + \boldsymbol{real}\big(G_M(s)\big) \quad , \quad m_{e_{IMAG}} = \boldsymbol{imag}\big(G_M(s)\big),$$

$$G_M(s) = \frac{m_r(k_r+s\,c_r)}{m_r s^2+(k_r+s\,c_r)+2(k_H+s\,c_H)}, \quad \text{and} \quad s = i\,\omega \qquad (7.35)$$

The effective stiffness of the equivalent-system:

$$k_e = k + \boldsymbol{real}\big(G_k(s)\big) \tag{7.36}$$

where:

$$G_k(s) = \frac{(k_r + s\,c_r)[(k_T + s\,c_T) + (k_H + s\,c_H)]}{m_r s^2 + (k_r + s\,c_r) + 2(k_H + s\,c_H)} \tag{7.37}$$

The effective damping of the equivalent-system:

$$c_e = c + \frac{\boldsymbol{imag}\big(G_k(i\omega)\big)}{\omega} \tag{7.38}$$

Eq. (7.33) can be described in the frequency as follows:

$$-\big(m_{e_{REAL}} + i\,m_{e_{IMAG}}\big)\,\omega^2 X_i - (k_e + i\omega\,c_e)\,(X_{i-1} + X_{i+1} - 2X_i) = F_i$$

or

$$-\big(M_{e_{REAL}} + i\,M_{e_{IMAG}}\big)\,\omega^2 X_i + 2\,(K_e + i\,\omega\,C_e)\,X_i =$$

$$\underbrace{F_i + (K_e + i\,\omega\,C_e)(X_{i-1} + X_{i+1})}_{F_T}$$

This leads to:

$$-m_{e_{REAL}}\,\omega^2 X_i + i\omega\,\big(2\,c_e - \omega\,m_{e_{IMAG}}\big)\,X_i + 2k_e\,X_i = F_T \tag{7.39}$$

Eq. (7.17) can be rewritten as:

$$-m_{e_m}\omega^2 X_i + i\omega\, c_{e_m} X_i + k_{e_m} X_i = F_T \tag{7.40}$$

where:

$$m_{e_m} = m_{e_{REAL}} \tag{7.41}$$

$$c_{e_m} = 2\, c_e - \omega\, m_{e_{IMAG}} \tag{7.42}$$

$$k_{e_m} = 2\, k_e \tag{7.43}$$

$$F_T = F_i + (k_e + i\,\omega\, c_e)(X_{i-1} + X_{i+1}) \tag{7.44}$$

7.2.6. Numerical Examples and Discussions:

Performance of The Active Acoustic Metamaterial with simultaneous transmission line and Helmholtz control boundaries, control configuration 2 :

Consider the active acoustic metamaterial with simultaneous transmission line and Helmholtz control boundaries. The system has the physical parameters listed in Table 7.4 for a high frequency case, in Table 7.5 for the mid-range frequency case, and Table 7.6 for the high frequency case. The metamaterial is excited at node 1 at the beginning of the transmission line with a swept sine wave and the response is monitored at node 4 at the end of the transmission line.

Table 7.4 Physical parameters of the active acoustic metamaterial with simultaneous transmission line and Helmholtz control boundaries, control configuration 2, for the High frequency case

Parameter	m (kg)	k (N/m)	c (Ns/m)	m_r (kg)	k_r (N/m)	c_r (Ns/m)	k_c (N/m)	c_c (Ns/m)	No. of Cells
Values	0.01	2000	0.5	0.5	1000	0.002	2100	0.1	4

Parameter	k_H (N/m)	c_H (Ns/m)	k_T (N/m)	c_T (Ns/m)
Values	$50k_c$	$0.0001c_c$	$100k_c$	$0.0001c_c$

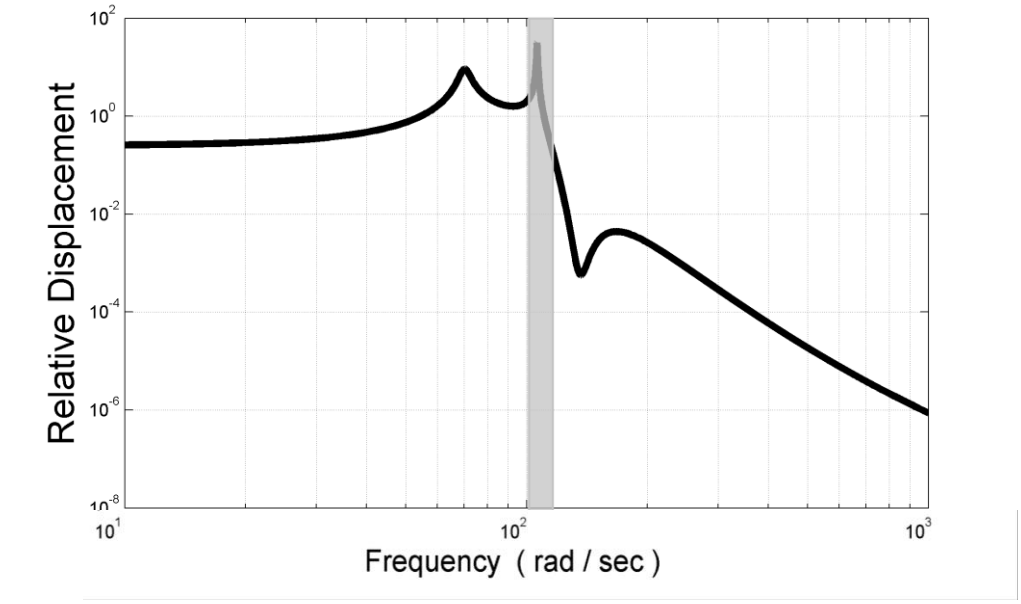

(a)

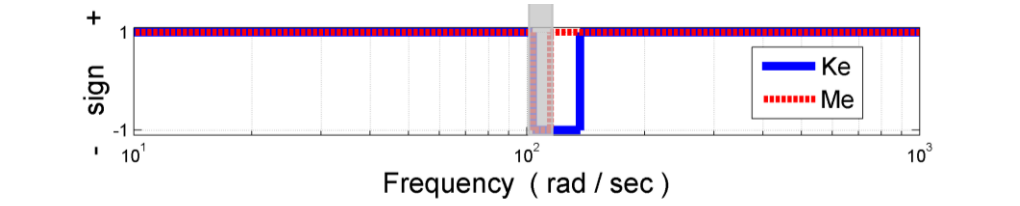

(b)

Fig. 7.7: The frequency response (a) and sign of the effective mass and stiffness (b) for an *AAMM/THC* configuration 2 at high frequency

Fig. 7.7a displays the frequency response of the magnitude of the transfer function $|X_4/X_1|$. Fig. 7.7b shows the sign of the effective mass m_e and stiffness k_e of the metamaterial array. It can be easily seen that between 103-115 *rad/s*, the metamaterial array exhibits negative effective mass whereas its effective stiffness has a negative value over a band between 104-137 *rad/s*. Therefore, using the *AAMM/THC* resonators results in simultaneous double negative properties in the frequency range 104-115 *rad/s*.

Table 7.5 Physical parameters of the active acoustic metamaterial with simultaneous transmission line and Helmholtz control boundaries, control configuration 2, for the mid-range frequency case

Parameter	m (kg)	k (N/m)	c (Ns/m)	m_r (kg)	k_r (N/m)	c_r (Ns/m)	k_c (N/m)	c_c (Ns/m)	No. of Cells
Values	0.01	2000	0.5	0.5	1000	0.002	2100	0.1	4

Parameter	k_H (N/m)	c_H (Ns/m)	k_T (N/m)	c_T (Ns/m)
Values	$10k_c$	$0.00001c_c$	$100k_c$	c_c

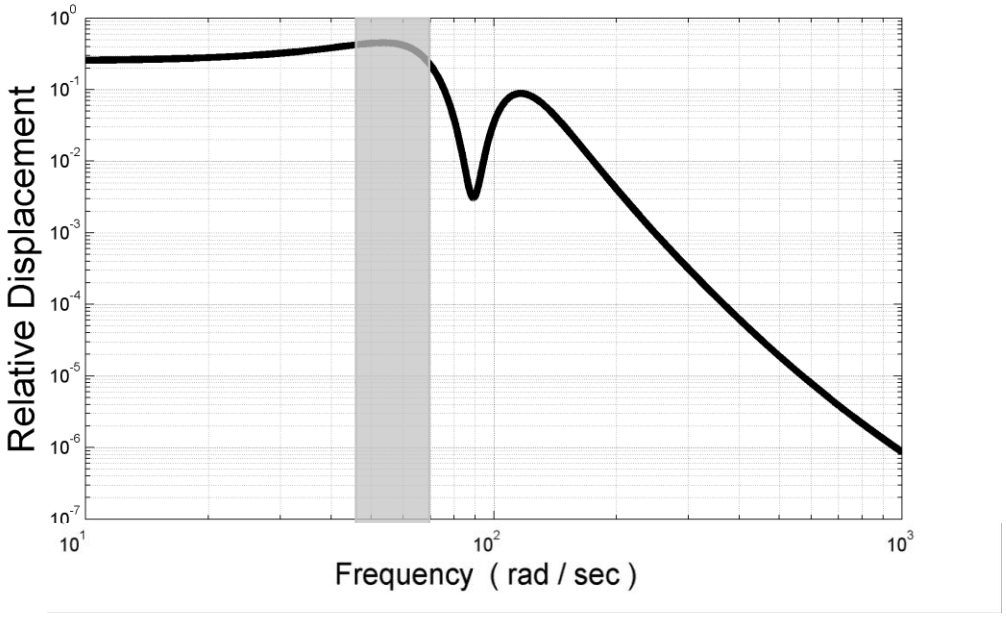

(a)

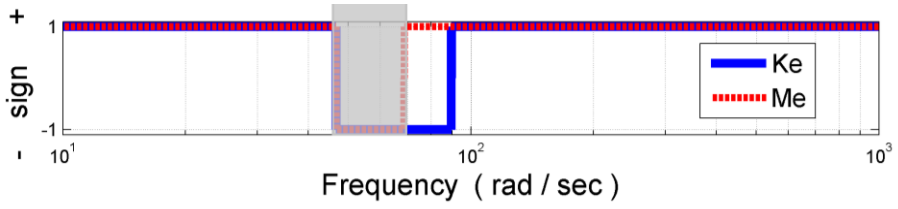

(b)

Fig. 7.8: The frequency response (a) and sign of the effective mass and stiffness (b) for an *AAMM/THC* configuration 2 at mid-range frequency

Fig. 7.8a displays the frequency response of the magnitude of the transfer function $|X_4/X_1|$. Fig. 7.8b shows the sign of the effective mass m_e and stiffness k_e of the metamaterial array. It can be easily seen that between 46-69 *rad/s*, the metamaterial array exhibits negative effective mass whereas its effective stiffness has a negative value over a band between 46-90 *rad/s*. Therefore, using the *AAMM/THC* resonators results in simultaneous double negative properties in the frequency range 46-69 *rad/s*.

Table 7.6 Physical parameters of the active acoustic metamaterial with simultaneous transmission line and Helmholtz control boundaries, control configuration 2, for the low frequency case

Parameter	m (kg)	k (N/m)	c (Ns/m)	m_r (kg)	k_r (N/m)	c_r (Ns/m)	k_c (N/m)	c_c (Ns/m)	No. of Cells
Values	0.01	2000	0.1	0.9	1000	0.002	2100	0.1	4

Parameter	k_H (N/m)	c_H (Ns/m)	k_T (N/m)	c_T (Ns/m)
Values	$1k_c$	$0.01c_c$	$10k_c$	$0.01c_c$

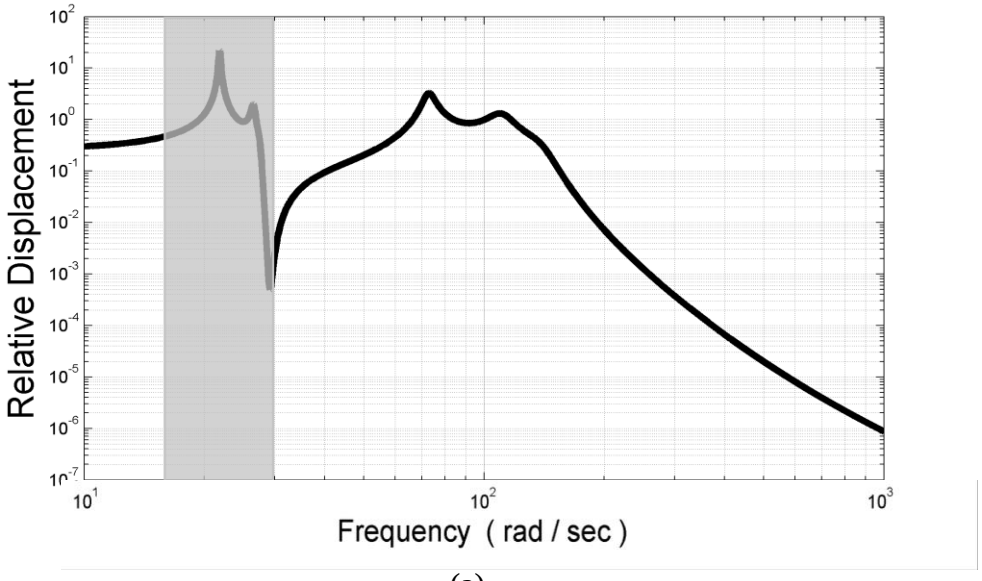

(a)

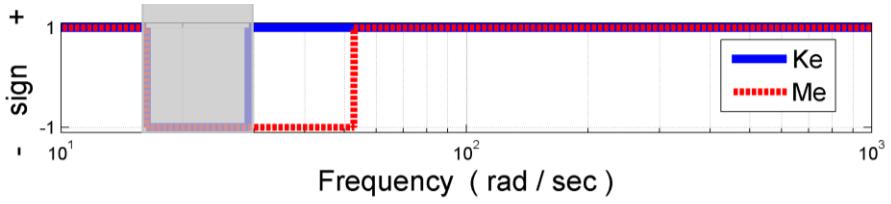

(b)

Fig. 7.9: The frequency response (a) and sign of the effective mass and stiffness (b) for an *AAMM/THC* configuration 2 at low frequency

Fig. 7.9a displays the frequency response of the magnitude of the transfer function $|X_4/X_1|$. Fig. 7.9b shows the sign of the effective mass m_e and stiffness k_e of the metamaterial array. It can be easily seen that between 16-53 *rad/s*, the metamaterial array exhibits negative effective mass whereas its effective stiffness has a negative value over a band between 16-30 *rad/s*. Therefore, using the *AAMM/THC* resonators results in simultaneous double negative properties in the frequency range 16-30 *rad/s*.

Figures 7.7, 7.8, and 7.9 show the capability of the *AAMM/THC*, configuration 2, on achieving a double negative property response on various frequency ranges. The *AAMM/THC* can be tuned to bring double negativity to high, mid-range, and low frequency regions. This tuning-ability feature of the active acoustic metamaterial is depending mainly on the passive and active parameters.

7.3. Summary

This chapter has presented *AAMM* configurations consisting of array of Helmholtz resonators with active boundaries, piezoelectric boundaries. These active Helmholtz resonators are attached to the transmission line. The transmission line, however, has been sectioned into cavities. Each cavity has been also provided with active boundaries, piezoelectric boundaries. This dual-controllability feature insures the achievement of double negative parameter response of the metamaterial either through the Helmholtz resonator or the transmission line or both.

Various control configurations have been presented in this chapter. Each of these control configurations has offered a great deal of negativity response over certain frequency bandwidths. Moreover, the control configurations have succeeded in bringing the double negative parameter response into various frequency ranges, high, mid-range and low frequency ranges.

8.1 Metamaterial Unit Cell and Experimental Setup

A prototype of the active acoustic metamaterial cell incorporates three different materials as shown in Fig. 8.1. Water, in a cylindrical pipe, is confined from both ends with two *PZT*4 piezoelectric bimorphs. In the middle of the acoustic cavity a Helmholtz resonator cavity has been attached, in which the rigid cap is replaced with the same *PZT*4 bimorph as in the main cavity. The bimorph itself is composed of intermediate brass disk with *PZT*4 layers deposited on both surfaces. The internal cell diameter is 0.035m, its overall length is 0.045m and the overall diaphragm thickness is 0.5*mm* of which 0.135*mm* brass intermediate disk thickness.

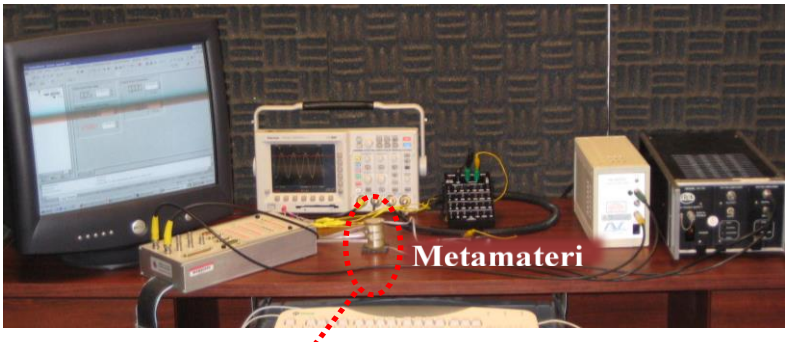

(a) – photograph of the experimental setup

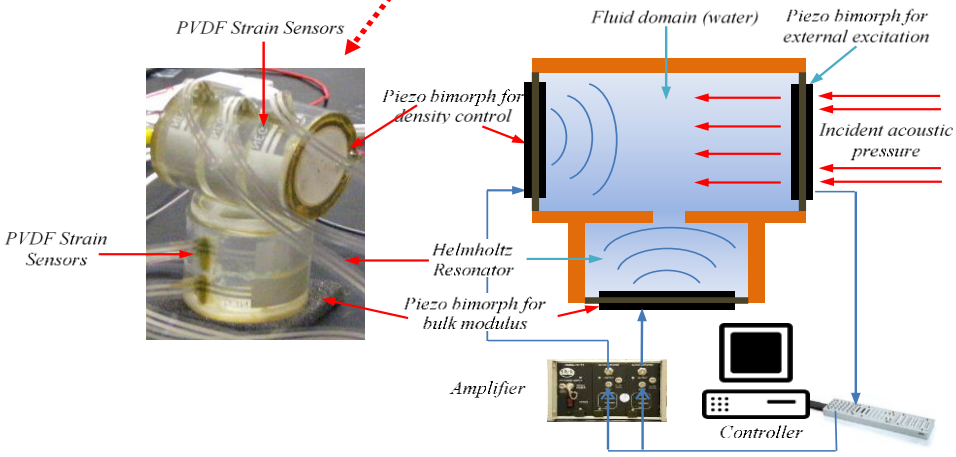

(b) – unit cell (c) – schematic drawing of the experimental setup

Fig. 8.1: Experimental setup of the active metamaterial cell

The cell is manufactured from an acrylic cylinder to form the main fluid cavity and the Helmholtz resonator. The piezoelectric bimorph diaphragms are wired, then coated with electrical insulating coating and then glued to the annular faces of the cylinder confining a fixed volume. Water is then injected through the 3*mm* circumferential hole until it fills the entire cylindrical volume leaving no air bubbles inside the cell. The hole is then sealed, leaving a composite water-PZT metamaterial cell for testing and evaluation. The main cavity length ($2\times l_f$) = 44.5*mm*, diameter = 32.6*mm*, Helmholtz resonator cavity length (l_H)=22.25*mm*, diameter = 32.6*mm*, Helmholtz resonator neck length (l) = 3*mm* and diameter = 3*mm*.

The basic concept of the *AAMM* lies in that the (sensing bimorph) measures the acoustic pressure passing throughout the cell and submits the measured signal to a feedback control circuit to generate a consequent control signal to the actuating bimorphs via a power amplifier to change their stiffness. Due to the incompressible nature of the confined fluid, direct coupling to the actuating bimorphs is established forming a homogeneous fluid-solid domain that acts as a single degree of freedom (*DOF*) system, provided the excitation wavelength is much larger than the dimension of the entire composite cell. Hence, changing the stiffness of one of the actuating piezoelectric bimorphs affects directly the stiffness of the second one, resulting in a controllable dynamic density (resulting from the effect of the face-mounted bimorph) and the bulk modulus (resulting from the effect of the Helmholtz mounted bimorph) of the entire single *DOF* fluid domain.

In summary, the main cavity of the metamaterial cell included three *PZT*4 piezoelectric bimorphs of 37 *mm* diameter. The first of these actuating bimorphs, on the right of the acoustic cavity, is used to generate a sinusoidal excitation at frequencies ranging from 200-2*k Hz*. The second bimorph, located at the left of the acoustic cavity, is utilized to control the effective density of the metamaterial unit cell. The third bimorph, is mounted at the bottom of the Helmholtz resonator, to control the bulk modulus of the cell.

8.2 Programmable Density:

A direct measure of the dynamic density of the metamaterial acoustic domain is the pressure gradient as indicated by Euler's equation. Therefore, the acoustic pressure is measured at the 3 equally-spaced locations using three *PVDF* piezosensors bonded to the walls of the acoustic cavity. These sensors generate electric signals which are proportional to the dynamic pressure acting on them. Accordingly, taking the difference between these signals can be used to compute the spatial pressure gradient along the cell. Using closed-loop feedback control, where the desired dynamic density value is fed as the reference signal. The difference between the measured and reference density values, forms the control error signal, is forwarded to a controller to activate the left piezoelectric bimorph as shown in Fig. 8.1.

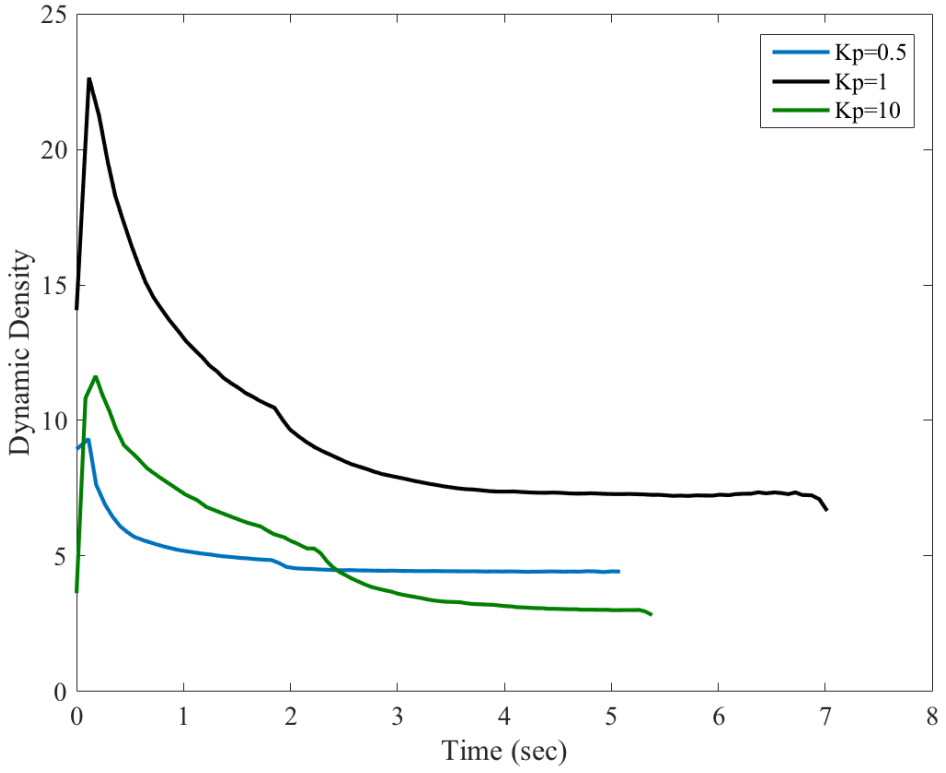

Fig. 8.2: Time response for the Active Acoustic Metamaterial cell with proportional gain. The dynamic density is set to achieve dynamic levels that are double the original static levels.

The displayed control system is used to generate stable values of effective dynamic densities ranging from 2-20 times the original fluid domain static density.

Figs 8.2 and 8.3 display the time response and the control voltage of the active metamaterial cell for reference dynamic density that is two times the original density respectively. The cell is subjected to sinusoidal excitation at 1000 *Hz*. The figures display also the associated control voltages which are necessary to generate the desired densities.

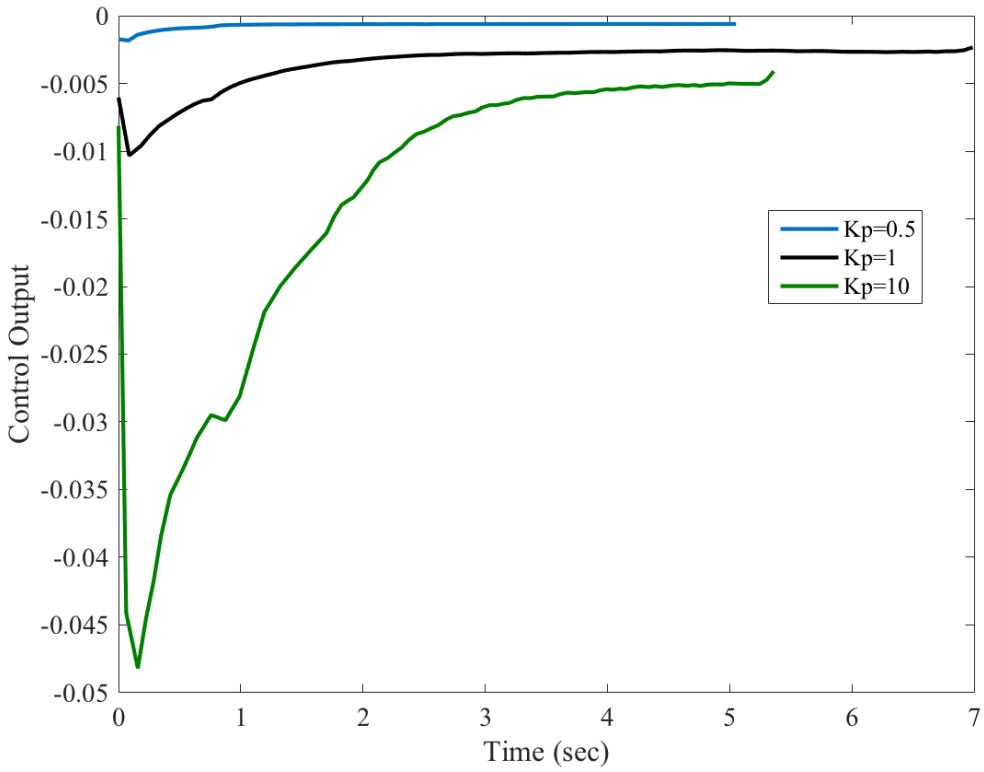

Fig. 8.3: Control response of the Active Acoustic Metamaterial cell with proportional gain. The dynamic density is set to achieve dynamic levels that are double the original static levels.

Due to the physical and geometrical parameters of the active metamaterial cell, it possesses a fundamental frequency of 800 *Hz*. For frequencies below 800 Hz, any control action has limited effect on the achievable relative density values as can be seen

from. Therefore, excitations above the first natural frequency are employed to enable the realization of wide range of effective dynamic densities.

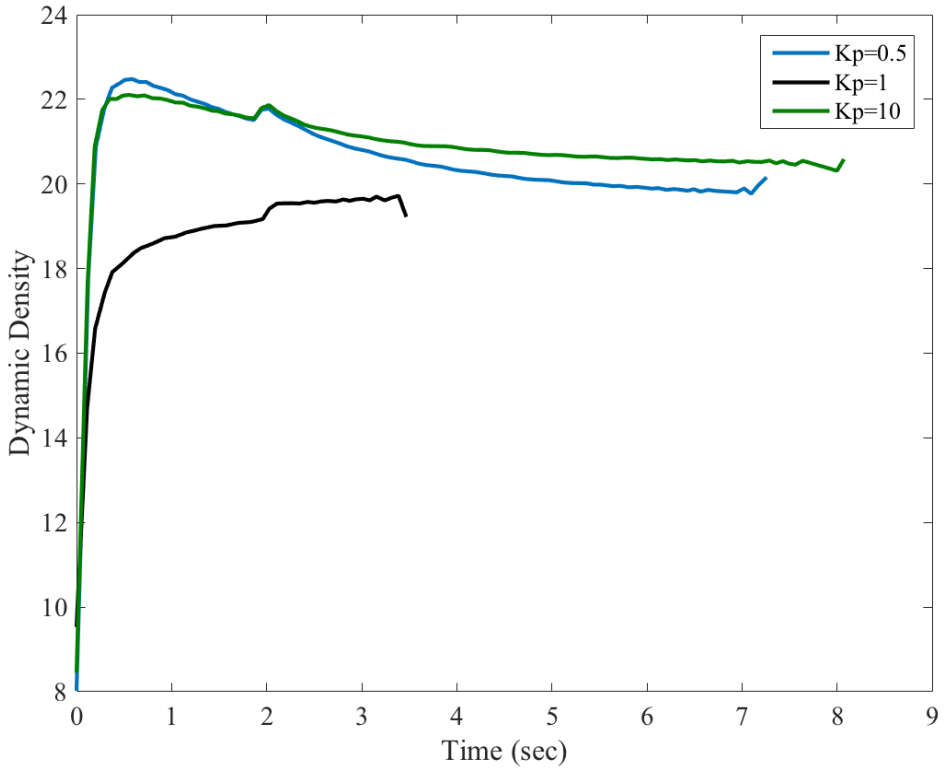

Figure 8.4: Time response for the Active Acoustic Metamaterial cell with proportional gain. The dynamic density is set to achieve dynamic levels that are twenty times higher than the original static levels.

At first, a controller with proportional gain has been applied to the Active Acoustic Metamaterial cell to generate a controlled signal required to maintain the density level at two times higher than the static level.

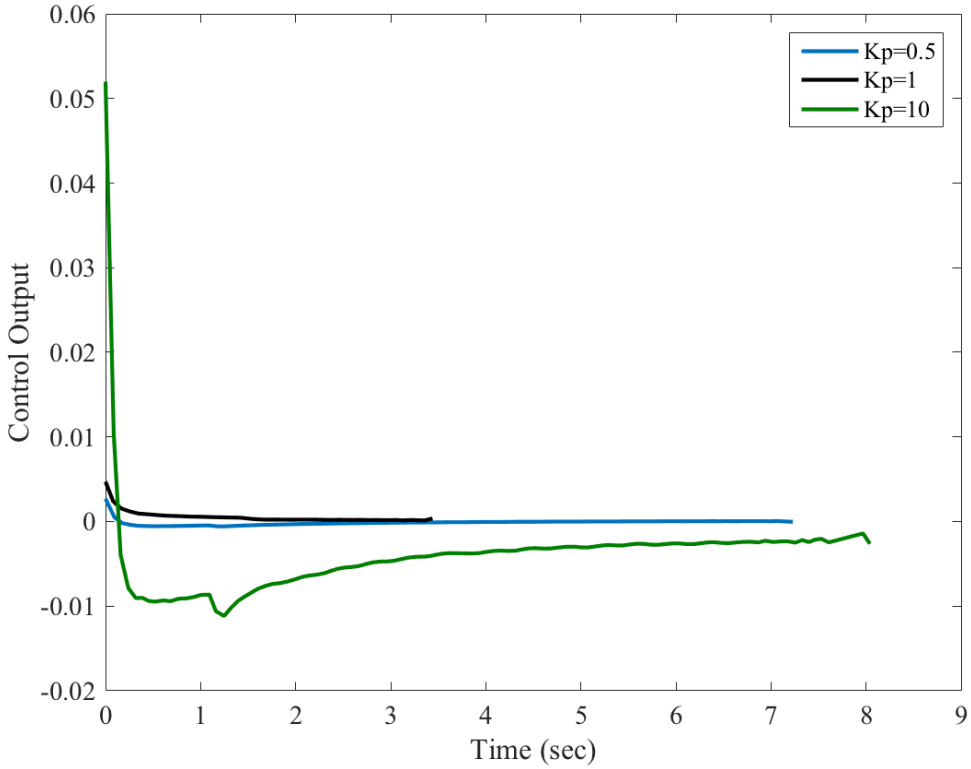

Figure 8.5: Control output of the Active Acoustic Metamaterial cell with proportional gain. The dynamic density is set to achieve dynamic levels that are twenty times higher than the original static levels.

Fig.8.2 displays the *AAMM* cell's time response and control output undertaken by the proportional-type controller. The controller is set at proportional gains ranging from 0.5 to 10. Fig. 8.3 shows the corresponding control voltage needed to control the desired dynamic density level which is double the original measured levels.

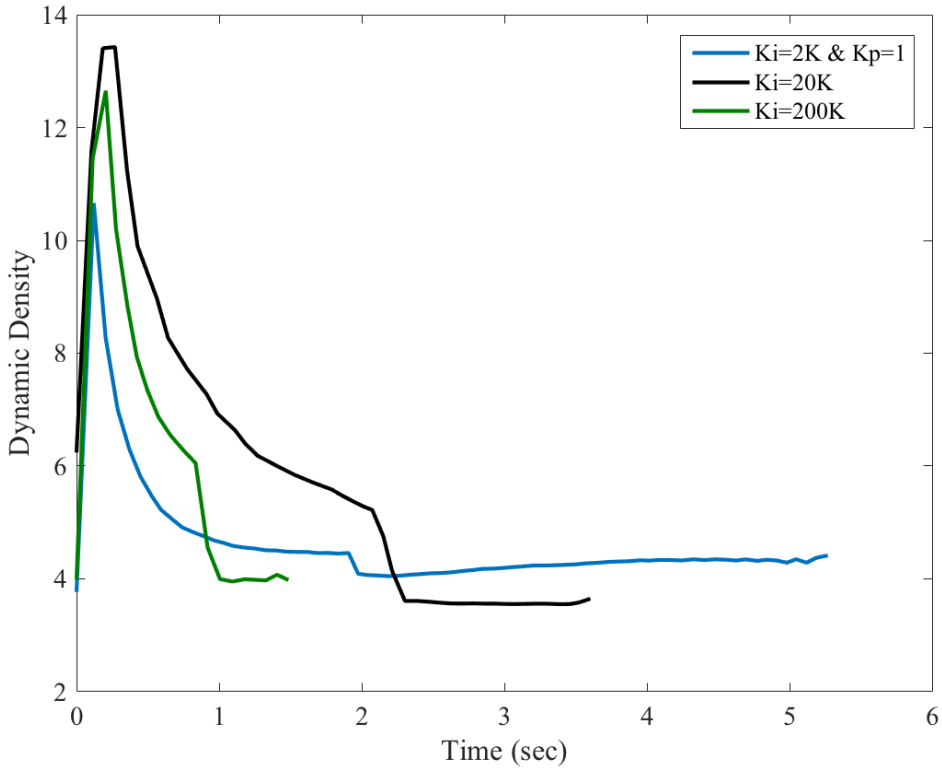

Figure 8.6: Time response for the Active Acoustic Metamaterial cell with proportional-integral controller. The proportional gain is set at fixed value of 1 while altering the integral gains 2K, 20K, and 200K. The dynamic density is set to achieve dynamic levels that are double the original static levels.

Fig.8.4 displays the *AAMM* cell's time response and control output undertaken by the proportional-type controller when the reference dynamic density is set a level that is twenty times higher than the original density level. The controller is set at proportional gains ranging from 0.5 to 10. Fig. 8.5 shows the corresponding control voltage needed to maintain the dynamic density at the desired level.

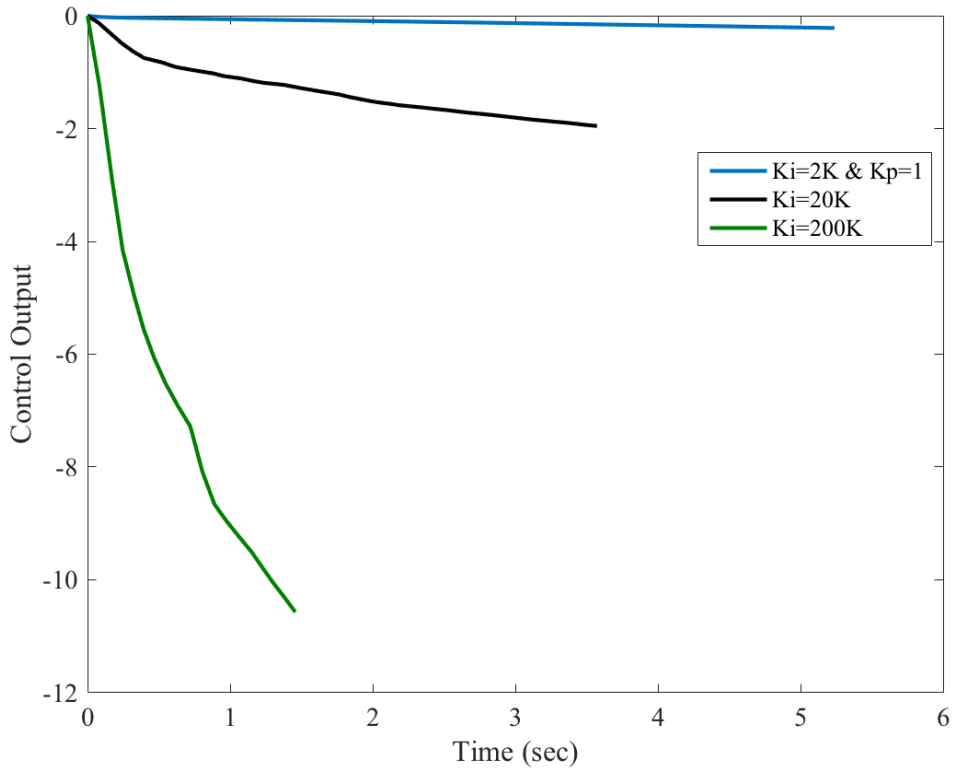

Figure 8.7: Control output of the Active Acoustic Metamaterial cell with proportional-integral controller. The proportional gain is set at fixed value of 1 while altering the integral gains 2K, 20K, and 200K. The dynamic density is set to achieve dynamic levels that are double the original static levels.

Attempts are carried out to reduce the steady state error caused by the proportional part of the controller. As a result a Proportional and Integral controller is used to eliminate the steady state error. In Figures 8.6 and 8.7 the time and control response of the Active Acoustic Metamaterial cell of the *PI* controller have been illustrated for the first case when the desired dynamic density level is two times the original density level. The displayed characteristics are obtained when the proportional gain K_p=1 and the integral gain is set to obtain the optimal response of the system.

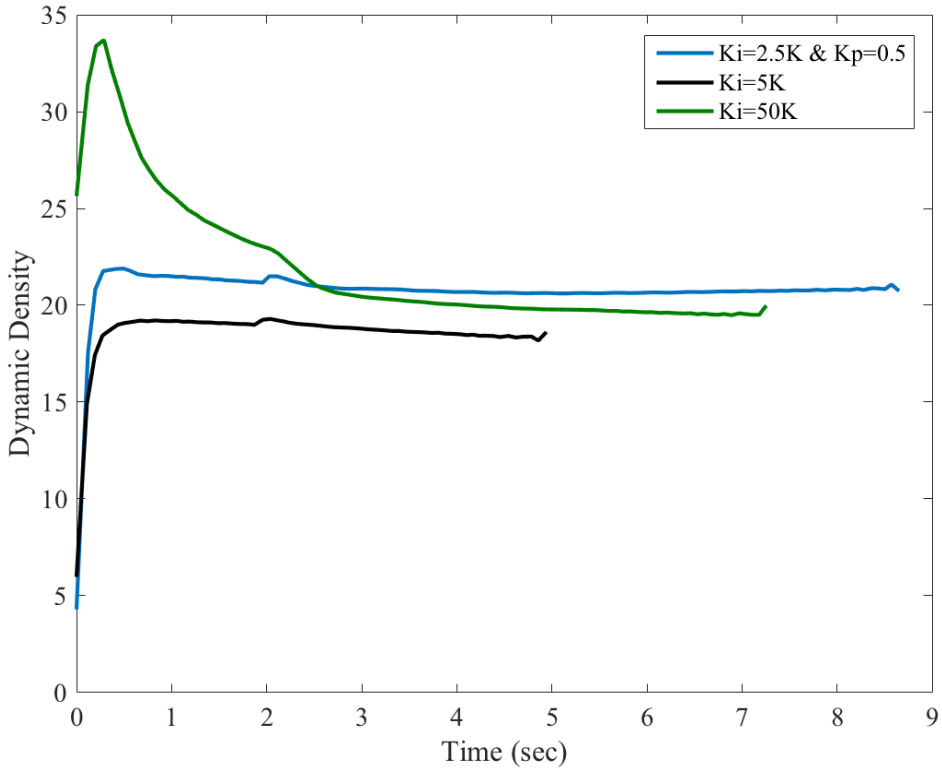

Figure 8.8: Time response for the Active Acoustic Metamaterial cell with proportional-integral controller. The proportional gain is set at fixed value of 0.5 while altering the integral gains 2.5K, 5K, and 50K. The dynamic density is set to achieve dynamic levels that are twenty times higher than the original static levels.

In Figures 8.8 and 8.9, the time and control responses of the Active Acoustic Metamaterial cell of the *PI* controller have been illustrated for the second case when the desired dynamic density is at twenty times higher than the static density level. As the integral gains have been altered to find the optimal gain value, the proportional gain in this case is maintained at K_p=0.5.

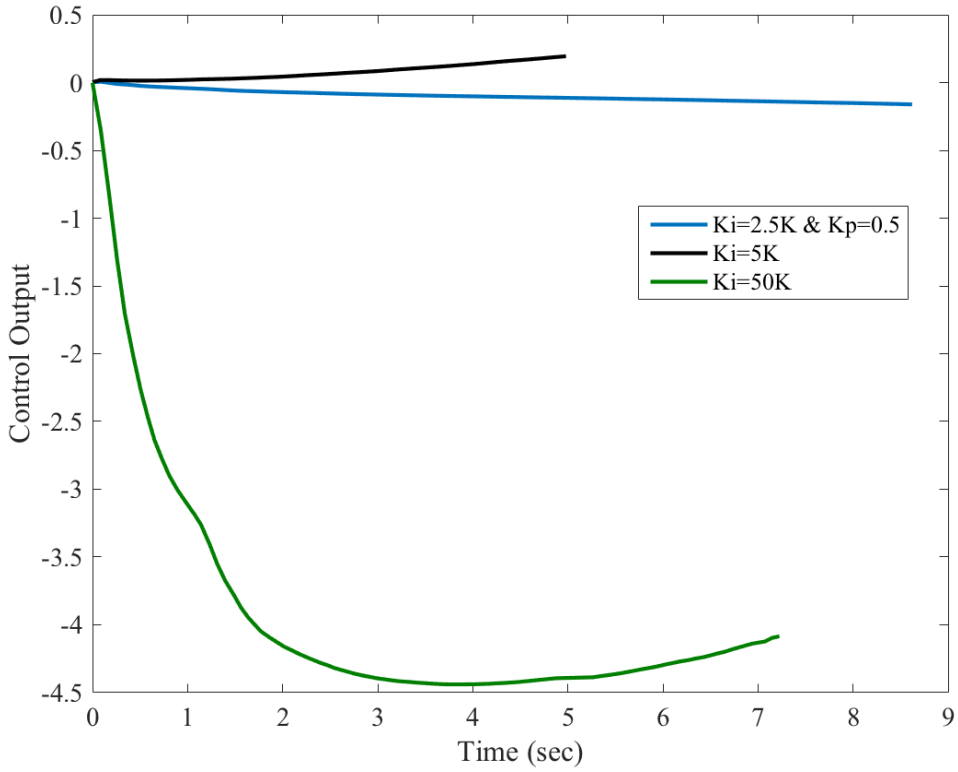

Figure 8.9: Control output for the Active Acoustic Metamaterial cell with proportional-integral controller. The proportional gain is set at fixed value of 0.5 while altering the integral gains 2.5K, 5K, and 50K. The dynamic density is set to achieve dynamic levels that are twenty times higher than the original static level

To summarize the performance of the Active Acoustic Metamaterial with Tunable Dynamic Density, a summary figure, Fig 8.10, consisting of two parts, one for the P controller and the other for a PI controller, has been generated. In the summary figure, the settled values for the dynamic density that are set at desired levels of two to twenty times the original levels are plotted. In part (a) of Fig 8.10, the desired dynamic density values at given proportional gains, using a proportional controller, is shown. Similarly, the integral gains with their corresponding dynamic density values are displayed in part (b) of Fig 8.10.

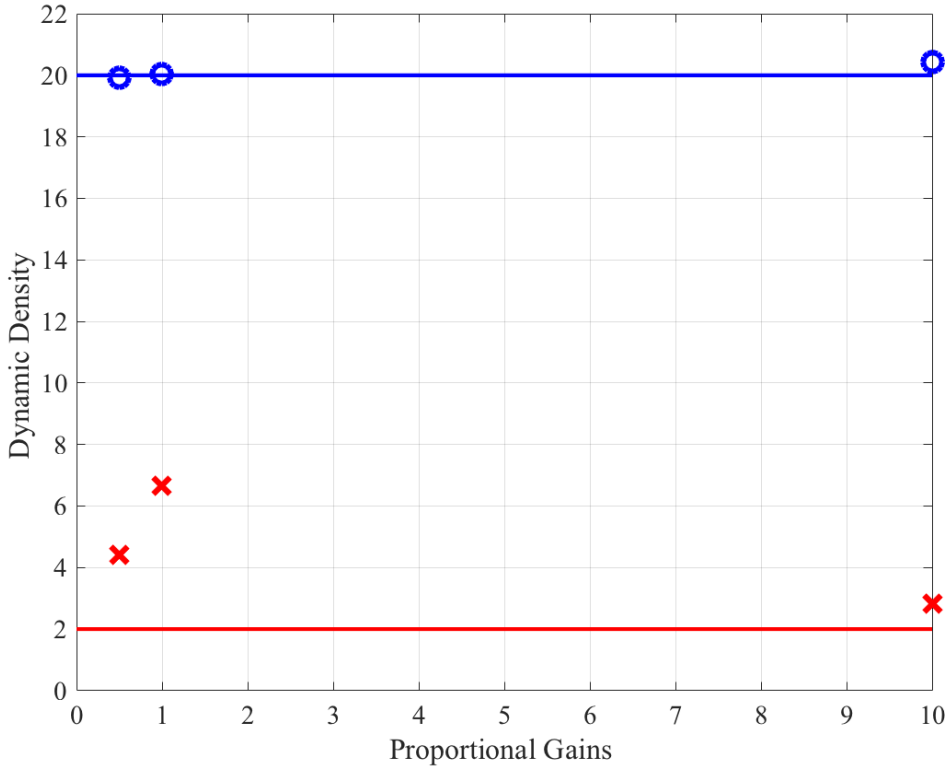

(a)

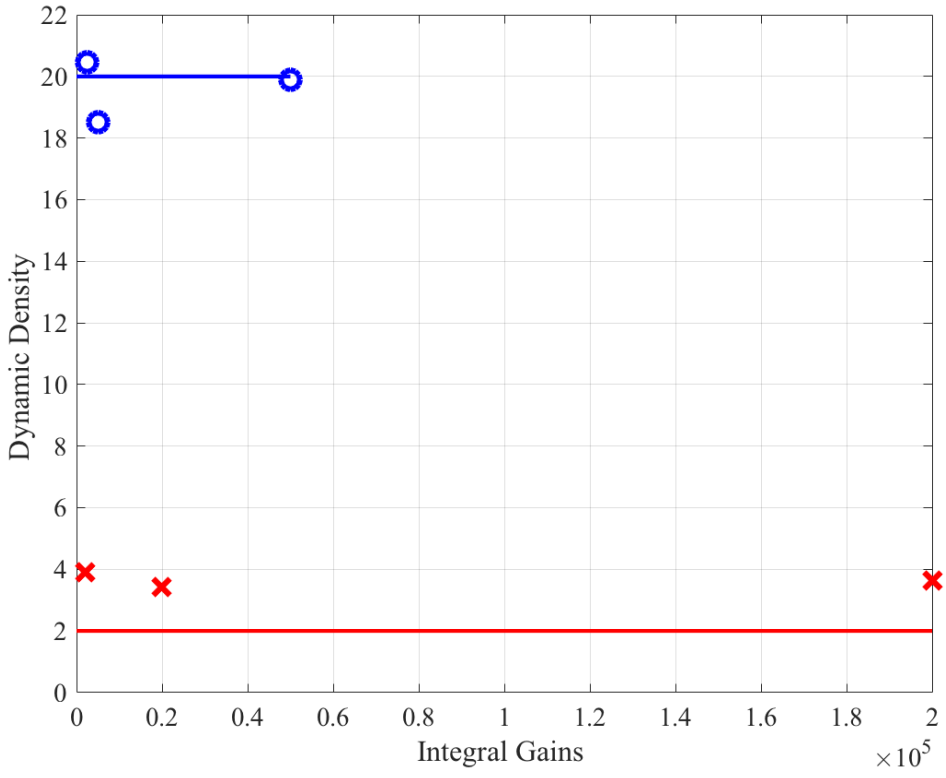

(b)

Figure 8.10: A summary figure for dynamic density levels achieved by the Active Acoustic Metamaterial at the desired levels of two and twenty times the original levels. (a) shows the dynamic density levels using a proportional controller plotted against the change in the proportional gains. (b) is displaying the dynamic density as a result of altering the integral gains using a PI controller.

By using a proportional controller and specifically at the desired level of twenty times higher, the dynamic density values of the AAMM seem to be at comparable levels as we increase the proportional gains. One can observe that the best value for the dynamic density has been accomplished when the proportional gain is at 1. On the other hand, when the desired value is set at levels that are twenty times higher, the P controller would bring an optimal value when the proportional gain is set at 10.

The implementation of the Proportional and Integral controller can assist to achieve an optimal value of the dynamic density at an integral gain of 50K, when the desired level of the *AAMM* is set at twenty times the static level. For the case of double

the original levels, it is noticeable that increasing the integral gains beyond 20K have no impact on the dynamic density. Hence, the *AAMM* with PI controller in this case has an optimal value at an integral gain of 20K.

8.2.1 System Identification of the Active Acoustic Metamaterial system:

For dynamical systems, system identification is a procedure used to develop a mathematical model of the corresponding system. Any system consists mainly of an exerted variable called input and an observed variable, output. These two system variables, input and output, are essential ingredients in the system identification process.

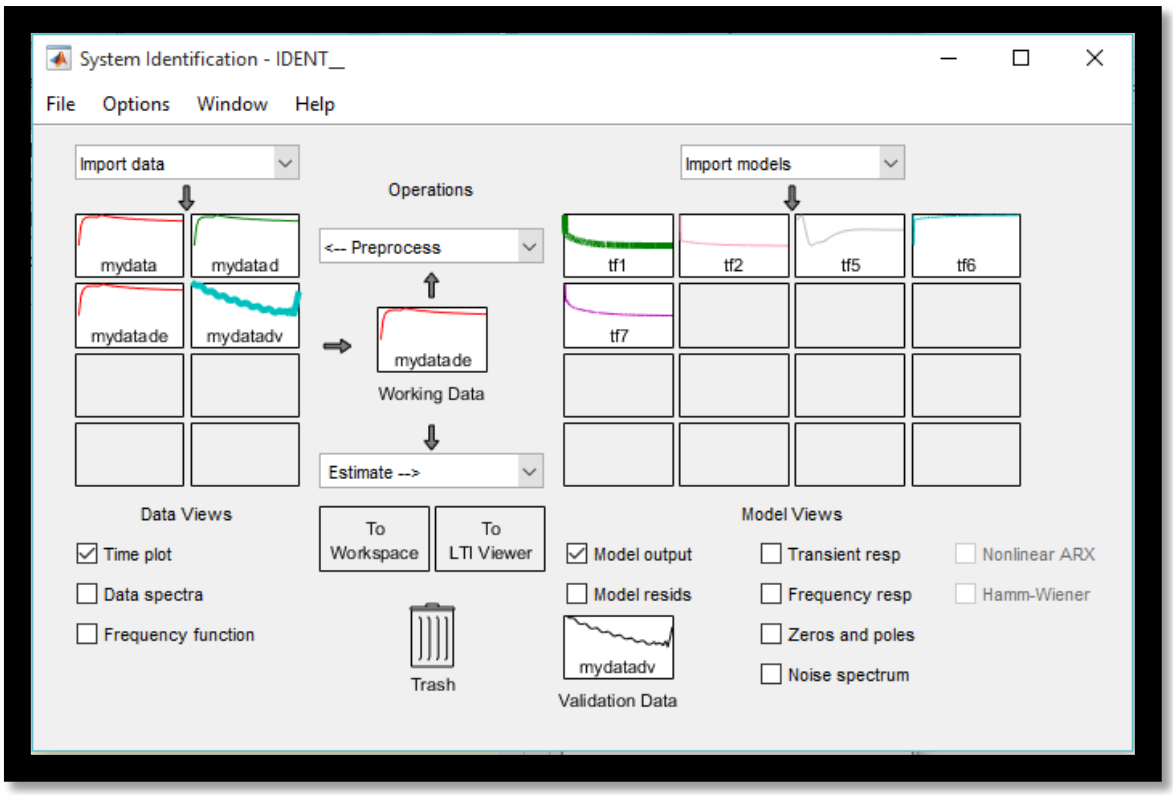

Figure 8.11: System Identification Tool Box, *ident,* computer window for the *AAMM* with Tunable Dynamic Density.

The system's variables, input and output, are recorded during the experiment. The recorded data of the system is stored and provided to the System Identification Tool Box for data analysis. A Matlab designed System Identification Tool Box, ident, is used for this purpose, see Fig. 8.11.

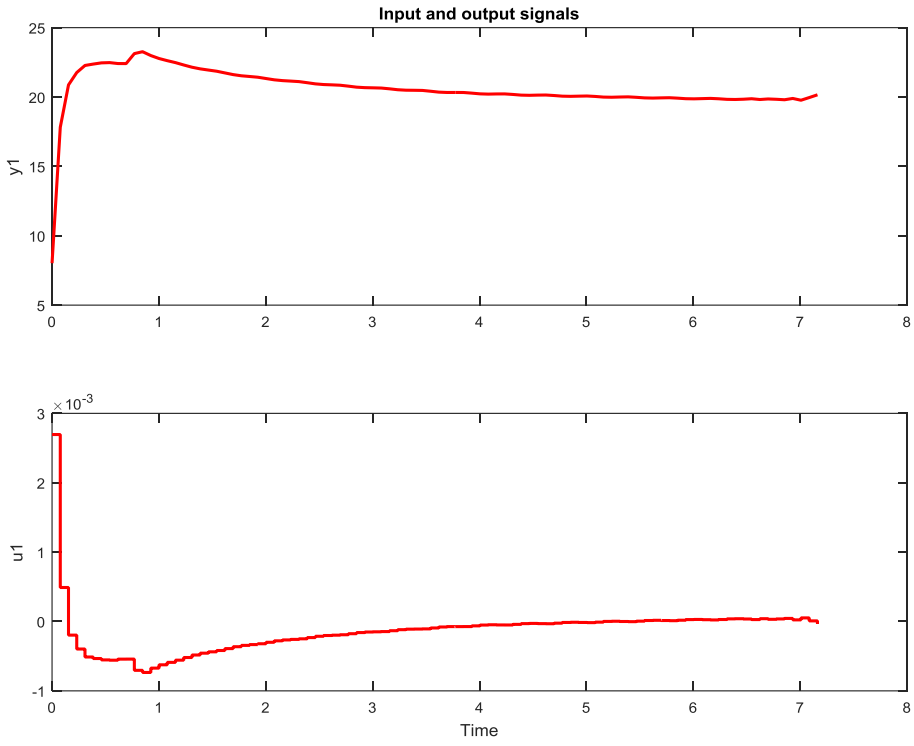

Figure 8.12: The system's input and output, u1 and y1 respectively, using System Identification Tool Box.

In this section the system in which the System Identification procedure would be applied to is the *AAMM* with programmable dynamic density. The input variable to the system is the generated electric signal. On the other hand, the output variable for the system is the dynamic density.

In the system identification application ident, a Matlab product, the system variables are imported as time-domain signals. The case when the desired dynamic density is at 20 times higher than the original static levels is used to be systematically

identified. For the system of the *AAMM* with programmable dynamic density, the input and output variables are plotted in Fig. 8.12. After importing the system's data, the transfer function model is estimated according to the chosen number of poles and zeros. Different Transfer Function models have been studied for the best model of the identified system.

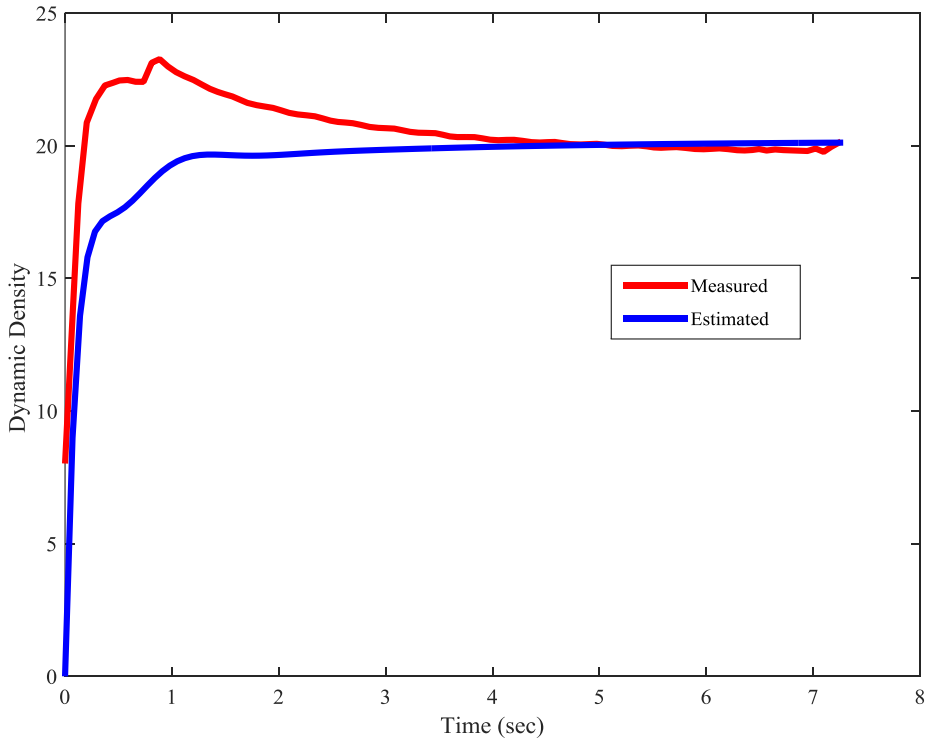

Figure 8.13: The measured vs estimated dynamic density response.

The Transfer Function model has been exported from the System Identification application for further analysis. From the exported model, the close loop system at a gain of $k = o.ooo16$ is generated. For comparison purposes, the estimated model is plotted against the measured model as displayed in Fig.8.13.

8.3 Programmable Bulk Modulus

The performance characteristics of the active acoustic metamaterial cell during the control of the effective bulk modulus are displayed in Fig. 8.14.

Fig. 8.14 shows the window of the bulk modulus controller which displays all the monitored and controlled parameters. The window of the controller shows in real time the obtained time response of bulk modulus for a desired effective bulk modulus.

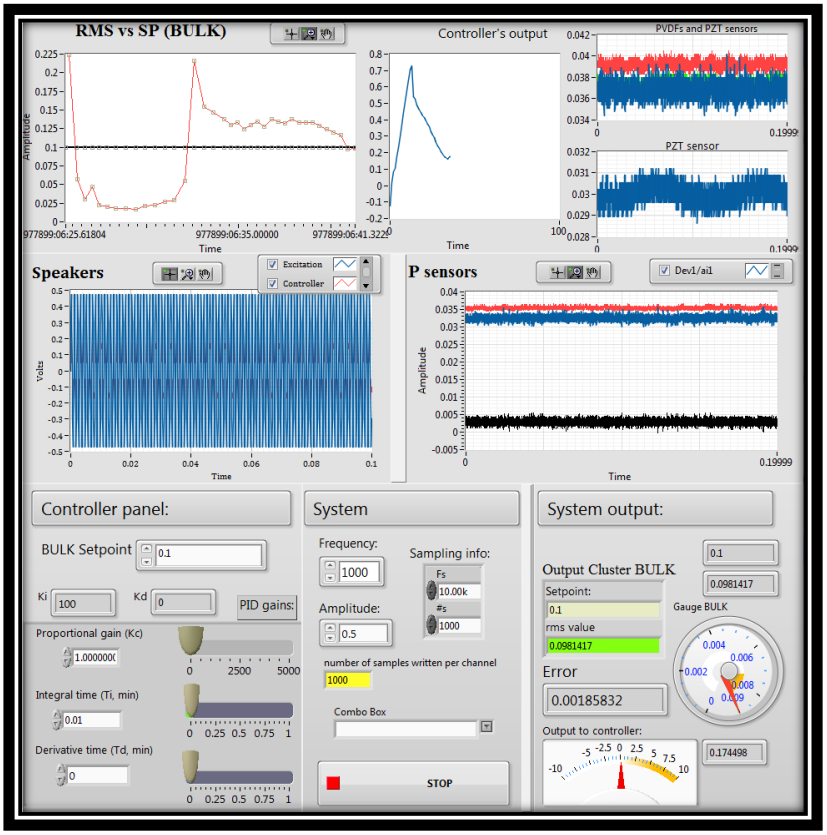

Fig. 8.14: Window of the bulk modulus controller of the active acoustic metamaterial cell

Time response of the bulk modulus of the active metamaterial cell for reference dynamic bulk moduli κ_r of multiple times higher and lower than that of the ambient will be invistigated in this section. These characteristics are obtained when the cell is subjected to sinusoidal excitation at 1000 *Hz*. Note that the same active metamaterial cell can be programmed to achieve bulk moduli that are set at different levels from the original static level.

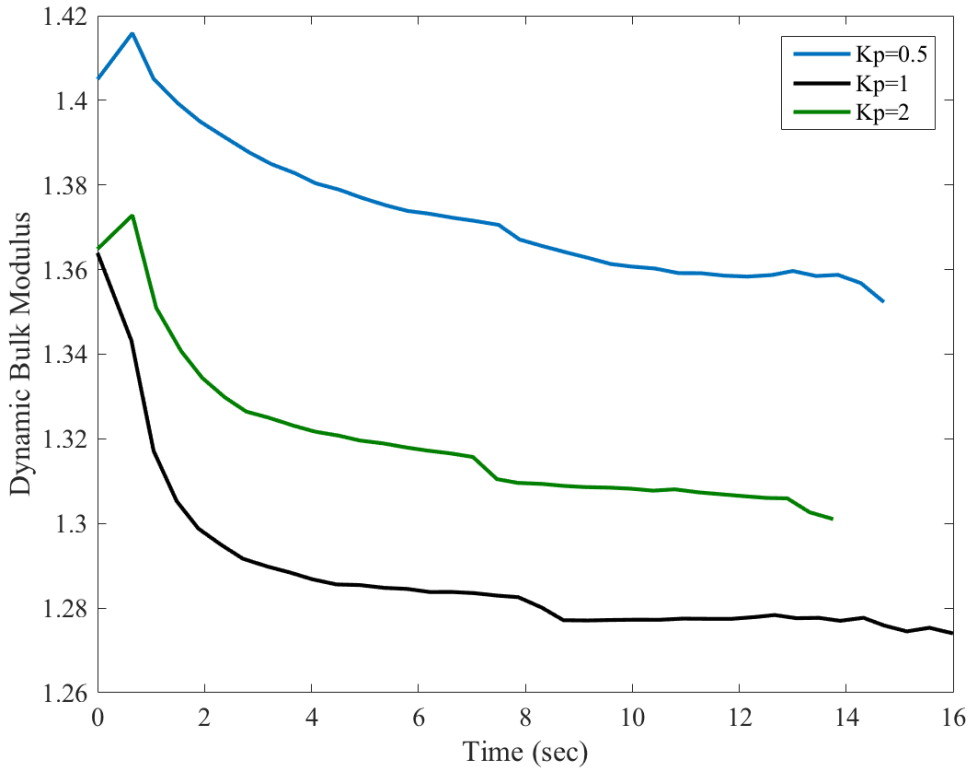

(a)

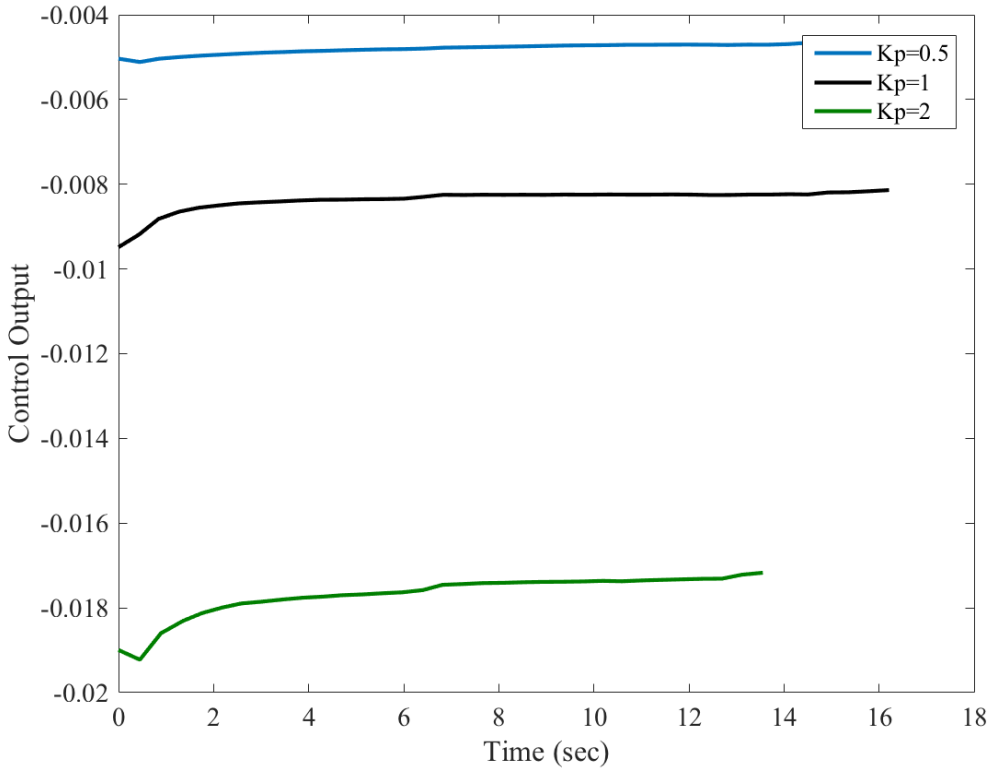

(b)

Figure 8.15: Dynamic bulk modulus, (a), and Control Outputs, (b), for the Active Acoustic Metamaterial cell using a proportional controller. The dynamic bulk modulus is set at only 70% of the original level. The proportional gains are given as 0.5,1, and 2.

Figure 8.15 shows the time and control response of the Active Acoustic Metamaterial cell when the desired dynamic bulk modulus is set at 70 % of the original static level. The proportional gain is maintained at values K_P of 0.5, 1, and 2.

In order to reduce the steady state error caused by the proportional part of the controller, a Proportional and Integral controller is used. The time and control response of the Active Acoustic Metamaterial cell with Tunable Bulk Modulus of the *PI* controller have been illustrated for the three chosen cases on a lower and higher scale from the original measure. The desired dynamic bulk modulus level at 70 % less, thirty five, and almost seventy times higher than the static level of bulk modulus.

The desired levels of the dynamic bulk modulus are set at extremely high levels as an attempt to exercise the *AAMM* to reach the highest levels possible. Although these levels are unrealistic, the resulted dynamic bulk modulus levels will be defining the ceiling in which the *AAMM* cannot exceed.

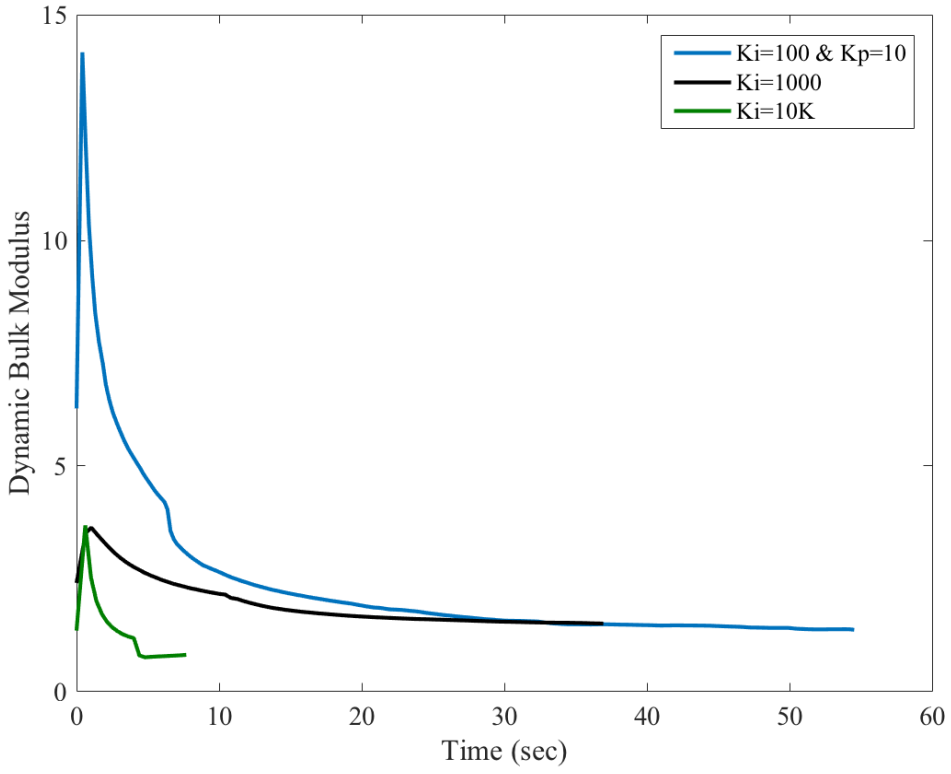

(a)

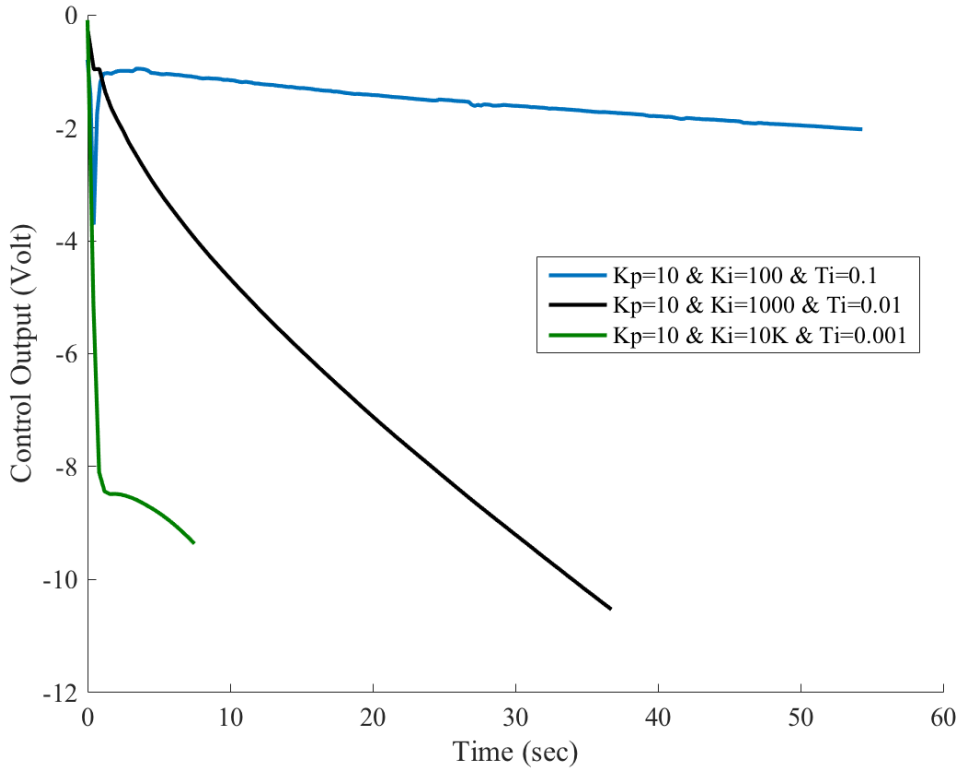

(b)

Figure 8.16: Dynamic bulk modulus, (a), and Control Outputs, (b), for the Active Acoustic Metamaterial cell using a proportional-integral controller (PI). The bulk modulus is set at 70 % of the original static level. The proportional gain is maintained at a fixed value where the integral gains are varying between 100,1000, and 10K.

Figure 8.16 displays the time and control response of the Active Acoustic Metamaterial cell when the desired dynamic bulk modulus is set at 70 % of the original static level. The proportional gain is maintained at a fixed value K_P= 10 where the integral gains are varying between 100,1000, and 10K.

Figure 8.17 shows the time and control response of the Active Acoustic Metamaterial cell when the desired dynamic bulk modulus is set at 35 times higher than the original static level. The proportional gain is maintained at values K_P of 0.5, 1, and 5.

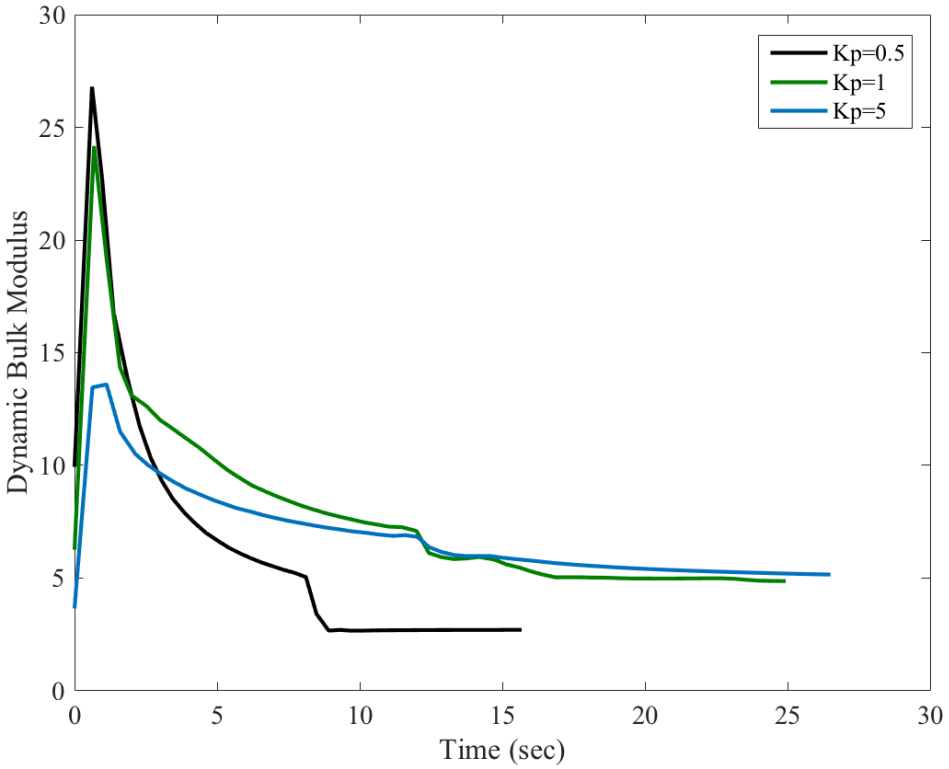

(a)

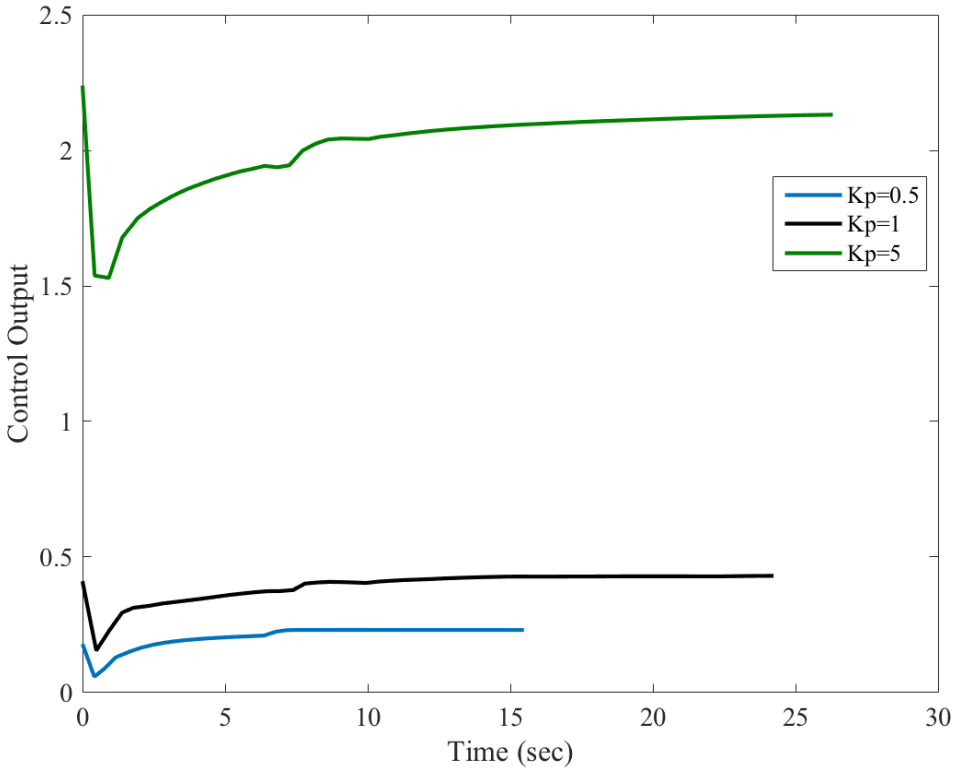

(b)

Figure 8.17: Dynamic bulk modulus, (a), and Control Outputs, (b), for the Active Acoustic Metamaterial cell using a proportional controller. The bulk modulus is set at 35 times higher than the original static level. The proportional gains are given as 0.5,1, and 5.

Figure 8.18 displays the time and control response of the Active Acoustic Metamaterial cell when the bulk modulus is set at 35 times higher than the original static level. The proportional gain is maintained at a fixed value K_P=1 where the integral gains are varying between 10,100, and 1000.

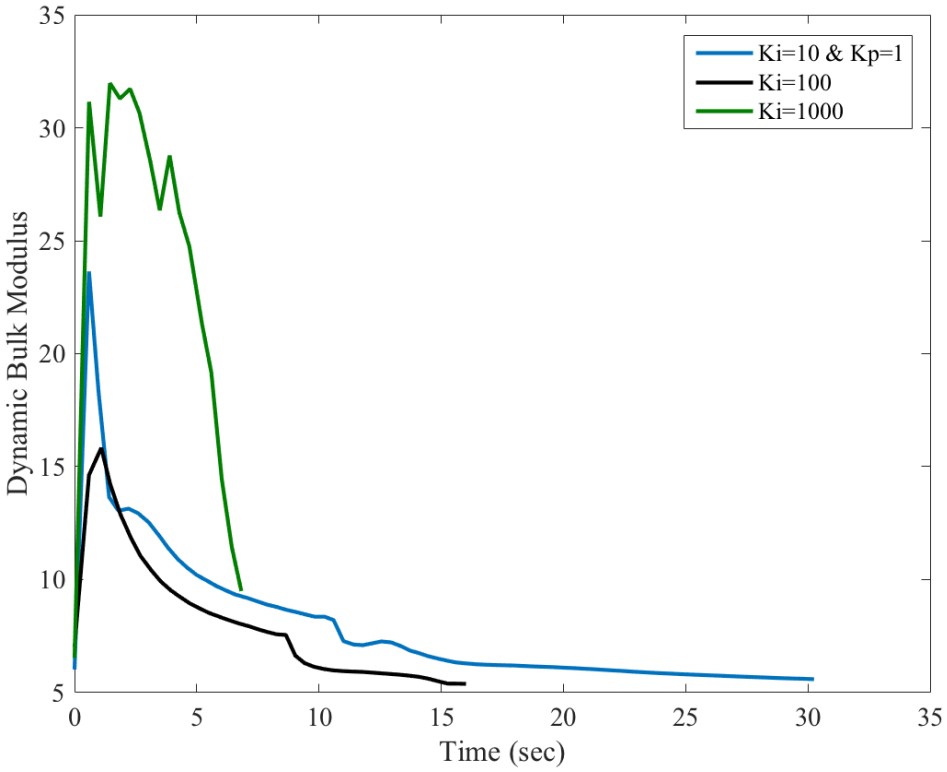
Ki=10 & Kp=1
Ki=100
Ki=1000
Dynamic Bulk Modulus
Time (sec)
35
30
25
20
15
10
5
0
5
10
15
20
25
30
35

(a)

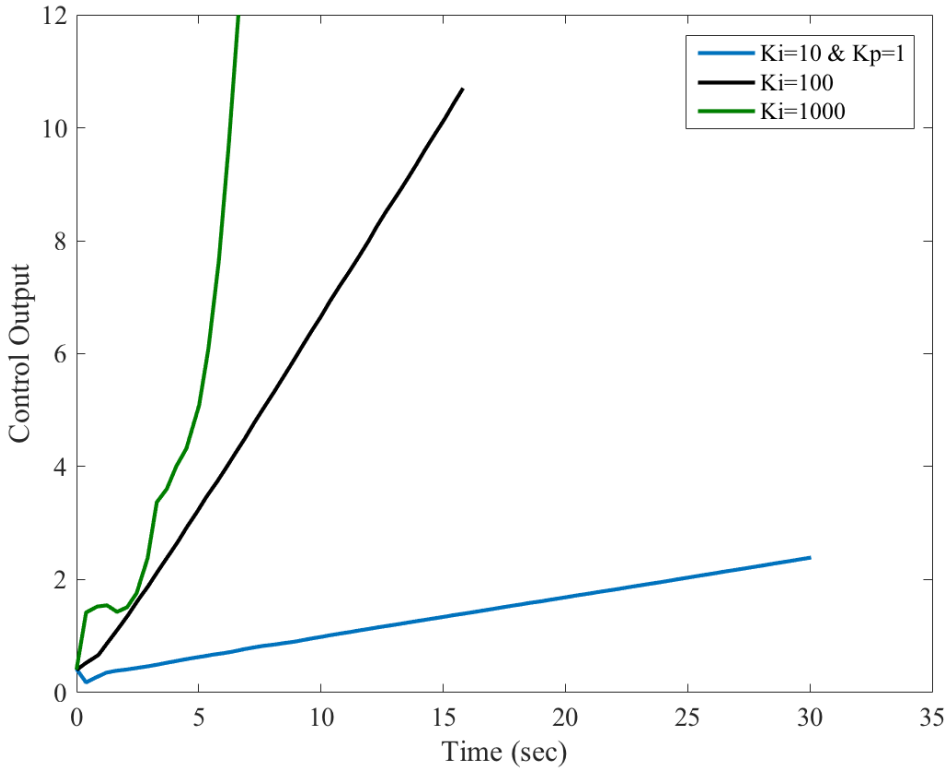

(b)

Figure 8.18: Dynamic bulk modulus, (a), and Control Outputs, (b), for the Active Acoustic Metamaterial cell using a proportional-integral controller (PI). The bulk modulus is set at 35 times higher than the original static level. The proportional gain is maintained at a fixed value where the integral gains are varying between 10,100, and 1000.

Figure 8.19 shows the time and control response of the Active Acoustic Metamaterial cell when the bulk modulus is set at almost 70 times higher than the original static level. The proportional gain is maintained at values K_P of 0.5, 1, 5, and 10.

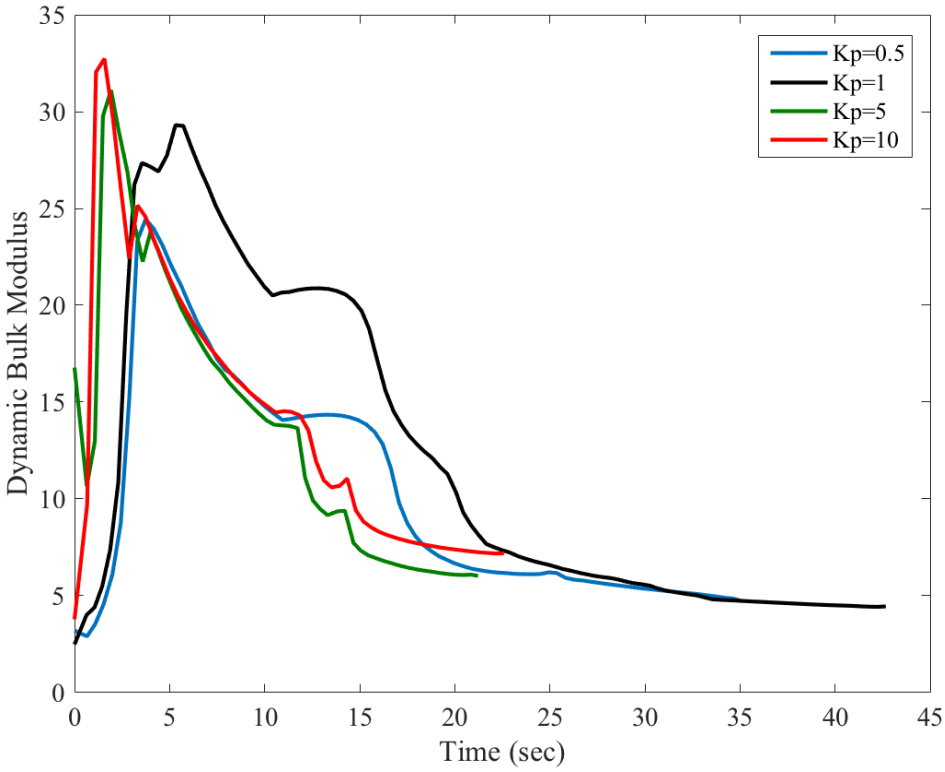
Kp=0.5
Kp=1
Kp=5
Kp=10
Dynamic Bulk Modulus
Time (sec)
0
5
10
15
20
25
30
35
40
45

(a)

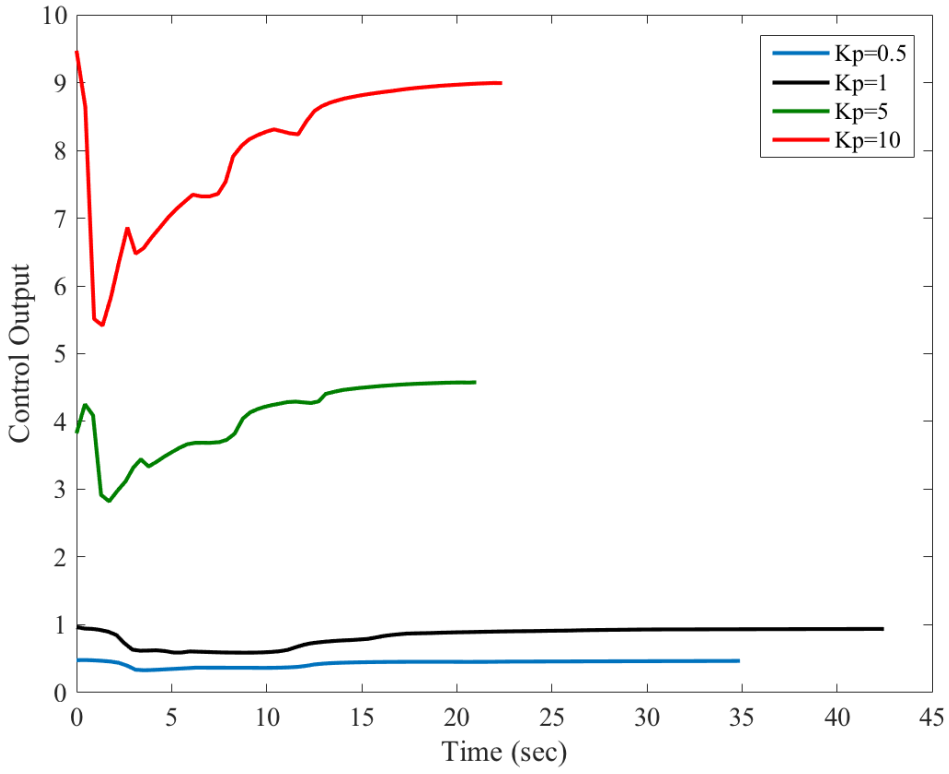

(b)

Figure 8.19: Dynamic bulk modulus, (a), and Control Outputs, (b), for the Active Acoustic Metamaterial cell using a proportional controller. The bulk modulus is set at 70 times higher than the original static level. The proportional gains are given as 0.5,1, 5, and 10.

Figure 8.20 displays the time and control response of the Active Acoustic Metamaterial cell when the bulk modulus is set at 70 times higher than the original static level. The proportional gain is maintained at a fixed value K_P=0.5 where the integral gains are varying between 0.5, 5, and 50.

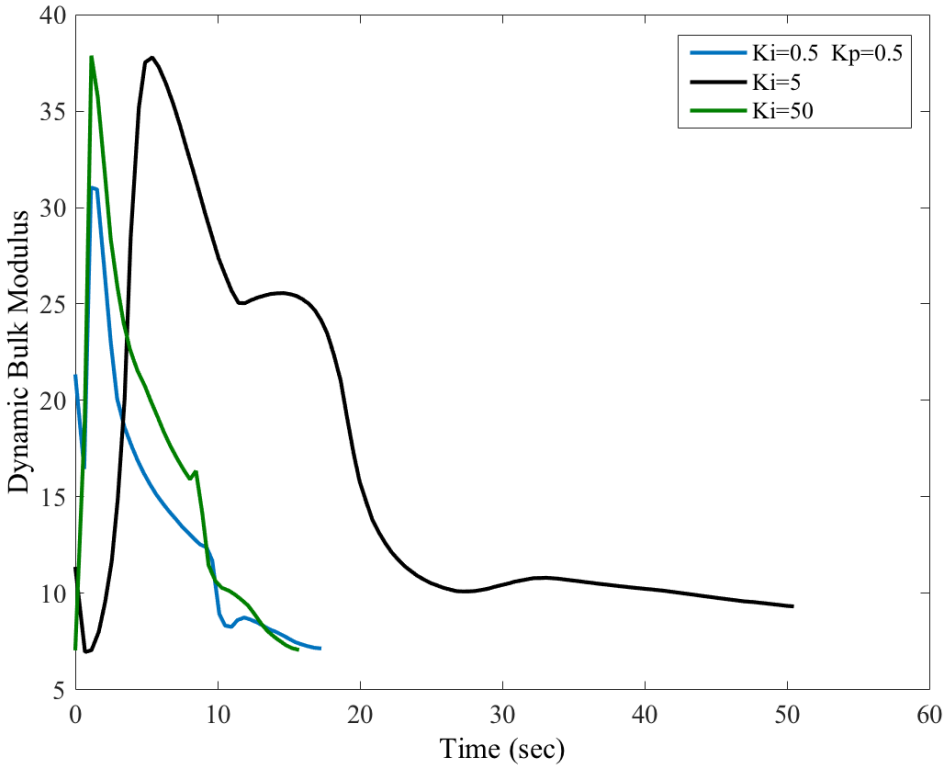
Ki=0.5 Kp=0.5
Ki=5
Ki=50
Dynamic Bulk Modulus
Time (sec)
40
35
30
25
20
15
10
5
0
10
20
30
40
50
60

(a)

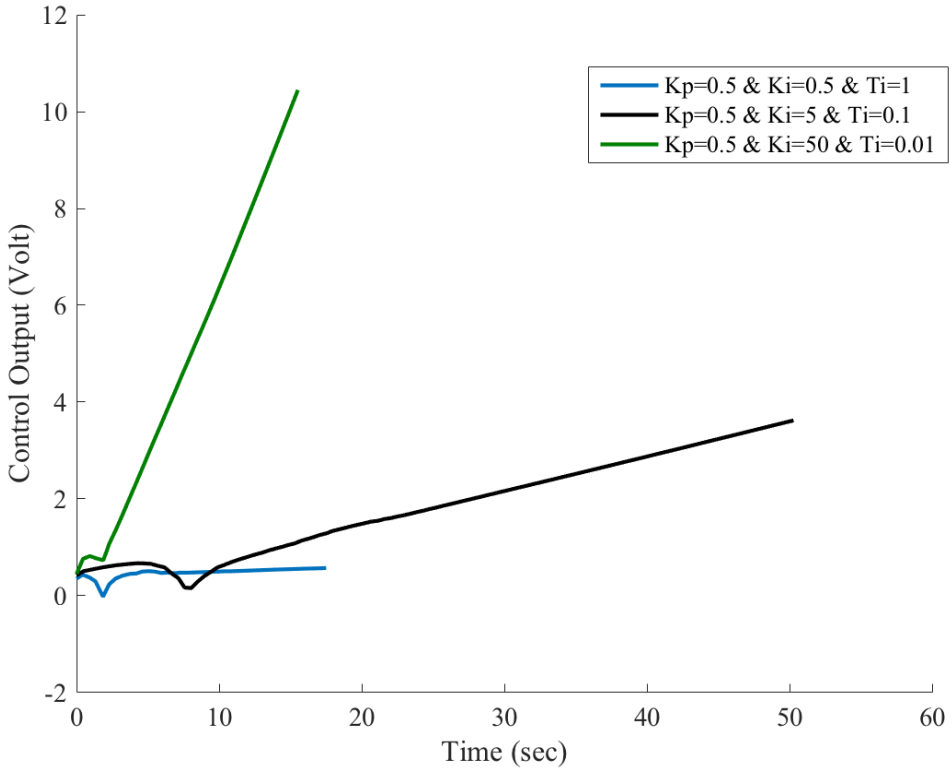

(b)

Figure 8.20: Relative Bulk Levels, (a), and Control Outputs, (b), for the Active Acoustic Metamaterial cell using a proportional-integral controller (PI). The Bulk Modulus is set at 70 times higher than the original static level. The proportional gain is maintained at a fixed value where the integral gains are varying between 0.5,5, and 50.

To better analyse the performance of the Active Acoustic Metamaterial with Tunable Bulk Modulus, summary figures have been generated, Fig 8.21. The performance of the *AAMM* with the proportional and PI controllers is also illustrated in (a), (b) and (c) of Fig 8.21. The settled values of the dynamic bulk modulus at the desired levels of 0.7, 35 and 70 of the original levels are displayed for the P-type and PI controllers. The *AAMM* with Proportional controller with various proportional gains at the chosen desired levels is shown in (a) of Fig 8.21. Similarly when using a PI controller, the integral gains with their corresponding dynamic bulk modulus values are displayed in part (b) and (c) of Fig 8.21.

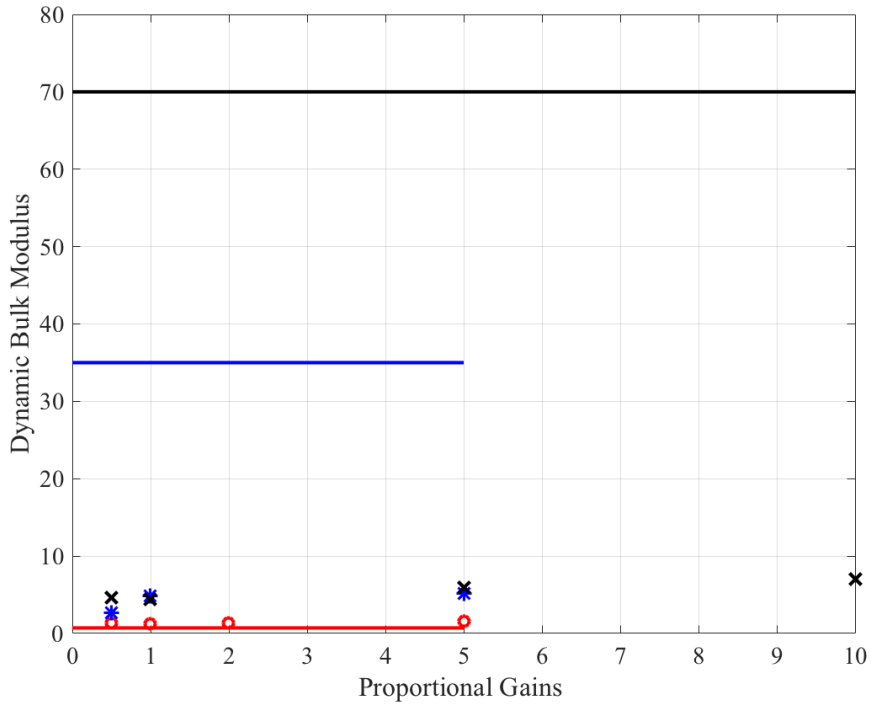
Dynamic Bulk Modulus
Proportional Gains
0
10
20
30
40
50
60
70
80
0
1
2
3
4
5
6
7
8
9
10

(a)

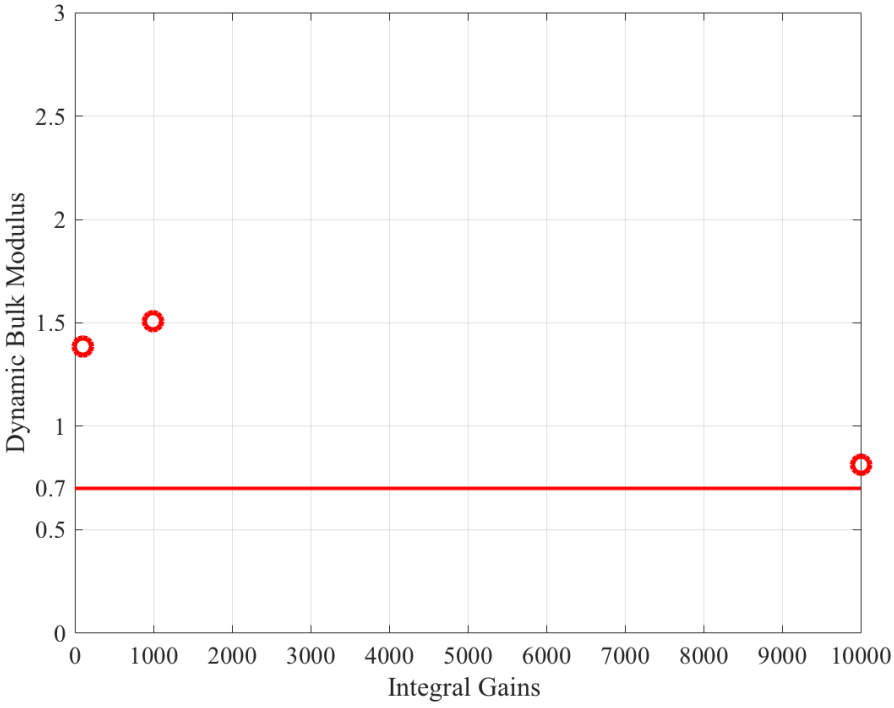
Dynamic Bulk Modulus
Integral Gains
0
0.5
0.7
1
1.5
2
2.5
3
0
1000
2000
3000
4000
5000
6000
7000
8000
9000
10000

(b)

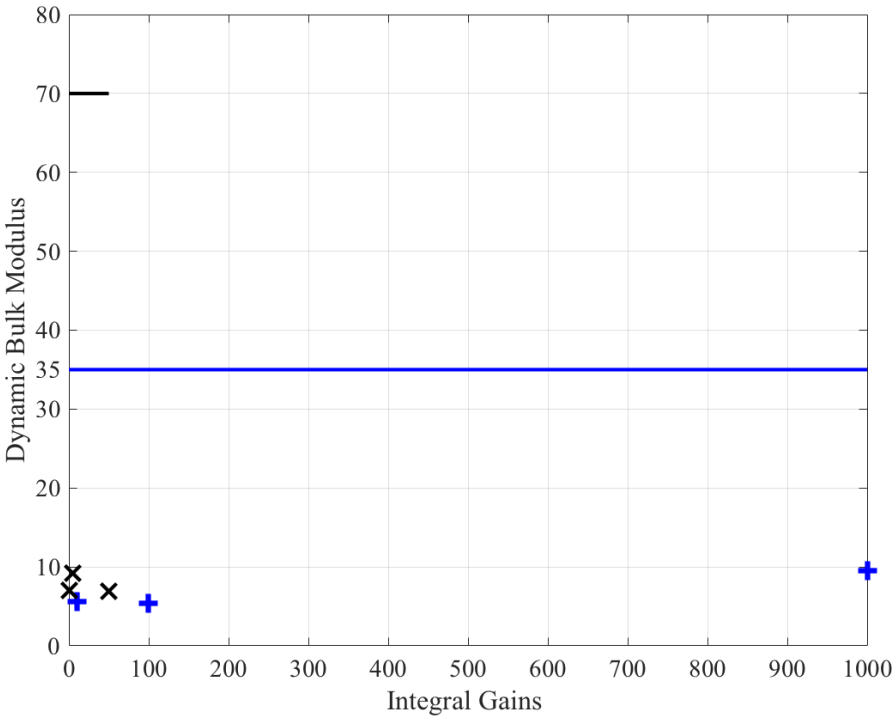

(c)

Figure 8.21: A summary figure for dynamic bulk modulus levels achieved by the Active Acoustic Metamaterial at the desired levels of 0.7, 35 and 70 times the original levels. (a) shows the dynamic bulk modulus levels using a proportional controller plotted against the change in the proportional gains. (b) and (c) is displaying the dynamic bulk modulus as a result of altering the integral gains using a PI controller.

By using a proportional controller and specifically at the desired level of 0.7 times less, the dynamic bulk modulus values of the AAMM seem to be at comparable levels as we increase the proportional gains. One can observe that the best value for the dynamic density has been accomplished when the proportional gain is at 0.5, see Fig 8.21 (a) as they are colored in Red. For the other cases when the desired levels were chosen at 35 and 70 times higher, increasing the proportional gains appear to bring the resulted dynamic bulk modulus to the desired values. Therefore, the optimum values for the range of the given proportional gains for the desired levels' cases of 35 and 70 were 5 and 10, respectively.

The implementation of the Proportional and Integral controller can assist to achieve an optimal value of the dynamic bulk modulus at an integral gain of 10K, when the desired level of the *AAMM* is set at 0.7 times less than the static level, (b) of Fig 8.21. For the case of 35 times the original levels, it is noticeable that at a very small integral gain, at 5, the *AAMM* was be able to achieve the highest possible level in this case. Likewise, in the case of 70 times the original the closest, yet the highest, to the desired level was accomplished at an integral of 1000.

8.3.1 System Identification of the Active Acoustic Metamaterial:

Developing a mathematical model for any given system is a procedure known as System Identification. By relating the input and output variables of the system, the system identification procedure will be able to extract meaningful information about the properties of the processed system.

The system's variables, input and output, are stored during the experiment. The acquired data of the system is provided to the System Identification Tool Box for data analysis.

A System Identification Tool Box named as ident which is a product of Matlab is used to identify the system, see Fig. 8.22.

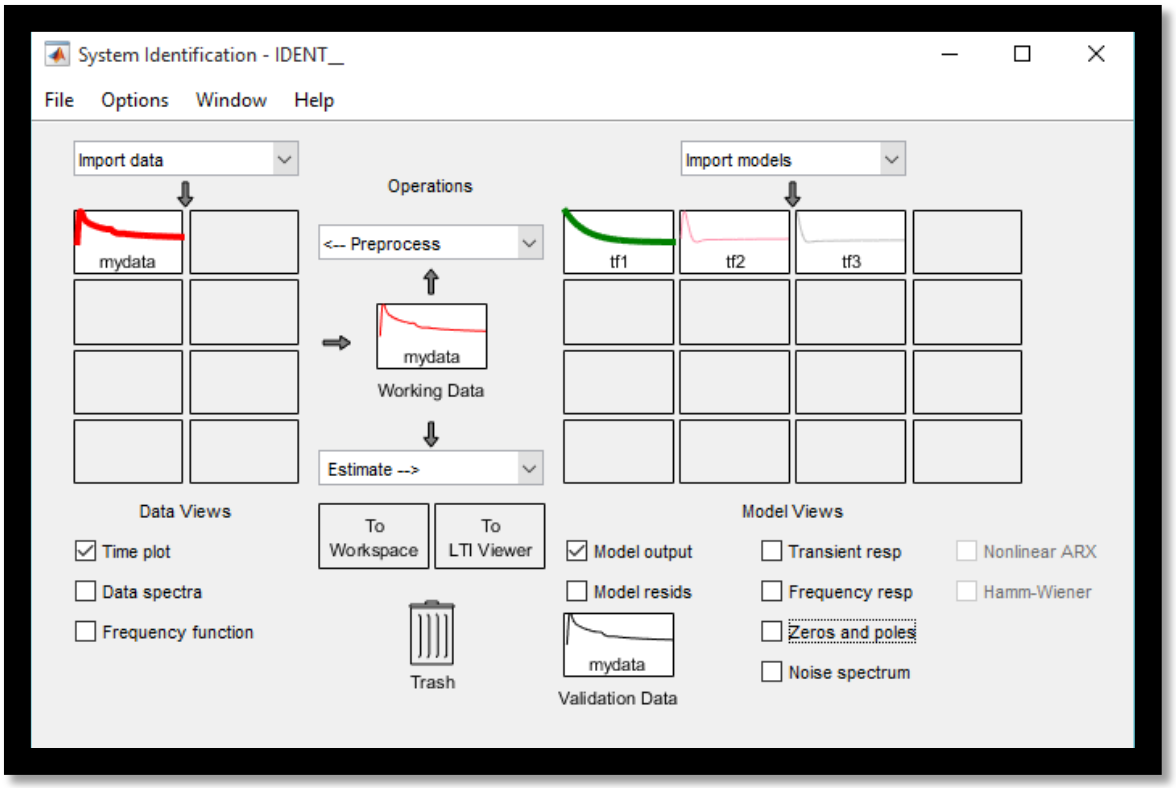

Figure 8.22: System Identification Tool Box, *ident,* computer window for the *AAMM* with Tunable Dynamic Bulk Modulus.

In this section the system in which the System Identification procedure would be applied to is the AAMM with programmable bulk modulus. The input variable to the system is the generated electric signal. On the other hand, the output variable for the system is the bulk modulus.

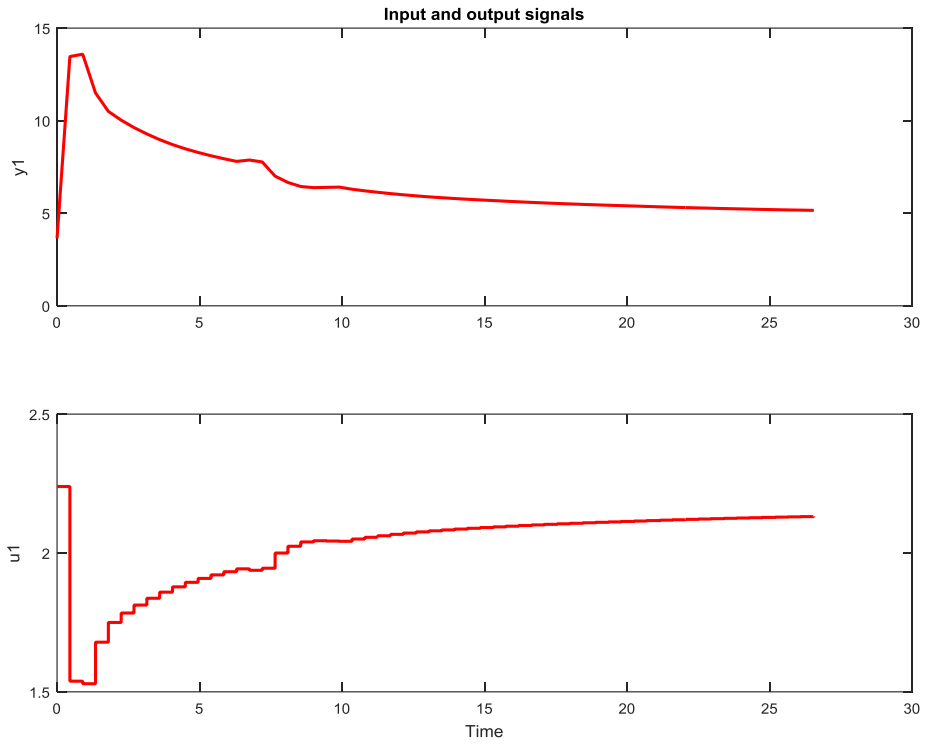

Figure 8.23: The system's input and output, u1 and y1 respectively, using System Identification Tool Box.

The system variables are imported as time-domain signals using the system identification application, ident. Here, the second case when the desired dynamic bulk modulus is 35 times higher than the original is used to be systimatically identified. For the system of the AAMM with programmable bulk modulus, the input and output variables are plotted in Fig. 8.23. After importing the system's data, the transfer function model is estimated according to the chosen number of poles and zeros. Different Transfer Function models have been studied to determine the best model of the identified system.

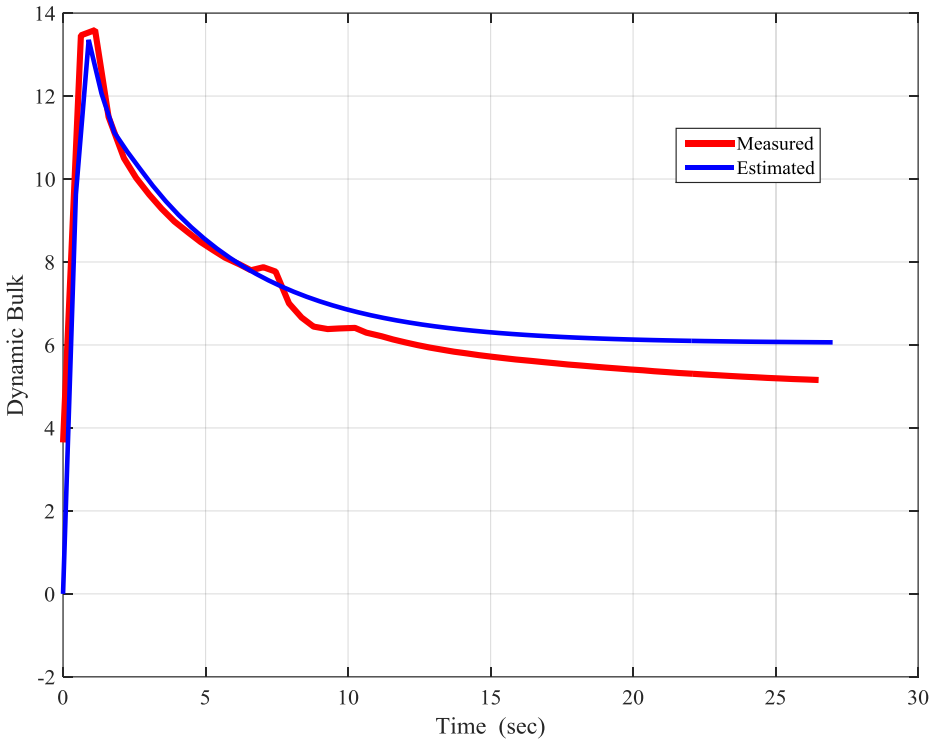

Figure 8.24: The measured vs estimated dynamic bulk modulus response.

The Transfer Function model has been exported from the System Identification application for further analysis. From the exported model, the close loop system at a gain of 0.005 is generated. For comparison purposes, the estimated model is plotted against the measured model as displayed in Fig 8.24.

8.4 Active Acoustic Metamaterial with Double Negative Parameters:

In this section, the goal is to bring both properties, mass density and bulk modulus, to embrace negative values simultaneously compared to the original levels measured at static conditions. In addition to invistigating its ability to achieve desirable and tunable properties levels seperately or together with negative or postive values. The Active Acooustic Metamaterial unit cell used for this purpose is equipped with several piezoelectric sensors of different types. Peizofilm sensors, *PVDF* type, attached to the inside of the cell are used in this *AAMM* cell. In addition to a piezoelectric bimorphic disk, PZT type, mounted to the end of the Helmholtz cavity. At rest, the piezoelectric sensors gather data necessary to measure the static levels of the cell's properties- mass density and bulk modulus-. To excite the Active Acoustic Metamaterial cell, piezoelectric actuators are incorporated. Actuators of bimorphic-PZT type are mounted to the three ends of the *AAMM* cell in which one is dedicated to apply a sinosuidal excitation. The remaining two actuators are used as controllers to serve obtaining the desired levels of the specific property. In the following sections, two different *AAMM* cell expermintal setups aimed to achieve simultaneously tunable properties, double-positive and then double-negative, using separate actuators and a single actuator are introduced.

8.4.1 Active Acoustic Metamaterial with Simultaneously Tunable Properties

Using Separate Actuators:

The Active Acoustic Metamaterial unit-cell in this setup is engaging all the piezoelectric actuators in the operation. In addition to the main actuator dedicated for sinosuidal excitation, this *AAMM* cell has two separate controllers/actuators to achieve the desired double negativity or positivity. Each controlling actuator is aimed to individually maintain one property at a certain specified level.

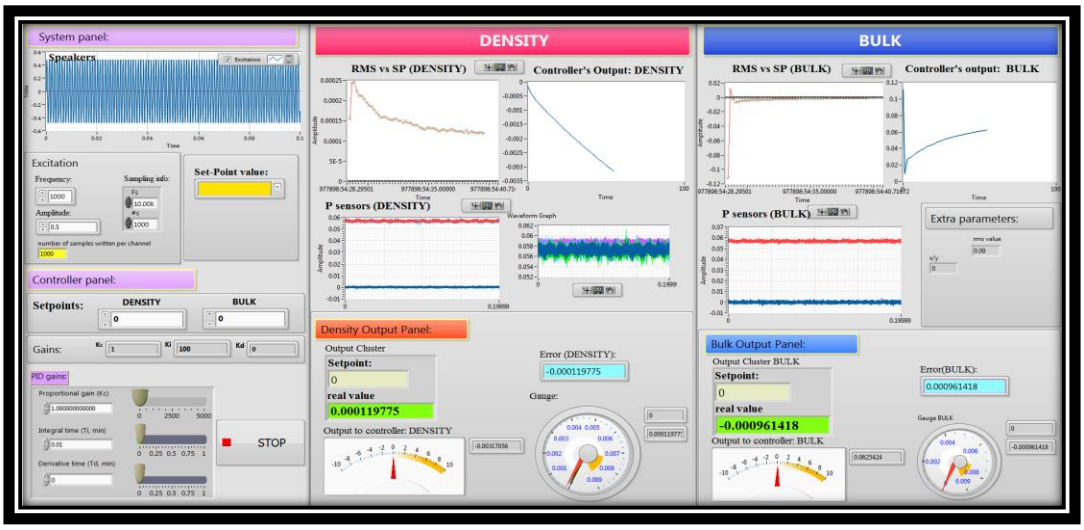

Figure 8.25: A computer window shows the control panel used to operate the Active Acoustic Metamaterial with Simultaneously Programmable Properties cell.

Figure 8.25 is showing a computer window of the Active Acoustic Metamaterial with Simulatenously Programmable Properties cell's control panel.

8.4.2 Active Acoustic Metamaterial with Simultaneously Tunable Positive Properties Using Separate Actuators:

The *AAMM* is subjected to a sinosuidal excitation at operating frequency of 1000 Hertz. In this case with separate actuators, the mass density and bulk modulus have obtained levels that are at 10 and 100 times the ambient levels of both properties at the same time.

Various controllers' types are used to achieve the goal of having both properties of the dynamic denstiy and bulk modulus to be at the same positive levels assigned to the *AAMM*. At first, the proportional controller applied to the *AAMM* with simultaneosly positive dynamic density and bulk modulus, double-positive *AAMM,* cell at various proportional gains K_p of 0.5,1,5,10, and 100.

In order to reduce the steady state error caused by the proportional part of the controller, a Proportional and Integral controller is used. The time and control response of the Active Acoustic Metamaterial cell with Simultaneously Tunable Properties by using the *PI* controller have been thoroughly studies for the chosen desired levels, ten to hundred times higher scale from the original measure.

The desired levels of the dynamic density and bulk modulus are set at extremely high levels as an attempt to push the *AAMM* to reach the highest levels possible. Although these levels are unrealistic, the resulted dynamic properties' levels will be defining the ceiling in which the *AAMM* cannot exceed.

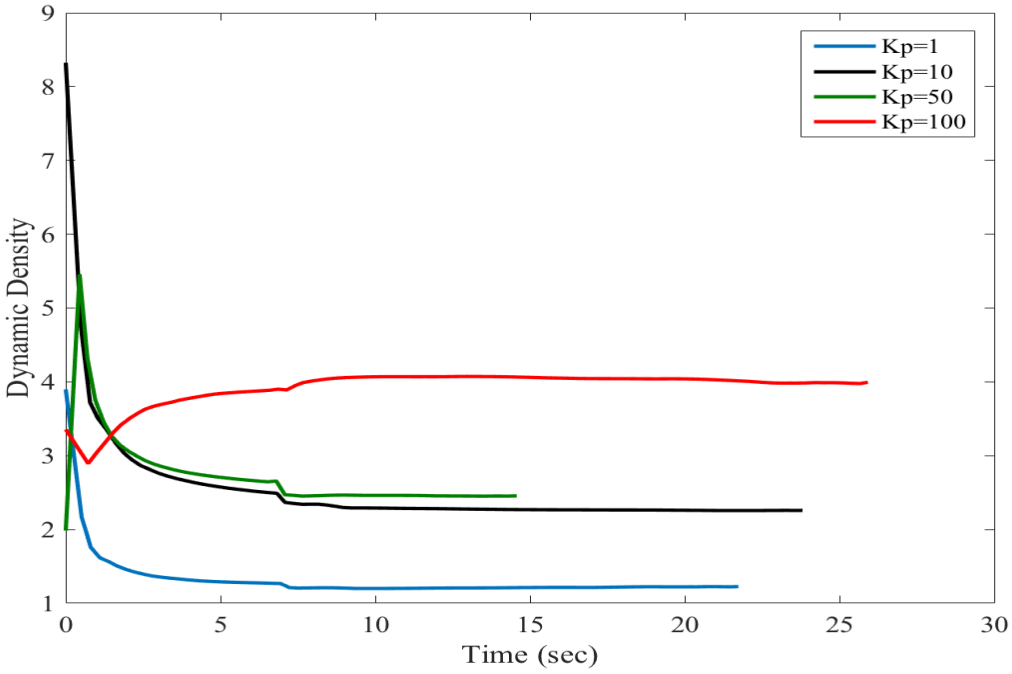

(a)

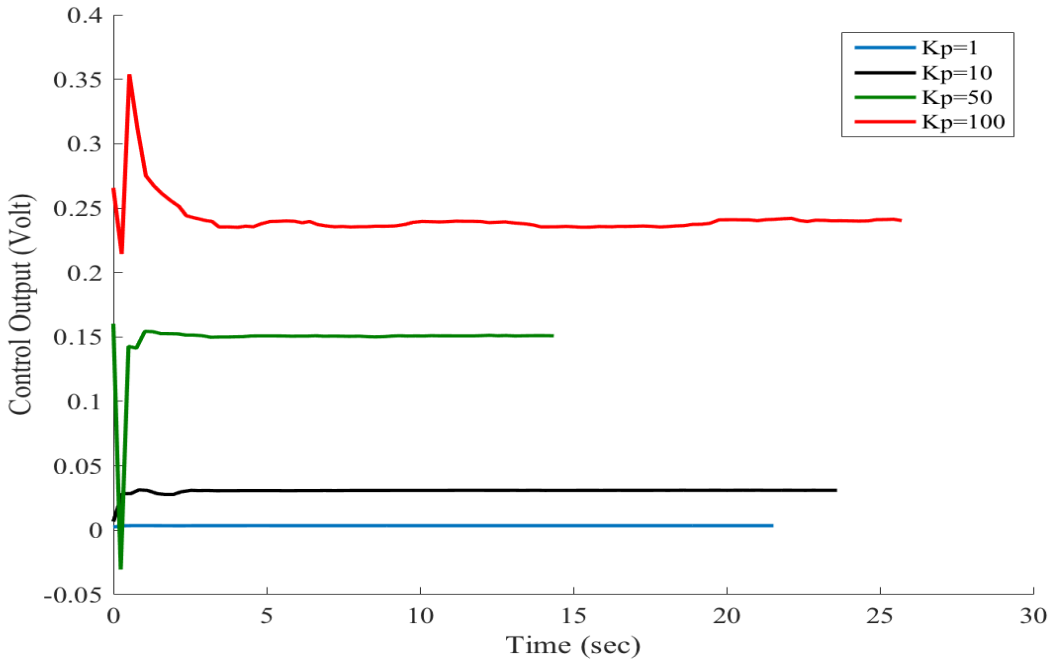

(b)

Figure 8.26: Dynamic Density, (a), and Control Outputs, (b), for the Active Acoustic Metamaterial cell using a proportional controller. The proportional gains are given as 1, 10, 50, and 100. The desired dynamic density is set at ten times the original level.

Figures 8.26 and 8.27 show the time response and the control voltage of the dynamic mass desnsity when the desired dynamic density is set to be 10 times the original density and the control outputs resulted from *P* and *PI* controllers respectively.

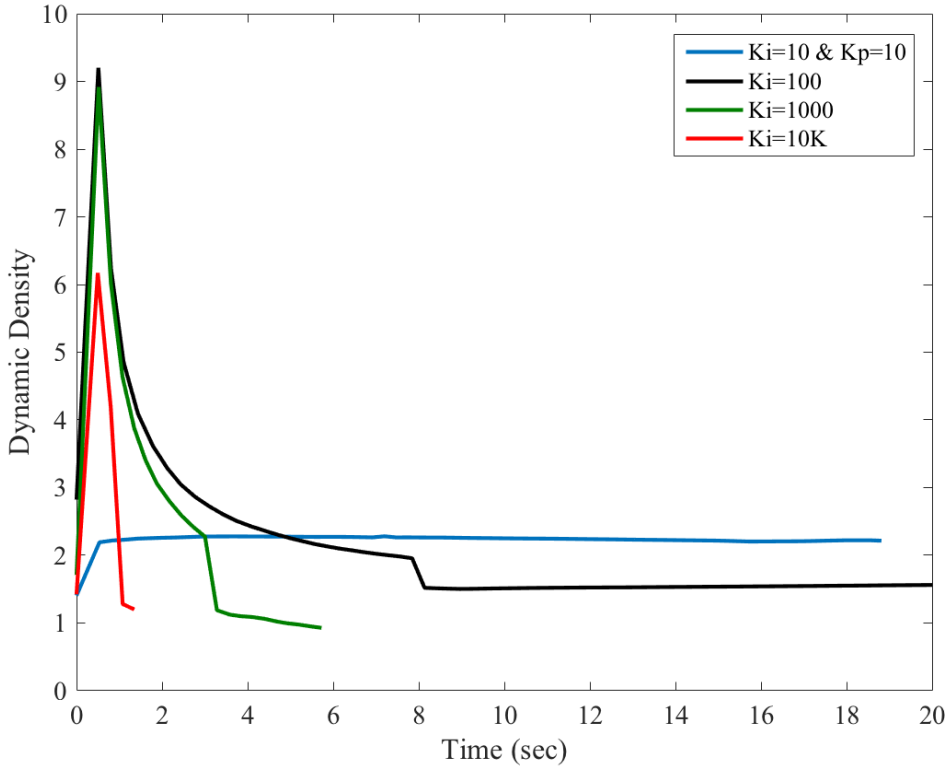

(a)

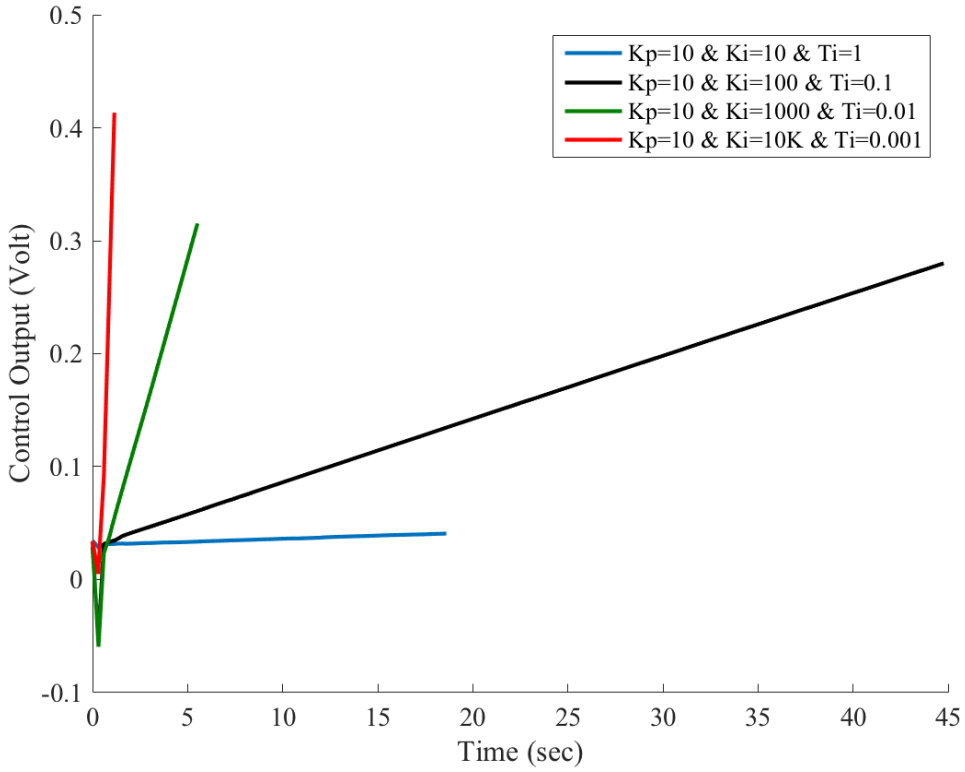

(b)

Figure 8.27: Dynamic Density, (a), and Control Outputs, (b), for the Active Acoustic Metamaterial cell using a proportional-integral (PI) controller. The integral gains are given as 10, 100, 1000, and 10K while keeping the proportional gain fixed at 10. The desired dynamic density is ten times the original level.

Likewise, Figure 8.28 and 8.29 show the corresponding characteristics when the dynamic bulk modulus is controlled to assume a reference value of 10 times the original bulk modulus using *P* and *PI* controllers respectively.

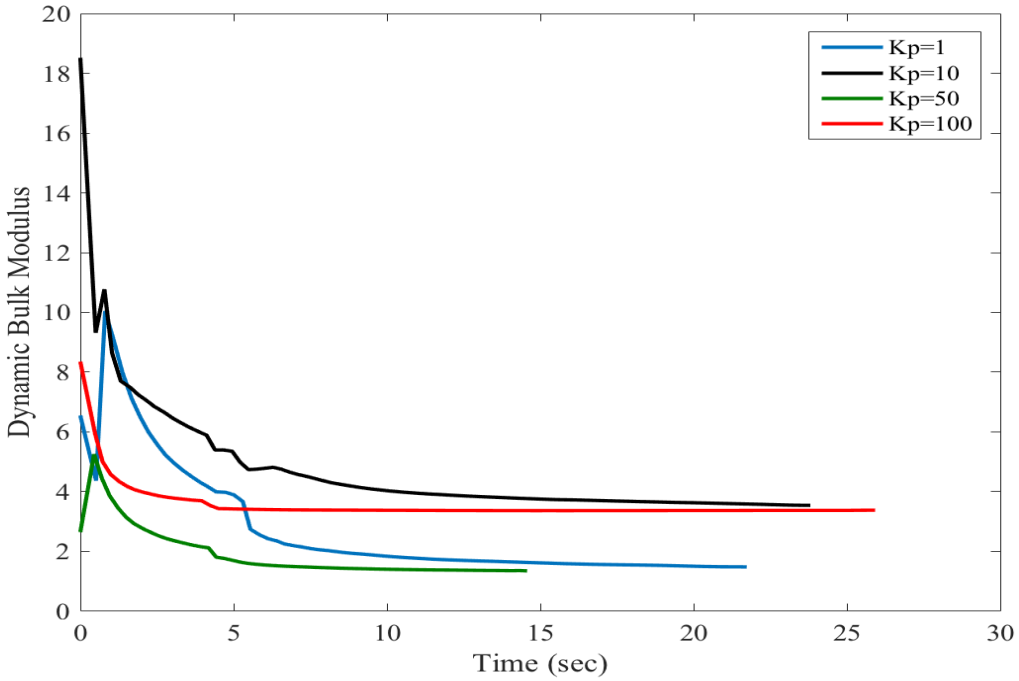

(a)

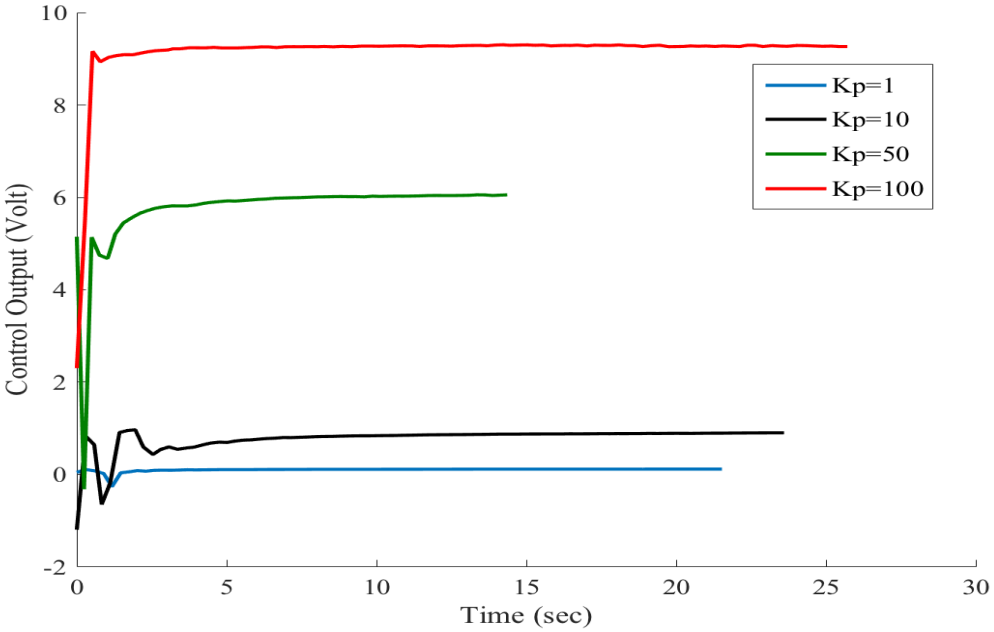

(b)

Figure 8.28: Dynamic bulk Modulus, (a), and Control Outputs, (b), for the Active Acoustic Metamaterial cell using a proportional controller. The proportional gains are given as 1, 10, 50, and 100. The desired dynamic bulk modulus is ten times the original level.

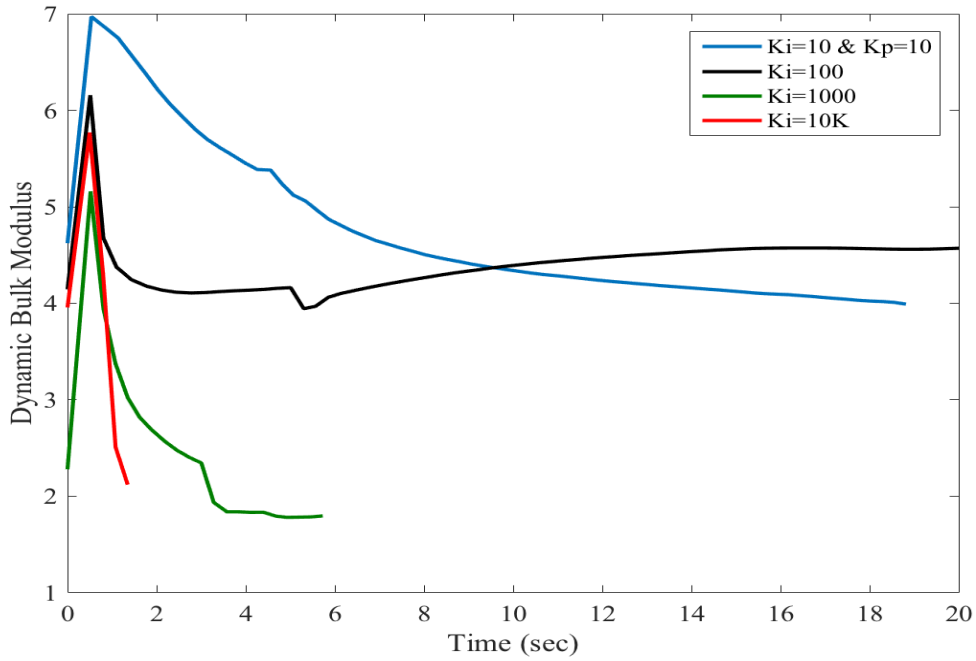

(a)

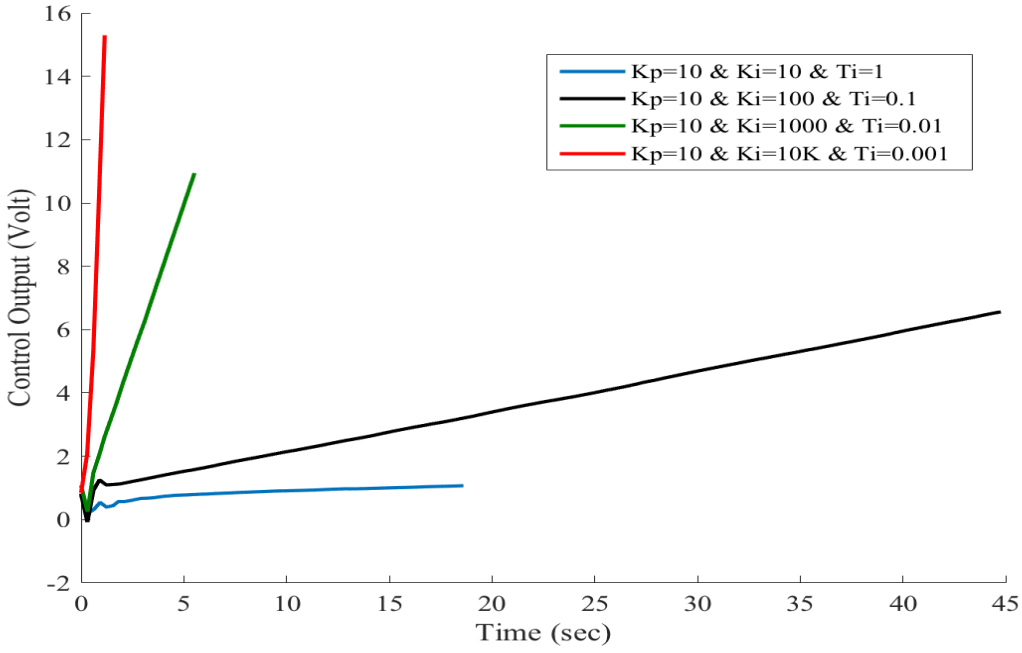

(b)

Figure 8.29: Dynamic bulk modulus, (a), and Control Outputs, (b), for the Active Acoustic Metamaterial cell using a proportional-integral (PI) controller. The integral gains are given as 10, 100, 1000, and 10K while keeping the proportional gain fixed at 10. The desired dynamic bulk modulus is ten times the original level.

When the desired dynamic density is set to be 100 times the original density, the time response and the control voltage of the mass desnsity and the control outputs resulted from *P* and *PI* controllers are illustrated in Figures 8.30 and 8.31.

The proportional controller is set at proportional gains of 1,5, and 7 to invistigate the optimal proportional gain in which the *AAMM* is be able to acquire the best possible response. Similarly, at integral gains of 0.01, 0.1, 1 and 10 the PI controller is tested for the optimal gain.

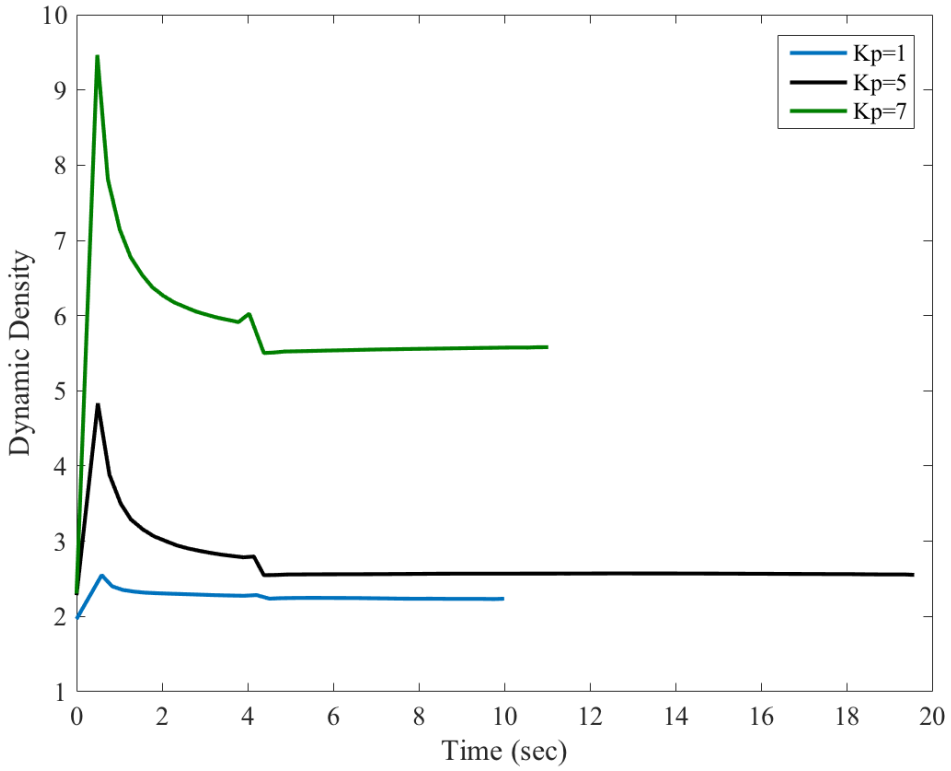

(a)

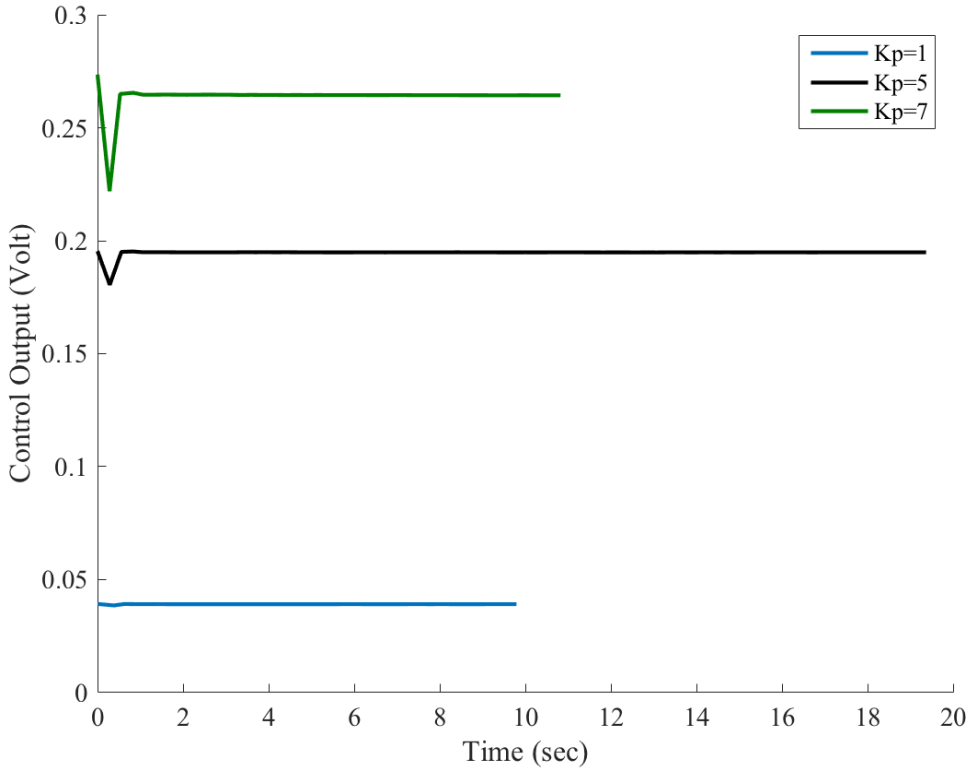

(b)

Figure 8.30: Dynamic density, (a), and Control Outputs, (b), for the Active Acoustic Metamaterial cell using a proportional controller. The proportional gains are given as 1, 5, and 7. The desired dynamic density level is hundred times the original level.

Figure 8.32 and 8.33 show the corresponding characteristics when the dynamic bulk modulus is controlled to assume a reference value of 100 times the original bulk modulus using *P* and *PI* controllers respectively.

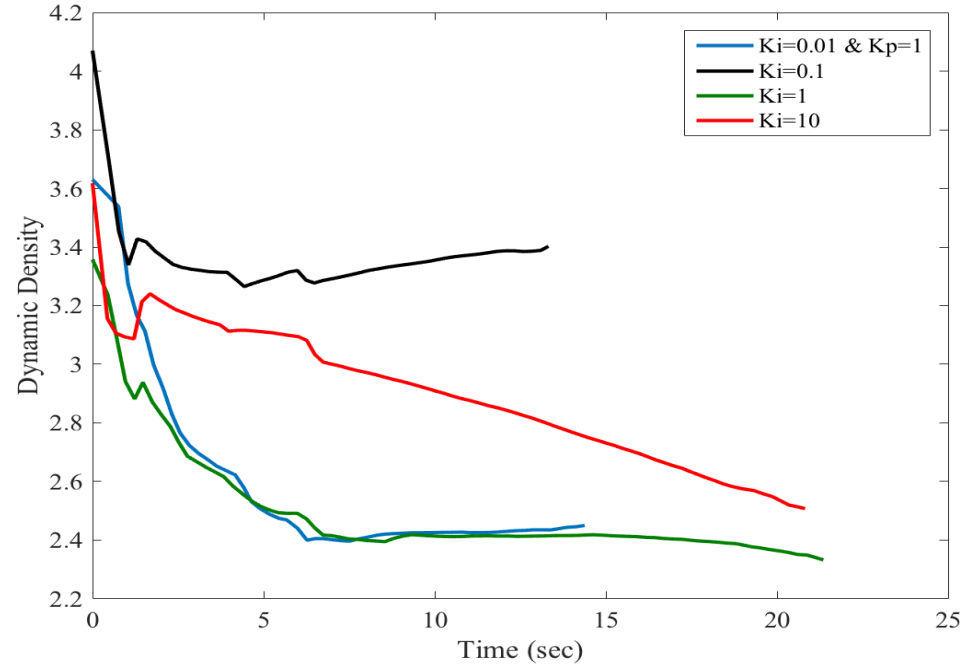

(a)

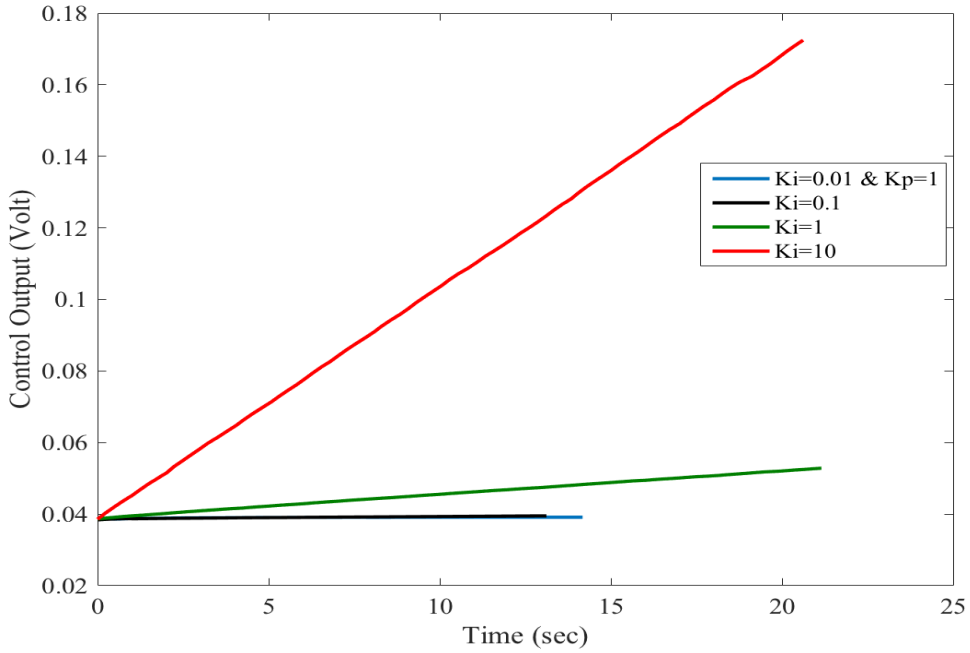

(b)

Figure 8.31: Dynamic Density Levels, (a), and Control Outputs, (b), for the Active Acoustic Metamaterial cell using a proportional-integral (PI) controller. The integral gains are given as 0.01, 0.1, 1, 10, and 100 while keeping the proportional gain fixed at 1. The desired dynamic density level is hundred times the original level.

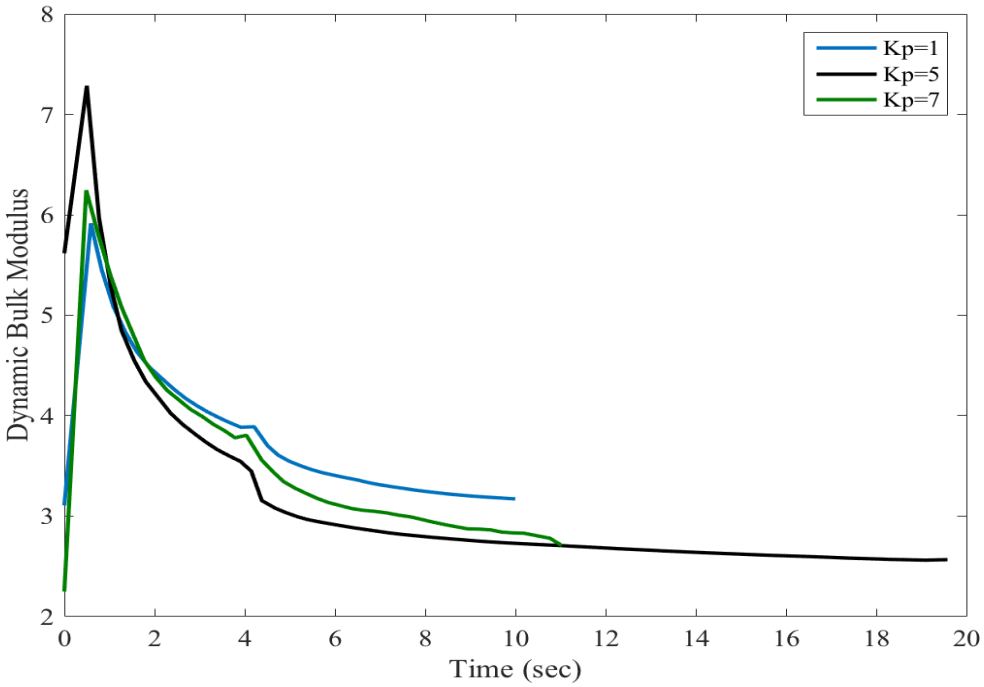

(a)

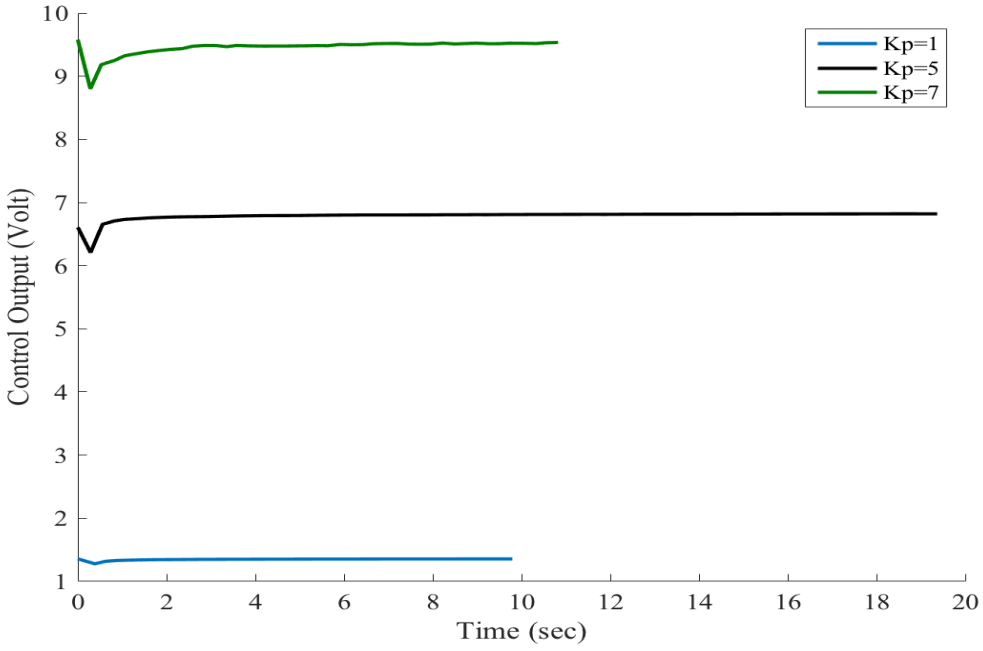

(b)

Figure 8.32: Dynamic Bulk Modulus, (a), and Control Outputs, (b), for the Active Acoustic Metamaterial cell using a proportional controller. The proportional gains are given as 1, 5, and 7. The desired dynamic bulk modulus is hundred times the original level.

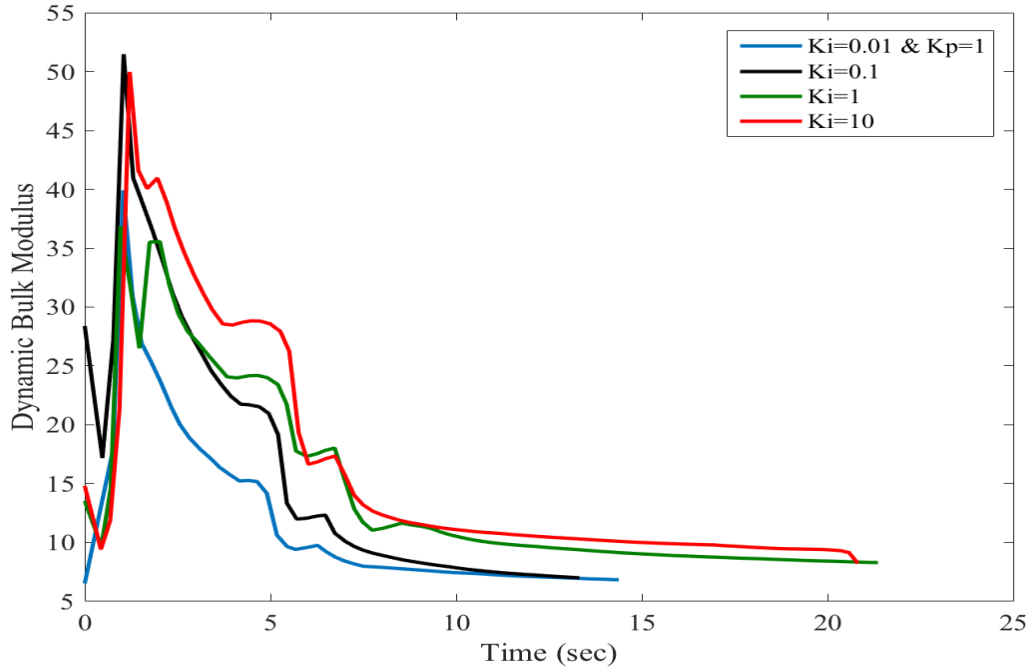

(a)

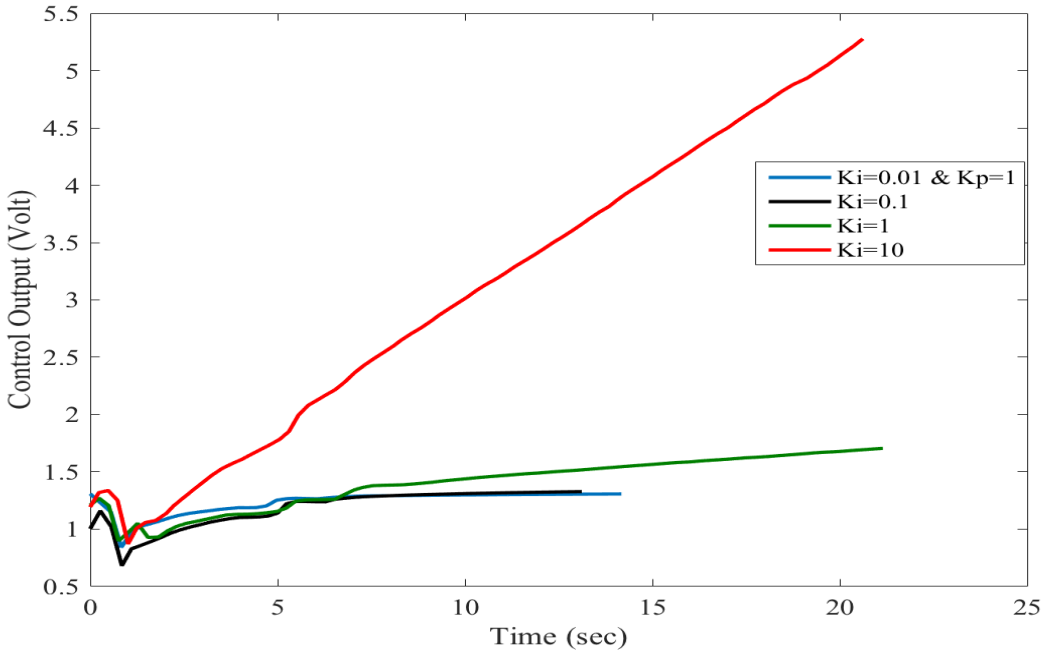

(b)

Figure 8.33: Dynamic Bulk modulus, (a), and Control Outputs, (b), for the Active Acoustic Metamaterial cell using a proportional-integral (PI) controller. The integral gains are given as 0.01, 0.1, 1, 10, and 100 while keeping the proportional gain fixed at 1. The desired dynamic bulk modulus level is set to be hundred times the original level.

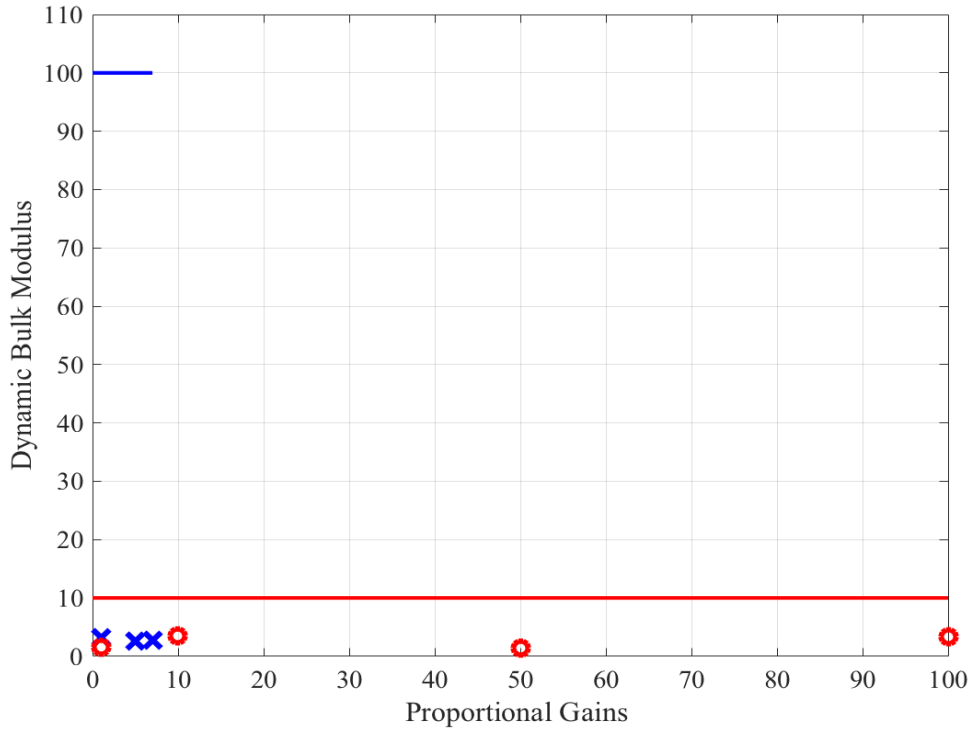

(a)

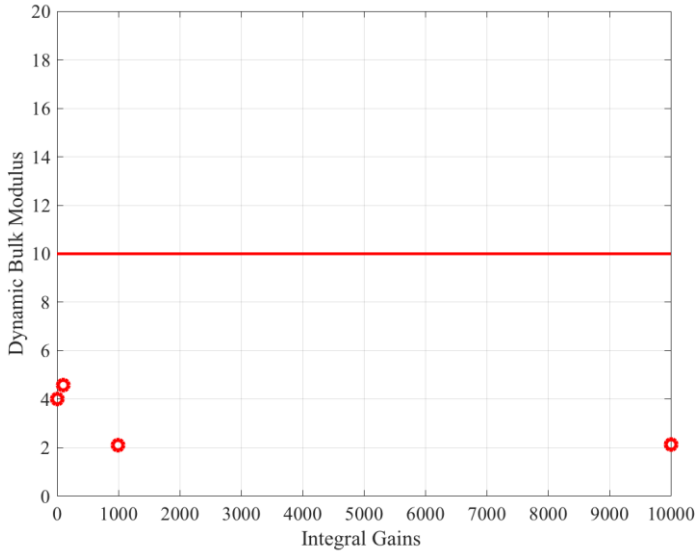

(b)

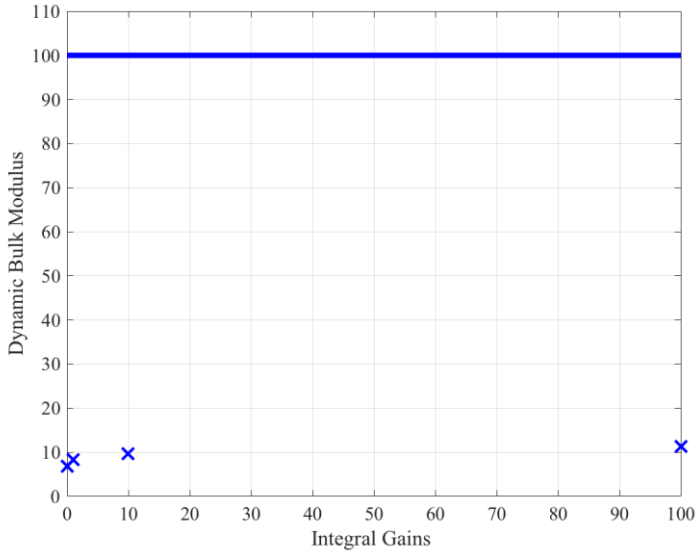

(c)

Figure 8.34: A summary figure for dynamic bulk modulus levels achieved by the Active Acoustic Metamaterial at the desired levels of 10 and 100 times the original levels. (a) shows the dynamic bulk modulus levels using a proportional controller plotted against the change in the proportional gains. (b) and (c) is displaying the dynamic bulk modulus for the two cases as a result of altering the integral gains using a PI controller.

To better analyse the performance of the Active Acoustic Metamaterial with Simultaneously Tunable Bulk Modulus and Density, summary figures have been generated for every property, Fig 8.34 and Fig 8.35, respectively. The performance of the *AAMM* with the proportional and PI controllers is also illustrated in (a), (b) and (c) of Fig 8.34 and Fig 8.35. The settled values of the dynamic bulk modulus and density at the desired levels of 10 and 100 of the original levels are displayed for the P-type and PI controllers. The *AAMM* with Proportional controller with various proportional gains at the chosen desired levels is shown in (a) of Fig 8.34 and Fig 8.35. Similarly when using a PI controller, the integral gains with their corresponding dynamic properties values are displayed in part (b) and (c) of Figs 8.34 and 8.35.

By using a proportional controller for both of the desired levels of 10 and 100 times, the dynamic bulk modulus values of the AAMM seem to be at comparable levels as we alter the proportional gains. One can observe that the best value for the dynamic density, for the 10 times case, has been accomplished when the proportional gain is at 10, see Fig 8.34 (a) as they are colored in Red. For the other case when the desired levels were chosen at 100 times higher, increasing the proportional gains appear to have no impact on the resulted dynamic bulk modulus. Therefore, the optimum values for the range of the given proportional gains for the desired was at 1.

The implementation of the Proportional and Integral controller can assist to achieve an ideal value of the dynamic bulk modulus at an integral gain of 100, when the desired level of the *AAMM* is set at 10 times higher than the static level, (b) of Fig 8.34. For the case of 100 times the original levels, it is noticeable that increasing the integral gain value can slightly enhance the response. At an integral gain of a 100, the *AAMM* was be able to achieve the highest possible level in this case.

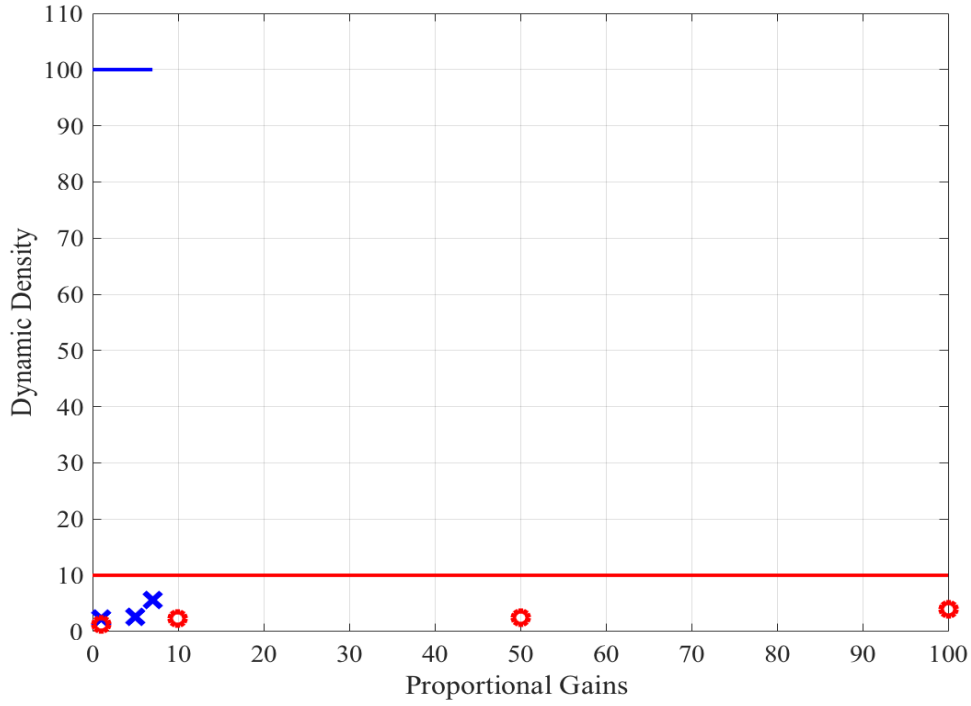

(a)

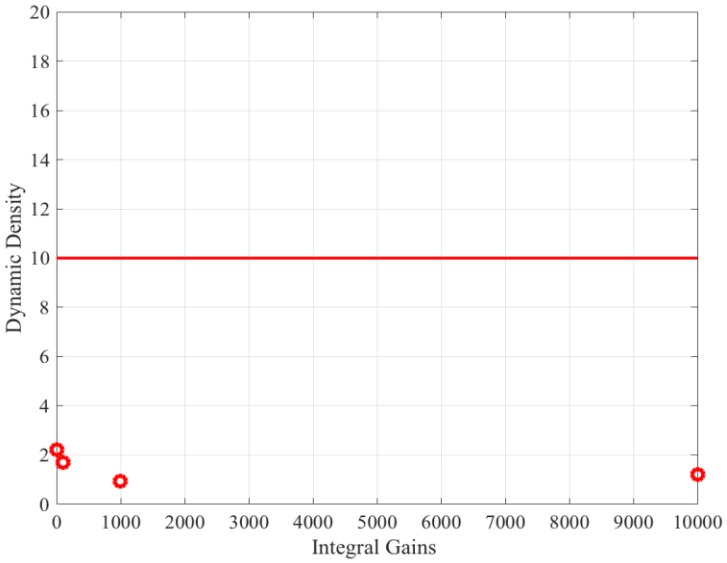

(b)

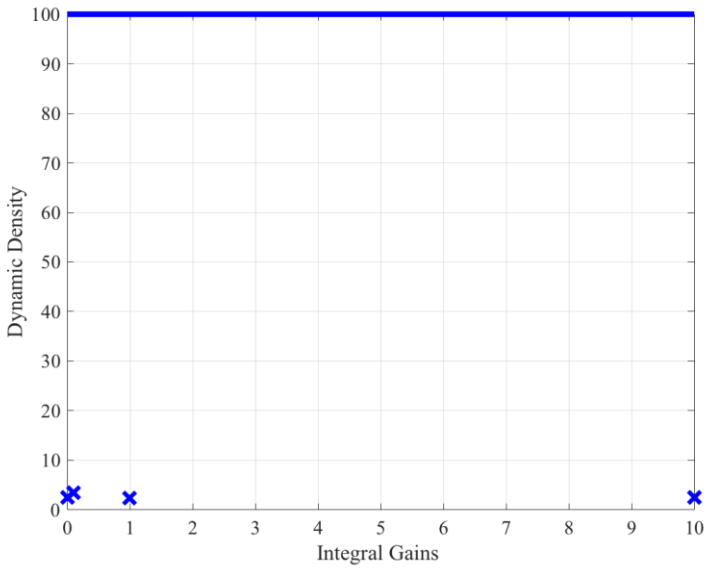

(c)

Figure 8.35: A summary figure for dynamic density levels achieved by the Active Acoustic Metamaterial at the desired levels of 10 and 100 times the original levels. (a) shows the dynamic density levels using a proportional controller plotted against the change in the proportional gains. (b) and (c) is displaying the dynamic density for the two cases as a result of altering the integral gains using a PI controller.

At the desired level of 10 times larger than the static levels and by using a proportional controller, the dynamic density values of the double-negative *AAMM* seem to be converging slightly as we increase the proportional gains. One can observe that the best value for the dynamic density has been accomplished when the proportional gain is at 100, see Fig 8.35 (a) as they are colored in Red. For the other case when the desired level was chosen to be at 100 times higher, increasing the proportional gains appear to bring the resulted dynamic density to the desired values. Therefore, the optimum value for the range of the given proportional gains for the desired level case of 100 was 7.

The implementation of the Proportional and Integral controller can assist to achieve an optimal value of the dynamic density at an integral gain of 10K, when the desired level of the *AAMM* is set at 10 times higher than the static level, (b) of Fig 8.35. For the case when the desired level is 100 times the original level, it is noticeable that increasing integral gains has no effect. At an integral gain of 0.1, the *AAMM* was be able to achieve the highest possible level in this case, (c) of Fig 8.35.

8.4.3 Active Acoustic Metamaterial with Simultaneously Double Negative Parameters:

The dynamic negative levels of the mass density and bulk modulus are investigated in this section. Previously, the Active Acoustic Metamaterial was exercised to only achieve simultaneously positive properties. On the contrary, the goal of the *AAMM* with simultaneously negative properties, double-negative *AAMM*, is to bring the dynamic properties to negative levels at the same time.

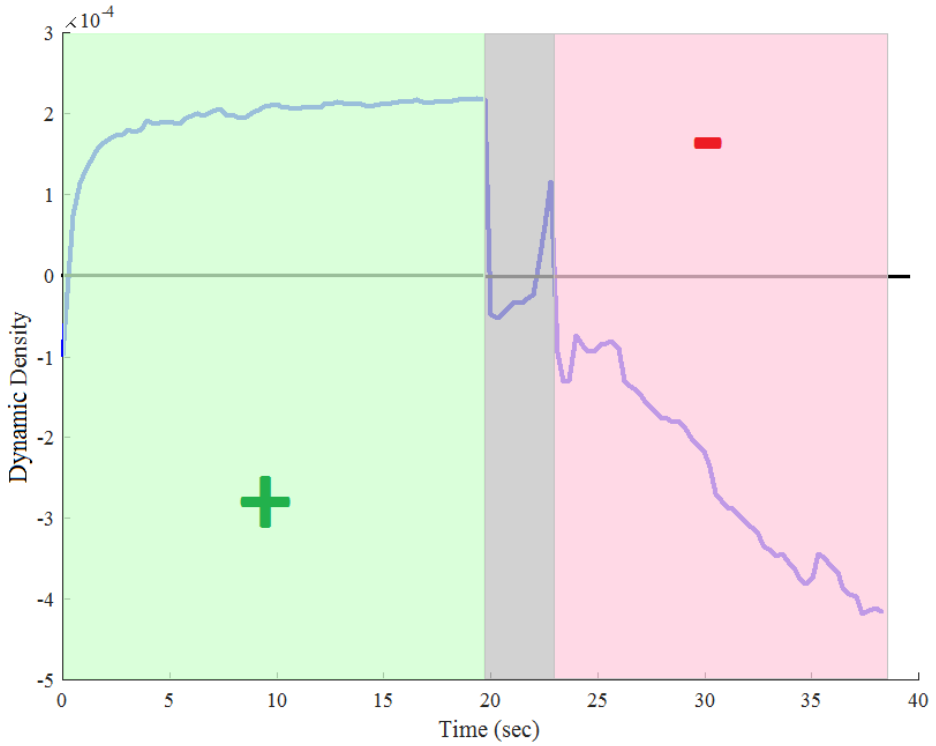

Figure 8.36: Dynamic Density of the Double-Negative Active Acoustic Metamaterial. Green zone shows that the relative property is positive. Whereas, red zone indicates the relative property is negative.

The Double-Negative Active Acoustic Metamaterial is set to operate at no-excitation conditions for about twenty seconds, and then the cell is set to be excited at 1000 Hz, see Fig. 8.34. It's evident that the Double-Negative *AAMM* is transitioning from the positive levels at rest to the negative levels. The mass density and bulk modulus properties exhibited the negativity concurrently, Figures 8.34 and 8.35.

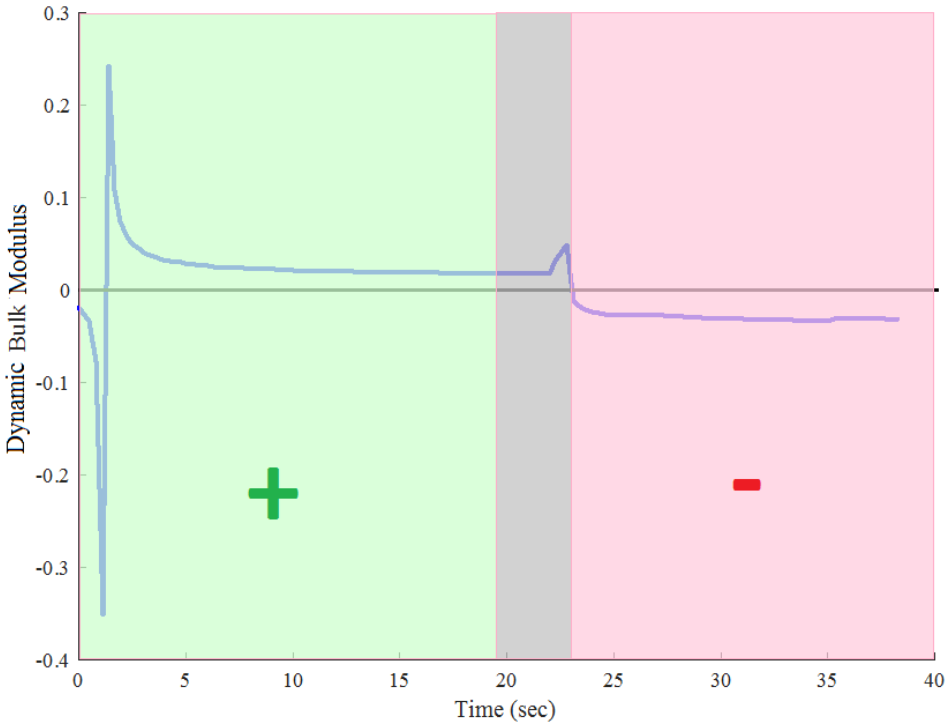

Figure 8.37: Dynamic Bulk Modulus of the Double-Negative Active Acoustic Metamaterial. Green zone shows that the relative property is positive. Whereas, red zone indicates the relative property is negative.

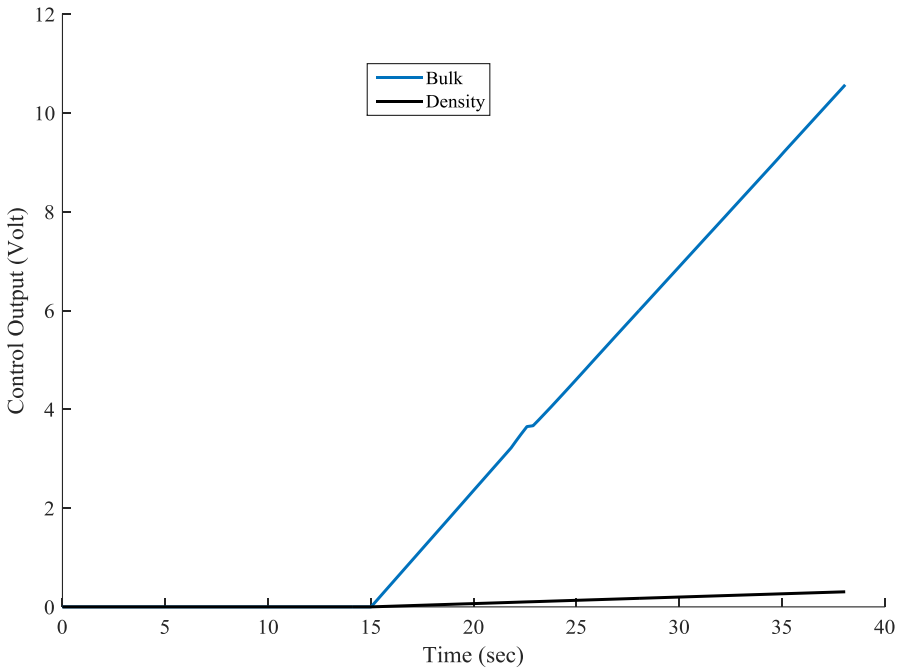

Figure 8.38: Control outputs for dynamic density and bulk modulus properties of the Double-Negative Active Acoustic Metamaterial.

The corresponding control voltage for the dynamic density and bulk modulus of the Active Acoustic Metamaterial with Simultaneously Negative Properties is displayed in Figure 8.38.

8.5 Active Acoustic Metamaterial with Simultaneously Negative Properties Using Single Actuator:

In this section, the control action of the Double-Negative Active Acoustic Metamaterial is achieved by only incorporating a single actuator in the operation. In addition to the main actuator that is dedicated for a sinosuidal excitation, this *AAMM* cell has one controller/actuator to achieve the desired double negativity. The single actuator is aimed to maintain both properties of mass denstiy and bulk modulus at negative relative levels simultaneously.

The controller in this setup is carefully designed to assure accomplishing the purpose of the double negativity in which the *AAMM* has to have its relative properties to be negative at the same time.

In this configuration, the control action is generated to be proportional to a linear combination of the Helmholtz displacement x_{r_i} and the displacements of the neighboring transmission line elements x_i's as $\left(X_{i-1} + X_{i+1} - 2X_{r_i}\right)$, the controller equation was first proposed by Pope and Daley (2010).

Figure 8.39 is showing a computer window of the Double-Negative Active Acoustic Metamaterial cell's control panel.

The Double-Negative *AAMM* is subjected to a sinosuidal excitation at operating frequency of 1000 Hertz.

In the previous case with separate actuators, the dynamic mass density $\boldsymbol{\rho}$ and bulk modulus $\boldsymbol{\beta}$ properties have obtained levels that are at zero, 10, 100 times the ambient levels of both properties at the same time. In the currnet design, the double-negative *AAMM* has achieved the purpose of having its properties to be simultaneously negatie by following the desired levels set for the system variable. The system variable is formed as $\left(X_{i-1} + X_{i+1} - 2X_{r_i}\right)$, which is the linear combination of the resonant

mass and neighboring transmission mass displacements , X_r, X_{i-1} and X_{i+1} respectively.

Various controllers' types are used to achieve the Double Negativity goal. At first, the proportional controller applied to the Double-Negative *AAMM* cell at various proportional gains K_p of 0.5,1,2, and 10.

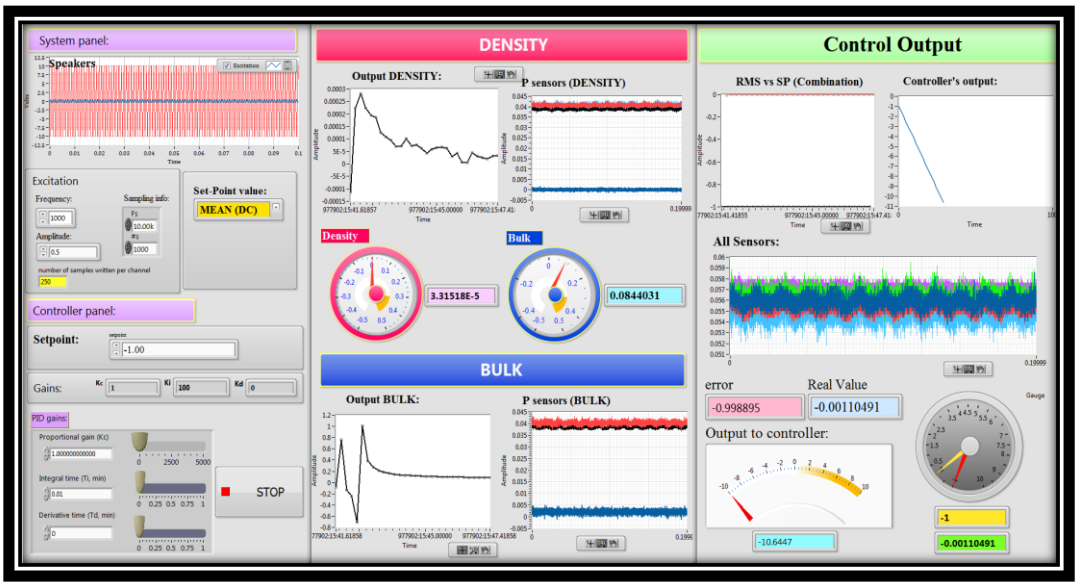

Figure 8.39: A computer window shows the control panel used to operate the Double-Negative Active Acoustic Metamaterial cell using a single actuator.

Figures 8.39 and 8.40 display the simultaneous control of the relative dynamic mass desnsity and dynamic bulk moudlus for a set reference system response of -1 using *P* and *PD* controllers respectively.

Figures 8.41 and 8.42 display the simultaneous control of the relative dynamic mass desnsity and dynamic bulk moudlus for a set reference system response of -5 using proportiona, *P*, and proportional-derivative ,*PD*, controllers respectively.

Similarly, Figures 8.43 and 8.44 display the simultaneous control of the relative dynamic mass desnsity and dynamic bulk moudlus for a set reference system response of -10 using P and PD controllers respectively.

It is important to note that the Double-Negative *AAMM* cell's properties are measured in the open-loop case. Hence, for the mass density and bulk modulus, $\rho_0 = 0.0002 \; and \; \beta_0 = 0.009$, respectively.

The original levels of the *D-N AAMM's* properties are considered as datum levels from which the operations and measurements of the closed-loop are related to.

In order to reach our goal of achieveing double negativity in an *AAMM*, the resulted relative density levels $\frac{\boldsymbol{\rho}}{\boldsymbol{\rho_0}}$ and relative bulk modulus $\frac{\boldsymbol{\beta}}{\boldsymbol{\beta_0}}$ will be negative when related to the original levels.

The linear comboniation of the Double-Negative *AAMM* states, $\left(X_{i-1} + X_{i+1} - 2X_{r_i}\right)$, is set as the system variable. The set point was selected carefully to force the *D-N AAMM* to have its properties to be relatively negative at the same time, such as $\frac{\boldsymbol{\rho}}{\boldsymbol{\rho_0}}$ and $\frac{\boldsymbol{\beta}}{\boldsymbol{\beta_0}}$.

Finally, Figure 8.44 displays the relative dynamic mass density, bulk modulus and control outputs using the PID controllers.

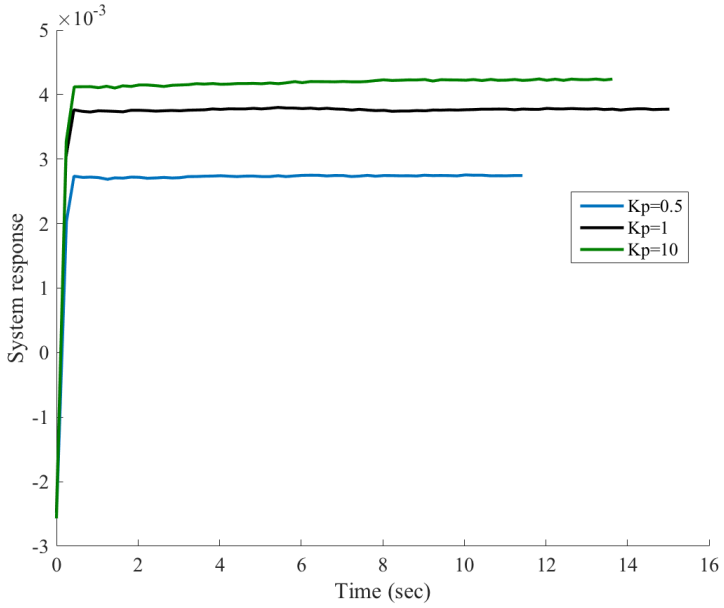

(a)

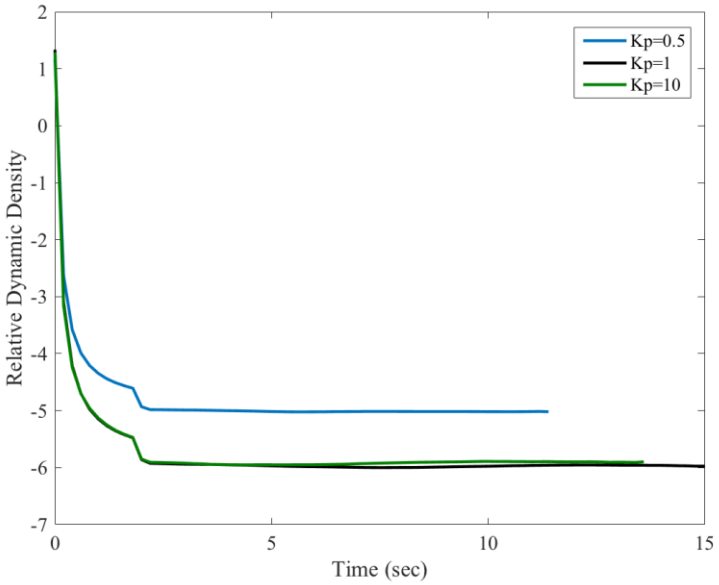

(b)

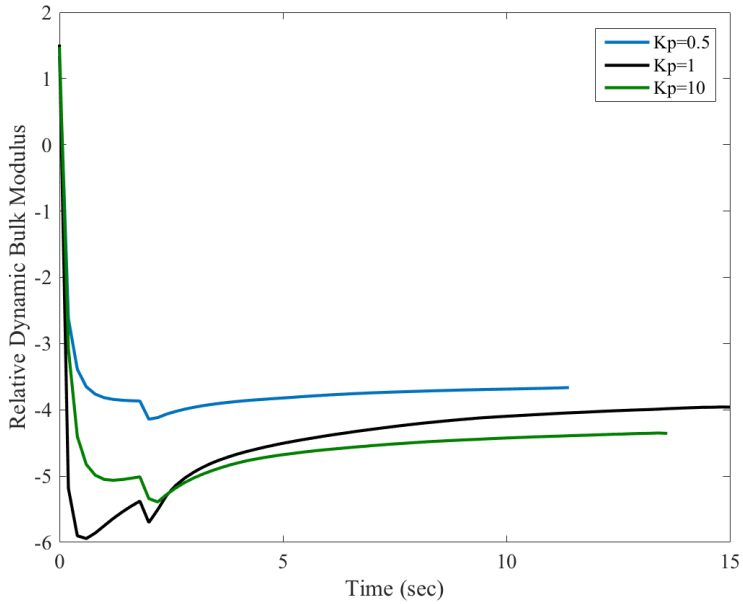

(c)

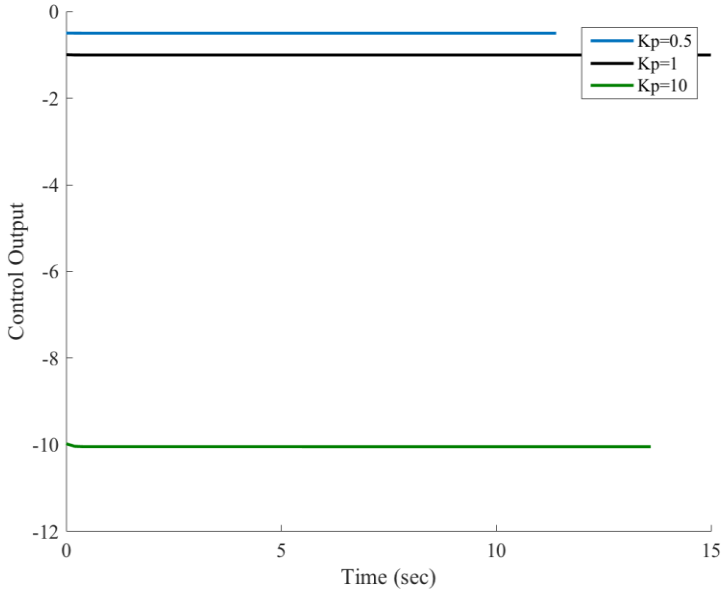

(d)

Figure 8.40: System response (a), Relative Dynamic Density $\frac{\rho}{\rho_0}$ (b), Relative Dynamic Bulk Modulus $\frac{\beta}{\beta_0}$ (c) and Control Outputs (d), for the Active Acoustic Metamaterial cell using a proportional controller. The setpoint is set at -1. The proportional gains are given as 0.5, 1, and 10.

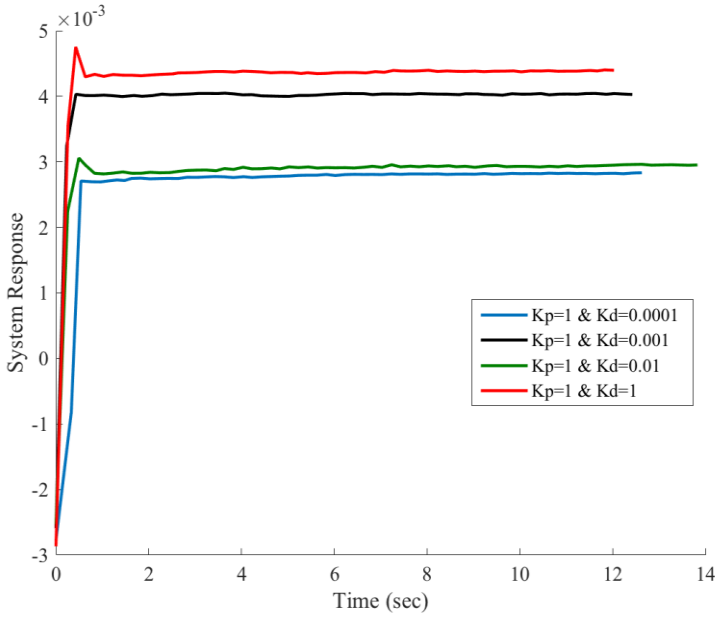

(a)

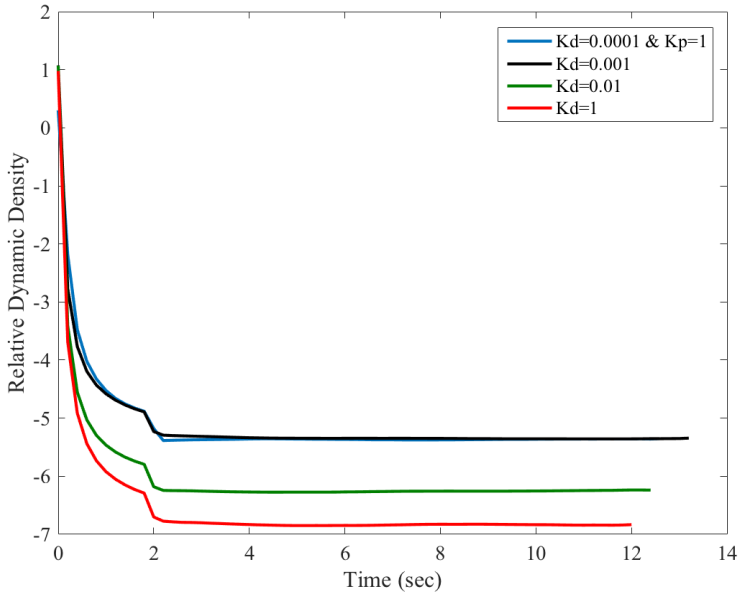

(b)

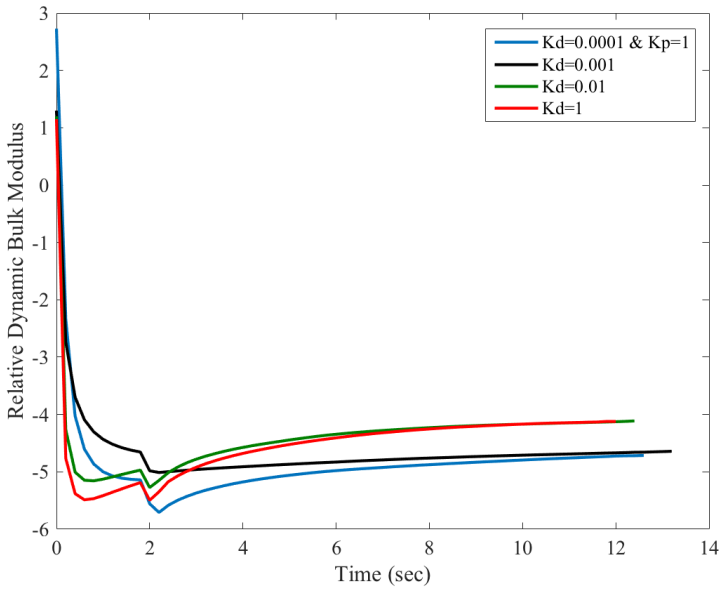

(c)

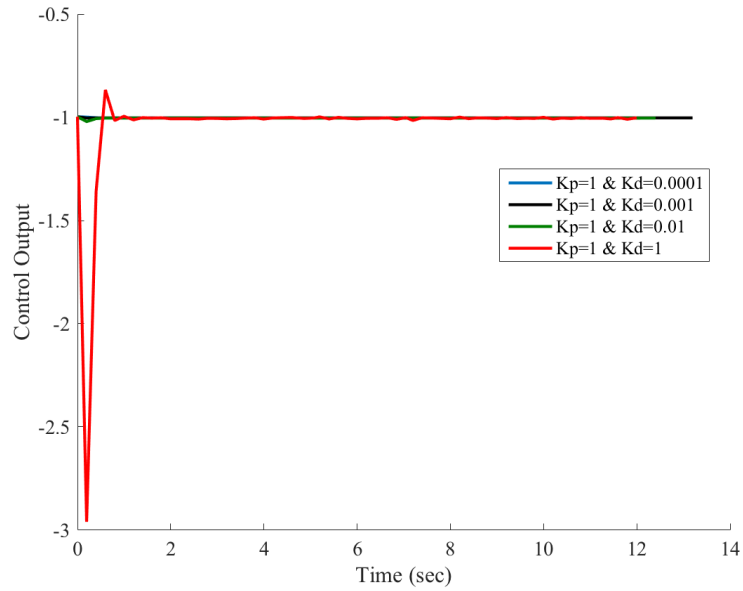

(d)

Figure 8.41: System response (a), Relative Dynamic Density $\frac{\rho}{\rho_0}$ (b), Relative Dynamic Bulk Modulus $\frac{\beta}{\beta_0}$ (c) and Control Outputs (d), for the Active Acoustic Metamaterial cell using a proportional-derivative PD controller. The setpoint is set at -1. The proportional gain is set at 1 while altering the derivative gains between 0.0001, 0.001, 0.01, and 1.

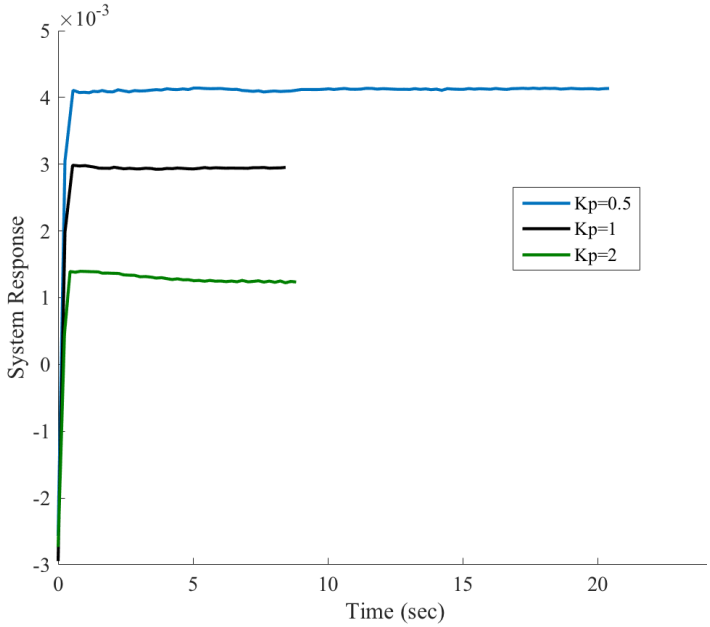

(a)

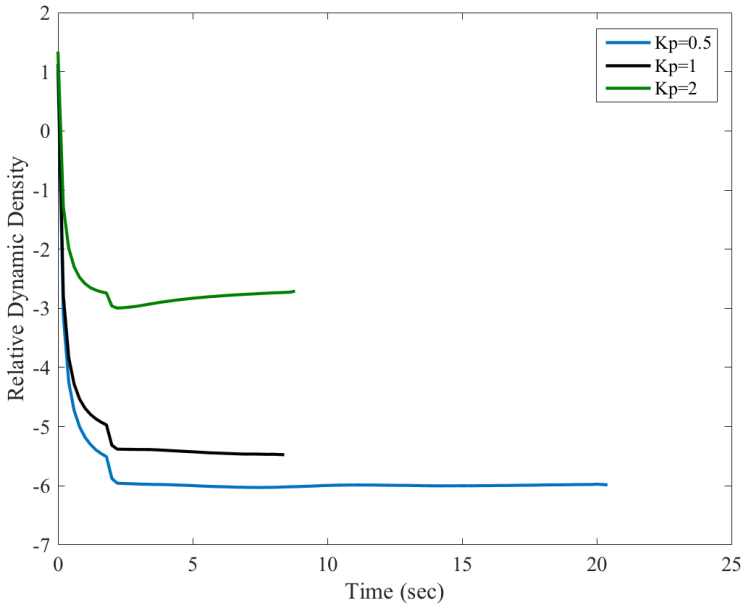

(b)

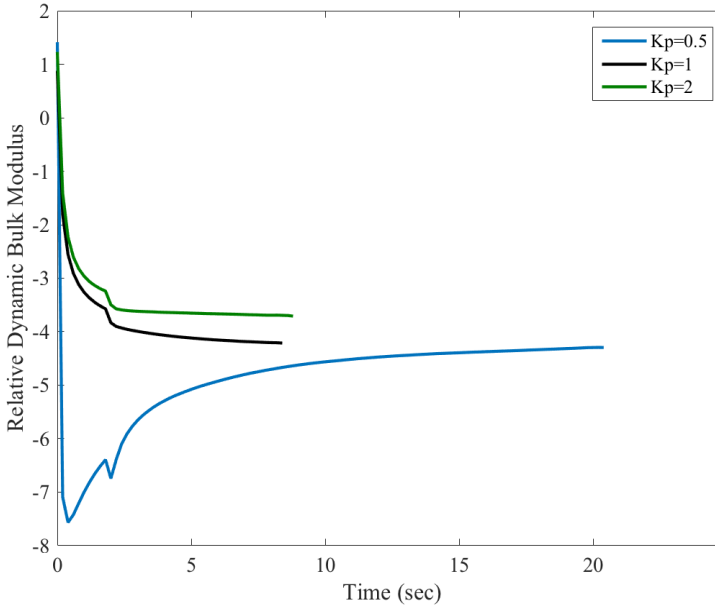

(c)

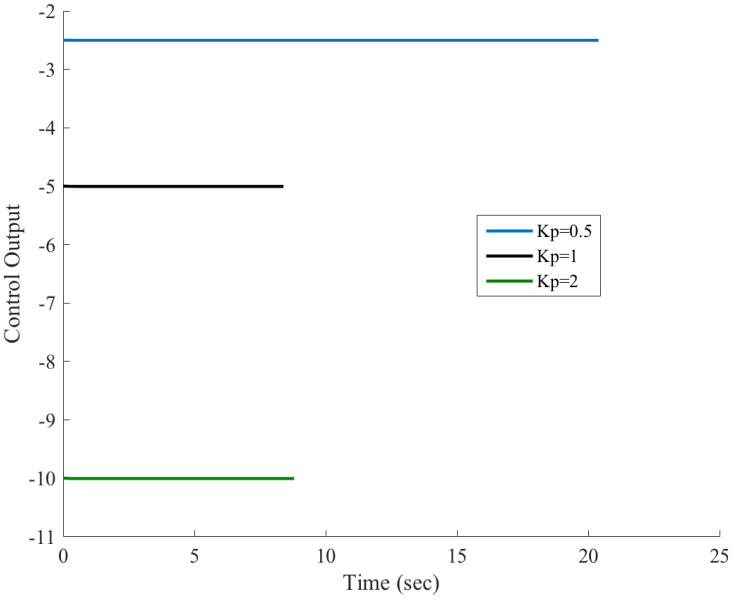

(d)

Figure 8.42: System response (a), Relative Dynamic Density $\frac{\rho}{\rho_0}$ (b), Relative Dynamic Bulk Modulus $\frac{\beta}{\beta_0}$ (c) and Control Outputs (d), for the Active Acoustic Metamaterial cell using a proportional controller. The setpoint is set at -5. The proportional gains are given as 0.5, 1, and 2.

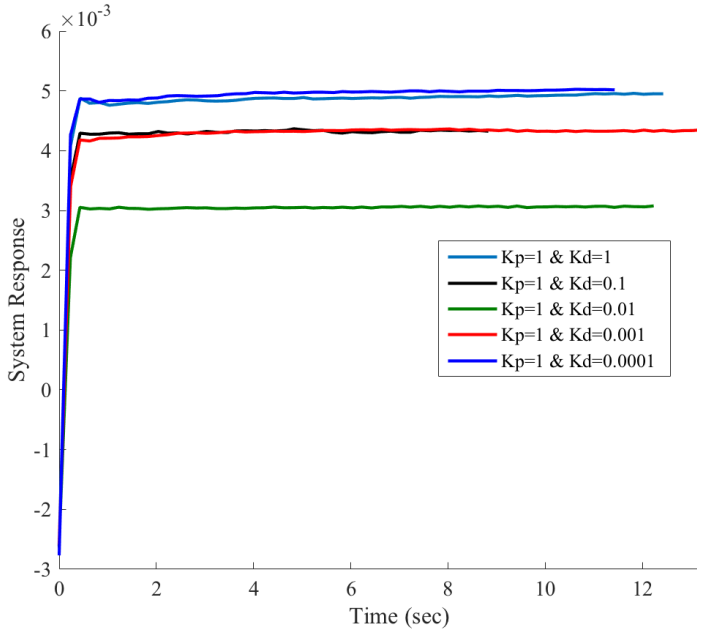

(a)

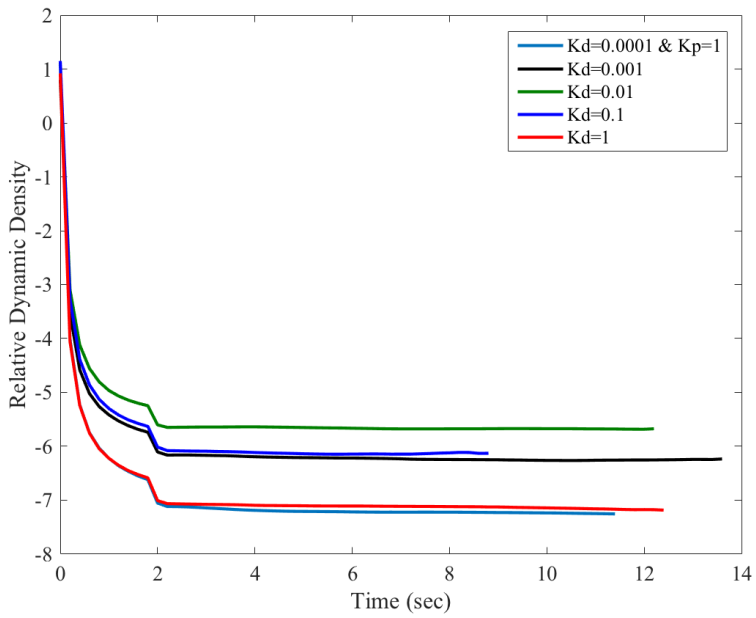

(b)

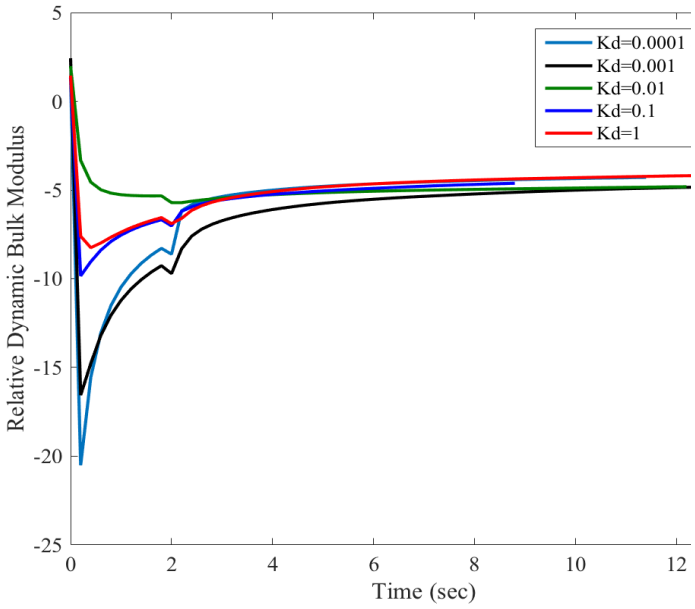

(c)

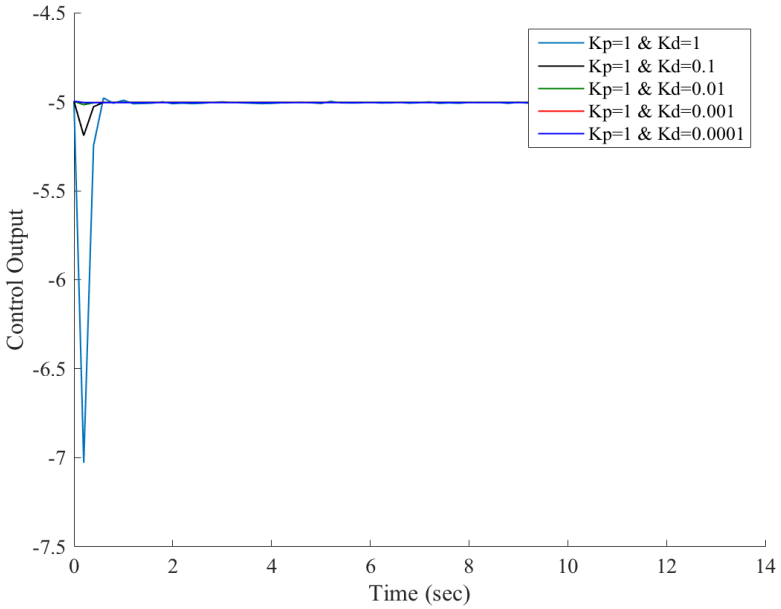

(d)

Figure 8.43: System response (a), Relative Dynamic Density $\frac{\rho}{\rho_0}$ (b), Relative Dynamic Bulk Modulus $\frac{\beta}{\beta_0}$ (c) and Control Outputs (d), for the Active Acoustic Metamaterial cell using a proportional-derivative PD controller. The setpoint is set at -5. The proportional gain is set at 1 while altering the derivative gains between 0.0001, 0.001, 0.01, 0.1, and 1.

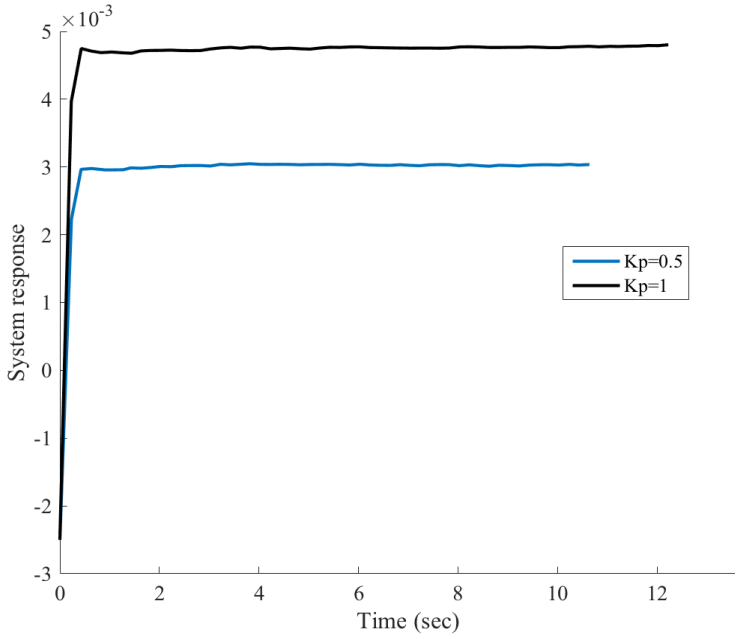

(a)

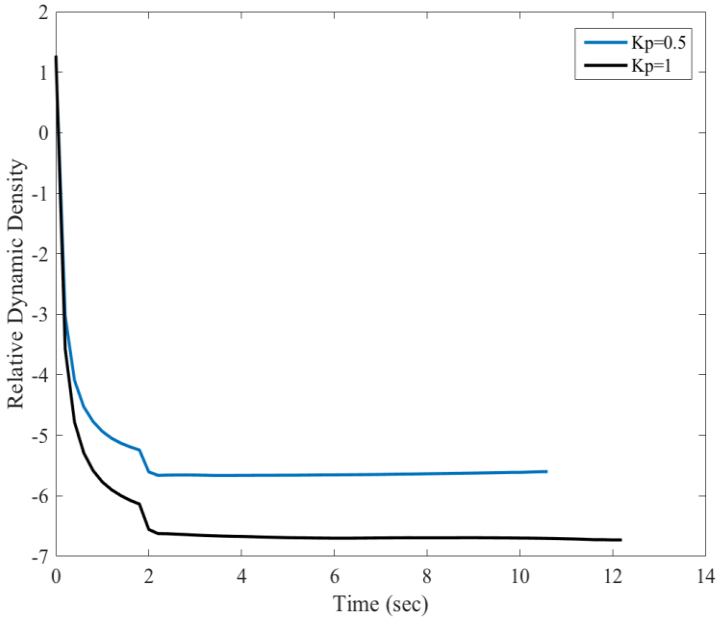

(b)

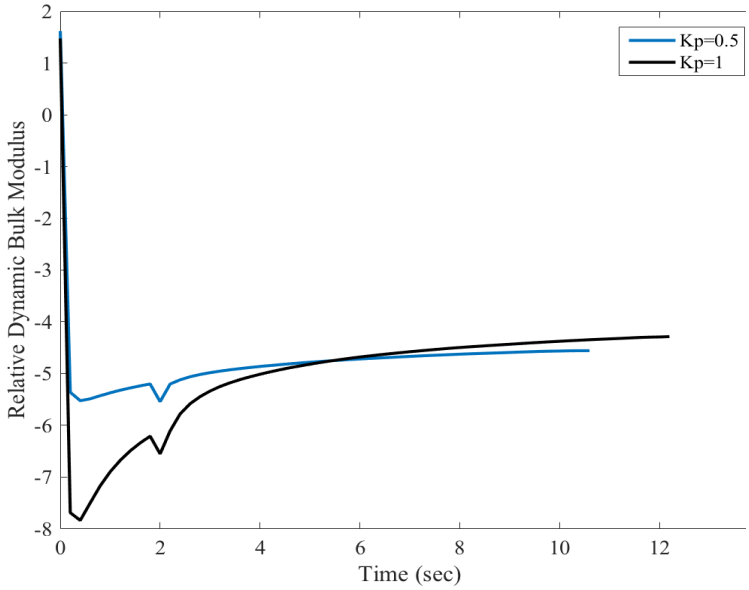

(c)

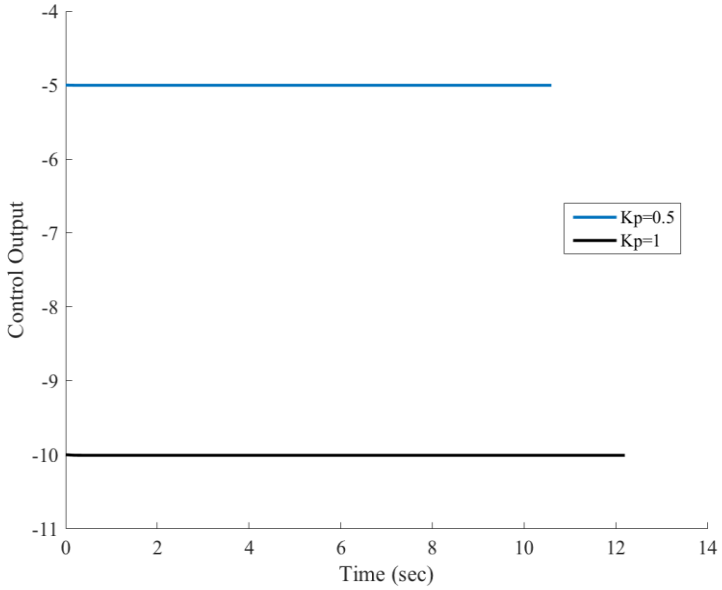

(d)

Figure 8.44: System response (a), Relative Dynamic Density $\frac{\rho}{\rho_0}$ (b), Relative Dynamic Bulk Modulus $\frac{\beta}{\beta_0}$ (c) and Control Outputs (d), for the Active Acoustic Metamaterial cell using a proportional controller. The setpoint is set at -10. The proportional gains are given as 0.5, and 1.

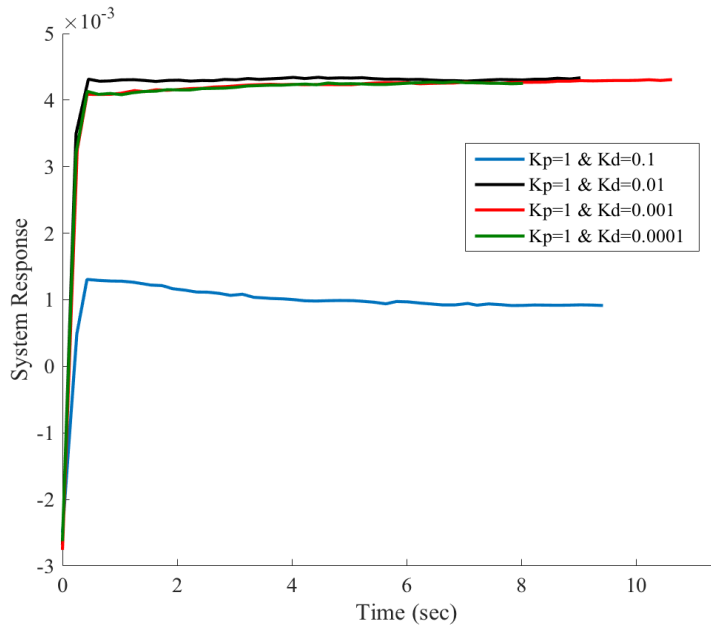

(a)

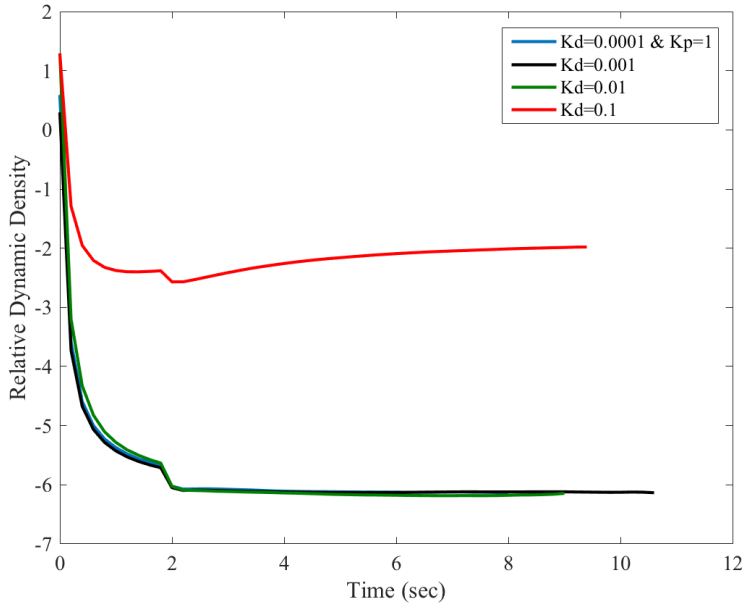

(b)

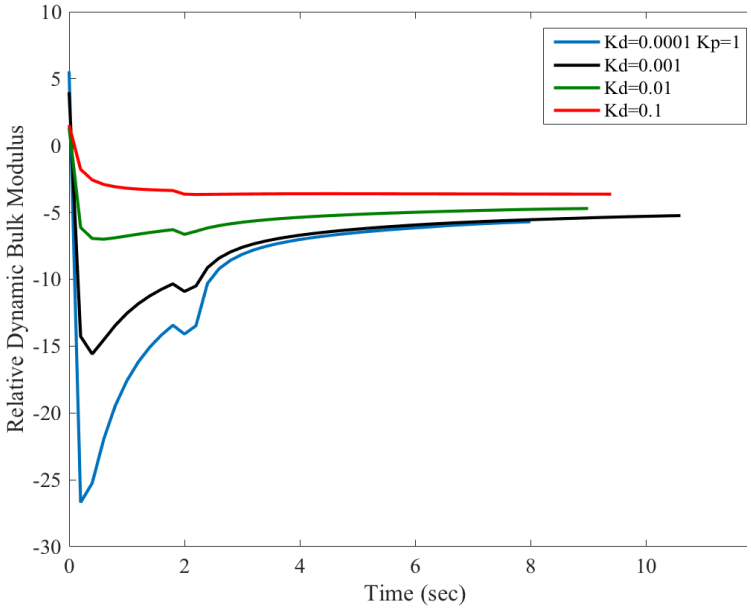

(c)

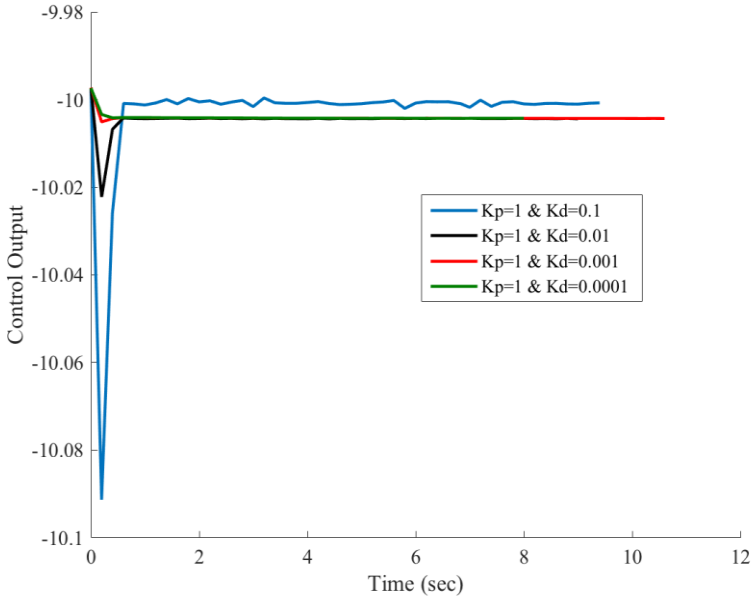

(d)

Figure 8.45: System response (a), Relative Dynamic Density $\frac{\rho}{\rho_0}$ (b), Relative Dynamic Bulk Modulus $\frac{\beta}{\beta_0}$ (c) and Control Outputs (d), for the Active Acoustic Metamaterial cell using a proportional-derivative PD controller. The setpoint is set at -10. The proportional gain is set at 1 while altering the derivative gains between 0.0001, 0.001, 0.01, and 0.1.

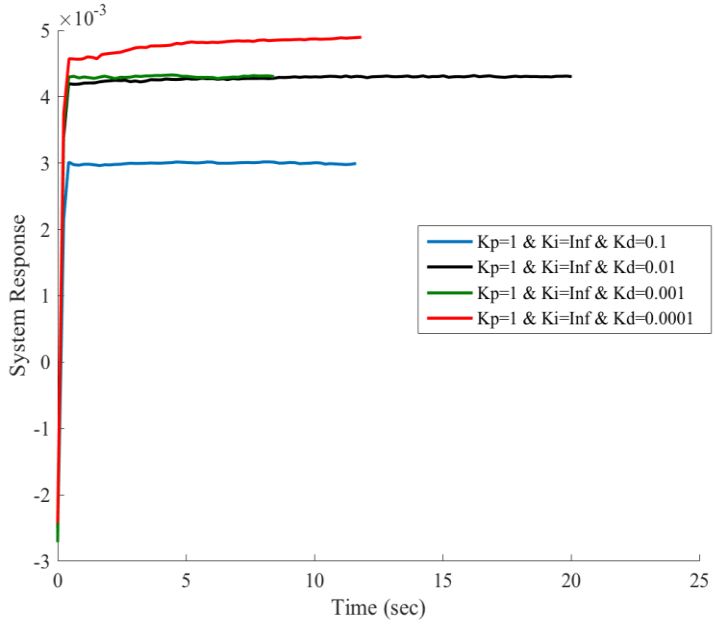

(a)

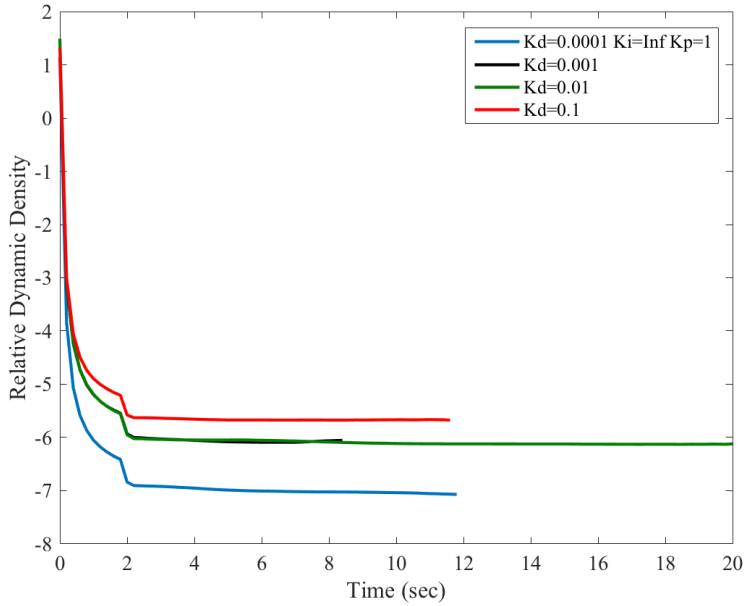

(b)

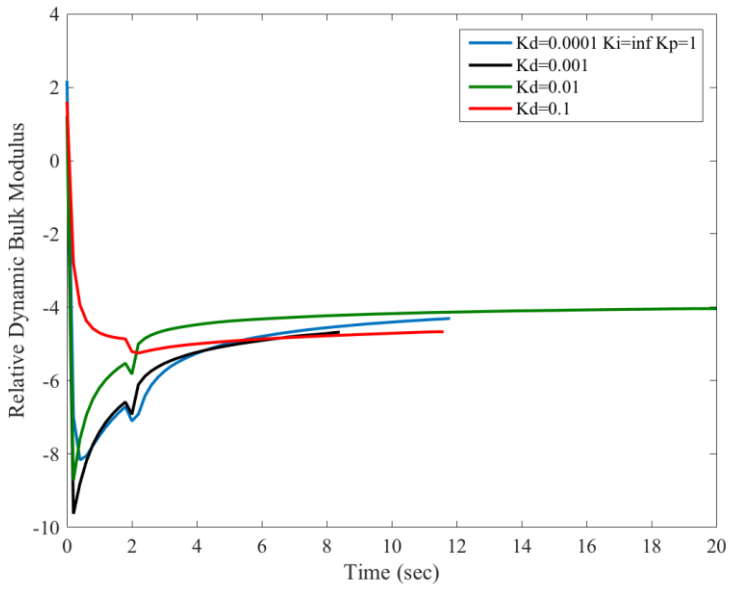

(c)

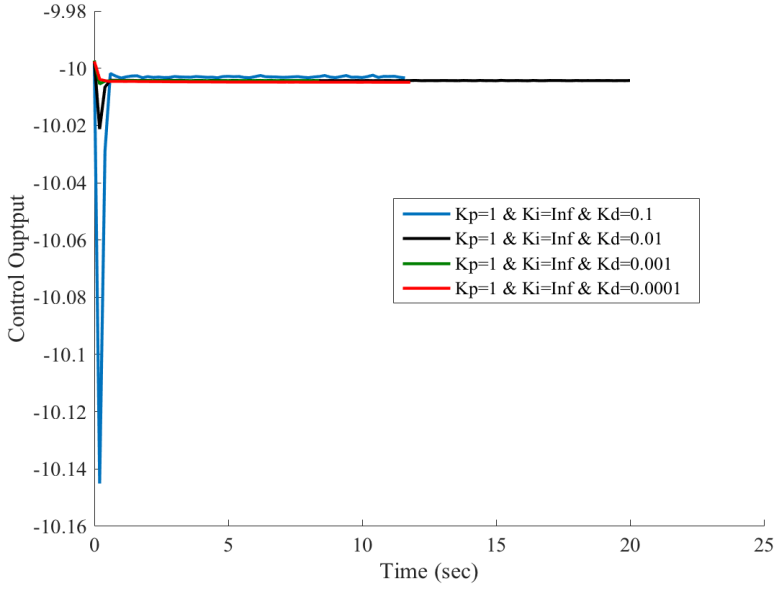

(d)

Figure 8.46: System response (a), Relative Dynamic Density $\frac{\rho}{\rho_0}$ (b), Relative Dynamic Bulk Modulus $\frac{\beta}{\beta_0}$ (c) and Control Outputs (d), for the Active Acoustic Metamaterial cell using a proportional-derivative PD controller. The setpoint is set at -10. The proportional gain is set at 1 and the integral gain is set at Inf while altering the derivative gains between 0.0001, 0.001, 0.01, and 0.1.

For the illustrated experimental cases of the *AAMM*, it is quite obvious that the relative dynamic properties, $\boldsymbol{\rho/\rho_0}$ and $\boldsymbol{\beta/\beta_0}$, of the unit cell have been maintaining on their negative levels at the same time .

8.6 Summary

This chapter has demonstrated that the performance of the Active Acoustic Metamaterial can be controlled in a programmable manner. Specifically, the dynamic property levels for the density and bulk modulus can be controlled separately using two separate actuators. The control actions considered here are proportional and proportional-integral controllers. The control gains are selected to achieve stable and near optimal performance characteristics of the *AAMM*.

This chapter has presented experimental results whereby the density and bulk modulus of the Active Acoustic Metamaterial are controlled to achieve positive relative property levels.

Later, the same *AAMM* controller has been utilized to generate negative relative levels for the acoustic properties using separate actuators/controllers. For good *AAMM* response, proportional and proportional-integral controllers are used to bring optimal results of the properties levels.

The Active Acoustic Metamaterial is then controlled using a single actuator to simultaneously control the density and bulk modulus simultaneously. This efficient control approach is evaluated to demonstrate that the density and bulk modulus can both assume negative relative levels at the same time. The implementation of the proportional, proportional-derivative, and proportional-derivative-integral controllers in the *AAMM*'s single actuator is demonstrated in achieving the negative duality of the *AAMM* properties.

Chapter 9: Conclusions and Recommendations

9.1 Overview

This chapter summarizes the conclusions arrive at during the course of implementation of the present dissertation and the recommendations of the future directions as well as the natural extensions of the work.

Included also in this chapter are the major contributions of the dissertation in relation to the current state-of-the-art.

9.2. Conclusions

This dissertation has presented new directions for the development of a class of active acoustic metamaterials with programmable acoustic properties.

In chapter 3, two configurations of the *AAMM* whereby the control actions are generated either by linear *PD* and nonlinear *FD* controllers. In the first considered configuration, the local control action f_{c_i} is generated to be proportional to the Helmholtz displacement x_{r_i} only. This strategy enables the control of only the effective mass of the *AAMM* while the effective stiffness remains unaffected or uncontrolled. Accordingly, an additional controller is needed to control the stiffness of the *AAMM*.

However, in the second configuration of the *AAMM*, the local control action f_{c_i} is generated to be a linear combination of the Helmholtz displacement x_{r_i} and the displacements of the neighboring transmission line elements x_i's. This strategy enables the simultaneous control of the effective mass and stiffness of the *AAMM* with one control actuator. Accordingly, this simplifies considerably the design, physical and practical realization, and reliability of the *AAMM*.

A major contribution of this chapter is the consideration of a nonlinear fractional derivative (*FD*) controller to control the acoustic properties of the *AAMM* instead of the conventional proportional and derivative (*PD*) controller. It is demonstrated here that the use of the *FD* controller has significantly magnified the frequency bandwidth where negative effective mass and stiffness are obtained simultaneously as compared to that obtained by using the *PD* controller. Such

significant magnification is shown to be achieved without compromising the stable operation of the *AAMM*.

In Chapter 4, a viable configuration of the *AAMM* which consists of an array of stacked Helmholtz resonators which are coupled with an acoustic transmission line is presented.

The equations governing the interactions of the stacked Helmholtz resonators with the transmission line are developed. The performance characteristics of the *AAMM/SHR* system are presented when linear *PD* or nonlinear *FD* controllers are employed. Comparisons are established between the characteristics of the *AAMM/SHR* with the different controllers to emphasize the effectiveness and merits of the nonlinear *FD* controller as compared to the linear *PD* controller.

It is seen that the use of the double-necked Helmholtz resonators has resulted in broadening the frequency bandwidth of double negative properties zone and shifting of the zone to lower frequency range. It is observed that the employing *FD* controller has enhanced considerably the characteristics of the *AAMM* by further stretching the frequency bandwidth of double negative properties zone and shifting it more to much lower frequency range

Chapter 5 has presented *AAMM* configurations consisting of multiple Helmholtz resonators (*MHR*) which are evenly distributed along the circumference of the unit cell. These multiple sets are intended as means for increasing the width of the double negative properties zones. Emphasis is placed in this chapter on using *MHR* with double and triple Helmholtz resonators.

It is shown that increasing the number of the *MHR* associated with each transmission element results in considerable improvement of the width of the double negative properties zones.

In chapter 6, *AAMM* configuration is presented which consists of arrays of transmission line cavities that are separated by and provided with piezoelectric boundaries. These boundaries control the stiffness of the individual cavity and in turn control its dynamical density and bulk modulus. Connected to these transmission line cavities are a set of Helmholtz resonators which have passive flexible boundaries. The transmission line control action insures the achievement of double negative parameter response of the metamaterial.

Various control configurations have been presented in this chapter. Each of these control configurations has offered a great deal of negativity response over certain frequency bandwidths. Moreover, the control configurations have succeeded in bringing the double negative parameter response into various frequency ranges, high, mid-range and low frequency ranges.

Chapter 7 has presented *AAMM* configurations consisting of array of Helmholtz resonators with active boundaries, piezoelectric boundaries. These active Helmholtz resonators are attached to the transmission line. The transmission line, however, has been sectioned into cavities. Each cavity has been also provided with active boundaries, piezoelectric boundaries. This dual-controllability feature insures the achievement of double negative parameter response of the metamaterial either through the Helmholtz resonator or the transmission line or both.

Various control configurations have been presented in this chapter. Each of these control configurations has offered a great deal of negativity response over certain frequency bandwidths. Moreover, the control configurations have succeeded in bringing the double negative parameter response into various frequency ranges, high, mid-range and low frequency ranges.

Chapter 8 has demonstrated that the performance of the Active Acoustic Metamaterial can be controlled in a programmable manner. Specifically, the relative property levels for the density and bulk modulus can be controlled separately using two separate actuators. The control actions considered here are proportional and proportional-integral controllers. The control gains are selected to achieve stable and near optimal performance characteristics of the *AAMM*.

This chapter has presented experimental results whereby the density and bulk modulus of the Active Acoustic Metamaterial are controlled to achieve positive relative property levels.

Later, the same *AAMM* controller has been utilized to generate negative levels for the acoustic properties using separate actuators/controllers. For good *AAMM* response, proportional and proportional-integral controllers are used to bring optimal results of the properties levels.

The Active Acoustic Metamaterial is then controlled using a single actuator to simultaneously control the density and bulk modulus simultaneously. This efficient control approach is evaluated to demonstrate that the density and bulk modulus can

both assume negative relative levels at the same time. The implementation of the proportional, proportional-derivative, and proportional-derivative-integral controllers in the *AAMM*'s single actuator is demonstrated in achieving the negative duality of the *AAMM* properties.

9.3. Recommendations

In all the work presented in chapters 2 through 7, the control action is carried out in the form of an open-loop. There is no reference inputs, no measurements of the actual acoustic properties, and accordingly there is no feedback control correction of any encountered errors. However, in chapter 8, attempts are exerted to implement closed-loop control strategies.

Furthermore, the control gains considered in chapters 2 through 8 are selected based on trial and error rather than by rigorous application of the control theory.

Emphasis should be placed on developing closed-loop controllers of the different *AAMM* configurations and particularly the experimental configuration. With such capabilities, it would be possible to target specific performance characteristics and more importantly to establish comparisons between the theoretical predictions and the experimental outcomes.

The closed-loop control system will enable the control of the actual effective mass and stiffness (m_a, k_a) of the *AAMM* unit cell to target the reference values (m_R, k_R) through proper selection of the control gain K.

The selection of the control gain can be achieved by using *PD* and *FD* control actions. Appropriate analyses should be conducted for the ensuring stability of the closed-loop *AAMM* unit cell.

9.4 Major Contributions of the Dissertation

This dissertation has presented various configurations of passive and active acoustic metamaterials along with their performance characteristics.

The comprehensive presentation of the active acoustic metamaterials through mathematical modeling and experimental realization and evaluation emphasizes the

following major contributions of the work to the current state-of-the-art of acoustic metamaterials:

1. Developing various configurations of the *AAMM* starting with simple transmission line elements integrated with arrays of single uncoupled Helmholtz resonators as well as coupled Helmholtz resonators.

2. Developing various configurations of the *AAMM* including transmission line elements integrated with arrays of stacked uncoupled Helmholtz resonators.

3. Developing various configurations of the *AAMM* including transmission line elements integrated with arrays of multiple Helmholtz resonators.

4. Developing *AAMM* configuration whereby the acoustic properties can be controlled through either the transmission line piezo-boundaries or the Helmholtz piezo-boundaries.

5. Control of the effective mass and stiffness of the different configurations using linear proportional-derivative (*PD*) controller as well as fractional derivative (*FD*) controller.

6. Simultaneous control of the effective mass and stiffness of a unit cell of the *AAMM* using a single actuator.

7. With the development of the various configurations of *AAMM* and control strategies, it has demonstrated that the width of the double negative properties zones can be significantly enhanced.

8. The experimental demonstration of the *AAMM* unit cell with controlled density and bulk modulus

9. Development of the closed-loop strategies of separate and simultaneous control of the density and bulk modulus is one of the very important contributions of this dissertation.

9.5 Summary

This chapter has summarized the discussions, recommendations and future work which can be carried out as a natural extension of this dissertation.

The chapter has included also are the major contributions of the dissertation in relation to the current state-of-the-art.

References

S. Pope and S. Daley, “Viscoelastic locally resonant double negative metamaterials with controllable effective density and elasticity”, *Physics Letters A* 374 (2010) 4250–4255

S. Althamer, and A. Baz. "Active acoustic metamaterial with fractional derivative controller." *SPIE Smart Structures and Materials+ Nondestructive Evaluation and Health Monitoring*. International Society for Optics and Photonics, 2014.

W. Akl and A. Baz, “Interior Acoustic Cloak”, *AIP Advances* **4**, 124305, 2014, http://dx.doi.org/10.1063/1.4902100

W. Akl, and A. Baz, “Multi-cell active acoustic metamaterial with programmable bulk’s modulus”, *Journal of Intelligent Material Systems and Structures*, Vol. 21, pp. 541-556, March 2010.

W Akl and A Baz, “Stability analysis of active acoustic metamaterial with programmable bulk modulus”, *Journal of Smart Materials and Structures*, Vol. 20, No. 12, 125010, Dec. 2011.

W. Akl and A. Baz, “Analysis and experimental demonstration of an active acoustic metamaterial cell”, *J. Appl. Phys*. Vol. 111, No. 4, 044505, 2012.

W. Akl and A. Baz, “A technique for physical realization of anisotropic density matrices with application to acoustic beam shifters”, *J. Appl. Phys*. Vol. 111, No. 2, 024907, 2012.

W. Akl and A. Baz, “Multicell active acoustic metamaterial with programmable effective densities”, *ASME Journal of Dynamic Systems, Measurement, and Control*, Vol. 134 , No. 6, pp. 061001-(1-11), 2012.

W. Akl, A. Elsabbagh, and A. Baz, Acoustic metamaterials with circular sector cavities and programmable densities”, *Journal of the Acoustical Society of America*, Vol. 132, No. 4, Pt. 2, pp. 2857-2865, October 2012

A. Baz, "The structure of an active acoustic metamaterial with tunable effective density", *New Journal of Physics*, Vol. 11, 1230102009, 2009.

A. Baz, "An active acoustic metamaterial with tunable effective density*", ASME* Journal of Vibration & Acoustics, Vol. 132, No. 4, 041011 1-9 , 2010.

Cheng, Y., Yang, F., Xu, J. Y., and Liu, X. J., 2008, "A Multilayer Structured Acoustic Cloak with Homogeneous Isotropic Materials", *Appl. Phys. Lett*. **92**, 151913.

Chen, H.-Y., Yang, T., Luo, X.-D. and Ma, H.-R., 2008, "Impedance-Matched Reduced Acoustic Cloaking with Realizable Mass and Its Layered Design", *Chinese Phys. Lett.* , **25** (10), pp. 3696-3699.

Cheng, Y., Xu, J. Y., and Liu, X. J., 2008, "One-Dimensional Structured Ultrasonic Metamaterials with Simultaneously Negative Dynamic Density and Modulus", *Physical Review* B, **77**, 045134.

Cheng, Y. and Liu, X. J., 2009, "Three Dimensional Multilayered Acoustic Cloak with Homogeneous Isotropic Materials", *Journal Applied Physics A: Materials Science & Processing*, **94** (1), pp. 25-30.

Cummer, S. A. and Schurig, D., 2007**, "**One Path to Acoustic Cloaking", *New Journal of Physics*, **9**, 45.

Cummer S. A., Rahm, M., and Schurig, D., 2008a, "Material Parameters and Vector Scaling in Transformation Acoustics", *New Journal of Physics*, **10**, 115025.

Cummer, S. A., Popa, B.-I., Schurig, D., Smith, D. R., Pendry, J., Rahm, M. and Starr, A., 2008b, "Scattering Derivation of a 3D Acoustic Cloaking Shell", *Phys. Rev. Lett*. **100** 024301.

Gil, M., Bonache, J., and Martín, F. , 2008, "Metamaterial Filters: A review", *Metamaterials*, **2**, pp. 186–197.

Lapine, M., 2007**,** "The Age of Metamaterials", *Metamaterials*, **1**, pp. 1.

Lee, S. H., Park, C. M., Seo, Y. M., Wang, Z. G., and Kim, C. K., 2009a, **"**Negative Effective Density in An Acoustic Metamaterial", *arXiv 0812.2954v3* [cond-mat-mtrl-sci].

Lee, S. H., Park, C. M., Seo, Y. M., Wang, Z. G., and Kim, C. K., 2009b, "Reverse Doppler Effect of Sound", *arXiv 0901.2772v2* [cond-mat.other].

Kinsler, L., Frey, A., Coppens, A., and Sanders, J., 2000, *Fundamentals of Acoustics*, *4th* ed., J. Wiley & Sons, Inc.

Milton, G. W., Briane, M. and Willis, J. R., 2006**,** "On Cloaking for Elasticity and Physical Equations with a Transformation Invariant Form", *New Journal of Physics*, **8**, 248.

C. A. Monje, Y. Q. Chen, B. M. Vinagre, D. Y Xue, V. Feliu, *Fractional-order Systems and Controls: Fundamentals and Applications*, Springer-Verlag London Ltd., 2010.

Norris, A. N., 2008**,** "Acoustic Cloaking Theory", *Proceedings of the Royal Society A: Mathematical, Physical and Engineering Sciences*, **464** (2097), pp. 2411-2434.

Norris, A. N. , 2009, "Acoustic metafluids", *J. Acoust. Soc. Am.*, **125** (2), pp. 839-849.

Prasad S., Gallas, Q., Horowitz, S., Homeijer, B., Sankar, B., Cattafesta, L., and Sheplak, M., 2006, "Analytical Electroacoustic Model of a Piezoelectric Composite Circular Plate", *AIAA Journal*, **44** (10), pp. 2311-2318.

Pendry, J. B. and Li, J., 2008**,** "An Acoustic Metafluid: Realizing a Broadband Acoustic Cloak", *New J. Phys.*, **10**, 115032.

Popa, B. I. and Cummer, S., 2009, "Cloaking with Optimized Homogenous Anistropic Layers", *Physical Review A*, **79**, 023806.

Shamonina, E. and Solymar, L., 2007**,** "Metamaterials: How the Subject Started", *Metamaterials*, **1**, pp. 12–18.

Torrent, D. and Sanchez-Dehesa, J., 2008**, "**Acoustic Cloaking in Two Dimensions: A Feasible Approach", *New Journal of Physics*, **10**, 063015.

Yao, S., Zhou, X. and Hu, G., 2008**, "**Experimental Study on Negative Effective Mass in a 1D Mass–Spring System", *New Journal of Physics*, **10**, 043020.

M. Reynolds and S. Daley, 2014, "An active viscoelastic metamaterial for isolation applications", *Smart Mater. Struct.* 23 045030